Investigation on the Effects of Entrained Air in Pipelines

Von der Fakultät Bau- und Umweltingenieurwissenschaften
der Universität Stuttgart zur Erlangung der Würde eines
Doktors-Ingenieurs (Dr.-Ing.) genehmigte Abhandlung

Vorgelegt von

Oscar Pozos Estrada

aus Mexiko Stadt, Mexiko

Hauptberichter: **Prof. em. Dr.-Ing. habil. Dr.-Ing. E.h. Jürgen Giesecke**

Mitberichter: **Prof. Dr.-Ing. Eberhard Göde**

Mitberichter: **PD Dr.-Ing. Walter Marx, AOR**

Tag der mündlichen Prüfung: 10.01.2007

Institut für Wasserbau der Universität Stuttgart

2007

Heft 158 Investigation on the Effects of Entrained Air in Pipelines

von
Dr.-Ing. Oscar Pozos Estrada

Eigenverlag des Instituts für Wasserbau der Universität Stuttgart

D93 Investigation on the Effects of Entrained Air in Pipelines

Titelaufnahme der Deutschen Bibliothek:

Pozos Estrada, Oscar:

Investigation on the Effects of Entrained Air in Pipelines/
von Oscar Pozos Estrada. - Stuttgart: Inst. für Wasserbau, 2007

(Mitteilungen/Institut für Wasserbau, Universität Stuttgart: H. 158)
Zugl.: Stuttgart, Univ., Diss., 2007
ISBN 3-933761-62-X
NE: Institut für Wasserbau <Stuttgart>: Mitteilungen

Herausgeber 2007 vom Eigenverlag des Instituts für Wasserbau
Druck: e.kurz + co druck und medientecknik GmbH, Stuttgart

Vorwort

1. Veranlassung

1.1 Dynamische Strömungsvorgänge, Druckstöße in Rohrleitungen

Bei jeder Geschwindigkeitsänderung in durchflossenen Gerinnen oder Rohrleitungen entstehen Druckschwankungen. Während in einem offenen Gerinne bei plötzlicher Durchflussänderung ein Ausgleich der Bewegungsenergie durch ein Anheben oder Absenken des Wasserspiegels (Schwall- bzw. Sunkwelle) erfolgt, entsteht bei geschlossenen Druckrohrleitungen ein Ausgleich der Bewegungsenergie durch die Elastizität der Rohrwandungen und des Wassers selbst. Dieses bedeutet bei einer Verzögerung der Fließgeschwindigkeit eine Umwandlung der Bewegungsenergie in Druckenergie (Druckstoß). Der Druckstoß ist demnach eine Folge derjenigen Kraft, welche die träge Flüssigkeitsmasse der Änderung ihres Bewegungszustandes entgegensetzt. Bei einer Beschleunigung wird Lageenergie in Bewegungsenergie umgesetzt. Diese plötzlichen Druckänderungen in einer Rohrleitung können erhebliche Größen annehmen und sind bei der Bemessung unbedingt zu berücksichtigen.

In Rohrleitungen, die vollständig mit einer Flüssigkeit gefüllt sind, kommt es insbesondere dann zu Druckstößen, wenn Absperr- oder Regelorgane betätigt bzw. Turbinen und Pumpen ein- und ausgeschaltet werden. Druckstöße treten auch beim zu schnellen Füllen von Rohrleitungen, bei ungenügender Entlüftung, beim pulsierenden Austritt von größeren Luftansammlungen aus Druckleitungen, schließlich bei unregelmäßiger Förderung von Pumpen als Folge ungenügender Saugrohrentlüftung und bei Kavitationserscheinungen auf.

Bei langen Rohrleitungen und kurzen Regelzeiten müssen bei der Berechnung von Druckstößen die weitgehende Inkompressibilität der Flüssigkeit und die Elastizität der Rohrwand berücksichtigt werden, da es an der Störstelle (Regelorgan, Turbinen, Pumpen etc.) zu einer Dichteänderung, die sich stets mit der Druckwellengeschwindigkeit fortpflanzt, kommt.

1.2 Be- und Entlüftungsventile bei Rohrleitungen

Neben Verschluss- und Regelorganen gehören auch Be- und Entlüftungsventile zu der Ausrüstung einer Fernleitung. Belüftungsventile gleichen den bei der Entleerung der Leitung auftretenden Unterdruck aus. Erheblicher Unterdruck kann sich vor allem dann ausbilden, wenn infolge der Drosselung einer Armatur der ursprüngliche Abfluss von der Zulaufseite unter dem bestehenden Druckgefälle nicht mehr alleine nachläuft und die Anschlussleitung zu saugen beginnt, um die erforderliche Nachströmung zu erhalten.

Hochpunkte und Knickpunkte der Rohrleitung sind ebenfalls durch Unterdruckbildung gefährdet. Aus Strömungsstörungen resultierende, zum Überdruck und Unterdruck wechselnde Druckwellen durchlaufen die Rohrleitung und können an diesen Punkten ein Abreißen der Wassersäule herbeiführen. Umgekehrt entstehen gefährliche, steile Druckspitzen beim Zusammenstoßen ursprünglich getrennter Flüssigkeitssäulen.

Als nächste Aufgabe haben die Be- und Entlüftungsventile die in der Rohrleitung vorhandenen Gase (Luft, Flüssigkeitsdampf etc.) entweichen zu lassen, die sich durch Anhäufung oder durch Ausscheiden aus dem Wasser im Laufe des Betriebes an besonderen Rohrstellen angesammelt haben und den freien Strömungsquerschnitt verringern sowie Energieverluste und ebenso unerwünschte Druckstöße verursachen können.

Entlüftungen sind normalerweise an geodätischen und in Bezug auf den Verlauf von Rohrleitungsdrucklinien an hydraulischen Hochpunkten von Rohrleitungssträngen erforderlich, wo es durch Druckerniedrigung oder durch Temperaturerhöhung zur Ansammlung von Luft kommen kann.

Für Füll- und Entleerungsvorgänge sind gleichfalls Be- und Entlüftungsventile notwendig. Sie befinden sich generell an Leitungshochpunkten und im Abstand von ca. 750 m bei langen geneigten Rohrleitungssträngen. Größe und Anzahl richten sich nach Leitungsdurchmesser, Füllvolumen und zulässiger Strömungsgeschwindigkeit der Luft im kleinsten Strömungsquerschnitt des Ventils.

1.3 Auswirkungen von gashaltigen Flüssigkeitsströmungen auf Druckstöße

Die an Hochpunkten einer Rohrleitung sich allmählich ansammelnde Luft kann einerseits als Luftpolster dämpfend auf Druckstoßwellen einwirken, andererseits aber auch nachteilig in Pumpendruckleitungen sein, wenn sich mit dem Start der Pumpen und der einsetzenden Flüssigkeitsströmung hier ein erhöhter Druck je nach Luftmenge und Ausdehnung, auch durch Reflektion, einstellt. Lufteinschlüsse verhindern ebenso die in Unterdruckbereichen auf Flüssigkeitsdampfbildung zurückzuführende Kavitation.

Bei flüssigkeitsdampf- bzw. gas- (z. B. luft-) haltigen Flüssigkeitsströmungen wird nach Zweiphasenströmungen bzw. Zweikomponentenströmungen unterschieden. Während erstere Schäden im Rohrleitungssystem verursachen, können Lufteinschlüsse aufweisende Wasserströmungen hinsichtlich der Druckwellenausbreitung sich unterschiedlich verhalten. Derartige Wasser-Luft-Gemische erfahren interne Reflektionen von Druckwellen mit der Folge, dass die Hauptwelle in Wellen kleinerer Ausdehnung gebrochen wird und sich die Druckwellengeschwindigkeit verringert.

Es liegt daher auf der Hand, dass die Luftmenge, die Luftblasenverteilung und die Größe sowie die Anzahl sich entlang einem unterschiedlich geneigten Rohrstrang bildenden Lufttaschen eine erhebliche Rolle für die Ausbreitung und Intensität von Druckstößen spielen, wenn schon nicht mit völlig luftfreier Flüssigkeitsbewegung über kilometerlange Rohrleitungssysteme gerechnet werden kann. Da kleinere Lufteinschlüsse an Hochpunkten eines Rohrleitungssystems offensichtlich zu einer nicht vernachlässigbaren Erhöhung der Druckschwankungen infolge plötzlicher Pumpenabschaltungen führen können, bedarf es eingehenderer Untersuchungen dieses Problemkreises. Jüngste Forschungsergebnisse weisen vereinzelt darauf hin, dass es nicht bei der bisherigen Praxis bleiben kann, grundsätzlich von homogenen, einphasigen, ausschließlich den Strömungsquerschnitt ausfüllenden Flüssigkeitsströmungen, d. h. frei von Dampfblasen und Lufteinschlüssen, auszugehen.

1.4 Zielsetzung der Dissertation

Die vorgenannte Problemstellung ergab sich bei einer in Mexiko, der Heimat des Doktoranden, ausgeführten Fernwasserversorgung. Ihrer nahm sich die Heimat-Universität Universidad Nacional Autonoma de México an. Hier wurden bereits zielgerechte

Modellversuche ausgeführt und Lösungsvorschläge für bauliche und betriebliche Änderungen ausgearbeitet. Letztere sollten nunmehr wissenschaftlich vertieft und zu allgemeinen Bemessungsregeln, möglichst auf analytischer Basis, übergeführt werden. Vornehmlich stehen die Bewegungsvorgänge von kompakten Lufteinschlüssen und Wasser-Luft-Gemischen (Zweiphasenkomponenten-Strömung) in Pumpendruckleitungen und deren Verhalten beim plötzlichen Abschalten der Pumpenaggregate im Vordergrund.

Hierzu gewährte die vom Staat Mexiko eingerichtete Forschungsgemeinschaft CONACYT ein mehrjähriges Stipendium für den Aufenthalt von Herrn Pozos an der Universität Stuttgart, Institut für Wasserbau.

2. Zum Inhalt der vorliegenden Schrift

Im **1. Kapitel** legt der Autor ausführlich die Problemstellung und die ersten Ansätze zur Erfassung lufthaltiger Wasserströmungen dar, die auf experimenteller Basis gewonnen und in bekannte Beziehungen der Strömungsmechanik eingebunden worden sind. Im Regelfall sammelt sich die Luft entlang der Rohrleitung an Knickpunkten, insbesondere an Hochpunkten der Rohrtrasse, und verdichtet sich zu einer Lufttasche, die mehr und mehr ein Luftpolster für durchlaufende Druckwellen mit Dämpfungswirkung und Teilreflexionen bildet. Kleine Luftblasen nehmen die Form eines Ellipsoids von 1 bis 6 mm Längsausdehnung an.

Durch die Häufung von Luftblasen an einzelnen prädestinierten Stellen der Rohrleitungsströmung können durchaus den ganzen Strömungsquerschnitt ausfüllende Volumina entstehen, wenn Luft z. B. bei Füllung der Leitung infolge Turbulenzen oder aus dem Pumpensumpf von Pumpenleitungen, ferner an Armaturen und Rohrverbindungen in stärkerem Maße eingetragen wird. Bei abnehmendem Strömungsdruck bis hin zum Unterdruck ist ein Ausgasen einer lufthaltigen Wasserströmung möglich, ebenso kann es bei einer Unterschreitung des Dampfdruckes der Flüssigkeit zur Bildung von Flüssigkeitsdampfblasen führen. Eine ähnliche Wirkung lösen Temperaturerhöhungen aus. Entsteht örtlich in einer Strömung eines Wasserluftgemisches ein partieller Füllungsgrad für das Wasser und unterschreitet sogar die Wassertiefe unterhalb einer Lufttasche die kritische Tiefe, kommt es zu einem hydraulischen Wechselsprung.

Erfolgt keine Abführung der Luftansammlung durch standortgerechte Entlüftungsventile, ergeben sich vielfach Probleme wie Strömungsbehinderung, Energieverluste, Korrosionsanfälligkeit stählerner Rohrleitungen durch Sauerstoff, ferner Schwingungen bis hin zu gefahrvollen Resonanzschwingungen von Bauteilen, Druckstöße bis hin zum entlastenden plötzlichen Zurückschlagen einer größeren Luftblase. Hierdurch ausgelöste Zerstörungen in einem Fernwasserversorgungssystem in Mexiko waren nicht zuletzt der Anlass für die vorliegende Dissertation.

Die Fortbewegung einer größeren Luftblase hängt vom Kräftegleichgewicht aus Strömungsdruck bzw. statischer Druckhöhe und Geschwindigkeitshöhe, aus Schleppkraft und Auftrieb, damit aber auch vom Rohrleitungsgefälle und von den Druckverlusten des Luftwassergemisches ab. Hierfür gibt der partielle Strömungsquerschnitt des bewegten Wassers im Vergleich zum gesamten Rohrquerschnitt den Ausschlag, ebenso der an der Schnittstelle beider Medien Luft und Wasser eintretende hydraulische Wechselsprung.

Hinsichtlich der Fragestellungen des Verbleibens und des Weiterwanderns von Lufttaschen aufgrund der örtlichen Strömungsbedingungen oder der Luftabführung durch unterschiedliche Be- und Entlüftungsventile legte der Doktorand ausführlich die bisherigen Forschungsergebnisse und praktischen Handhabungen dar. Hierbei stellte er auch neben den rechnerischen Ansätzen insbesondere jenen in den Mittelpunkt, den er zusammen mit dem Betreuer seiner Masterarbeit an der Universidad Nacional Autónoma de México, México, aufgestellt hat. Dieser Ansatz spiegelt den auf Modellversuchen und theoretischen Untersuchungen aufbauenden Zusammenhang zwischen Durchfluss, Rohrdurchmesser, Neigung des Rohrstranges und Erdbeschleunigung wider, nachdem sich eine Lufttasche im Anschluss an den Ort des hydraulischen Wechselsprunges im abwärts geneigten Rohrstrang entweder nach oben zurück oder nach unten fortbewegt, Letzteres nach Überschreiten einer sog. kritischen Strömungsgeschwindigkeit.

Im **2. Kapitel** befasst sich der Autor im Detail mit der Analyse der vorerwähnten, mit auf ihn zurückgehenden Formel für die Luftblasenbewegung, ferner mit den zugehörigen Modelluntersuchungen und der Aufstellung eines Rechenprogrammes. Dieses bindet er in die Schilderung zweier Ausführungsbeispiele von Fernwasserversorgungssystemen in Mexiko ein.

Sowohl die rechnerischen als auch die durchgeführten Modelluntersuchungen bestätigten die treffsicheren Aussagen über die Bewegungsabläufe von kleinen Luftblasen als auch von großen Lufttaschen stromaufwärts und stromabwärts, sofern sie nicht von Turbulenzen beeinträchtigt werden. Hierauf stützt sich die vom Doktoranden entwickelte Software für Simulationsrechnungen, mit deren Hilfe die Notwendigkeit von Be- und Entlüftungsventilen je nach Rohrleitungsverlauf und Lufteintrag beurteilt werden kann oder statt dessen aus ökonomischen Gründen deren Anzahl zu verringern sein könnte, wenn auf einzelnen Leitungsabschnitten eine den Betrieb gefährdende Luftblasenanhäufung dank einer gesicherten Fortbewegung von Lufteinschlüssen ausgeschlossen werden kann.

Die beiden ausführlich geschilderten Beispiele einer Trinkwasserversorgung in Mexiko, das eine mit 54,5 km langen Doppelrohrleitungen aus Spannbeton, das andere mit 6,9 km langer Stahlrohrleitung, belegen eindeutig hinsichtlich völlig unerwarteten Betriebsverhaltens und eingetretener Schäden an Bauwerken, welche Bedeutung Lufteinschlüssen in großer Menge in ausgedehnten Lufttaschen ohne ausreichende Entlüftung beizumessen ist. In beiden Versorgungssystemen kam es aufgrund von extremen Luftansammlungen infolge turbulenter Strömungen und unterschiedlicher Strömungsraten, ferner ungenügender Anordnung von zusätzlichen, teilweise nicht funktionsgerechten Entlüftungsventilen besonders bei größeren Durchsätzen im ersten Fall zu erheblichen, auf Druckstoß zurückzuführenden Schäden an Bauwerken und im zweiten Fall zum Überlaufen von offenen Wasserbehältern aufgrund außerordentlicher Aufschwingungen des Wasserkörpers.

Im **3. Kapitel** erfolgen die grundsätzlichen experimentellen und theoretischen Untersuchungen zur Erfassung sich an Hochpunkten der Rohrleitung ansammelnder Lufttaschen. Untersuchungskriterien sind bei den hier verfolgten Pumpendruckleitungen das Wasserluftgemisch, d. h. die mit Luftblasen mehr oder weniger gleichmäßig durchsetzte Wasserströmung, die Bildung großer, sich verselbständigender Luftblasen, die sich durch Ausgasung an Hochpunkten der Leitungstrasse einstellen. Je nach den Durchfluss- sowie den Druck- bzw. Strömungsverhältnissen verharren Letztere an diesen Stellen oder wandern mit der aufgeteilten Wasserströmung, besonders längs Leitungsgefällsstrecken, weiter, bis ein durch die beiden Medien bedingter Wechselsprung eintritt und die Luftblasen sich wieder mit dem Wasser vermischen.

Die Bildung der Luftblasen setzt vor Erreichen des betrachteten Hochpunktes ein; die Luftblase nimmt eine bestimmte axiale Länge und damit ein gewisses Volumen ein, das im Modellversuch ausgemessen werden kann. Ab einer oberstromigen Grenzlage wächst die Luftblase bei weiterem Zufluss bzw. weiterer Luftzufuhr nur noch nach der Unterwasserseite hin. Die oberstromige Begrenzung hängt von der Größe des Durchflusses und der kritischen Wassertiefe der längs der Unterseite der Luftblase vorbeiziehenden Wasserströmung ab. Der schließlich am unterstromigen Ende der Luftblase entstehende hydraulische Wechselsprung bedingt Energieverluste.

Die experimentellen Untersuchungen wurden im vorgenannten Universitätsinstitut in Mexico City mit mehreren Varianten der Bestimmungsgrößen und ausgeklügelter Messtechnik ausgeführt, so dass neben der Boyle-Mariotteschen-Zustandsgleichung für Gase hierauf die hydromechanischen Beziehungen als Basis der rechnerischen Analysen gestützt werden konnten. Diese beinhalten die Länge und die Volumengröße der Luftblasen, den herrschenden Druck, den Reibungsbeiwert, den hydraulischen Radius, die Neigung der Leitungsabschnitte, die Wassertiefen unterhalb der Lufttasche und die Fließgeschwindigkeit, schließlich die Froude-Zahl. Die Berechnung des die Lufttasche längs begrenzenden Wasserspiegels und des Lufteinschlusses selbst erfolgt in 13 Schritten. Die in Tabellen und Grafiken dargelegten Rechenergebnisse korrelieren bestens mit den Versuchsdaten.

Im **4. Kapitel** werden die vorgenannten Untersuchungsergebnisse in ihrer praktischen Nutzanwendung für Pumpendruckleitungen von Wasserversorgungssystemen weiterverfolgt. Gewöhnlich beträgt der Luftgehalt von Wasser je nach den vorherrschenden Druck- und Temperaturverhältnissen ca. 2 %. Beim Einsatz von Förderpumpen werden auf der Saugseite (z. B. Entnahmebrunnen, Wasserbehälter) 5 bis 10 % Luft in den Flüssigkeitsstrom eingetragen. Weitere Luftaufnahmen können an Verschluss- und Regelorganen sowie ggfs. an Rohrverbindungen geschehen, die in der Summe zu beachtlichen Einschränkungen der Förderkapazität und zu gefährlichen Druckstößen führen können, sofern nicht für ausreichende Entlüftung durch Be- und Entlüftungsventile an Leitungshochpunkten gesorgt wird.

Der Verfasser stellt nach Diskussion von rund einem Dutzend anderweitiger wissenschaftlicher Forschungsberichte diesen ein Rechenmodell gegenüber, das mit dem Charakteristikenverfahren zur Verfolgung von Lufttaschen innerhalb des eine

Zweikomponentenströmung darstellenden Wasserluftgemisches entwickelt worden ist. Die Anwendung geht übersichtlich aus dem zugehörigen Flussdiagramm hervor, das auch die Grundlage für eine anschließende Fallstudie bildet für eine Pumpendruckleitung mit vier parallel geschalteten Kreiselpunkten, 2,3 km langer Stahlleitung von 1,2 m Durchmesser und einem zu versorgenden, 397 m höher gelegenen Wasserbehälter bei unterschiedlichen Fördermengen und Luftvolumina. Um die verschiedenartigen Auswirkungen letzterer zu demonstrieren, wurde gänzlich auf Entlüftungsventile verzichtet.

Die Untersuchungsvarianten zeigen anhand der Verläufe der Drucklinien deutlich deren Schwankungsbreite zwischen der Förderung von nicht-lufthaltigem Wasser und mit Lufttaschen belastetem Fördermedium. Die durch plötzliche Pumpenabschaltung entstehenden Druckwellen werden je nach Luftvolumen und Ausdehnung der an verschiedenen Standorten sich ansiedelnden Lufttaschen entweder beachtlich gedämpft oder gar reflektiert, sie werden oberstromseitig zum Pumpenstandort und unterstromseitig zum Wasserbehälter zurückgeleitet bzw. fortgeführt. Mit wachsendem Luftvolumen nehmen die Druckhöhen ab. Mit anderen Worten: Kleine Luftblasen vergrößern gegenüber einer luftfreien Wasserströmung in der Rohrleitung eher die instationären Druckdifferenzen, während größere Luftblasenvolumen einen vergleichsweise günstigen Einfluss haben, indem sie die instationären Druckschwankungen verkleinern.

Aus Gründen der Betriebssicherheit sind die Auswirkungen verschieden großer Lufttaschenvolumen von Bedeutung. Hiernach richten sich die Eigenschaften des sich im Blasenbereich einstellenden Freispiegelabflusses und damit die instationären Druckverhältnisse, z. B. nach Ausfall der Förderpumpen. Daher ist die vorhandene Sicherheit durch Variation der Luftblasengröße, der Lage und der Ausdehnung der Lufttaschen innerhalb realistischer Grenzen jeweils zu überprüfen. Dieses kann durch die vom Autor frei zugänglichen Programm-Module zur instationären Rohrleitungsberechnung geschehen.

Das **5. Kapitel** ist in Erweiterung der vorausgegangenen Grundsatzbetrachtungen dem gleichzeitigen Auftreten von Lufttaschen an Leitungshochpunkten und gezielt der nach Unterstrom gerichteten Fortbewegung eines Wasserluftgemisches aus Wasserströmung und darin verteilten feinen Luftblasen als Folge eines hydraulischen Wechselsprunges am unterstromigen Ende der Lufttasche gewidmet. Wiederum sollen keinerlei Entlüftungsventile in das Leitungssystem eingebunden sein. Die verschiedensten Ausbildungen einer

Zweikomponentenströmung aus Luft und Wasser, die der Doktorand vereinfachend als Zweiphasenströmung bezeichnet, werden zusammen mit aus Modellversuchen gewonnenen Bildern im Einzelnen diskutiert. In gleicher Weise geht der Autor auf die Fließzustände und Strömungsbilder eines immer homogener werdenden Wasserluftgemisches ein, das nach dem Wechselsprung aus der Lufttasche und dem diese begleitenden Wasserstrom entstanden ist.

Wiederum werden in der analytischen Ergründung der theoretischen Zusammenhänge eine große Reihe an vorausgegangenen, veröffentlichten Forschungsarbeiten herangezogen und der eigene Rechenansatz mit dem oben erwähnten Stufenmodell unter Einbindung eines eindimensionalen Modelles für das als homogen betrachtete Wasserluftgemisch fortgeführt. Erneut werden die erforderlichen Rechenschritte in einem übersichtlichen Flussdiagramm zusammengefasst. Die Verfahrensschritte bis hin zur grafischen Darstellung der variantenreichen Ergebnisse werden anhand des gleichen Wasserversorgungssystems mit vier Pumpenaggregaten, Fernrohrleitung und Endbehälter, wie im vorigen Kapitel herangezogen, dargestellt. Durch den zusätzlichen Dämpfungseffekt, den das einer Lufttasche nachfolgende, über den hydraulischen Wechselsprung mehr oder weniger zustande gekommene Wasserluftgemisch ausübt, fallen im Vergleich zu den Ergebnissen einer nur die Lufttaschen berücksichtigenden Berechnung nunmehr die Abminderungen der Druckhöhen erheblich deutlicher aus. Innerhalb des Wasserluftgemisches kommt es durch Teilreflexionen der durch plötzlichen Pumpenstillstand erzeugten Druckwelle an den einzelnen Luftblasen zu deren Aufspaltung in einzelne kleinere Druckwellen, die weitaus ungefährlicher für den Bestand der Rohrleitung sind. Wiederum ist der Dämpfungseffekt am größten, wenn die Lufttasche ein beträchtliches Volumen hat und ein intensiver Luftweitertransport auf deren Unterstromseite mittels des Wasserluftgemisches stattfindet.

In zehn Einzeluntersuchungen mit verschiedenen Ausgangsbedingungen hinsichtlich Fördermenge, Pumpeneinsatz, mit bis zu vier Standorten und Volumengrößen der Lufttasche sowie mit Luftweiterleitung unterhalb der Lufttasche lassen sich die für die Praxis interessanten Ergebnislagen anhand der Drucklinienverläufe verfolgen. Ein aufschlussreicher Vergleich mit der Situation bei luftfreier Wasserförderung einerseits und mit der Situation bei Unterbindung einer Luftweiterleitung auf der Unterstromseite einer Lufttasche andererseits ist gleichfalls gegeben.

Im abschließenden **6. Kapitel** werden die wichtigsten Ergebnisse nochmals erörtert und in Verbindung mit praktischen Anforderungen bei Planung, Ausführung und Betrieb von Pumpendruckleitungen in Wasserversorgungssystemen gebracht. Gerade im Hinblick auf die immer wieder gemachten Erfahrungen, dass die Fernleitungen für Flüssigkeitstransport als Folge von Lufteinschlüssen in Transportmedien namhafte Schäden erleiden können, wenn nicht sachgemäße Abhilfe durch Anordnung von funktionstüchtigen Be- und Entlüftungsventilen unterschiedlichen Bautyps oder durch höchstmögliche Vermeidung von Lufteinträgen getroffen wird, sind die vorgelegten Experimente und rechnerischen Ergebnisse von grundsätzlichem Wert.

3. Zusammenfassende Betrachtung

Herr Oscar Pozos Estrada legte eine interessante Promotionsschrift in englischer Sprache vor, die ihren Ausgang von in seinem Heimatland Mexiko aufgetretenen Schadensfällen bei Trinkwasserfernversorgungen mit mehreren zehn Kilometer langen Rohrleitungen genommen hat. Diese waren auf überraschende Einträge größerer Luftmengen in das Fördersystem und auf entweder gänzlich entfallende oder nicht den Anforderungen genügende Be- und Entlüftungseinrichtungen zurückzuführen. Zur eindeutigen Klärung der Ursachen galt es, ein Simulationsmodell zur rechnerischen Analyse von Lufteinschlüssen in unterschiedlicher Form als Wasserluftgemisch (Zweikomponentenströmung) und als Lufttaschen größerer Ausdehnung vornehmlich an Hochpunkten einer Rohrleitung zu entwickeln. Dabei spielen eine Rolle die Boyle-Mariottesche-Zustandsgleichung, die verschiedenen hydromechanischen Gesetze für Strömungsabläufe, das Verhalten von getrenntem Luftpolster und Wasserkörper, von mehr oder weniger homogenen mit Luft angereicherten Wasserströmungen und die durch Luftblasen oder gar Lufttaschen ermöglichte Dämpfung von Druckwellen. Nach Möglichkeit sollten auch experimentelle Untersuchungen die numerischen Simulationen ergänzen und eine Übereinstimmung von Versuch und Rechnung nachweisen.

Tatsächlich ist es gelungen, jeder Zeit nachvollziehbare Lösungswege aufzuzeigen und zu für die Baupraxis interessanten Schlussfolgerungen zu gelangen.

Stuttgart, im Januar 2007 Jürgen Giesecke

Acknowledgments

I would like to express my sincere thanks to my advisors Prof. em. Dr.-Ing. habil. Dr.-Ing. E.h. Jürgen Giesecke and PD Dr.-Ing. Walter Marx, AOR for the encouragement and guidance throughout this work.

I also owe a sincere gratitude to Prof. Dr.-Ing. Eberhard Göde and his invaluable comments and suggestions on the work.

My Profound gratitude goes to my family (Mom, Dad and my brother). It is they who gave me the courage and strength to continue my step along this work.

My thanks also go to Dipl.-Ing Jörg Franke and Dr.-Ing. Andreas Bielinski, with whom I had many helpful discussions during this work.

Financial support from the Consejo Nacional de Ciencia y Tecnología CONACYT and German Academic Exchange Service DAAD is gratefully acknowledged.

I am grateful to M. I. Eduardo Rodal C. and M. I. Alejandro Sanchez H. from University of Mexico (UNAM) for the permission to use the experimental apparatus at the Hydromechanics Laboratory and to conduct the investigation related with this dissertation.

I also want to give my thanks to my colleagues and friends for their help inside and outside my academic life. This started from the first day I came to Germany.

Oscar

Investigation on the Effects of Entrained Air in Pipelines

Table of contents

LIST OF FIGURES

LIST OF TABLES

LIST OF SYMBOLS

a	transient wave speed	[m/s]
a_{mix}	velocity of the pressure wave in a water-air mixture	[m/s]
a	numerical coefficient	[-]
A	total cross section area of the pipe	[m^2]
A_1	water area at the upstream end of the pipe reach	[m^2]
A_2	water area at the downstream end of the pipe reach	[m^2]
BS	dimensionless parameter to characterise the size of air bubbles and pockets	[-]
c	constant determined from the initial steady state condition for the air pocket	[-]
C	drag coefficient	[-]
$C_{(-)}$	negative characteristic	[m^3/s]
$C_{(+)}$	positive characteristic	[m^3/s]
d	length of the free surface of the receiving body of water	[m]
D	pipe diameter	[m]
e	pipe wall thickness	[m]
E	Young's modulus of elasticity of the pipe material	[kg/m^2]
E_a	modulus of elasticity of air	[kg/m^2]
E_w	modulus of elasticity of water	[kg/m^2]
E_1	specific energy at the downstream end of the pipe reach	[m]
E_2	specific energy at the upstream end of the pipe reach	[m]
F_1	Froude number upstream of the hydraulic jump	[-]
g	acceleration due to gravity	[m/s^2]
H	instantaneous head	[m]
H_A	absolute head	[m]
$H_{U_{i,n+1}}$	piezometric head above the datum at the section (i,n+1) at the end of the time step	[m]
H_b	barometric pressure head	[m]
K	constant depending on the air bubble/pocket shape	[-]
L	length of conduit	[m]
L_d	linear dimension of the air bubble/pocket	[m]
$L_{Hyd\ Jump}$	length of the hydraulic jump	[m]
L_{pipe}	length of the pipeline	[m]
L_{pocket}	length of the air pocket	[m]
$L_{profile\ at\ S01}$	length of the flow profile at the upgrade pipe	[m]
$L_{profile\ at\ S02}$	length of the flow profile at the downgrade pipe	[m]
L_{ts}	length of the test section	[m]
n	coefficient of Manning	[s/$m^{1/3}$]
p	average pressure at the particular cross section	[kg/m^2]
P_1	atmospheric pressure in Mexico City, equal to 8.03	[mH_2O]
P_2	absolute pressure of the air pocket during test 2	[mH_2O]
Q	instantaneous water flow rate	[m^3/s]
Q_a	air flow rate	[m^3/s]
Q_w	water flow rate	[m^3/s]
$Q_{i,n+1}$	water flow rate at the upstream end of the air pocket at the beginning of the time step	[m^3/s]

$Q_{U_{i,n+1}}$	water flow rate at the upstream end of the air pocket at the end of the time step	[m^3/s]
$Q_{i+1,1}$	water flow rate at the downstream end of the air pocket at the beginning of the time step	[m^3/s]
$Q_{U_{i+1,1}}$	water flow rate at the downstream end of the air pocket at the end of the time step	[m^3/s]
R	hydraulic radius	[m]
R_e	Reynolds number	[-]
S	pipe slope	[-]
S_f	safety factor	[-]
S_f	friction slope	[-]
S_{sub}	subcritical slope	[-]
S_{sup}	supercritical slope	[-]
S_{01}	slope of the upstream pipe leg	[-]
S_{02}	slope of the downstream pipe leg	[-]
t	time	[s]
T´	dimensionless gas pocket number	[-]
v	water velocity in the pipe	[m/s]
v_a	average air velocity	[m/s]
v_{br}	bubble rise velocity	[m/s]
v_c	cleaning velocity of the flow	[m/s]
v_{crit}	critical mean water velocity acting on a stationary air bubble	[m/s]
$v_{critical}$	critical velocity for air removal or air pocket	[m/s]
v_{jet}	supercritical jet velocity	[m/s]
v_m	mixture velocity	[m/s]
v_{min}	minimum mean water velocity required to clear a given volume of air	[m/s]
v_{nom}	nominal velocity (velocity when no air pocket exist)	[m/s]
v_r	rise velocity of the air pocket	[m/s]
v_0	outlet water velocity	[m/s]
v_0^*	critical outlet velocity to transport air	[m/s]
v_1	water velocity upstream of the hydraulic jump	[m/s]
V	volume of air	[m^3]
V_1	volume of air injected in the line at atmospheric pressure	[m^3]
V_2	volume of air in the test section during test 2	[m^3]
$V_{1,2}$	volume of air at the pipe reach	[m^3]
V	volume of air	[m^3]
V_{U_i}	volume of the air at the end of the time step	[m^3]
V_i	volume of the air at the beginning of the time step	[m^3]
V_{Up}	volume of the air pocket upstream of the control section	[m^3]
V_{Down}	volume of the air pocket downstream of the control section	[m^3]
$v_1^2/2g$	velocity head at the upstream end of the pipe reach	[m]
$v_2^2/2g$	velocity head at the upstream end of the pipe reach	[m]
y_1	initial depth	[m]
y_1	initial depth	[m]
y_e	effective depth	[m]

Y_c	critical depth	[m]
Y_n	normal depth	[m]
Y_1	water depth at the upstream end of the pipe reach	[m]
Y_2	water depth at the downstream end of the pipe reach	[m]
x	axial distance along the pipe	[m]
z	height of the pipe axis above the datum	[m]
α	void fraction	[-]
β	ratio of air flow rate to water flow rate	[-]
γ	specific weight of water	[kg/m^3]
Γ	gas production rate per unit volume	[kg/m^3/s]
Δh_{APi}	head loss caused by the presence of the air pocket	[m]
Δh	head loss generated by the air pocket	[m]
Δh	difference in elevation in the manometer	[m]
Δt	size of the time step	[s]
Δx	length of the reach	[m]
$\Delta x_{1,2}$	length of the pipe reach	[m]
ξ	empirical dimensionless coefficient	[-]
θ	angle of pipe inclination from the horizontal	[°]
λ	friction factor of Darcy-Weisbach	[-]
λ_{exp}	experimental friction factor	[-]
μ	pipe constraint factor	[-]
ν	kinematic viscosity	[cm^2/s]
ρ	water density	[kgs^2/m^4]
ρ_a	air density	[kgs^2/m^4]
σ	surface tension	[kg/m]
τ_o	boundary shear stress	[kg/m^2]
ψ	polytropic index	[-]
$\varphi_1, \varphi_2, \varphi_3$	terms in the characteristic equations	[-]
$\zeta_1, \zeta_2, \zeta_3$	terms in the characteristic equations	[-]

ABSTRACT

The main goal of this work is the development of a computational program for the quantitative assessment of the effects of entrained air in pipeline systems with respect to their operational safety. Likewise, two specific problems are investigated. (1) The effect of entrained air in form of pockets on hydraulic transients, during pump shutdown. It can be considered the most dangerous maneuver within a pumping pipeline. The computations corresponding to this study were evaluated by using the method of characteristics. (2) The numerical simulation of fluid transients caused by the shutdown of pumps, considering air pockets located at the high points of pumping pipeline systems and a water-air bubble mixture immediately downstream of the pockets. The constitutive equations – conservation of the gas mass, of the liquid mass, and the mixture momentum – yield a set of differential equations that will be solved by the method of characteristics. For the homogeneous model presented herein the two phases or components are treated as a single pseudofluid with average properties. It is assumed that there is no relative motion or slip between the phases, as well as for the momentum equation for the mixture. In the same way to the compressibility of the gas, the liquid compressibility and the pipe wall elasticity are included in the system of equations. The equation of energy is not used due to the moderate change in temperature of the mixture during the transient. In the case of negative impacts on the safety and operability of pipeline systems resulting from air entrainment, operational remediation measures will be suggested.

In a previous research a computational program has been developed supported on a proposed equation, which was validated with experimental investigation made in laboratory. Two hydraulic models were designed and constructed to analyze the behavior of stationary air pockets located at high points of gravity pipelines, as well as to analyze the air entrained by the hydraulic jump at the end of the pocket located in the downward sloping pipe section of the models. From a comparison of the experimental measures with the results obtained with the program, it can be stated that these agreed well. In addition, a new subroutine was implemented to be used in this work to locate the air pockets that are likely to accumulate at the high points of pumping pipeline systems. The results obtained with the implementation adjusted well with the predictions obtained from other investigators for the pipeline configuration analyzed in the case study.

The new computational implementations were developed to provide the pipeline designers with a quantitative method for studying the movement of air bubbles and pockets and identifying the high points in pipelines that are susceptible to accumulate air, as well as the effect of entrained air on hydraulic transients caused by the sudden shutdown of pumps can be simulated. The program can be used to analyze either pipeline systems during the design stage or existing pipeline performance.

Hydraulic model investigations have been carried out in the laboratory with the main aim of measuring the volumes of air that form the pockets, as well as to study and observe large air pockets located at the high points of the pumping pipeline systems. The experimental measures were made in an experimental apparatus composed of a pump with a maximum water flow rate of 2.5 l/s; a constant head tank of 5.0 x 1.1 m at the base and 1.0 m height and a pipe test section of a 76.2 mm internal diameter acrylic pipe mounted on metallic frames. It was formed by an upstream pipe of 6.8 m long followed by a flexible pipe with a length of 50 cm and by another pipe section of 6.4 m in length. Both pipe sections could be varied in slope. During the experiments the water depths underneath the large air pocket for pressurized conduit flow, as well as at atmospheric pressure were recorded. The measurements were compared with the analytical results obtained with the direct step method used in the analysis of gradually varied flow. It was seen, that the flow profiles underneath the air pocket determined experimentally and those computed by using the dynamic equation of the gradually varied flow showed excellent correlation with the flow profiles.

The air pocket volumes were calculated by applying an equation based on the direct step method and were compared with the experimental results obtained in laboratory. The computed values are lower than the volumes of air measured in the experiments. Hence, it can be stated that the volumes of air estimated with the variables obtained with the direct step method increase the factor of safety in pipeline design. This is because the author and other investigators have found that small air pockets located at intermediate and high points can exacerbate the magnitude of the pressure transients experienced by a sudden or routine pump shutdown. However, it can be stated that there is a limit to the air pocket volumes having this effect on hydraulic transients. Therefore, it is important to find the critical air pocket volumes for any given pipeline configuration to be taken into account during the design stage of pipelines to reduce any potential detrimental effect.

A photographic study was developed to reinforce the assumptions made in the analytical model for the simulation of pressure transients with air pockets and a water-air mixture downstream of them.

A case study of a pumping pipeline system without surge suppression devices was simulated to demonstrate the potential effect of air pockets with and without a water-air mixture downstream of them on hydraulic transients. The boundary condition at the upstream end is a pumping station and at the downstream end a constant head tank. Only hydraulic transients generated by the shutdown of the pumps are taken into account in this analysis. The pumping station operates with four centrifugal pumps connected in parallel and each unit is able to deliver a maximum flow discharge of 0.625 m^3/s to the constant head tank 396.92 m above the sump pump level. The conduction is 2289 m in length and made up of steel pipe with an inner diameter of 1.22 m.

The purpose of this research is to demonstrate the potential detrimental and beneficial effects on pressure transients of air pockets with and without a water-air mixture downstream of them, located at the high points of pumping pipeline systems. The numerical investigation developed during this work could serve the designer as guidance to predict more accurately the critical conditions for various pipeline configurations.

KURZFASSUNG

Einleitung

Es gibt zahlreiche Fälle in der Praxis, in welchen eine Flüssigkeit, die in einem Rohr fließt, entweder Dampf oder Gas oder beides als Mischung enthält. Eine fließende Mischung aus Dampf und Flüssigkeit der gleichen chemischen Substanz wird Zweiphasenströmung genannt, während eine Gas-Flüssigkeitskombination unterschiedlicher Substanzen wie Luft und Wasser Zweikomponentenströmung genannt wird. Vereinfachend wird die Bezeichnung „Zweiphasenströmung“ häufig auch für Zweikomponentenströmungen eingesetzt. Jedoch kann der Effekt des Vorhandenseins von Dampf (Zweiphasenströmung) oder Gas (Zweikomponentenströmung) weit reichende Auswirkungen auf Druckstoßvorgänge haben.
Während der Einfluss der Dampfblasenbildung normalerweise in Bezug auf Druckstoßvorgänge schädlich ist, kann freies Gas entweder vorteilhaft oder schädlich sein. Dies ist abhängig von der Menge und der Position des kondensierbaren Gases. Offensichtlich spielen der Anteil des Dampfes oder des Gases - oder von beiden - in einem Strömungssystem eine wichtige Rolle auf die resultierenden Drücke, ebenso wie die Art des Druckstoßes.

Die wesentlichen Effekte der Luft auf Druckstoßvorgänge sind bekannt. Wenn sich Luft beispielsweise an einem Hochpunkt ansammelt, dann wirkt sie wie ein Luftpolster, das die Druckstoßwellen dämpft, sie kann den Druckstoß aber auch vergrößern, *Ewing* (1980). Wenn die Luft gleichmäßig in Form kleiner Luftblasen verteilt ist, sind die Auswirkungen schwieriger vorherzusagen. Der signifikanteste Effekt ist eine Verringerung der Druckwellengeschwindigkeit, auch schon bei kleinen Mengen an Luft im System. Die daraus resultierende Dämpfung der Druckwelle hat einen vorteilhaften Effekt auf das Rohrleitungssystem. *Ewing* (1980) gab an, dass die Hauptwelle in Wellen kleinerer Länge gebrochen wird, woraus ein schnelleres Abklingen resultiert. Nach *Pearsall* (1965) wird die Dämpfung in Wasser-Luft-Gemischen durch eine interne Reflexion der Druckwelle an der luftblasenführenden Flüssigkeit erreicht.

Numerische Methode

Ein Berechnungsprogramm wurde entwickelt, um die Effekte vorhandener Luft in Rohrleitungssystemen auf Druckstoßvorgänge resultierend aus Stromausfällen zu untersuchen. Das Programm besteht aus zwei Teilprogrammen.

Das ***Teilprogramm 1*** wurde mit dem Hauptziel entwickelt, den Effekt von Lufttaschen auf Druckstoßvorgänge in Hochpunkten von Rohrleitungen während Stromausfall zu zeigen. Dies ist vielleicht der relevanteste Bemessungsfall für eine Pumpendruckleitung. Die Berechnungen dieser Studie basieren auf dem Charakteristikenverfahren und verwenden die Methode, die von Wylie und von Streeter (1978) dargestellt und von Wylie et al. (1993) ausgewertet wurde.

Teilprogramm 2 verwendet die homogenen Fließgesetze, um Druckstoßvorgänge von Strömungen mit Wasser-Luft-Gemischen zu berechnen. Die aufbauenden Gleichungen - Erhaltung der Gasmasse, der flüssigen Masse und das Mischungsgleichgewicht - ergeben mehrere Differentialgleichungen, die unter Zuhilfenahme des Charakteristikenverfahrens gelöst werden. Für das homogene Modell in diesem Programmteil werden die zwei Phasen oder Komponenten als Pseudofluid mit durchschnittlichen Eigenschaften behandelt.
Wie von *Martin et al.* (1976) und später in *Wiggert und Sundquist* (1979) beschrieben, wird angenommen, dass es keine relative Bewegung oder Reibung zwischen den Phasen gibt,

zudem wird den Berechnungen für die Mischung der Impulssatz zu Grunde gelegt. In der gleichen Weise wie die Kompressibilität des Gases sind die Kompressibilität der Flüssigkeit und die Rohrwandelastizität im Gleichungssystem berücksichtigt. Der Energieerhaltungssatz wird aufgrund der geringen Temperaturänderungen der Mischung während des Druckstoßvorgangs nicht verwendet.

In einer vorhergehenden Forschungsarbeit wurde vom Verfasser ein Berechnungsprogramm entwickelt, das sich auf eine aus Laborversuchen resultierende und validierte Gleichung bezieht. Zwei hydraulische Modelle wurden entworfen und konstruiert, um das Verhalten der stationären Lufttaschen an den Hochpunkten der Rohrleitung zu analysieren. Ebenso ist untersucht worden, wie sich die Luft in einer abwärtsgeneigten Rohrleitung am Wechselsprung am unteren Ende der Tasche verhält. Ein Vergleich der Laborversuche mit den Berechnungen zeigt eine gute Übereinstimmung. Zusätzlich wurde für diese Arbeit ein neues Teilprogram entwickelt, um diejenigen Hochpunkte in Pumpendruckleitungssystemen zu ermitteln, an denen Lufttaschen anzutreffen sind. Die Berechnungsergebnisse korrellieren gut mit den Aussagen, die andere Forscher für die gleiche Rohrleitungskonfiguration getroffen haben, wie sie in der Fallstudie analysiert wurde.

Die neuen Teile des Berechnungsprogrammes wurden entwickelt, um den Konstrukteuren von Rohrleitungssystemen einen numerischen Algorithmus zur Verfügung zu stellen. Das Programm kann verwendet werden, um Rohrleitungssysteme während des Entwurfs oder die Leistung schon vorhandener Rohrleitungen zu analysieren. Ebenso wurden Laborversuche durchgeführt, um das Verhalten der Lufteinschlüsse an den Hochpunkten von Rohrleitungen zu untersuchen und das Volumen der Luft dieser Lufttaschen zu bestimmen.

Laborversuche

Laborversuche wurden im Labor durchgeführt, um das Volumen der Luft, das zur Taschenbildung führt, zu messen sowie das Verhalten der großen Lufteinschlüsse an den Hochpunkten der Rohrleitungssysteme zu untersuchen. Der Versuchsaufbau bestand aus einer Pumpe mit einem maximalen Durchfluss von 2,5 l/s; einem Oberwassertank von 5,0 x 1,1 m Grundfläche und 1,0 m Höhe und einer Rohrleitung mit einem Innendurchmesser von 76,2 Millimeter aus Acryl, welche in einem metallischen Rahmen gehalten war. An den Oberwassertank schloss sich ein 6,8 m langer Rohrleitungsabschnitt an, der über eine flexible, 50 cm lange Verbindung mit einem weiteren, 6,4 m langen Abschnitt verbunden war. Die Neigung beider Rohrleitungsabschnitte war veränderlich. Der Versuchsaufbau ist in Abbildung 1 dargestellt.

Während den Versuchen wurden die Wassertiefen unter den Lufttaschen bei atmosphärischem Druck sowie unter Druck aufgezeichnet.

Die Versuchsergebnisse wurden mit den analytischen Resultaten der direct step method verglichen, die in der Analyse des stufenweise veränderten Flusses verwendet wurde. Die analytischen Berechnungen ergeben für Lufttaschen sehr ähnliche Formen wie diejenigen, die in den Laborversuchen ermittelt wurden. Die Fließprofile in der teilgefüllten Rohrleitung unter den Lufttaschen, die aus der dynamischen Gleichung des leicht ungleichförmigen Abflusses berechnet wurden, zeigen eine ausgezeichnete Übereinstimmung mit denen aus den Laborversuchen.

Die Werte aus den analytischen Berechnungen sind etwas niedriger als die in den Laborversuchen bestimmten Luftvolumina. Daher erhöhen die Ergebnisse aus den

Berechnungen mit der direct step method den Sicherheitsbeiwert beim Rohrleitungsentwurf. Nach Meinung des Autors und anderer Forschern führen kleinere Lufteinschlüsse an den Zwischenhoch- und Hochpunkten eines Rohrleitungssystems zu einer Erhöhung der Druckschwankungen aus einer plötzlichen oder routinemäßigen Pumpenabschaltung. Es könnte ernsthafte Folgen haben, wenn im Rohrleitungssystem vorhandene Luft während des Entwurfs des Rohrleitungssystems nicht beachtet wird.

Zu Untermauerung der Annahmen des analytischen Modells für die Simulation der Druckstoßvorgänge mit Lufttaschen und einem daran anschließenden Transport von Luft-Wasser-Gemischen wurde eine fotographische Studie durchgeführt. Es wurden schießender Abfluss sowie unter Druck stehende vollgefüllte Rohrleitungen getestet, als auch die Eigenschaften von Wechselsprüngen in den kreisförmigen Rohrleitungen bei atmosphärischem Druck und unter Druck. Die Beobachtungen zeigen, dass dem Luft-Wasser-Gemisch durch den Wechselsprung eine beträchtliche Luftmenge hinzugefügt wird.

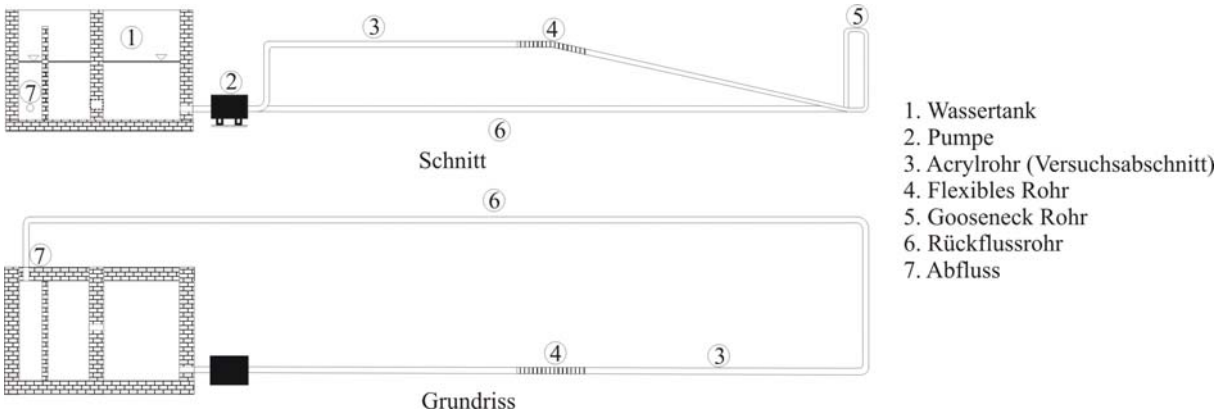

Abbildung 1 Schnitt und Grundriss des Versuchsaufbaus

Fallstudie

Die Fallstudie eines ausgeführten Pumpendruckleitungssystems ohne druckstoßdämpfende Bauteile wurde durchgeführt, um den möglichen Effekt der Lufttaschen mit und ohne den Transport eines Luft-Wasser-Gemischs hinter den Luftpolstern auf Druckstoßvorgänge zu zeigen. Die Randbedingung auf der einen Seite ist eine Pumpstation und auf der anderen Seite ein Hochbehälter. Nur die Druckstöße aus Pumpenabschaltung werden in dieser Analyse betrachtet. In der Pumpstation sind vier parallel geschaltete Kreiselpumpen installiert. Jede Pumpe hat eine maximale Kapazität von 0,625 m^3/s und kann damit Wasser in den 396,92 m über dem Pumpensumpfniveau gelegenen Hochbehälter fördern.

Der Leitungsabschnitt ist 2,289 m lang, und die Rohrleitung ist aus Stahl mit einem inneren Durchmesser von 1,22 m gefertigt. Die Skizze in Abbildung 2 zeigt einen schematischen Schnitt des untersuchten Rohrleitungssystems.

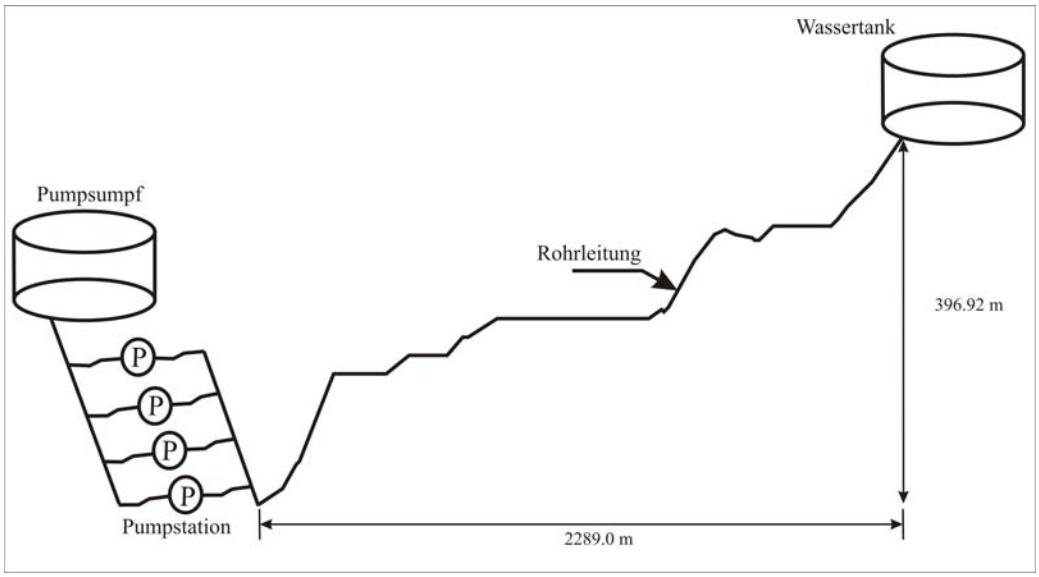

Abbildung 2 Schematisches Höhenprofil der Pumpendruckleitung

Ergebnisse des analytischen Modells

Im folgenden Abschnitt werden die Ergebnisse vorgestellt, die mit Hilfe des analytischen Modells erzielt wurden. Das Modell wurde für Druckstoßvorgänge in homogenen Zweiphasen- Wasser- Luftmischungen entwickelt.

Um den Effekt der Lufttaschen auf hydraulische Druckstoßvorgänge mit Hilfe des analytischen Modells zu untersuchen, wurde eine Methode entwickelt, die die Lage der Lufttaschen in Pumpendruckleitungen erkennt und deren Volumen quantifiziert. Verwendet wird eine lineare Gleichung, die von Gonzalez und Pozos (2000) für diese Fragestellung empfohlen wird. Diese Gleichung sagt aus, dass sich bei einer Pumpstation mit 3 Pumpen, höchstens vier Punkte ergeben, an denen sich die Luft ansammeln kann. Dieses Szenario stellte sich als das am meisten kritische für die Analyse heraus.

Die resultierende Einhüllende der maximalen und minimalen Druckhöhe wird mit dem Volumen der Lufttaschen in gleicher Höhe verglichen. In diesem Fall jedoch tritt eine abwärtsgerichtete Strömung des Wasser-Luft Gemisches ein. Darüber hinaus werden die Effekte der Wasser-Luft-Mischung auf die Umhüllende des maximalen und minimalen Gesamtdrucks untersucht. Der gravierende Unterschied bei den Ergebnisauswertungen der Versuche zeigt sich bei einer möglichen Verminderung während der Ausbreitung der Druckwelle entlang des Rohrleitungsprofils. Die Druckhöhe wird hauptsächlich durch die Wasser-Luft-Mischung und die Lufttaschen absorbiert.

Abbildung 3 zeigt, dass das größte Lufttaschenvolumen zusammen mit einer abwärts gerichteten Strömung der Wasser-Luft-Mischung eine Reduktion der maximalen und minimalen Druckhöhe in Pumpendruckleitungen verursacht. Hervorzuheben ist, dass der niedrigste und höchste Wert der minimalen und maximalen Umhüllenden, abhängig von dem Pumpendurchfluss, nahezu gleich ist. Von geringerer Bedeutung ist dagegen ein Abfluss ohne abwärts gerichtetes Wasser-Luft-Gemisch und die Annahme, dass eine Luftaufnahme ausgeschlossen wird.

Der dämpfende Effekt, hervorgerufen durch den Luftblasengehalt und das daraus resultierende große Luftvolumen, auf die maximalen Druckhöhe, ist von größerer Bedeutung als das Vorkommen des Wasser-Luft-Gemisches. Eine untergeordnete Rolle spielt der Vergleich der zwei Kurven ohne Beachtung des abwärts gerichteten Luft-Wasser-Gemisches.

Abbildung 4 zeigt das Auftreten eines Wasser-Luft-Gemisches unterstrom von den mittleren Lufttaschen, mit den Volumen (V_1 = 0.761 m^3, V_2 = 1.235 m^3, V_3 = 1.747 m^3, V_4 =0.856 m^3) und eine damit verbundene deutliche Reduktion der maximalen und minimalen Profile der Druckhöhe. Die Reflexion der instationären Druckwellen verschwindet fast vollständig durch den Lufttransport, obwohl eine Reflexion oberhalb der Hochpunkte, an denen sich die Lufttaschen befinden, und in Richtung des unterstromigen Randes sichtbar wird. Dieser Effekt scheint jedoch das System nicht zu zerstören.

Die Ergebnisse, die in Abbildung 5 dargestellt sind, zeigen, dass die kritischste Situation bei den vier kleinsten Lufttaschen auftritt (V = 0.145 m^3, 0.448 m^3, 1.038 m^3, 0.412 m^3). Obwohl direkt unterstrom von jeder Lufttasche ein Netto-Lufttransport auftritt, ist dieser nicht groß genug, um die Energie der instationären Welle maßgeblich zu absorbieren. Ebenso ist die maximale Druckhöhe am Pumpenauslass größer als ohne die Luftakkumulation in der Pipeline. Eine geringe Reflexion der maximalen Druckhöhe wird durch die Lufttaschen am unterstromigen Ende verursacht.

Zusammenfassend kann die Aussage getroffen werden, dass mittlere und große Lufttaschen im Zusammenspiel mit einem Netto-Lufttransport in unterstromige Richtung einen wichtigen Effekt verursachen, indem sie den instationären Druck reduzieren. Der dämpfende Effekt macht sich in den maximalen Druckhöhen stärker bemerkbar. Die Simulation, die kleine Lufttaschen und ein Wasser-Luft-Gemisch enthält, zeigt eine bedeutende Zunahme der Druckhöhe in Richtung der oberstromigen und unterstromigen Ränder des Systems.

Die erzeugten Druckstöße zeigen, dass die minimalen Druckhöhen nach dem Abschalten von drei Pumpen erzeugt wurden. Für den Fall von vier Lufttaschen an den Hochpunkten und einem Netto-Lufttransport nach Unterstrom wurden die Druckstöße niemals geringer als bei den Berechnungen ohne Luft und ohne Netto-Lufttransport. Ebenso zeigen die Ergebnisse der maximalen und minimalen Gesamtdrücke für ein bis vier Lufttaschen und entsprechenden Netto-Lufttransport an den Hochpunkten, dass die Form der Umhüllenden ungefähr gleich bleibt und dass weder Leerraumanteil noch Volumen der Lufttaschen die Prozesse bestimmen.

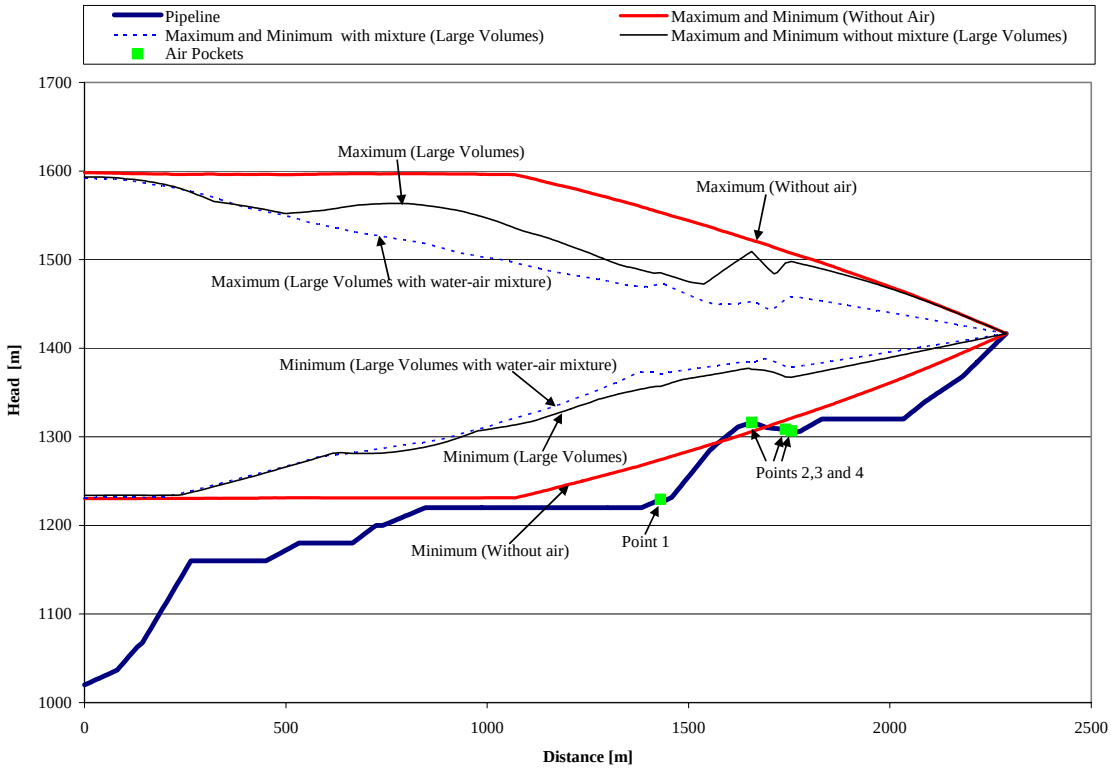

Abbildung 3: Maximale und minimale Druckhöhe bei 4 großen Lufttaschen an den Punkten 1, 2, 3 und 4 mit und ohne Wasser-Luft Mischung flussabwärts

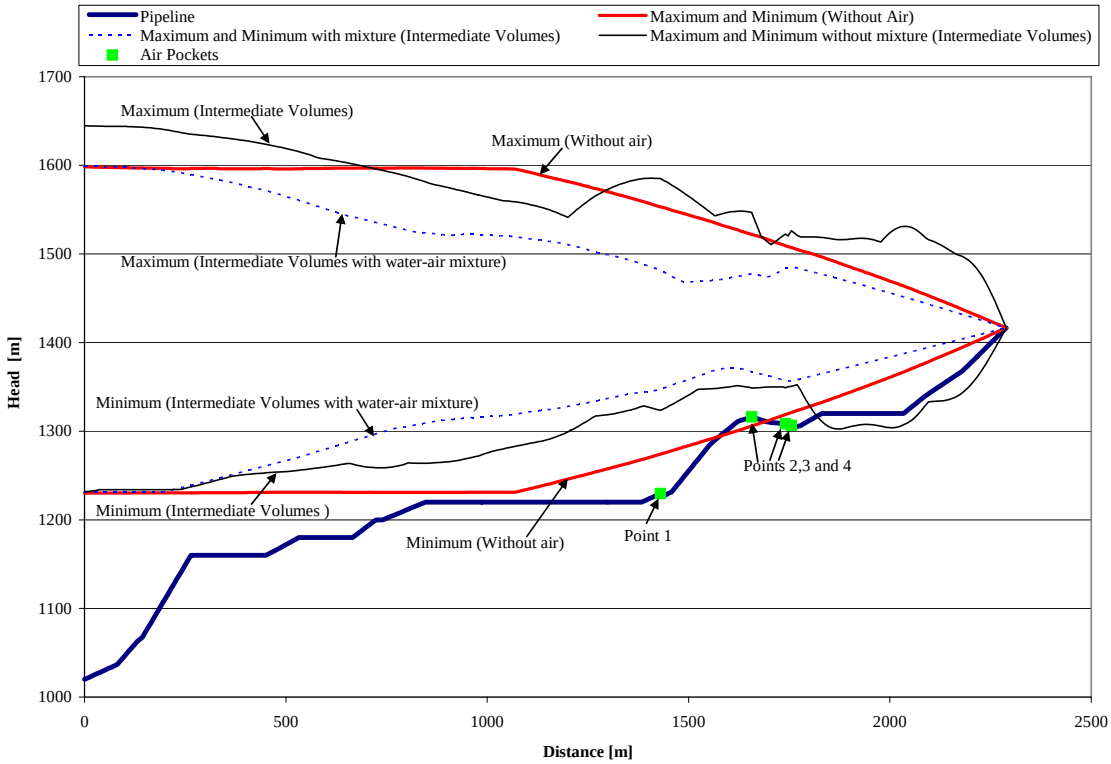

Abbildung 4: Maximale und minimale Druckhöhe bei 4 mittleren Lufttaschen an den Punkten 1, 2, 3 und 4 mit und ohne Wasser-Luft Mischung flussabwärts

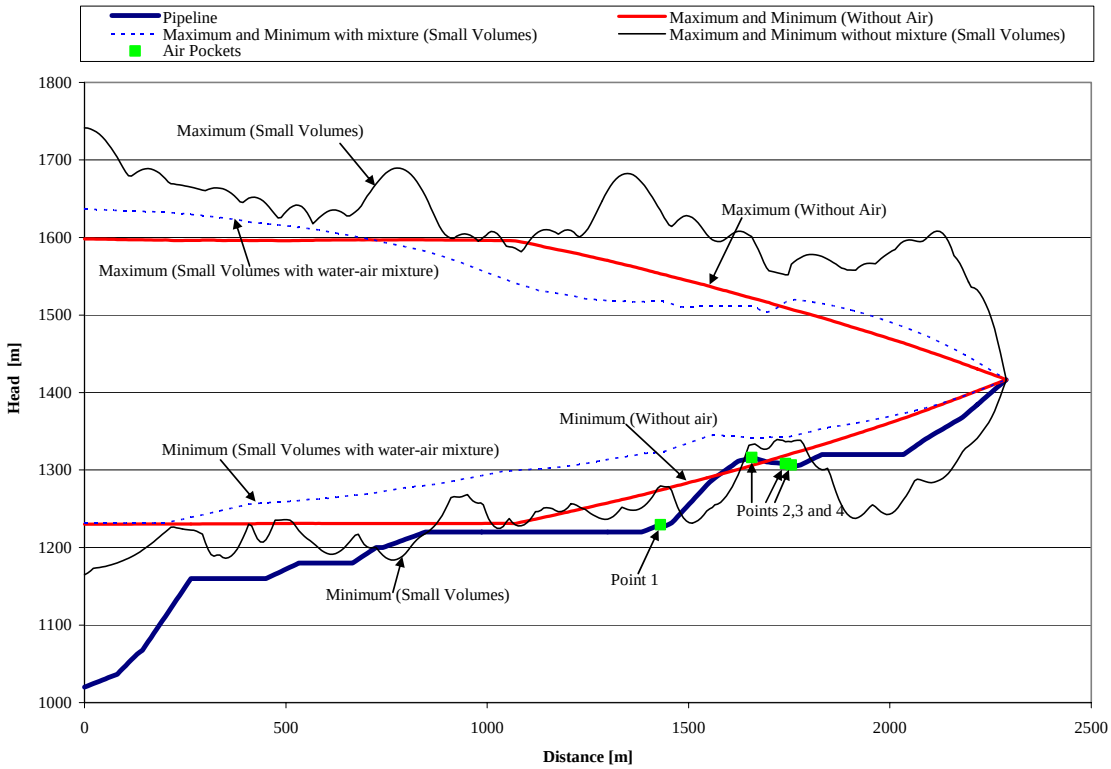

Abbildung 5: Maximale und minimale Druckhöhe bei 4 kleinen Lufttaschen an den Punkten 1, 2, 3 und 4 mit und ohne Wasser-Luft Mischung flussabwärts

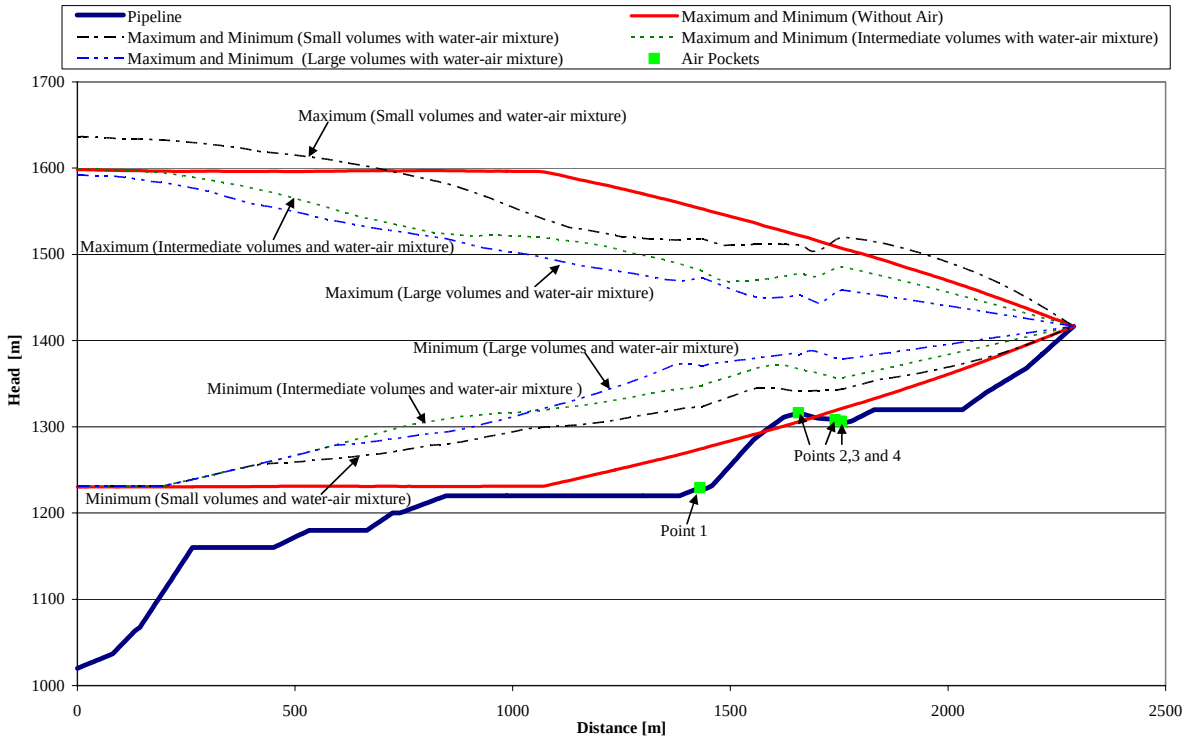

Abbildung 6: Vergleich der maximalen und minimalen Druckhöhe bei den unterschiedlichen Lufteinschlussvolumina an den Punkten 1, 2, 3 und 4 mit und ohne eine Wasser-Luft Mischung flussabwärts

Empfehlungen

Luftansammlungen in den Rohrleitungsystemen sind sowohl unbeabsichtigt als auch unvermeidbar und können nicht immer vollständig beseitigt werden. Durch Erkentnisse über den Lufteintrag kann der Ingenieur die Auftretenshäufigkeit reduzieren. Viele Ingenieure planen fälschlicher Weise mit der Annahme, dass der Rohrleitungsquerschnitt immer vollständig und nie teilweise benetzt durchströmt wird. Dies kann zu kritischen Problemen führen, weil die vorhandene eingeschlossene Luft für die Berechnungen nicht in Betracht gezogen wird. Folglich sollte ein Planer von Rohrleitungen in der Lage sein, „worstcase“-Szenarien vorherzusagen und im Falle einer wahrscheinlich negativen Auswirkung das Profil der Rohrleitung entsprechend anzupassen oder auch Betriebseinrichtungen einzuplanen, um die negativen Effekte zu verringern. Es ist bekannt, dass schon einfachste Rohrleitungssysteme unter der eingeschlossenen Luft leiden. Folglich müssen bei allen Systemen, insbesondere die mit Steigungsänderungen, alle Fließzustände im Detail analysiert werden, ob sich in möglichen Höchst- und Zwischenhochpunkten Luft angesammelt haben könnte. Zusätzlich basiert die hydraulisch instationäre Berechnung normalerweise auf der Annahme, dass sich keine Luft im Rohrleitungssystem ansammelt. Dies könnte das Versagen bzw. den Bruch von Leitungen erklären, welche mit Standardberechnungen nicht vorhergesagt werden konnten. Ebenso wenn der Verlauf einer vorhandenen Rohrleitung beispielsweise infolge eines Kanals oder Gebäudeneubaus verändert wird, muss eine komplett neue Berechnung durchgeführt werden.

Hochpunkte sind auf mögliche Luftansammlungen zu untersuchen. Besteht die Wahrscheinlichkeit, dass diese auftreten, muss eine Simulation der Druckstöße erfolgen, um negative Effekte zu verringern. Es wird empfohlen, Berechnungen mit eingeschlossener Luft routinemäßig anzuwenden, um glaubhaft in der Lage zu sein, betriebliche Szenarien darzustellen, welche Druckstöße zur Folge haben. Konstrukteure von Rohrleitungen könnten bemängeln, dass numerische und experimentelle Untersuchungen extrem zeitraubend und teuer sind. Jedoch können die Reparaturkosten der Rohrleitungen und Prozesse von Personen und Geschäftseigentümern bei einem Rohrleitungsausfall gegen den Betreiber dieser Systeme um ein Vielfaches zeitaufwendiger und teurer sein.

Zusammenfassende Anmerkungen

Der Vergleich der maximalen und minimalen Druckhöhenumhüllenden mit und ohne Luftwassergemisch hebt beide Effekte, Lufttaschen und Luftblasengehalt, bei Druckschwankungen hervor. Anschließend hat die Fallstudie gezeigt, dass große und mittelgroße Lufttaschen einen polsternden Effekt haben und die maximale Druckhöhe beim Stromausfall im Pumpbetrieb herabsetzen. Zusätzlich scheint es, dass kleine Lufttaschen Druckstöße beträchtlich erhöhen können.

Das Ziel dieser Arbeit war es, mögliche schädliche und vorteilhafte Effekte der eingeschlossenen Luft auf Druckstöße aufzuzeigen, wie beispielsweise bei Luftgasgemischen unterhalb von Lufttaschen. Eine Reihe numerischer Simulationen wurde durchgeführt, um eine Anleitung zur Vermeidung dieser Probleme zu geben oder zumindest eine Verringerung der Gefahr von Rohrleitungsbeschädigung.

Bei der Analyse von Druckstoßvorgängen muss berücksichtigt werden, dass alle Rohrleitungssysteme in Betrieb und Konfiguration unterschiedlich sind. Es ist nicht möglich, ein einfaches, definitives Ergebnis in Bezug auf die kritischen Volumina der Lufteinschlüsse und ihrer Position zu erhalten. Jedoch können die Ergebnisse dazu dienen, die Konstrukteure

von Rohrleitungssystemen beim genaueren Ermitteln von kritischen Situationen bei verschiedenen Rohrleitungskonfigurationen zu unterstützen. Resultierend aus dem Fortschritt der numerischen Methoden gibt es eine Tendenz, Rohrleitungssysteme nur durch numerische Simulationen zu entwerfen. Jedoch werden zusätzlich Laborversuche empfohlen, um eine ausführliche und genaue Analyse des Effektes der Lufttaschen mit und ohne Luft-Wasser-Gemisch auf Druckstöße zu ermitteln.

1 Air Problems in Pipeline Systems

1.1 Principal problems

The presence of air in pipelines can severally affect the water carrying capacity of the line. In gravity systems, stationary air pockets can lead to reducing the effective cross section for the passage of water. In pumping systems the presence of air can be reflected in increased energy consumption and flow reduction. These problems are still occurring up till now, even in pipeline systems constructed recently, due to a lack of design criteria that make gravity pipelines, as well as pumping systems, work more efficiently when air enters into the line.
Water pipelines are usually designed assuming no air in the water and sometimes pipeline designers do not take into account the causes of air entrainment and the potential problems that can be raised by entrained air.

Most of the times, pipelines contain air in the form of pockets which can build up at high points along the profile. The phenomenon occurs because air is lighter than water and therefore it will migrate to the high points.

Although free air is beneficial for cavitation prevention, for oxygenation purposes or damping effects in hydraulic transients; it can be also detrimental, for example, there are ranges of air volumes that can produce an undesirable pressure rise during the pumps start-up. The effect of air in both situations depends on the location and amount of the undissolved air as well as the configuration of the pipeline.

Landon (1997) [44] wrote: “It has been said that if a pipeline is properly deaerated, you cannot guarantee against a line break. However, if you do not properly deaerate a pipeline, you should be prepared for one”.

1.2 Air Bubbles Classification Used for the Research

Before explaining the causes of air entrainment and problems caused by air entrainment, the definitions of air bubble and air pocket which are used throughout the thesis are presented. Air can be found in water pipelines mainly as large or small moving bubbles and as large stationary pockets.

Wisner et al. (1975) [87] defined bubbles as small droplets of air with ellipsoidal shape, entrapped in water by turbulent action such as a hydraulic jump or the impact of a falling nappe of water. These bubbles have a size varying from 1 mm to 5 mm. *Kent* (1952) [40]

reported size of bubbles of 6.35 mm and smaller.

For the purpose of this work, the air cavities formed by the coalescence of air bubbles, which have a longitudinal length less than or equal to the diameter of the pipe will also be called bubbles. An air pocket will be defined as an air cavity in pipelines, when its longitudinal length is greater than the diameter of the pipe. The air pockets may be formed by the coalescence of air bubbles, because of entrapment of a large amount of air during the filling of the line, due to air leak in through mechanical equipment during vacuum pressure, or by air release when the pressure drops below the saturation vapor pressure or by other causes, that will be described in detail.

1.3 Causes of Air Entrainment in Pipelines

Air in pipelines cannot be always completely eliminated but understanding the ways how it enters a pipe helps the engineers to minimize its occurrence. Air in the line comes from different sources including the following:

A pipeline is full of air during its filling. If the air is not completely released through air valves, vents and standpipes, air may remain at high points throughout the system in the form of air pockets.

Air enters also through mechanical equipment, for example:

- Pumps introduce air by the vortex action of the suction in quantities of 5% to 10% of flow. Hence, air has to be released before the check valve opens.

- When vacuum pressure occurs in the pipeline, air can leak in through packing at joints and valves.

Water contains over 2% air by volume and air solubility in water is proportional to the pressure. Dissolved air may form a free gas phase at points in the pipeline where pressure drops or the temperature rises.

Pipelines are complex systems formed by hydraulic structures, such as dropshafts, siphons, tanks, etc. Air entrainment is commonly found in these structures and beyond their inlets the closed conduit sometimes flows partly full, and if the normal depth is less than the critical depth a hydraulic jump will occur. If the air cannot be removed by the flowing water or mechanical means such as air release valves, it may remain at some high points of the line.

The break pressure tank is an important source of air entrainment because of the vortex action generated in its intake. When the water level in the structure is very low, the core of the vortex can be deep enough to introduce considerable quantities of air into the pipe.

1.4 Problems Caused by Air Entrained

Air entrained in pipelines may lead to a variety of problems. For example, air accumulated at high points of the pipeline can reduce the effective pipe cross section, which results in an increase of head losses. Air enhances corrosion by making more oxygen available in ferrous pipes. Incorrect readings on measurement devices are produced by free air. Vibrations are caused by the transition from a partly full pipe to a full pipe because of the presence of air pockets. Important quantities of accumulated air cause blowbacks that drive to vibrations and structural damage. Air increases the energy consumption of pump equipment. Air may build up in important quantities that the air pockets can cause the partial or complete blockage of flowing water, reducing the capacity of the pumping systems as well as the gravity pipeline systems.

1.4.1 Increase of Head Losses caused by Entrained Air

Air entrained from different causes is conveyed through the pipeline by the inertia of flowing water and may accumulate at high points, forming an air pocket that can become larger if more air pockets or air bubbles join it. When a pocket reaches a downward slope the water pushes it down. If the air pocket is large enough the water flow may not overcome the pocket buoyancy force, then the pocket can remain stationary in the pipe and the friction force will go to zero. The forces acting on an air pocket are shown in Figure 1.1.

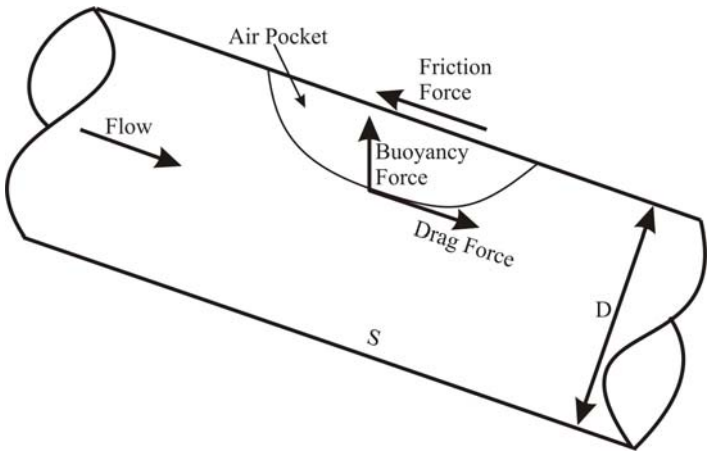

D pipe diameter [m]
S pipe slope [-]

Figure 1.1: Forces acting on an air pocket in a pipe flowing full

Air binding is a concept introduced by *Richards* (1957) [62] and refers to the trapping of air that reduces the cross section of the pipe in a manner that prevents the pipe from being entirely filled up. Thereby the pipe reverts to open channel flow beneath the air pocket and the energy gradient is roughly parallel to the pipe slope.

Air binding can be a source of head loss that can reduce the system capacity**.** Applying the energy equation between the top and the bottom of each air pocket, it will show that the loss of head is roughly equal to the vertical component of the length of the pocket, see Figures 1.2 and 1.3.

Richards (1962) [63] commented that is important to recognize that the major head loss is caused by the change in the gradient slope from the normal full pipe energy gradient to one which is roughly parallel to the pipe slope. The reduction of pipe cross section by the air is not the primary or even an important source of loss.

The pipelines that have downward slope sections in the direction of flow can be subjected to air accumulation. In pumping systems the air accumulation results in the rising energy consumption and flow reduction if air pockets located at high points of the pipeline cannot be carried downstream. It may occur that flow entirely stops because the cumulative head losses produced by the air pockets can be higher than the pump head capacity. Air buildup in gravity pipelines results in capacity reduction. In some gravity pipeline sections entrapped air has led to the overflow of vents. Since the available static head is not high enough to overcome the water columns separated by air standing at the high points. *Richards* (1962) [63]. Figures 1.2 and 1.3 show the effect of air accumulation.

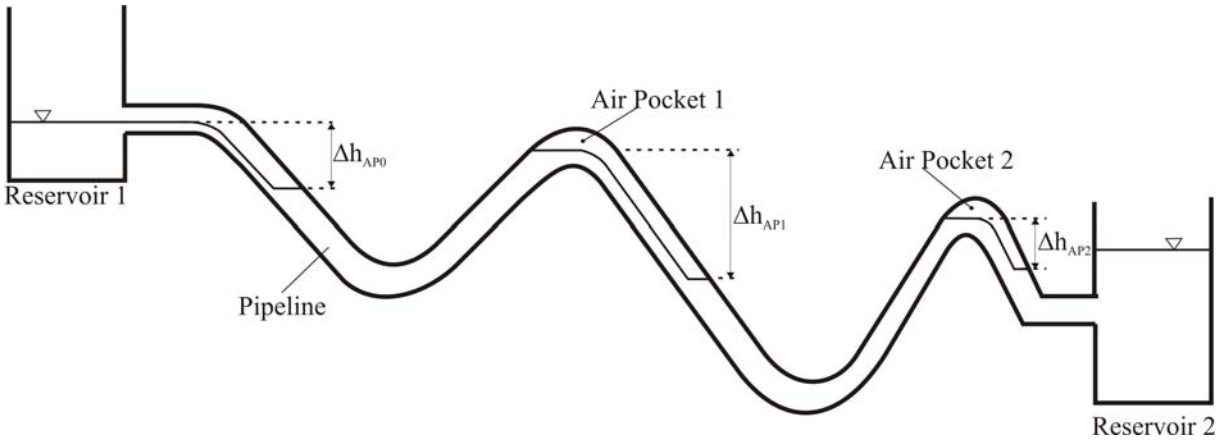

Δh_{APi} head loss caused by the presence of the air pocket [m]

Figure 1.2: Air pockets in a gravity pipeline system

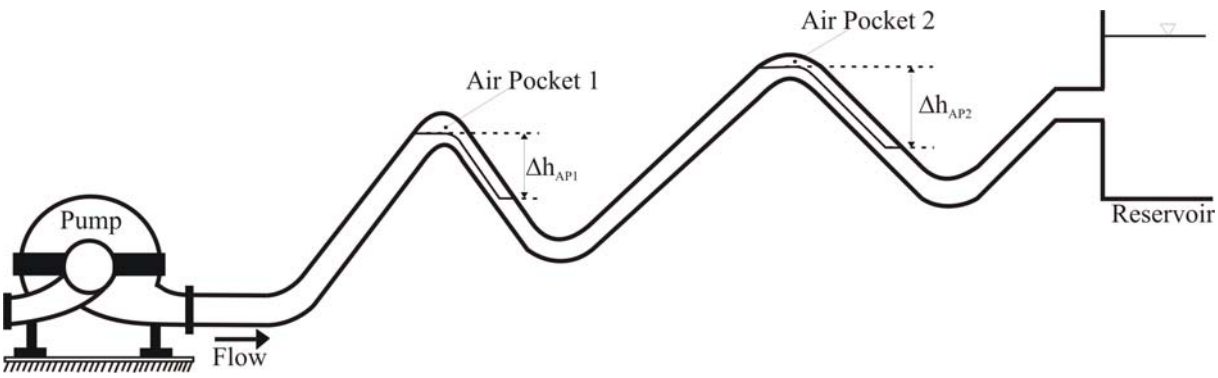

Δh_{APi} head loss caused by the presence of the air pocket [m]

Figure 1.3: Air pockets in a pumping pipeline system

The problems caused by the reduction of the pipe cross section in consequence of entrapped air may occur more oftentimes than records show. If the head losses are just a little less severe and do not cause spillage in vents or the complete stoppage of flow in pumping systems, then these problems can go unnoticed.

As air accumulates at high points during pipeline filling or any other causes of air entrainment, more head is lost. Therefore, the total head losses as a result of air accumulation can be evaluated as the sum of the individual head loss of each air pocket.

1.4.2 Blowbacks

The entrained air may accumulate at high points of the pipeline and form air pockets that can become relatively large. If the pipe slope is steep downward from the high point, the air pocket tends to stabilize along the top of the pipe. At the end of the air pockets a hydraulic jump usually occurs. The formation of a hydraulic jump at the end of the air pockets in water supply lines is a way by which air can be removed and carried away by the flowing water. Beyond the hydraulic jump the air entrained as bubbles can form air pockets and if these are large enough the drag force of water cannot overcome the buoyancy force. Then, the bubble or the pocket remains in the pipe, getting larger as more bubbles arrive to join them. The air pockets further increase their size and reduce their velocity as a result of the buoyant force increment. The air pocket can blow back with tremendous force through the hydraulic jump, taking water with it, and can partly or completely destroy hydraulic structures, such as break pressure tanks and surge tanks.

Sailer (1955) [66] investigated prototype cases in the San Diego aqueduct, which crosses several broad valleys in long siphons. The longest siphon has a length of 20.12 km. On these long structures a problem arose from the hydraulic jump at the inlet leg. Air entrained and

accumulated into large air pockets downstream from the jump. These air pockets blew back with enormous force, taking water with them, and destroying the reinforced concrete platform on the inlet structure of the siphon on the Belle Fourche Project in South Dakota, U.S.A. *Sailer* (1955) [66] and *Falvey* (1980) [20] recommended that the possibility of undesirable blowbacks must be always investigated in hydraulic models.

1.4.3 Water Hammer Induced by Air Evacuation

The increase in velocity beneath the air pocket may push away part or the entire pocket downstream. The abrupt and rapid change in the fluid velocity when the pocket is removed and stopped by another high point could lead to a high pressure surge (water hammer). Considerable damage to accessories, joins, or even the rupture of the line can occur. This phenomenon is the so called water hammer induced by air evacuation.

1.4.4 Reduction of the Pumping System Efficiency because of Entrained Air

Thomas (2003) [77] presented a useful comparison between the efficiency of the pipeline systems and the cost for removing the entrained air out of the water pipelines. It is estimated that 75% of the cost of operating a pipeline is the cost of pumping. Investigations on a variety of water pipelines throughout the world have revealed that entrapped air can reduce their efficiency by as much as 30%. Most pipeline systems are commonly operated with air contents that diminish system flow efficiencies by 15 to 20%. Pockets of compressed air present enormous obstacles to any efforts to pump fluids. Entrapped air increases head pressure by 20% and will force pumps to perform 20% harder, and thus demand 20% more electrical energy to overcome the restrictions.

In 1999 a large industrial city in South Canada spent 1,600,000 dollars on electricity to power the water pumps. Assuming that the machinery has to work 20% harder to push away the air blockages throughout their grid, the additional electrical demands cost $320,000. Almost a third of a million dollars, spent in a year, to overcome a poorly vented water pipeline system.

1.5 <u>Mechanisms of Air Removal</u>

The causes by which air enters pipelines have been described in the previous section, as well as the variety of problems that can take place in water systems because of entrapped air. Within this section the two methods to accomplish the removal of air are presented: (1) Hydraulic means, using the inertial flowing water to remove the air from pipe; and (2) Mechanical means as air valves, open vents and other devices to release the air.

1.5.1 Hydraulic Means

Up to now, there are no well accepted analytical solutions for the transport of air bubbles and air pockets. Therefore, the design of water pipelines is done using experimental investigations. The disadvantage is that recommendations of previous authors vary widely and for some pipelines design may not be adequate. The possible causes for this disagreement are that conditions adopted by different researchers are not general and the investigations were carried out in a diversity of small diameters compared to prototypes.

There is a diversity of clearing velocities found by various investigators. If one of these values is used for a specific design, the water velocity may not clear the air from prototype giving rise to the variety of problems described before.

Wisner et. al. (1975) [87] described the following terms which are used in this work:

1) **Sweeping velocity** to denote the minimum flow velocity to transport bodily an air pocket or air bubble.
2) **Generation** refers to the turbulent action at the downstream end of the pocket resembling a hydraulic jump which causes air bubbles to be ripped off.
3) **Entrainment** is used to describe the movement of the generated air bubbles to downstream.
4) **Clearing velocity** is the minimum velocity to remove an air pocket from the line.

Experiments have shown generation may not mean entrainment. Entrainment depends on the hydraulic conditions downstream of the air pocket.

Investigators have adopted different approaches to define a clearing velocity. Some used stationary pockets in flowing water as criterion, while others used the rising velocity of pockets in still water as an index. The recommendations of previous investigators are reviewed consecutively:

Kalinske and Robertson (1943) [38] studied the air entrainment due to a hydraulic jump in circular pipes. An experimental apparatus made of acrylic pipes with an inside diameter of 149.4 mm and about 10.7 m length could be set at downward slopes from 0° to 16.7°. The results are presented in two experimental graphs. Figure 1.4 represents the condition in which all the air entrained by the jump is carried along and discharged out of the line. Considering the rate of air entrainment by the hydraulic jump, it should depend on the water discharge and the

turbulent action of the jump. The intensive agitation of the hydraulic jump depends on the Froude number upstream of the jump, F_1. The values of air entrainment by the hydraulic jump can be estimated from the empirical relationship

$$\frac{Q_a}{Q_w} = 0.0066(F_1 - 1)^{1.4} \quad [-] \qquad (1.1)$$

where

Q_a air flow rate [m^3/s]
Q_w water flow rate [m^3/s]
F_1 Froude number upstream of the hydraulic jump [-]

The authors observed that the air pumped into the flowing water by the jump forms a large pocket beyond the jump which extends to the point where all the air leaves the pipeline.

Kalinske and Robertson (1943) [38] provided a second graph presented in Figure 1.5 that shows the Froude numbers below which the flowing water carries only a part of the air entrained by the hydraulic jump. For any value of y_1/D, where y_1 is the initial depth, there is a value of the Froude number below which only a part of the air entrained by the jump can be carried out of the line.

The authors concluded that above a certain critical condition the rate of air removal from an air pocket in a pipeline depends on the ability of the hydraulic jump to entrain air. The critical condition, for any pipe slope and for any relative flow depth in the air pocket, depends on the value of the Froude number of the flow ahead of the jump. Below this critical value of F_1 the flow beyond the jump will not be able to carry the air entrained by the jump and thus the air removal will not be a function of the jump characteristics but rather of the hydraulic features of the flow beyond the jump.

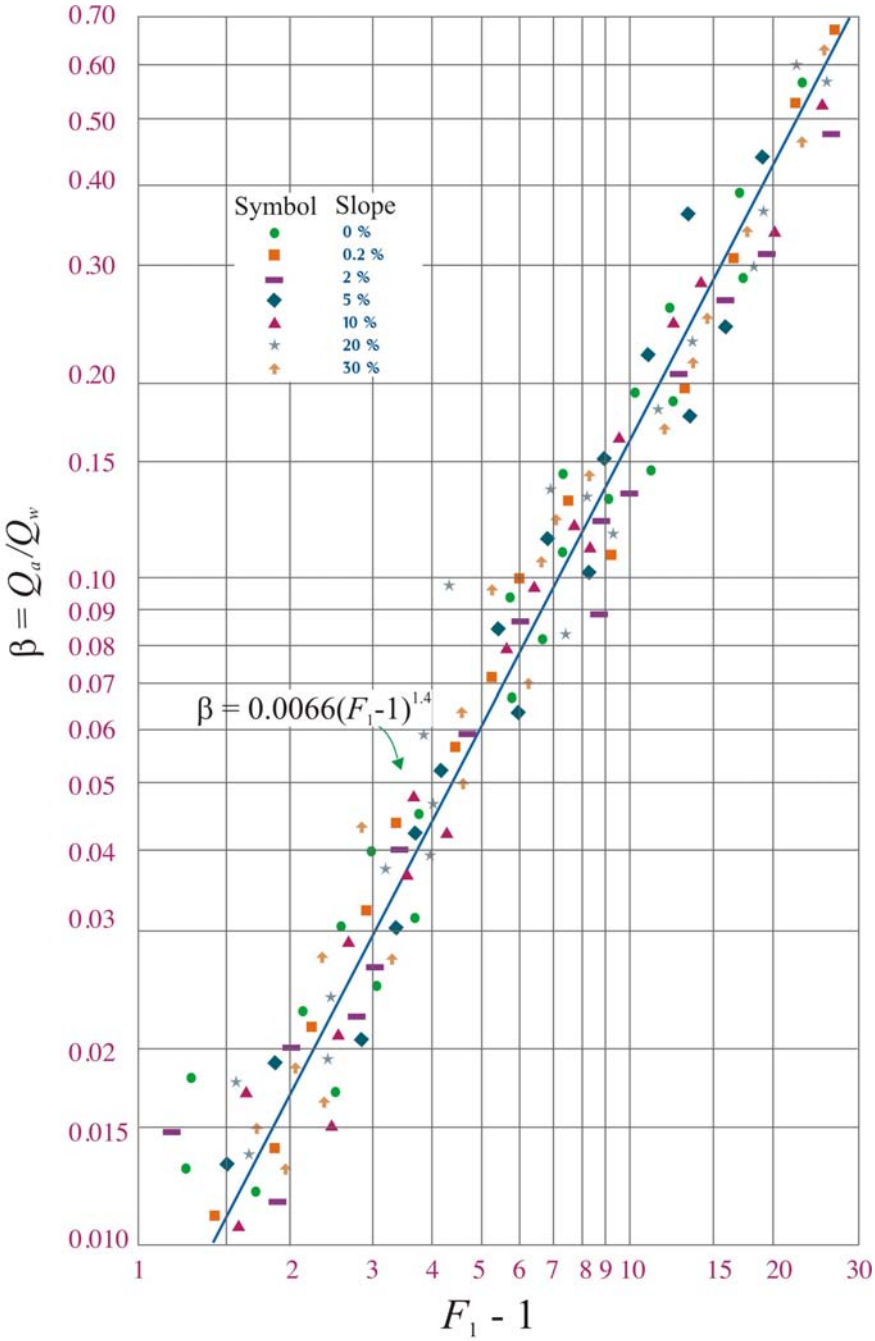

β ratio of air flow rate to water flow rate [-]
F_1 Froude number upstream of the hydraulic jump [-]
Q_a air flow rate [m^3/s]
Q_w water flow rate [m^3/s]

Figure 1.4: Correlation of data on rate of air entrained by hydraulic jump (after Kalinske and Robertson, 1943)

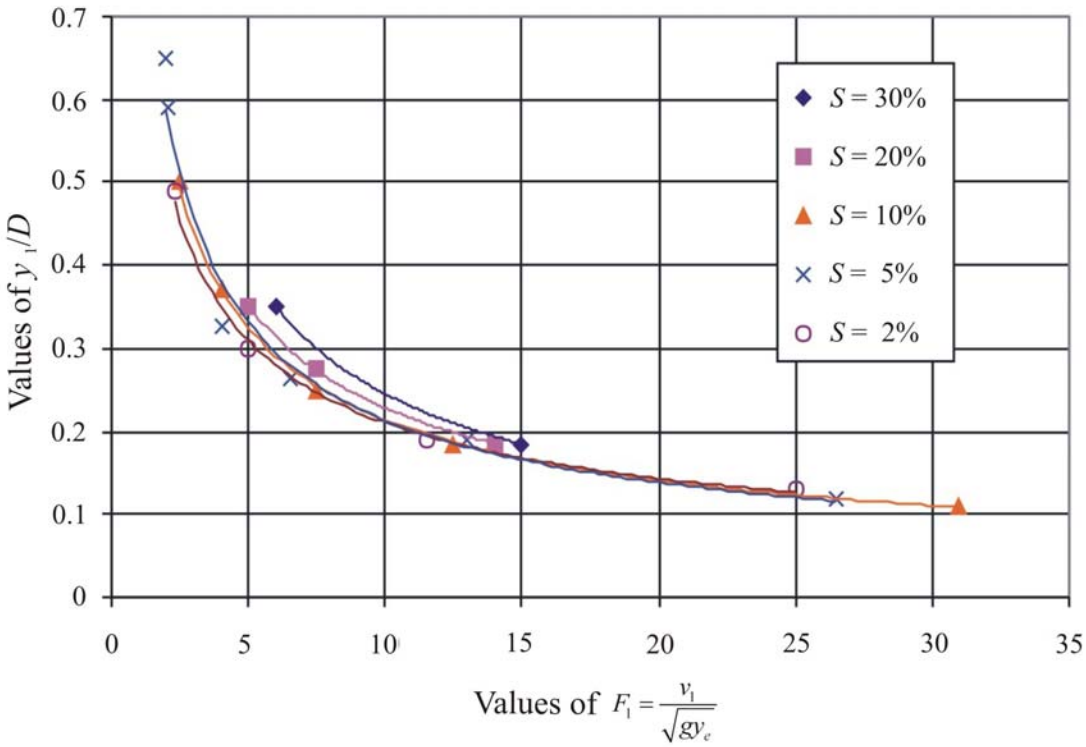

y_1 initial depth [m]
D pipe diameter [m]
F_1 Froude number upstream of the hydraulic jump [-]
v_1 water velocity upstream of the hydraulic jump [m/s]
g acceleration due to gravity [m/s^2]
y_e effective depth [m]
S pipe slope [-]

Figure 1.5: Experimental values of critical Froude number (after Kalinske and Robertson, 1943)

Gandenberger (1957) [26] studied the statistical information related with breaks in certain sections of 900 mm diameter cast iron mains. These most frequently occurred near high points and during periods when the velocity was lower than 0.3 m/s, and suggested that these failures can be attributed to pressure fluctuations caused by the presence of air. In contrast, in other mains with less favorable profiles but constantly higher flow rates, no problems resulting from air were encountered over a period of 50 years. To recognize the effect of accumulated air, Gandenberger accomplished hydraulic model investigations to study the movement of air in pipelines. The experiments on the movement of air bubbles and pockets were made in glass tubes with diameters of 10.5 mm, 26 mm, 45 mm, and 100 mm steel pipe with slopes varying from 0° to 90° and water flowing in upward and downward slopes. The results are presented in Figure 1.6 that gives the minimum mean water velocity required to clear a given volume of

air from a high point in the profile of a pipe of unit diameter for a certain downward slope. The dimensionless parameter to characterise the size of air bubbles and pockets, *BS* is defined for any pipe diameter, *D*, as $BS = 4V/(\pi D^3)$, where *V* is the volume of the air bubble or pocket. The graph covers the range from *BS* = 0.02 to *BS* > 1. For any given pipe diameter the clearing velocity increases with bubble size up to *BS* = 1 and thereafter is constant. Gandenberger concluded that the graph would be valid for pipe sizes greater than about 0.1 m and for air pockets with *BS* > 1. Later he corroborated his prior conclusion with satisfactory agreement, in a posterior test carried out in a pipe with a diameter of 500 mm, having a length of 455 m and a slope of 5°.

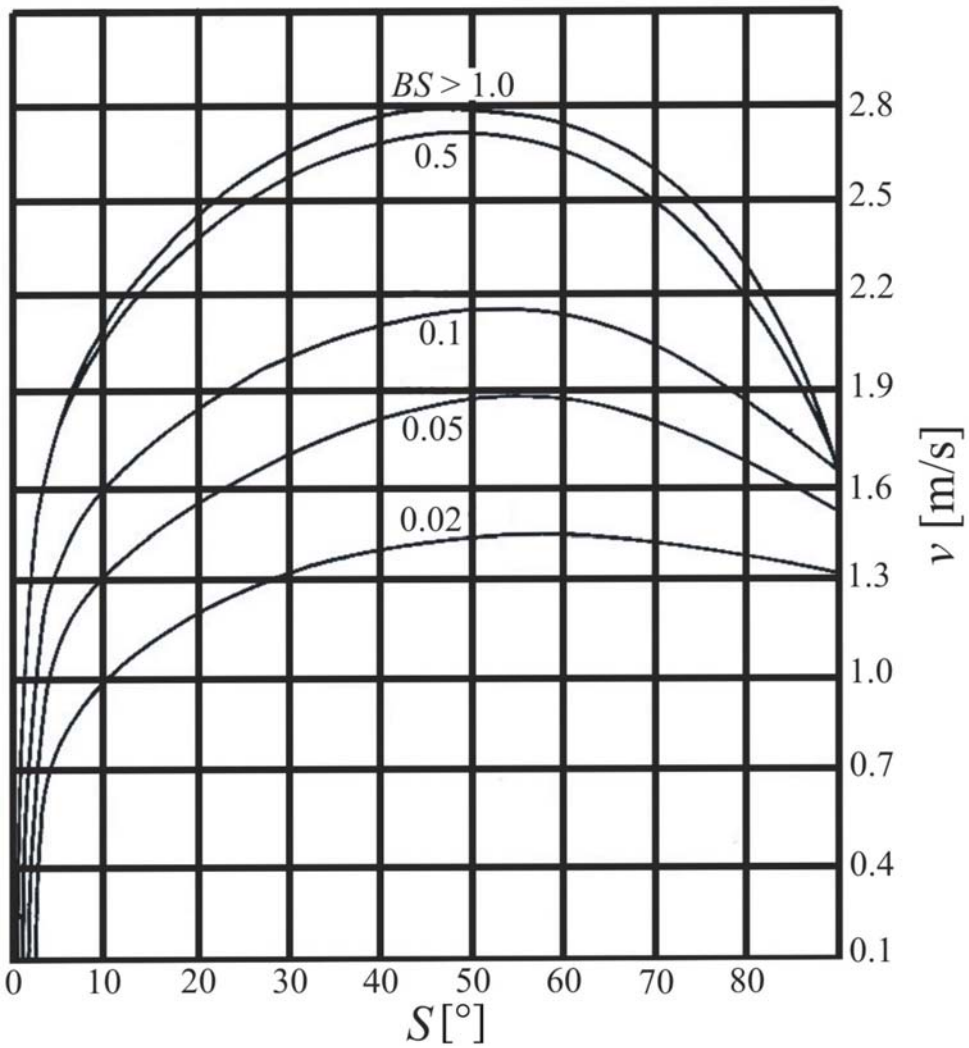

S pipe slope [-]
v water velocity in the pipe [m/s]
$BS = 4V/(\pi D^3)$ dimensionless parameter to characterise the size of air bubbles [-]

Figure 1.6: Movement of air bubbles of different sizes in downward slopes (after Gandenberger, 1957)

Kent (1952) [40] found that the rate of removing air by the hydraulic jump at the end of the air pocket is related to the drag force of water acting on the pocket. An effective rate of air removal exists when the mean velocity v of the water is equal to or greater than a certain minimum value, designated as v_{min}. Therefore, equating the drag force exerted by the flowing water and the buoyant force of an air pocket, the velocity v is equaled to v_{min}. Kent developed a semi-empirical relationship for the minimum velocity v_{min}, which is a function of S and D.

$$v_{\min} = C_0^{1/2}\sqrt{gDS} \quad \text{[m/s]} \qquad (1.2)$$

v_{min} minimum mean water velocity required to clear a given volume of air [m/s]
g acceleration due to gravity [m/s^2]
D pipe diameter [m]
S pipe slope [-]

$C_0^{1/2}$ is a function of the air pocket shape and from the experimental data was found that its values become constant for lengths of air pockets greater than 1.5D. Kent's formula is often used in practice because of its simplicity. However, an examination of the formula shows that there is a systematic deviation from his experimental results, see Figure 1.7. Kent's experiments were performed in an acrylic pipe line with 100 mm diameter and a straight section of 5.5 m.

Veronese (1937) [80] found a minimum velocity to keep a bubble stationary in the flow. He observed that at some higher velocity, generation and entrainment reduced all pockets to a small stable size which was defined as the limit bubble. Any increase on velocity did not further disrupt the limit bubble but carried it out. The velocity to maintain the limit bubble in equilibrium in flowing water is called limit velocity. Veronese suggested a clearing velocity of 0.59 m/s that should clear the air in pipes with diameters greater than 100 mm.

Kalinske and Bliss (1943) [37] presented information of direct use to the pipeline designer. They provided experimental data indicating the water discharge necessary to maintain air removal from any given size of pipe laid at any slope. The experimental investigation was carried out using acrylic pipes with diameters of 102 mm and 152 mm. The line went up to a summit and then was set at downward slopes between 0° and 17.5°.

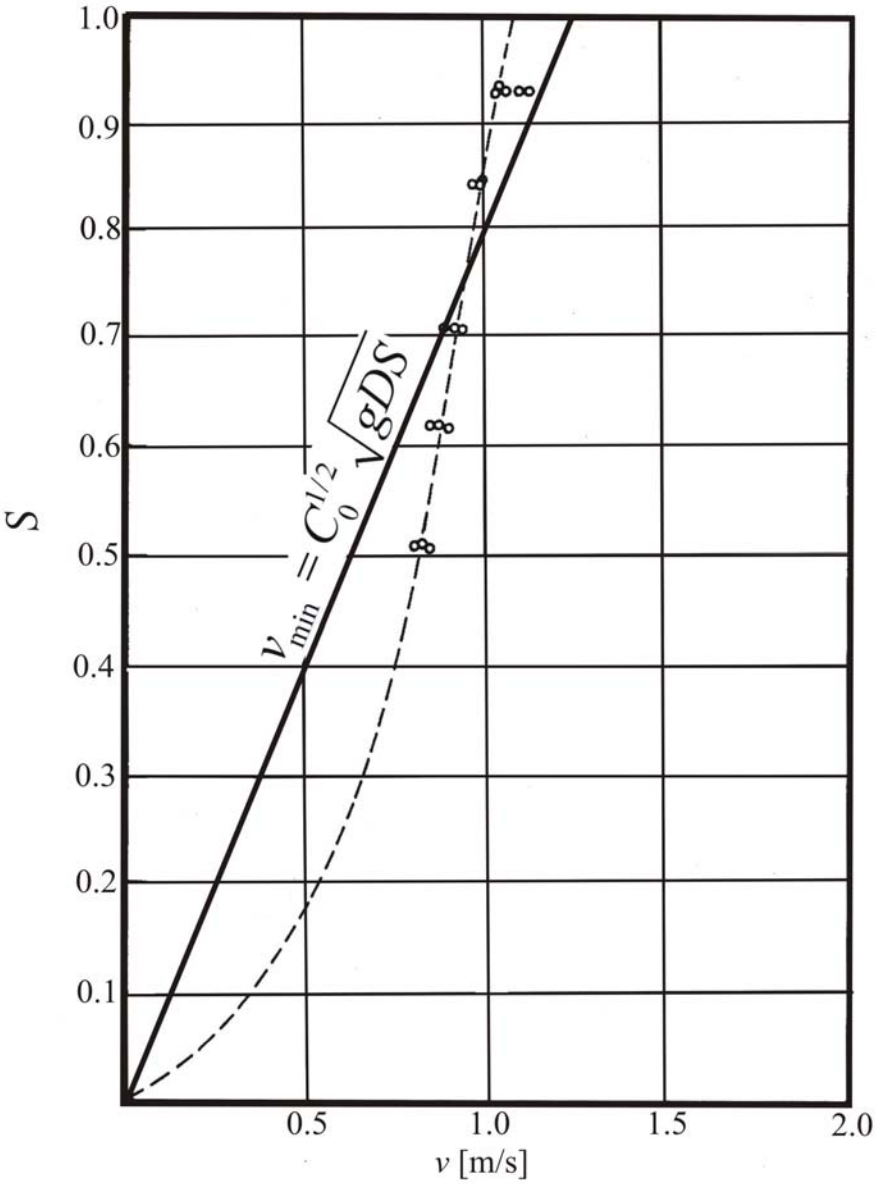

S pipe slope [-]
v water velocity in the pipe [m/s]

Figure 1.7: Relation of the minimum velocity and the downgrade slope (after Kent, 1952)

For all except the very flat slopes, the water was flowing down the sloping pipe in a hydraulic jump. The downstream depth of the jump was usually large enough to seal the pipe, although in some cases for low flows at flat slopes the jump did not fill the conduit. In such cases the depth beyond the jump increased gradually until the pipe was filled. Under such conditions the air removal phenomenon was considerably different from the case where the jump did fill the pipe.

The rate at which the jump entrained the air did not necessarily correspond to the rate at which air was removed from the pocket. Downstream of the jump the pipe flowed full, except for the air bubbles, and the rate at which the air was eventually removed from the pipe depended on the ability of the flowing water in the pipe beyond the jump to carry the air bubbles along. For higher water flow discharges the jump generated and entrained air at a higher rate than the flow beyond the jump could handle. The excess air then blew back periodically through the jump. For any pipe size and slope, there was a discharge at which air was carried down by the water flow beyond the jump. Below this discharge the removed air depended on the ability of the water downstream of the jump in the filled conduit to convey air along. Above this discharge the water velocity beyond the jump was sufficient to clear all the air entrained by the jump.

Kalinske and Bliss observed that the removal of air was controlled by two hydraulic phenomena. For higher discharges the air removal was controlled by the hydraulic jump, since the water flow beyond the jump was capable of carrying all the air entrained by the jump, and more if it were available. At lower discharges the air removal was controlled by the flow characteristics beyond the jump.

For smaller slopes it was found that the entire air pocket would be swept out of the pipe very quickly. However, this could always be prevented by having a singularity or rough protuberance near the pipe line peak, to which the end part of the pocket would cling. It was considered by the authors that in the prototype would always be sufficient surface roughness, particularly at joints, to cause the upper end of the air pocket to remain in the singularity.

It was noted that smaller air bubbles could be moved more easily than the larger ones. However, the smaller ones would gradually coalesce into large bubbles, which could not be moved by the water, and these would travel up the pipe and pass back through the jump.

The analysis done by Kalinske and Bliss indicated that the ratio of the volumetric rate of air removal to water discharge Q_a/Q_w is related to the pipe slope, S, and the dimensionless flow rate defined as Q_w^2/gD^5, where g is the gravitational acceleration and D the pipe diameter. The plotting of the data indicated the

existence of such a general relationship, the value of Q_a/Q_w increases with Q_w^2/gD^5 for any slope. The graph is shown in Figure 1.8.

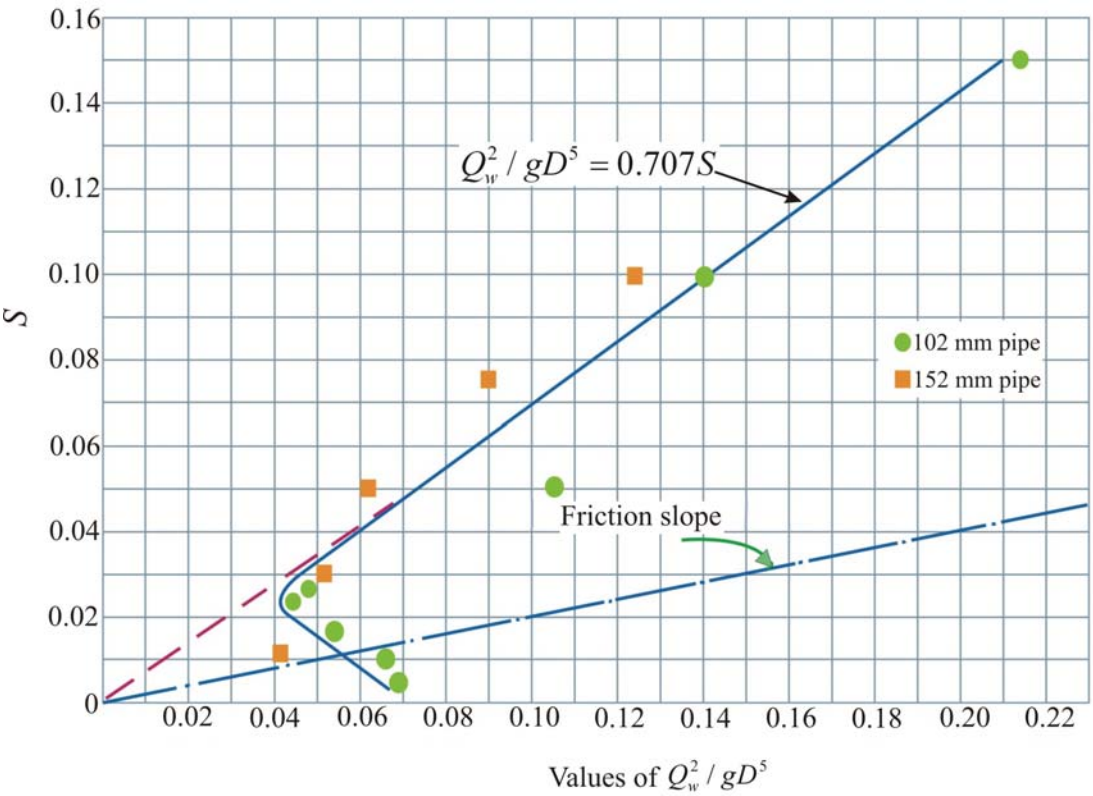

Figure 1.8 Experimental data showing the relation between pipe slope, pipe diameter, water flow rate, and hydraulic gradient when air removal starts (after Kalinske and Bliss, 1943).

The relationship can be written as

$$Q_w^2 / gD^5 = 0.707S \quad [-] \qquad (1.3)$$

Q_w water flow rate [m^3/s]
g acceleration due to gravity [m/s^2]
D pipe diameter [m]
S pipe slope [-]

Replacing the water flow rate, Q_w by the water velocity, v the equation can also be presented as

$$v^2 / gD = 1.146S \quad [-] \qquad (1.4)$$

v water velocity in the pipe [m/s]

The peculiar deviation of the data for the smaller slopes is quite different than expected. It was found that for pipe slopes less than 2.5% the experimental data deviated from the straight line relationship. This occurred when the hydraulic jump

at the lower end of the air pocket did not fill the pipe. Thus, the process of entraining air was quite different from that when the downstream depth of the jump was greater than the pipe diameter. It is apparent that for pipe slopes less than 2.5 % higher water discharges are required to initiate air removal. This appears to be a significant finding since it means that no advantage is gained by using very flat slopes. Kalinske and Bliss stated that even though the exact limiting water discharge was difficult to determine, the measurements obtained are sufficiently accurate for practical use.

Wisner et al. (1975) [87] simulated in a physical model, some conditions at which different investigators worked in order to appreciate previous authors' recommendations. They investigated the scale effect on the clearing velocity and recommended some tools to enable practicing engineers to identify the different aspects of air presence and methods for eliminating air, adopting remedial measures or both.

After a dimensional analysis Wisner et al. as well as Gandenberger expressed the bubble size as a dimensionless parameter *BS*, in which $BS = 4V/(\pi D^3)$, where V is the volume of the air pocket and *D* the pipe diameter.

A hydraulic model with acrylic pipes and a diameter of 244 mm and 7.3 m length was used to perform the experiments for moving water and still water situations. An experiment was performed to investigate Veronese's limit bubble. A large pocket was introduced in flowing water. The water velocity was changed to keep the pocket in equilibrium as disruption progressed. It was observed that the pocket was finally reduced to a small stable size and that any increase of the velocity does not further disrupt the pocket but sweeps it out. The results obtained extend Veronese's results. The experimental results clarified two important points. (1) The limit velocity does not become a constant quantity with increasing diameter as suggested by Veronese, but it decreased with diameter, at least in the range of Veronese and the writers; and (2) the limit length does not become a constant beyond 100 mm in diameter, but decreased at a decreasing flow rate. For the 244 mm pipe the limit length and limit velocity were found to be 46 mm and 0.72 m/s, respectively.

The experiments in still water were done to investigate the relationship between the Reynolds number R_e and $v_r / \sqrt{gD}$, where v_r is the rise velocity of the pocket. The experiments were performed in a downward slope with 18.5° and different air pockets sizes were allowed to rise in the still water. The values obtained were plotted in terms of $v_r / \sqrt{gD}$ and Re for 18.5° together with Gandenberger´s results for other pipe sizes. The authors concluded that for values of Reynolds number above 10^5, $v_r / \sqrt{gD}$ becomes independent of the Reynolds number. Also for the same slope results suggest that $v_r / \sqrt{gD}$ becomes independent for $BS \geq 0.8$. Wisner et al. plotted all available experimental results to provide a lower limit for the critical velocity for air removal $v_{critical}$.

$$v_{critical} / \sqrt{gD} = 0.25\sqrt{S} + 0.825 \qquad [-] \qquad (1.5)$$

$v_{critical}$ critical velocity for air removal [m/s]
g acceleration due to gravity [m/s^2]
D pipe diameter [m]
S pipe slope [-]

The authors recommended that the design values of the velocity parameter should not be much higher than this lower bound as this will introduce a problem of blowback.

Falvey (1980) [20] presented a graph showing the limits for air pockets and air bubble motion in closed conduits, based on the data presented by *Kalinske and Bliss* (1943) [37], *Runge and Wallis* (1965) [65] and *Colgate* (1966) [13]. The author comments that the direction of movement taken by the air bubbles or air pockets can be analyzed taking into account the relative magnitudes of the drag and buoyant forces upon a stationary bubble in the flow. For example bubbles move perpendicularly to the pipe axis only when the upstream component of the buoyant force vector is equal to the drag force component. Falvey also reproduced in the graph the results obtained by *Sailer* (1955) [66] related with prototype cases in which large air pockets move against the flow to completely destroy reinforced concrete platforms, see Figure 1.9.

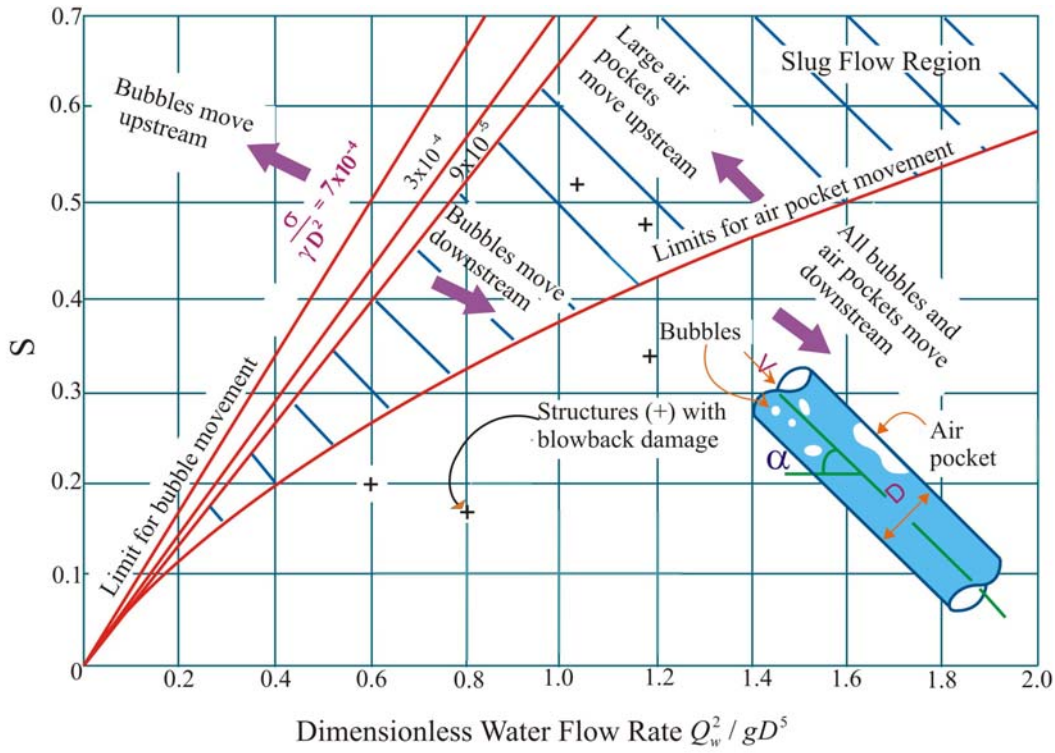

Q_w water flow rate [m^3/s]
g acceleration due to gravity [m/s^2]
γ specific weight of water [kg/m^3]
σ surface tension [kg/m]

Figure 1.9: Air bubbles and air pockets motion in closed conduits flowing full (after Falvey, 1980)

Gonzalez and Pozos (2000) [29] proposed a linear equation to study the behavior of air bubbles and air pockets downstream of a hydraulic jump located at the end of a large air pocket. Experimental and theoretical investigation was carried out to validate the practical use of the equation. The equation was developed based on *Kalinske and Bliss* (1943) [37] investigations, as well as research made by posterior investigators to Kalinske and Bliss. The proposed linear relationship is

$$Q_w^2 / gD^5 = S \quad [-] \qquad (1.6)$$

The term Q_w^2/gD^5 is named dimensionless water flow rate

Q_w water flow rate [m^3/s]
D pipe diameter [m]
g acceleration due to gravity [m/s^2]
S pipe slope [-]

For the analysis of the air pockets and air bubbles Q_w^2/gD^5 is compared with the downward sloping pipe sections of the pipeline system. When Q_w^2/gD^5 is greater than the pipe slope the air bubbles and pockets move downstream along the pipe. When it is lower than *S*, the air bubbles and pockets will move upstream. Measurements and observations in an experimental apparatus corroborated that the air behaved as the linear equation (1.6) predicted.
The experimental investigation was developed in a physical model of acrylic pipes with diameter of 101.6 mm. Likewise, the linear equations, as well as experimental and theoretical investigations are presented in detail in chapter 2.

Escarameia et. al (2005) [18] described experimental and numerical studies that were conducted to enable the development of design guidance on how to minimize the negative effects of the presence of air pockets in pipes, particularly for mild slopes.

The tests were carried out in a 150 mm internal diameter pipe at slopes varying between 0° and 22.5° but, in view of past research findings, the results can be taken as generally valid for slopes up to about 40°. The report describes the experimental apparatus, its operation, tests carried out and the development of design formulae on critical flow velocity for air pocket movement and on the rate of air removal by hydraulic jumps. The authors also presented the results of their experiments related to air pocket velocity, bubble velocity downstream of hydraulic jumps.

The general conclusions from the experiments are:

- Air moves freely in the direction of the flow on upward slopes of the line due to its own buoyancy with no flow. The velocities of air pockets in upward slopes are similar to the air pocket velocities observed in downward slopes.
- A critical or cleaning velocity is required to move air pockets along horizontal and downward slope sections of pipes.
- An equation for the estimation of critical flow velocity for air pocket movement was obtained from the experiments which showed the dependency of the critical flow velocity on the slope and air pocket size, and implicitly on the pipe diameter. The equation (1.7) was developed based on a range of air pocket sizes and the maximum values of critical velocity associated with each of the air pocket classes. It can therefore be said that the equation was based on an envelope to the data.

$$v/(gD)^{0.5} = S_f \{0.56(S)^{0.5} + a\} \quad [-] \qquad (1.7)$$

v water velocity in the pipe [m/s]
g acceleration due to gravity [m/s^2]
D pipe diameter [m]
S_f safety factor [-]
S pipe slope [-]
a numerical coefficient [-]

The values of a depend on the dimensionless parameter to characterise the size of air bubbles and pockets *BS*.

The authors recommended that equation (1.7) can be used with reasonable confidence for pipe diameters of up to 1.5 m. For this size, the required flow velocity for air pocket movement in a horizontal pipe as predicted by equation for large air pockets is 2.1 m/s and 2.6 m/s respectively. The applicability of the recommended equation to larger pipe diameters is a matter of debate as it would need to be verified in practice.

Little (2002) [49] used the information presented by other investigators and reviewed the experimental investigation on air transport movement in pipes with downward slopes and undulating profiles. Little's conclusions are presented here:

- Published data are not always consistent with each other or with case histories. Differences may be due to test procedures, data extraction, definitions used and variables other than those plotted.
- Test data show that air bubbles will be transported more easily than air pockets but will tend to agglomerate into air pockets at the pipe soffit, because irregularities in the pipe wall can cause air pockets to adhere to them.
- Under normal operating conditions air pockets should be transported forward down shallow slopes but will not be transported against steep slopes. There is a critical slope at which air pockets will be trapped, the value depending principally on pipe diameter and flow.
- In addition, free surface hydraulic conditions in the pipe must be studied if it is to be assumed that air will wander its way back against the flow. Where possible, air valves or vents should be used.
- Assessment must be made of the full range of flow conditions.
- Data on air transport in pipes at shallow slopes are few. On the basis of limited case histories, the line apparently based on work by *Kent* (1952) [39]; *Mosvoll* (1976) [54];

Edmunds (1979) [15]; *Wisner et. al.* (1975) [87] seems sensible as a guide in determining critical gradient within the limits given. Differences between this line and data presented elsewhere *Falvey* (1980) [20], *Kalinske & Bliss* (1943) [37], *Wisner et. al.* (1975) [87], *Ervine* (1998) [16] support the need for caution and may indicate particular cases where further study is required. The shape of the line at shallow slopes is not well substantiated.

- The range of data and case histories suggests that factors other than those identified, perhaps pipe roughness and local detail, may have some influence. Further research, tests, field data and case histories are needed, both for shallow and steep slopes.

Lauchlan et al. (2005) [47] collected and summarized existing knowledge and experience relating to air problems in pipelines. The conclusions of this literature review are the following:

There are no generally accepted formulae for the transport of air bubbles or pockets in pipelines and there is a wide variation between the various prediction equations. Dimensional analysis (*Bendiksen* (1984) [6], *Falvey* (1980) [20], and *Wisner et al.* (1975) [87]) has shown that the critical velocity, also called clearing velocity, to move an air bubbles or air pockets is a function of surface tension, Froude number, Reynolds number and pipe slope. Where the effects of surface tension are negligible, the critical velocity for a given pipe slope has been taken by several researchers as proportional to $(gD)^{1/2}$, where g is acceleration due to gravity and D is the pipe diameter.

Most formulae suggested by the various investigators relate the cleaning velocity of the flow v_c with the pipe diameter D and the pipe slope S, as well as with the acceleration due to gravity. It should be noted however that many authors' work was carried out using a single pipe diameter and therefore dependence on D could not be established from their experiments. The authors presented a graph, which plots $v_c /(gD)^{0.5}$ against $(S)^{0.5}$ summarizes the findings relating to air pockets and bubbles moving in downward sloping pipes, see *Lauchlan et al.* (2005) [47].

From an economical standpoint, the hydraulic means are the best to clear the air of the pipelines. If the water flow velocity is not high enough to remove the air bubbles and air pockets through the line, then mechanical methods must be adopted.

1.5.2 Mechanical Means

Around the beginning of the 20th century, engineers did not understand well the behavior of air into water pipelines. Many began placing standpipes believing that large amounts of air could be exhausted through them, but standpipes are a solution that can be used, only if the hydraulic gradient line is not so far above ground level. A manual control valve is used to connect the standpipe to the water main in such a manner that air can be discharged to the atmosphere.

Normally, open vents at intermediate summits are not feasible if the distance to the hydraulic line from the pipeline exceeds 6 to 10 m. According to *Falvey* (1980) [20] the maximum allowable vent high is determined from topographic, aesthetic and economic considerations.

Open fire hydrants are a solution adopted by some engineers and there are still some municipalities that use them connected to one side of the pipe to remove air, but a substantial amount of air leaves at the roof of the line, *Landon* (1994) [43]. Another solution was the placing of globe and gate valves at the high points of the system to manually exhaust the air. In large systems, it is not possible to predict when the valves have to be opened to relief the air. This method neither provides continual air release during system operation nor vacuum protection.

Air Valves

Air valves are the most used devices for exhausting the entrapped air during the filling of the pipeline or entering a high volume of air into the water line during dewatering, and discharging the air introduced after filling or released from solution. Their malfunction or total fail can lead to air accumulation since the valves are not able to intercept and release the air. Therefore, the correct sizing and appropriate placing of air valves throughout the entire length of the pipeline is very important. This also allows that the air valves remain working during fluid transients, avoiding problems as water column separation.

Balutto (1996) [4] described pipeline problems related with the malfunction of air valves. The inefficient operation of air valves can reduce flow by more than 30% and contributes to high energy consumption as pumps are forced to work harder to overcome the entrapped air in the line.

Estimations indicate that the cost of repairing pipeline breaks in Canada exceeds 100 million dollar annually. Based on investigations Balutto stated that the causes of these breaks originated from air and the use of conventional air valves, either as the primary causes or as a secondary contributing factor.

Types of Air Valves

Up to now air valves are commonly used on pipelines around the world. The mode of operation is to automatically release and admit air without personnel assistance. Many enterprises offer different configuration and designs of air valves for a wide range of applications.

The information on valve types, location, performance and sizing is based on information published by Vent-O-Mat, Val-Matic, APCO and the AWWA.

Normally the automatic air valves are divided into three types:

- Air Vacuum Valves or Single Large Orifice Valve
- Air Release Valves or Single Small Orifice Valve
- Combination Air Valves or Double Orifice Valve

Air Vacuum Valves (AVV)

Air vacuum valves admit a large amount of air to avoid destructive conditions from occurring in the water line due to water column separation or for dewatering the system. The AVV release air during the pump start-up and pipeline filling. The air exhausting should be done in a slowly form to avoid pressure surge or other destructive phenomena.

As air is removed from the line, water enters the valve and elevates the float to shut off the valve discharge port. The velocity of discharge airflow is a function of the pressure focused on the center point of the valve orifice. Air valve sizing criteria are a very important consideration, because the size of the valve controls the differential pressure at which the air is released.

During pump shut-down, draining of the system, breakage of pipeline or water column separation the valve float drops and permit air to re-enter the pipeline to prevent a vacuum. This safeguards the pipeline against collapse. Since the size of the AVV dictates the degree of vacuum, correct sizing of the valve is very important.

When the air has been removed from the line, the float will seal the AVV orifice. Nevertheless, under normal operation the AVV will not relieve built up air. Air Release Valves are needed for this purpose. Figure 1.10 shows the (AVV).

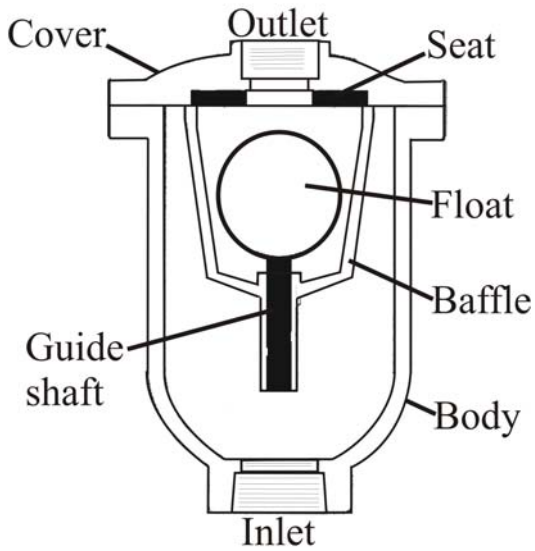

Figure 1.10 Air Vacuum Valve

Air Release Valves (ARV)

Air release valves have a small precision orifice to vent air pockets as they build up at high points of the system while the pipeline is operating. The ARV has a hydro-mechanical float to sense the presence of air and opens the orifice under full pipeline pressures.

During system performance, small amounts of air separate from water and enter the valve. Each particle of air displaces the same volume of liquid inside the valve and lowers the liquid level relative to the float. As the liquid is lowered by the air, the float will drop to open the valve orifice allowing the release of air. When air is exhausted, the liquid level within the valve rises to seal the orifice. This cycle repeats itself as often as air concentrates in the valve.

The ARV have a limited capacity for admitting and exhausting air. Therefore, they are not recommended for vacuum protection nor to release large amounts of air when a pipeline of large diameter has to be filled, due to their small orifices usually less than 1.27 cm. For this purpose a combination air valve is recommended. A sketch of the air release valve is presented in figure 1.11.

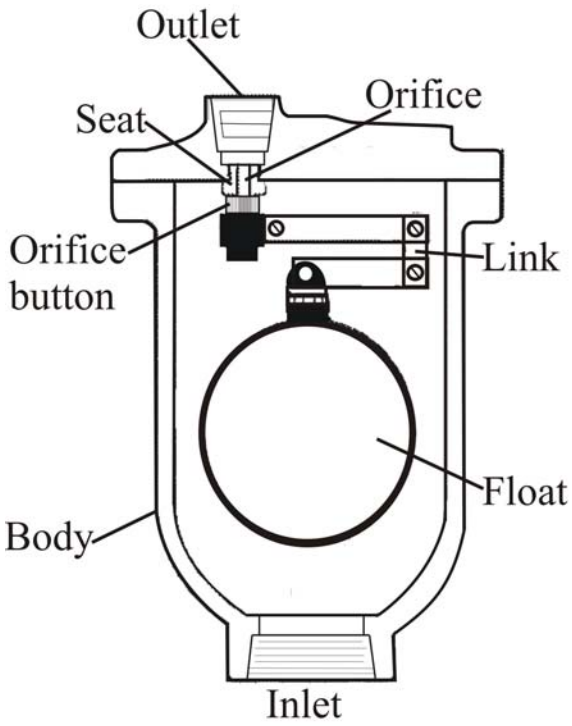

Figure 1.11 Air Release Valve

Combination Air Valves (CAV)

Combination air valves perform the functions of the Air Vacuum Valves and Air Release Valves. These devices are also called Double Orifice Valves DOV. A CAV contains an air vacuum port and a small air release orifice in one assembly. These valves are installed at all high points throughout the pipeline where air release and air vacuum valves are needed to protect and vent the system. Two body designs of CAV are available, (1) a single body combination and (2) a dual body combination. The single body unit has the advantage of being more compact and normally less costly and is used where compactness is preferred. The dual body combination design consisting of an ARV piped to an AVV. This dual body CAV has the advantage that a variety of ARV with a wide range of orifice with higher operating pressure can be used. During maintenance AVV is still working while the ARV is isolated and under repair. Since CAV include all air valve functions, some engineers use only these devices and do not leave the pipeline unprotected in case of a mistake in field installation or incorrect operation of the system.

The two types of combination air valves above described are shown in Figures 1.12 (a) – (b).

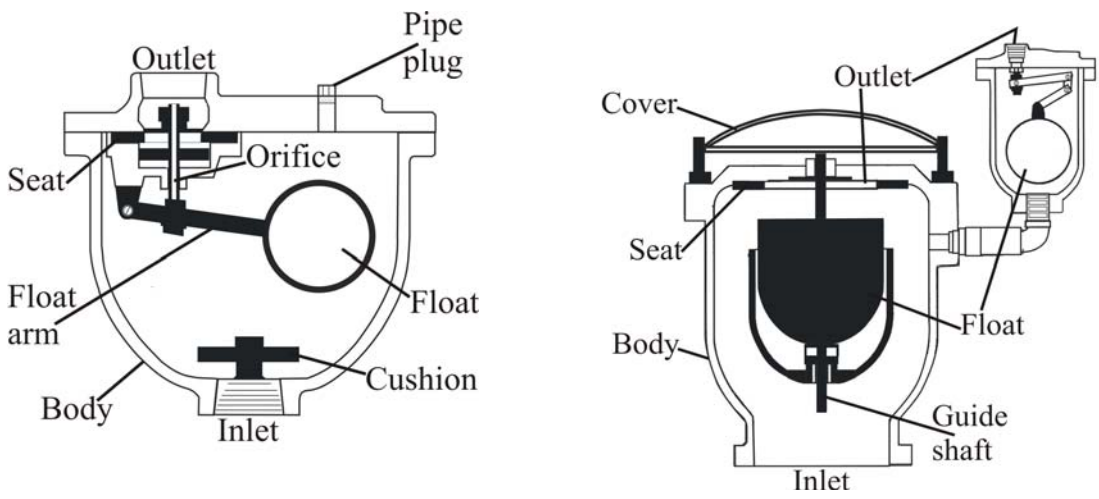

a) CAV Single Body b) CAV dual Body

Figure 1.12 Combination Air Valves

The Combination Air Valves or Double Orifice Valves described above can be distinguished as Kinetic Air Valves and Non-Kinetic Air Valves. These valves function with a large hollow spherical float which draws up to seal the orifice when air has released. During dewatering the valve allows air to enter into the line. Likewise, considerably changes in the design of the CAV have not been made in the last hundred years. Therefore, the hollow spherical float sealing the large orifice continues causing some operating problems, which are presented below.

Non-Kinetic Air Valves

A number of functional limitations of Non-Kinetic Valves designs include *Balutto* (1998) [5]:

Poor Sealing and Working Pressures. The hollow float must be perfectly spherical in order to produce a leak tight seal against a resilient seat located around the circumference of the discharge port of the valve. In practice, it is almost impossible to have a perfect sphere and to compensate the lack of uniformity; therefore, a very soft seating seal is often used. The adherence of the soft seal to the float can lead to the malfunction of the orifice.

Deformation and Jamming. The hollow structure of spherical floats makes them susceptible to permanent deformation and distortion when the valve works under high pressure. Field observations have shown that float elongates and becomes wedged into the orifice. Evidently

the orifice does not perform neither air intake nor exhausted functions if the float jammed into the orifice.

Premature Closure. Premature Closure is also called Dynamic Closure and refers to the tendency of the hollow spherical float to seal the orifice of the ball type air valves at very low differential pressures (0.02 - 0.05 bar) without any further discharge, resulting in the entrapment of a large volume of air in the pipeline.

Limitation of Orifice Size and Its Effect on Performance. Some manufacturers recommend that the spherical float should not have a diameter less than 3 times the large orifice diameter otherwise it may wedge into the orifice. From the economic point of view the large orifice diameters are restricted, because also the weight and size of the float increase proportionally. For this reason designers choose to reduce somewhat the large orifice, consequently the discharge performance is adversely affected.

Venturi Effect. All air valves designs with spherical floats tend to remain partially closed during air suction. As a result of the creation of a lower pressure zone on the upper part of the float compared to the pressure experienced in the pipeline.

Kinetic Air Valves

The main purpose of the kinetic valves is to overcome the phenomenon of premature closure or dynamic closure. The internal configuration of the valve is modified, thus its aerodynamic characteristic can prevent a dynamic closure. The details and effectiveness of such internal modifications differ for each valve manufacturer.

When these types of devices are discharging air at high velocities they can create serious problems for the operation of the pipeline system, some of which are (*Balutto* (1998) [5]):

Water Hammer. Air valves discharging air at high velocities and differential pressures will cause closure with damaging pressure transients. This is because of the water enters the valve abruptly. The effect on the pipeline dynamics is equivalent to the rapid closure of an isolating valve. Investigations conducted by authorities and manufacturers proved that the damage created by these devices, exhausting air at high velocities, is a problem that cannot be ignored in pipeline design. They recommended a differential pressure of 0.05 bar as limit to prevent the damage from high pressure transients.

Water Spillage. Water spillage can occur when the large orifice control float fails to react as water at high velocity enters the valve chamber. The water covers the control float, holding the float down, while exiting through the large orifice. The quantity of water spilled in this manner is substantial and floods the valve chamber. The spillage of the water can induce a pressure surge in the pipeline.

Seal Failure. Seal Failure is a peculiar phenomenon in kinetic air valves. The seal fails between the valve and the isolator. This can occur on closure of the large orifice and results in water spillage. It is as a result of the transient pressures created on closure. Research conducted by fabricants and authorities has concluded that this phenomenon occurs at 80 - 85 bar, which implies that the transients created by kinetic air valves, discharging at high deferential pressures are in excess of 85 bar.

Under Sizing. Kinetic air valves are more susceptible to being undersized than other air valve designs. This is because of the pipeline designers concentrating on their discharge requirements, selecting valves to discharge at high differential pressures, and thereby ignoring their vacuum requirements. Valve selection based totally on discharge requirements is detrimental to the pipeline under vacuum conditions, as the valve may not fully protect the pipeline under these conditions. This is especially true for plastic pipes, and pipeline seals which cannot withstand very high differential negative pressures.

Venturi Phenomenon. The Venturi phenomenon described under non kinetic air valves is also applicable to kinetic air valves.

1.6 Location and Sizing of Air Valves

Pump Discharge. An Air Vacuum Valve should be installed on the pump discharge side before the check valve to exhaust the air during pump start-up and to permit air to re-enter the line after shutdown. These types of devices are not necessary for pumps with positive suction head. The valve is sized with the discharge of the pump. It is important that the differential pressure does not exceed 0.05 bar during filling operation.

Increase Downslope. A Combination Air Valve is commonly located at abrupt changes in downward slope due to the possibility of vacuum and water column separation. The design water flow is used to know the size of the air valve required. The differential pressure across the large orifice should not be lower than 0.35 bar. During the selection of the air valve the “Venturi Effect” has to be taken into account.

Decrease Upslope. An Air Vacuum Valve or Combination Air Valve should be located at sharp upward slopes to avoid serious problems in case of water column separation or vacuum. The design water discharge is used to find the size of the air valve required. The problems and precautions are the same as in the last point.

Long Horizontal Runs. Combination Air Valves are placed at the beginning and end of long horizontal sections. Along the horizontal section Air Release Valves are located. Investigators and manufacturers recommend various intervals, between 380 and 760 meter, where the valves should be considered. Whenever possible long horizontal pipeline sections have to be avoided. If it is impossible then more valves should be positioned along the horizontal section. The sizing of these two types of devices should be based on the filling rate of the pipeline.

Long Ascents. An Air Vacuum Valve or a Combination Air Valve should be considered throughout the upward sections of the pipeline at intervals of 400 m to 800 m. These devices are required for an adequate discharge during filling of the system and for good ventilation when it is being dewatered. For the sizing of the air valves, the filling rate has to be compared with the intake demand, calculated for the breakage of the pipe and for the pump failure. If the filling rate is greater than the intake rate, the devices are sized based on the filling rate.

Long Descents. An air release valve or a combination air valve should be considered throughout of the downward sections of the pipeline at intervals of 400 m to 800 m.

High points. Combination Air Valves should be located at high points to avoid vacuum and water column separation and to release the air while filling operation, to discharge the air introduced after filling or released from solution and for air inflow during draining.

Generally the size of the valve is determined based on the pipeline rupture calculations.
The location of the air valves in the pipeline is shown in Figure 1.13 (a) to (g).

As the valves have been selected, it is recommended to analyze the pipeline as a whole to ensure that the valves and other devices selected for the adequate performance of the system work without problems to avoid the destructive phenomena already described.

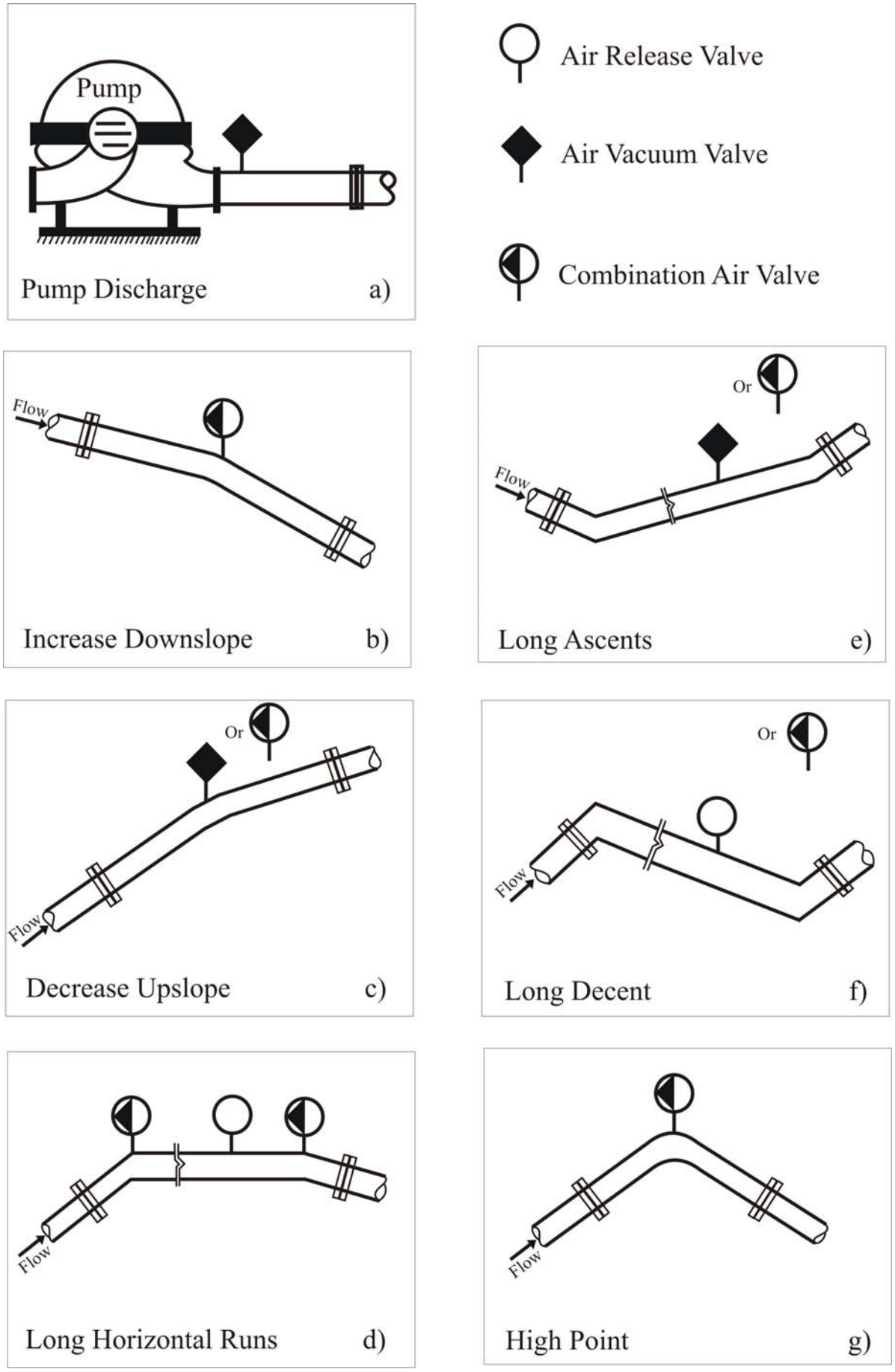

Figure 1.13: Location of the air valves in the pipeline

2 Analysis of Air Pockets Trapped in Gravity Pipeline Systems

2.1 Introduction

As described in the first chapter, *Gonzalez and Pozos* (2000) [29] proposed a linear equation to study the movement of air bubbles and air pockets downstream of a hydraulic jump located at the end of a large air pocket in a downward sloping pipe. The equation was developed based somewhat on *Kalinske and Bliss* (1943) [37] investigations, as well as research made by investigators posterior to Kalinske and Bliss.

The linear relationship herein presented is supported on theoretical analysis and hydraulic model investigation. A computer program was developed by using this equation and it is utilized to illustrate two real cases where overflows occurred due to air entrained.

2.2 Theoretical Analysis made to develop the linear relationship to analyze the movement of air bubbles and air pockets

The direction of movement of a stationary air bubble or air pocket in flowing water in a downward sloping pipe can be analyzed by balancing the magnitudes of the drag force of the water and the buoyant force on an air bubble or air pocket. This can be written as:

$$\text{Drag force} = \text{Buoyant force}$$

where

$$\text{Drag Force} = CL_d^2 \rho v_{crit}^2$$

C drag coefficient [-]
L_d linear dimension of the air bubble/pocket [m]
v_{crit} critical mean water velocity acting on a stationary air bubble or air pocket [m/s]
ρ water density [kgs^2/m^4]

The air density is neglected since it is much lower than water density.

$$\text{Buoyant force} = KL_d^3 \rho g S$$

K constant depending on the air bubble/pocket shape [-]
g acceleration due to the gravity [m/s^2]
S pipe slope [-]

Then

$$CL_d^2 \rho v_{crit}^2 = KL_d^3 \rho g S \quad [-] \qquad (2.1)$$

Rearranging the terms

$$v_{crit}^2 / gL_d = (K/C)S \quad [-] \qquad (2.2)$$

An assumption is made regarding the linear bubble dimension. If L_d simply depends on the pipe diameter D, then L_d / D becomes a constant. Consequently L_d can be replaced by D in equation (2.2).

$$v_{crit}^2 / gD = (K_1 / C)S \quad [-] \qquad (2.3)$$

Equation (2.3) can be also presented as

$$Q_{crit}^2 / gD = (K_2 / C)S \quad [-] \qquad (2.4)$$

Q_{crit} = critical water flow rate [m^3/s]

Equation (2.4) is the same relation obtained by *Kalinske and Bliss* (1943) [37]. However, they did not give values of the coefficients K and C that depend on the Reynolds number R_e.

Walski et al. (1994) [83] determined the values of drag coefficients for gas pockets in model but the results were not satisfactory, because the Reynolds numbers were on the order of 1000 which is often a range where drag coefficients are usually independent of the Reynolds number. Likewise, *Falvey* (1980) [20] stated that the drag coefficient can not be predicted for flow in a pipe, therefore the techniques of dimensional analysis must be used to determine the significant parameters for correlation that could lead to obtain a more complex equation, due to including more dimensionless numbers.

Kalinske and Bliss (1943) [37] found relatively good correlations for the initial movement of air bubbles by using the pipe slope S and the Eötvös number $\gamma D^2/\sigma$. Therefore, equation (2.4) can be rewritten as

$$Q_w^2 / gD^5 = f(S, \gamma D^2 / \sigma) \quad [-] \qquad (2.5)$$

Q_w water flow rate [m^3/s]
g acceleration due to the gravity [m/s^2]
D pipe diameter [m]
S pipe slope [-]
γ specific weight [N/m^3]
σ surface tension [N/m]

Zukoski (1966) [91] and *Viana et al.* (2003) [81] stated that for turbulent flow conditions, viscosity and surface tension effects will be minimal in pipe diameters of 175 mm or larger. Hence, the Eötvös number can be neglected. In addition, most of the equations recommended by various investigators associate the clearing velocity with the pipe slope S, pipe diameter D, as the acceleration of the gravity g. *Gonzalez and Pozos* (2000) [29] followed the arguments of the above authors and backed these statements by own experiments. On this basis the following formula as a modification of that proposed by Kalinske and Bliss was suggested, which is the same linear relationship presented in equation (1.6), chapter 1.

$$Q_w^2 / gD^5 = f(S) \quad [-] \qquad (2.6)$$

Q_w water flow rate [m^3/s]

Replacing the water flow rate, Q_w by the mean water velocity, v in the equation (1.6) or equation (2.6) yields

$$v^2 / gD = 1.62S \quad [-] \qquad (2.7)$$

v water velocity in the pipe [m/s]

The suggested equations by previous researchers to assess the clearing velocity in downward sloping pipes are listed in Table 2.1, as well as the results computed from the equations to compare the velocity obtained by *Babb et al.* (1968) [3] on a prototype siphon with a diameter of 3.66 m, water flow rate of 34.55 m^3/s and slope of 0.42. The clearing velocity measured by Babb et al. was 3.3 m/s.

Equations Proposed by	Value of the Clearing Velocity [m/s]
Kalinske and Bliss (1943) $v_c = 1.07\sqrt{gDS}$	4.16
Kent (1952) $v_{min} = 1.2\sqrt{gDS}$	4.65
Gonzalez and Pozos (2000) $v = 1.27\sqrt{gDS}$	4.93

Table 2.1: Equations to calculate the clearing velocity for D = 3.66 m, Q_w = 34.55 m^3/s, S = 0.42 (Clearing velocity measured by Babb et al. was v = 3.3 m/s)

Analysing the computed values, it can be readily seen that the highest clearing velocity is the one calculated with the equation proposed by *Gonzalez and Pozos* (2000) [29]. The results suggest that equation (2.6) is conservative and the value obtained by its application is on the safe side. Therefore, it is recommended to be used either in the design of water pipeline systems or to analyze the movement of air bubbles/pockets in existing water lines, because it is only a function of the pipe slope and has the advantage that empirical coefficients do not have to be taken into account.

2.3 Method of Analysis by Using the Linear Relationship of Gonzalez and Pozos

As discussed in the previous chapter, large air pockets can be trapped at high points of pipelines, when air valves are not located at summits likely to air accumulation. Even though air valves have been placed, they may fail and air would not be exhausted. When the large air pockets extend downstream in a steep slope the critical depth will be larger than the normal water depth, then a hydraulic jump can occur.

Observations in experimental apparatus indicated that large air pockets can accumulate along the control section located at the transition between the subcritical and supercritical slopes, *Walski et al.* (1994) [83]; *Gonzalez and Pozos* (2000) [29]. Likewise, *Mosvell* (1976) [55] stated that the water flow rate capacity to transport large air pockets decreases, when there is a transition between subcritical slope and supercritical slope. Figure 2.1 is a schematic description of a large air pocket collected at a high point.

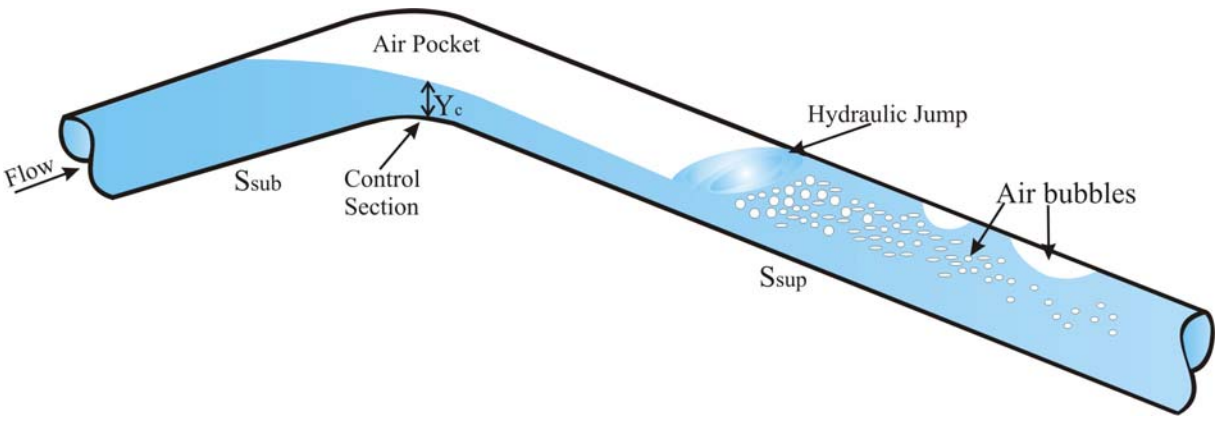

S_{sub} subcritical slope [-]
S_{sup} supercritical slope [-]
Y_c critical depth [m]

Figure 2.1: Large air pocket accumulate at the transition between S_{sub} and S_{sup}

Rodal et al. (2000) [64] found that the necessary critical water depth Y_c for removing a large air pocket from the control section must be equal to or greater than 90% of the pipe diameter. Measurements in a physical model permitted to conclude that even the nominal design flow rate may not be enough to remove the large pockets located at the control section.

The hydraulic jump at the end of the large pocket will entrain air in form of small bubbles, see Figure 2.1. The rate at which the air is removed from the line depends on the ability of the water flowing in the pipe below the jump. The equation (2.6) is used to analyze the movement of air bubbles and air pockets in a downward sloping conduit flowing full. Small bubbles entrained by the jump will rise to the pipe roof coalescing and forming air pockets. The pockets and bubbles may move upstream and pass back through the jump, remaining the same volume of air in the pipeline. However, if the pipe slopes upward in the direction of the flow, air pockets and air bubbles will move downstream. In addition to horizontal pipes, the upward component of the buoyancy force does not influence the air bubbles/pockets behaviour, therefore it would be expected that the flowing water drags the air.

To determine if large air pockets are likely to remain at slope transitions in the line, the dimensionless flow rate Q_w^2/gD^5 is assessed for the full range of flow conditions and compared with all the downward sloping pipes that make up the pipeline. When Q_w^2/gD^5 is greater than the downward slope *S*, air bubbles and air pockets will move with the flow. However, when Q_w^2/gD^5 is lower than *S*, the bubbles and pockets will turn and move backward relative to the current. In this case, the high or intermediate high point is identified as possible candidate for air accumulation, because the inertia of flow is not able to remove the air from the line. Therefore, the location of air valves or vents should be taken into account to remove mechanically the entrained air.

It is important to highlight that the linear relationship (2.6) does not predict the occurrence of destructive blowbacks in pipelines, as described by *Sailer* (1955) [66]. The method of analysis is included in a computational program called AIRE (presented at section 2.4) that has been used to predict the movement of air in existing gravity pipeline systems.

2.4 Experimental Investigation

In order to validate the application of the linear equation (2.6) presented in the previous section, experimental investigations were developed. The experimental apparatus was

designed and constructed to study the behavior of stationary air pockets at high and intermediate high points of pipelines, as well as to analyze the air entrained by the hydraulic jump at the end of the pocket located in a downward sloping line. The experimental investigation also included the measurement of air bubble velocities by using a high speed camera at different sections of the pipe behind the hydraulic jump, to define the boundary between the air entrainment and the transport of air to be able to give a limit to the application of the proposed linear relationship.

2.4.1 Description of the Experimental Apparatus

The experimental apparatus was designed and made of acrylic pipes with a diameter of 76.2 mm. In consequence of the presence of free surface flow the Froude number was used as design criterion. Figure 2.2 shows a sketch of the test section.

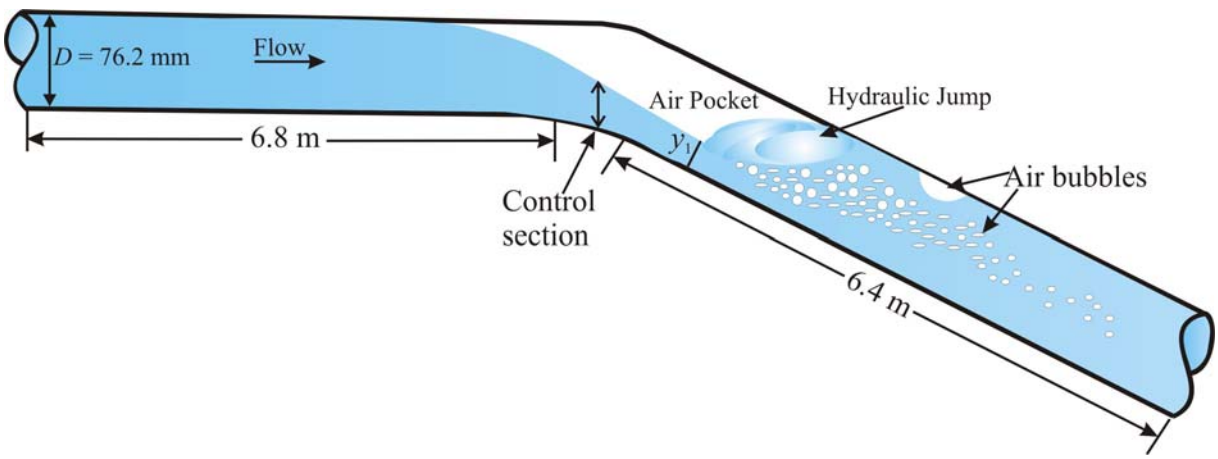

y_1 initial depth [m]

Figure 2.2: Test Section of the Experimental Apparatus

The downstream sloping section of the line was 6.8 m in length and could be varied in slope, whereas the horizontal upstream leg of the model was 6.4 m long. The water was supplied from a constant head tank. Two pumps connected in parallel fed the line. The water flow rate was controlled by two valves located at the pumps discharge side and measured by orifice plates.

2.4.2 Experimental Procedure

While the line was flowing full, air was injected into the pipe by using a compressor. Once in the experimental apparatus, air tended to accumulate at the control section in form of a large pocket ending in a hydraulic jump. Likewise, the turbulent action of the jump that sealed the

duct was able to entrain air that was swept downstream by flowing water. It was observed that small air bubbles coalesced into air pockets. Depending on the water flow rate and pipe slope, the bubbles and pockets either returned to the hydraulic jump or moved downward in the direction of flow. The conjugate depth was measured at the beginning of the jump to calculate the air flow rate Q_a introduced by the hydraulic jump with equation (1.1). This is the empirical relationship developed by *Kalinske and Robertson* (1943) [38].

The measurements were made for various water flow rates and the downward leg was placed at different slopes. During the tests, all the slopes were compared with the full range of dimensionless flow rates. *Gonzalez and Pozos* (2000) [29] observed in the experimental apparatus that air bubbles and pockets behaved, as the linear relationship (2.6) predicted. The advantage of the parameter Q_w^2/gD^5 is that it includes the water flow discharge Q_w and the pipe diameter D, therefore it allows the transfer of results from model to prototype.

Part of the results obtained in the experimental investigation is summarized in table 2.2.

S = 0.089					
y_1 (m)	**Q_a (m^3/s)**	**Q_a (l/s)**	**Q_w(m^3/s)**	**Q_w^2/gD^5**	**Air behavior**
0.019	0.00018	0.18	0.0015	0.0889	moves upstream
0.021	0.00017	0.17	0.0017	0.1147	moves downstream
0.024	0.00013	0.13	0.0019	0.1432	moves downstream
S = 0.060					
y_1 (m)	**Q_a (m^3/s)**	**Q_a (l/s)**	**Q_w(m^3/s)**	**Q_w^2/gD^5**	**Air behavior**
0.022	0.00010	0.10	0.0015	0.0889	moves downstream
0.023	0.00012	0.12	0.0017	0.1147	moves downstream
0.024	0.00013	0.13	0.0019	0.1432	moves downstream
S = 0.052					
y_1 (m)	**Q_a (m^3/s)**	**Q_a (l/s)**	**Q_w(m^3/s)**	**Q_w^2/gD^5**	**Air behavior**
0.021	0.00012	0.12	0.0015	0.0889	moves downstream
0.024	0.00010	0.10	0.0017	0.1147	moves downstream
0.025	0.00011	0.11	0.0019	0.1432	moves downstream

Table 2.2: Movement of air bubbles/pockets in the downward sloping pipe of model with D = 76.2 mm, y_1 initial depth, Q_a air flow rate, Q_w water flow discharge

2.4.3 Limits of the application of the linear relationship

During the experimental investigation a high speed camera was used to measure the mean and instantaneous velocities of air bubbles in flowing water beyond the hydraulic jump. The aim was to define the boundary between the air entrainment and air transport. The two phenomena are drawn in Figure 2.3.

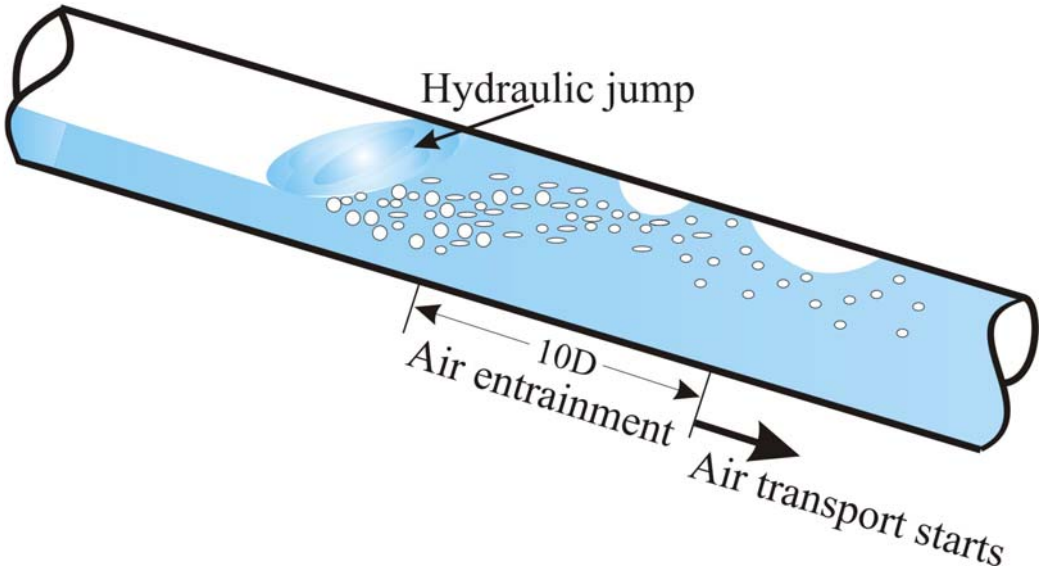

Figure 2.3: Limits of air entrainment and air transport

In order to characterize the behaviour of air bubbles introduced by the jump, these were filmed at different sections of a downward sloping pipe, i.e. at distances of 1, 5 and 10 diameters downstream of the hydraulic jump. The size of the air bubbles varied from 1mm to 2 mm, approximately. Three different water flow rates were used during the tests, Q_w = 1.0 l/s, Q_w = 1.5 l/s, Q_w = 2.0 l/s. The pipe slope remained constant during all the experiments, S = 0.089.

Further analysis of the images was made by a commercial software called OPTIMAS® [93] to determine the velocities of the air bubbles. At one diameter beyond the hydraulic jump the velocity profiles were strongly influenced by the turbulent action of the jump and the velocities distribution was irregular. When the velocities were measured 5 diameters downstream of the jump the velocity profiles showed a different behaviour, but the influence of the eddying action of the jump was still evident. As well, it was observed than 10 diameters behind the hydraulic jump the velocity distribution was very similar to a typical fully developed velocity profile in a circular conduit. Then, observations from the velocity profiles permitted to conclude that the linear relationship can only predict the movement of air bubbles, when these are out of the zone of influence of the turbulent action of the hydraulic jump. If the air bubbles are under the influence of turbulent action equation (2.6) should not be used, because it will not anticipate the behaviour of the air bubbles. The velocity profiles are shown in Figure 2.4.

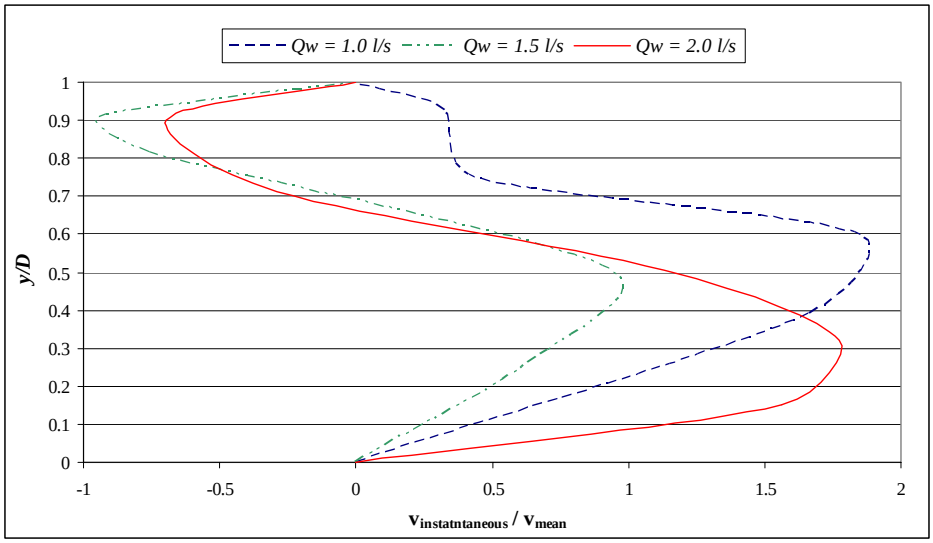

a) Velocity profiles of the air bubbles at 1 diameter downstream of the hydraulic jump

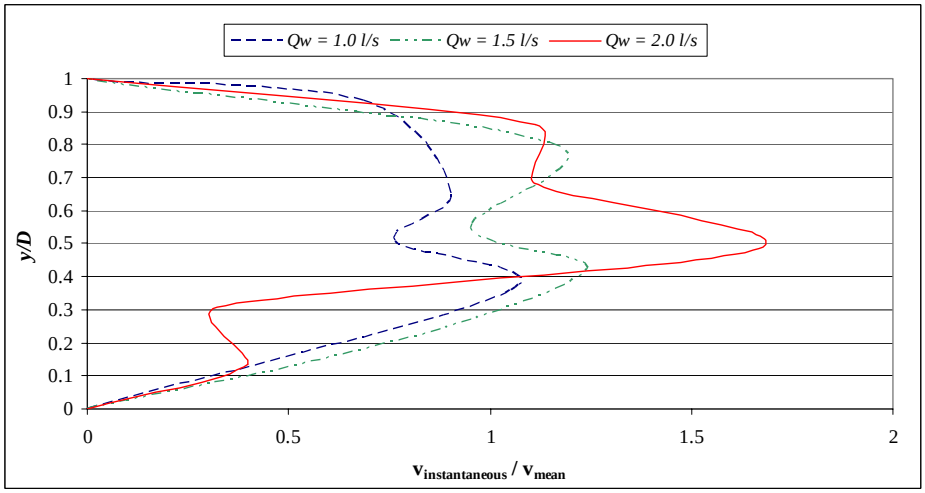

b) Velocity profiles of the air bubbles at 5 diameters downstream of the hydraulic jump

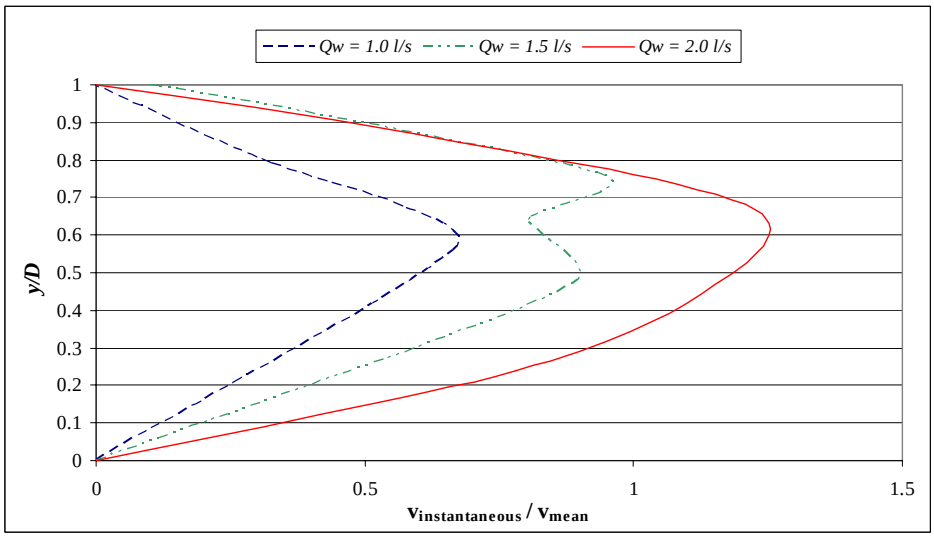

c) Velocity profiles of the air bubbles at 10 diameters downstream of the hydraulic jump

Figure 2.4: Velocity profiles measured by the high speed camera

2.5 Program AIRE

Many engineers design under the assumption that pipelines flow full all the time and never partly full. This hypothesis may lead to critical problems, therefore presence of entrained air should be taken into account during the design of pipelines.

The computer program AIRE was developed by the author based on equation (2.6), *Pozos Estrada* (2002) [58]. The purpose was to provide the pipeline designers a quantitative method for studying the movement of air bubbles and pockets and identifying the summits in pipelines that are susceptible to accumulate air. The program can be used to analyze either pipeline systems during the design stage or existing pipelines.

The program displays a table, which summarizes the behaviour of air bubbles beyond the influence of the turbulent action of the hydraulic jump. In addition, it generates graphs for the full range of flow conditions. The graphs show the pipeline profile, the hydraulic grade line, and the small squares indicate the high and intermediate high points likely to accumulate air. Where the hydraulic grade line intersects the pipeline profile, there will be a transition from open channel flow to pressure flow conditions. If the downward slope is steep the critical depth will be greater than the normal depth, then the transition will be through a hydraulic jump. The equation of Darcy-Weisbach was used to determine the hydraulic gradient line. Evidently the use of other equations is not restricted. Figure 2.5 is an example of a graph displayed by the program AIRE.

The simplest pipeline system can suffer from entrained air problems. Therefore, all systems, especially those with several slope changes, should be reviewed in detail to locate the potential high and intermediate high points, where air may be accumulated. Likewise, if the pipeline will operate with flow variations, the hydraulic grade line may intersect the profile. The necessity of air valves has to be considered. The proper location of air valves can minimize potential problems caused by any buildup of air. In addition, air accumulation cannot always be controlled by installing a large number of air valves and vents throughout the line at the beginning of all downward sloping pipes, because some of these devices would probably not be needed.

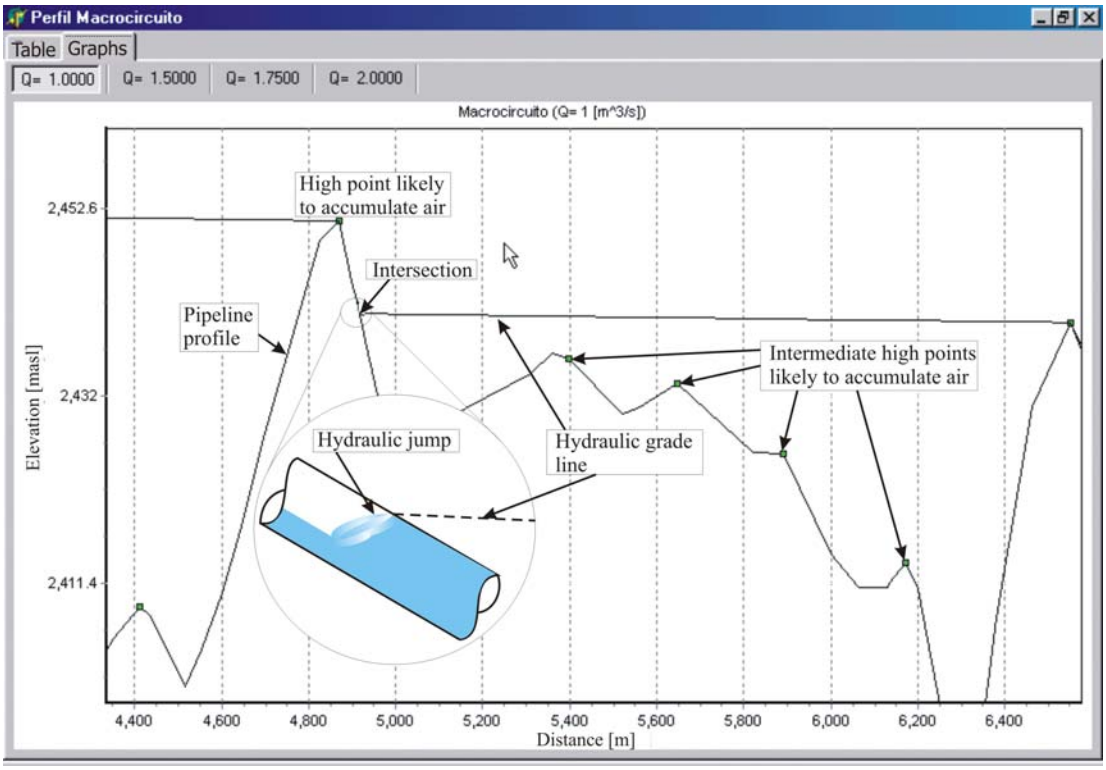

Figure 2.5: Graph displayed by the program AIRE

The program has been used to analyze problems related with air entrainment in existing pipeline systems. The proposal solutions have allowed a better development of these pipelines. Within the next section the program AIRE will be used to exemplify two problems related with air entrained, where air accumulation at intermediate high points caused overflow over hydraulic structures.

2.6 Presentation of real cases related with entrained air

The study of two gravity pipeline systems with air entrainment problems occurred in field is presented, as well as the solutions of these problems supported on the linear equation (2.6), hydraulic model investigations and the computer program AIRE.

2.6.1 Break Pressure Tank Valle de Paz (Macrocircuito)

The Macrocircuito is the main system for supplying potable water to the north and eastern municipalities of Mexico City. The distribution is made by two parallel lines. Line 1 and Line 2 are 54.5 km in length each. The system takes water from the north branch of the Cutzamala System by a tunnel. The section of interest begins at the Bellavista tank (Tank 1), approximately 8.5 km downstream of it the Break Pressure Tank Valle de Paz (Tank 2) is located, followed by the Emiliano Zapata tank (Tank 3), see Figure 2.6. The (Tank 2) has the

aim of limiting the maximum pressure downstream of it, because most of the conduction is made up of prestressed concrete pipe with an inner diameter of 1.22 m. Moreover, without (Tank 2) in the line the pipe could be damaged by the hydrostatic head, if the valve at the entry of (Tank 3) is closed and the pipeline profile from the (Tank 1) to (Tank 3) is completely full when the system is out of service, i.e. $Q_w = 0$ m^3/s.

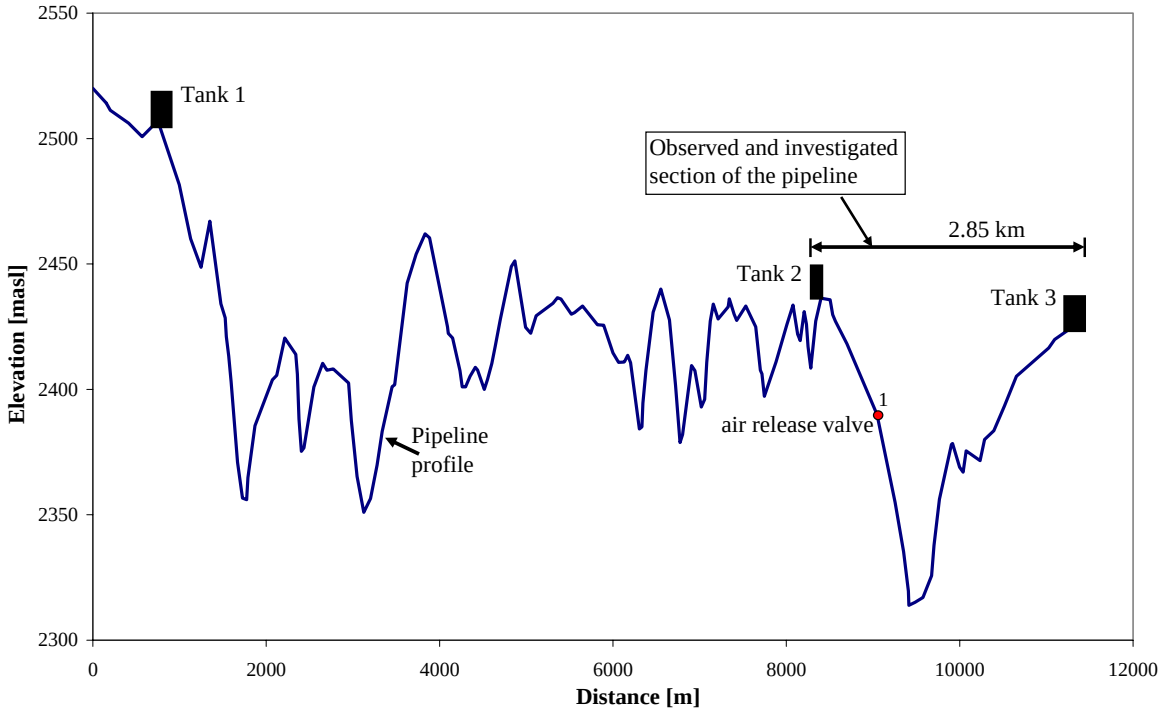

Figure 2.6: Section of interest of the Macrocircuito

The investigated section reaches from (Tank 2) located at station 8 + 399 to the (Tank 3) placed at the station 11 + 247.9, as illustrated in Figure 2.7. The analysis was done by using the equation proposed by Gonzalez and Pozos (2000) [29], equation (2.6). In addition, hydraulic model investigations were carried out. It was found that downstream of (Tank 2) at the change of the horizontal pipe, $S = 0.0$, to the steep slope, $S = 0.51$, see Figure 2.8, a great quantity of air can be accumulated in the form of a large air pocket that ends with a hydraulic jump. This air buildup gave rise to the overflow over the crown of (Tank 2). Supported on the analytical and experimental investigation, it was recommended to place an air release valve and a standpipe immediately upstream and downstream of this point, respectively, as shown in Figure 2.14 a). An air release valve was originally installed at point 1, see Figure 2.7, but the air was not exhausted because it behaved as predicted by equation (2.6), therefore the air returned through the hydraulic jump to the pocket.

It is important to point out that air did not accumulate in form of pockets at the intermediate and high points upstream of (Tank 2), because air release valves are placed where air is likely to build up.

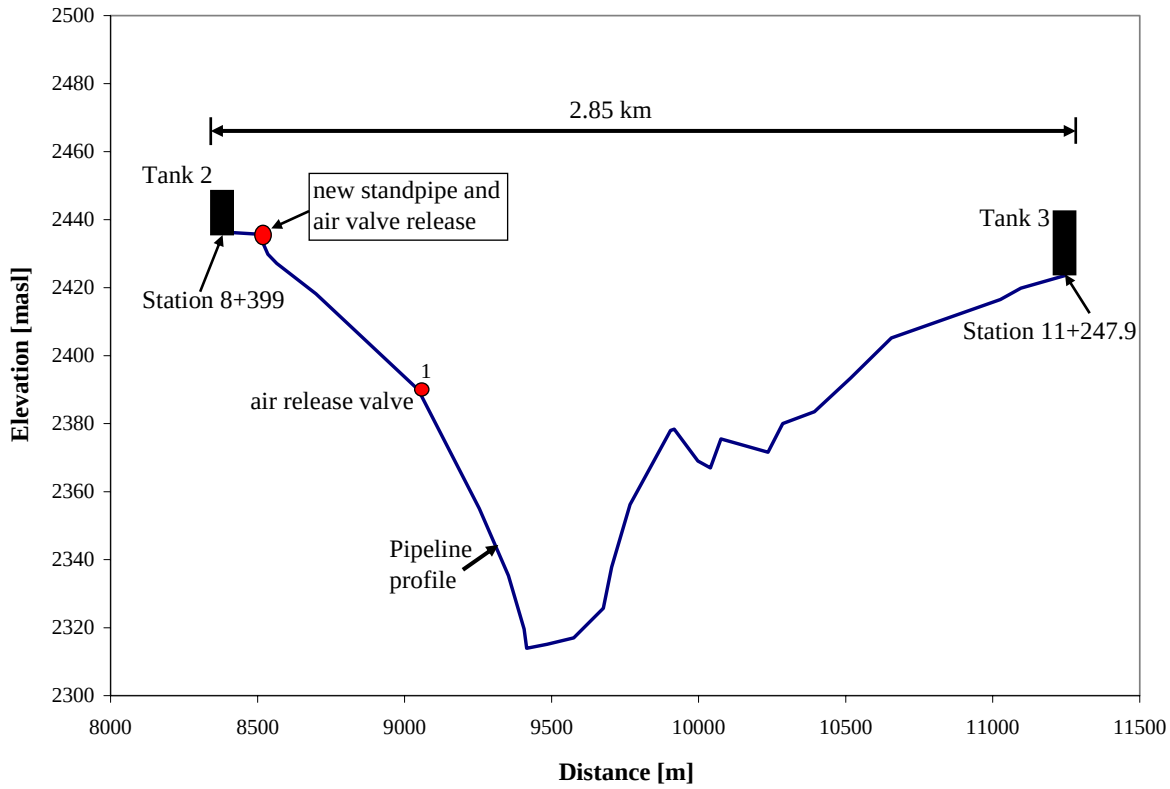

Figure 2.7: Investigated section of the Macrocircuito

The (Tank 2) configuration is shown in Figure 2.8. The dimensions of the tank are 6 x 6 m at the base and 4.5 m height. At the bottom of the tank a vertical segment of steel pipe of 2 m length is connected to an elbow of 90°, followed by a horizontal pipe of 35.3 m length with a inside diameter of 1.22 m. Two further downward sloping pipes come after with a diameter of 1.22 m, with lengths and slopes of 6.58 m and S = 0.51 and 31.0 m and S = 0.58, respectively. The beginning of the prestressed concrete pipe is at the end of the last steel pipe.

Within the next subsection the problem and the solution to the overflow of (Tank 2) is explained more in detail.

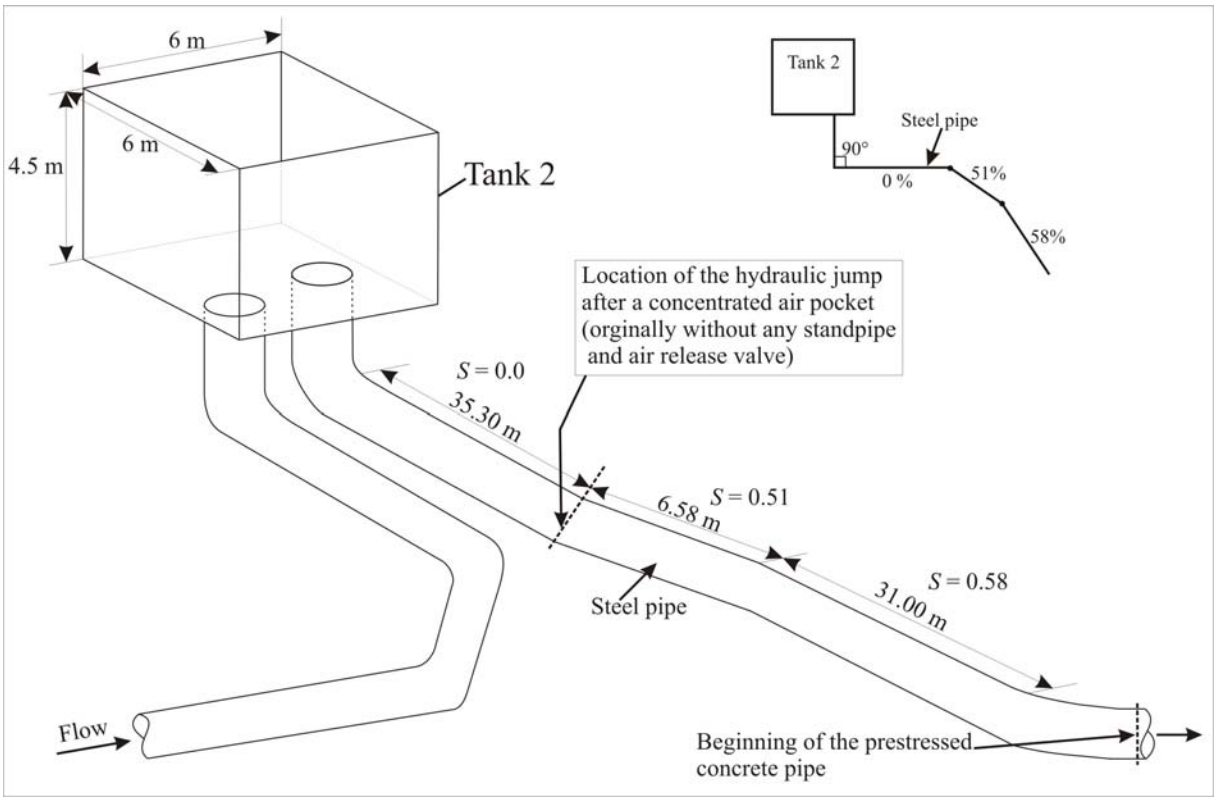

Figure 2.8: Configuration of the Tank 2

Description of the Problematic on the (Tank 2)

The Macrocircuito was designed to convey a water flow rate, Q_w = 3.0 m^3/s, but when the delivery through the line was 1.9 m^3/s, the (Tank 2) started spilling. Therefore, the National Water Commission entered into an agreement with the Institute of Engineering of the University of Mexico (UNAM), to conduct the investigation related with the overflow of the (Tank 2). Personnel of the Institute visited the tank with the purpose of being able to give a preliminary diagnosis. The personnel observed:

- Air entrained through the intake by vortex action in consequence of the low water level in the (Tank 2).
- Observing the behavior of the water in the (Tank 2) it was seen that the oscillations from the bottom to the top of the tank were in the order of 20 or 30 minutes, then the tank spilled.
- The personnel also heard a strong noise within the first downward sloping pipe section, S = 0.51, associated to the transition from partially pipe flow to full pipe flow through a hydraulic jump.

- An important volume of air in form of bubbles rose through the water in the tank, while strong vibrations were heard in periods of 20 minutes, approximately. This phenomenon was related with the air pockets that blew back upstream through the hydraulic jump.

A great amount of air entered into the line due to the vortex action at the (Tank 2) discharge. A photograph and a diagram of the vortex in the (Tank 2) are shown in Figure 2.9. Once in the pipe the air was swept downstream. A large air pocket with a hydraulic jump at its end accumulated along the transition between horizontal pipe, S = 0.0, and the steep slope, S = 0.51. The water flow rate was insufficient to overcome the buoyant force of the large air pocket, hence it remained stationary at the high point of the line. The hydraulic jump dispersed small air bubbles beyond the jump in consequence of its turbulent action. Since the drag forces are usually greater than the buoyant force for small bubbles, these will move downstream. During their downward motion, several of the small bubbles joined together to forming air pockets. When the air pockets grew, these reduced their velocity as a result of the buoyant force increase and blew back with tremendous force through the hydraulic jump, taking water with them. This force was big enough to cause cracks on the walls of the (Tank 2). Photographs of the damage caused to the tank by the blowbacks are shown in Figures 2.10.

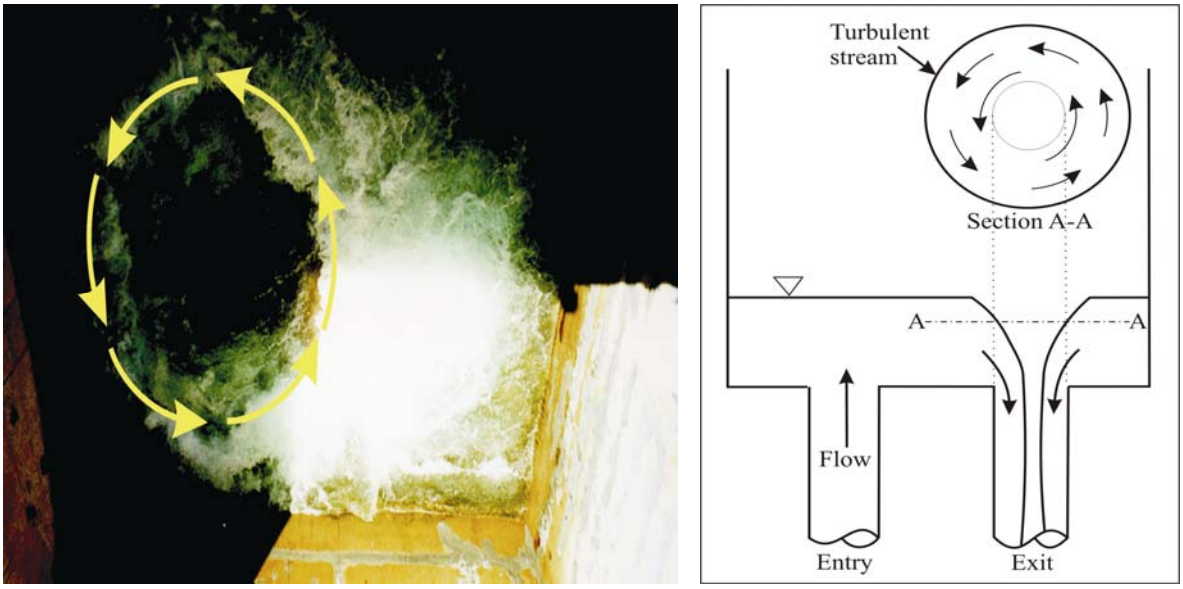

a) **b)**

Figure 2.9: Vortex in the (Tank 2): a) section of the vertical vortex, b) sketch of the vortex

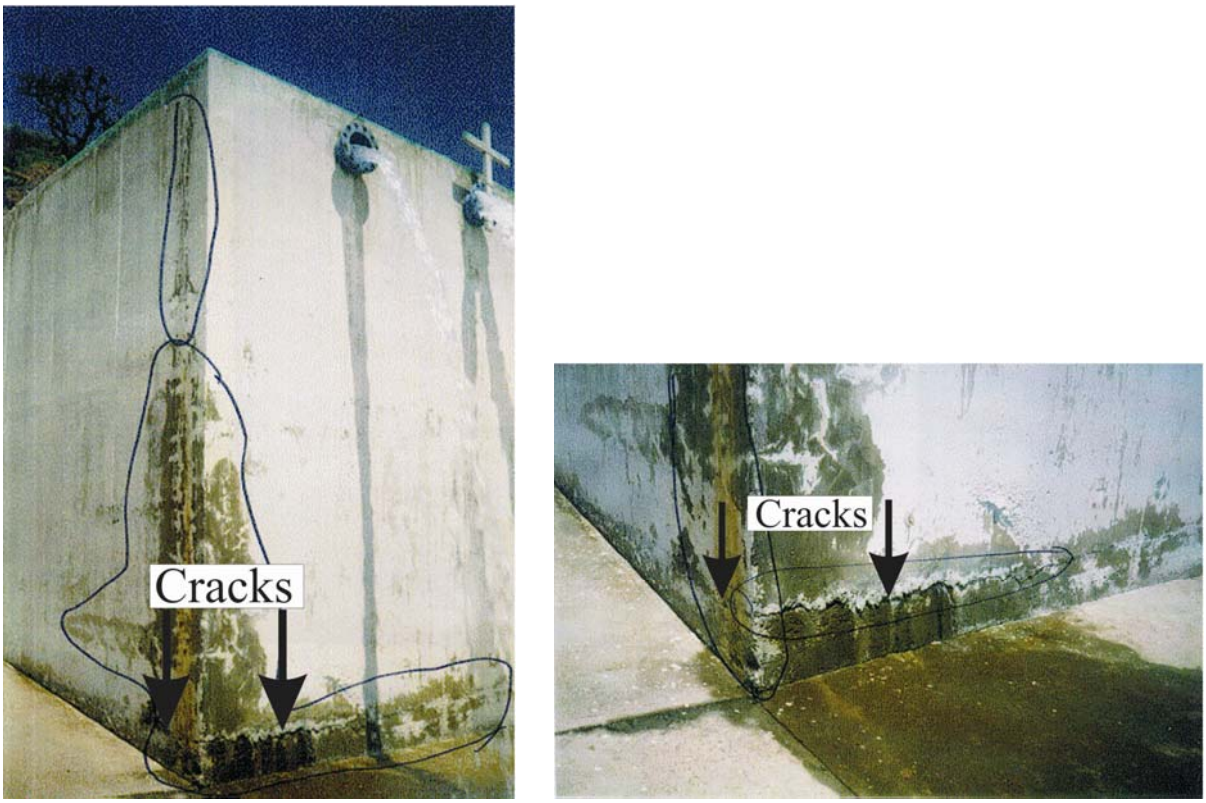

a) **b)**

Figure 2.10: Damage caused to the tank by the blowbacks: a) cracks on the wall of the (Tank 2), b) detail of the cracks

The stationary pocket extended on both sides of the control section reduced the effective cross section of passage of water. Hence, the water level in the (Tank 2) rose, stopping the inflow of air into the pipeline. Due to the availability of a greater hydraulic head, the velocity underneath the air pocket increased, then the air pocket was either swept out bodily or parts of the pocket could be removed to downstream remaining a smaller pocket that was disrupted as the velocity increased even more, and later removed out. In consequence of this behaviour the line was handling 1.9 m^3/s, the (Tank 2) drained after 20 or 30 minutes, allowing air to reenter and the phenomenon was repeated. The (Tank 2) during the overflow for 1.9 m^3/s is shown in Figure 2.11.

The slopes of the steel pipe sections downstream of the (Tank 2) were compared with the dimensionless water flow rate to analyze the movement of air, using the Q_w = 1.9 m^3/s, D = 1.22m and g = 9.81 m/s2. Q_w^2/gD^5 = 0.136. The predictions are summarized in Table 2.3.

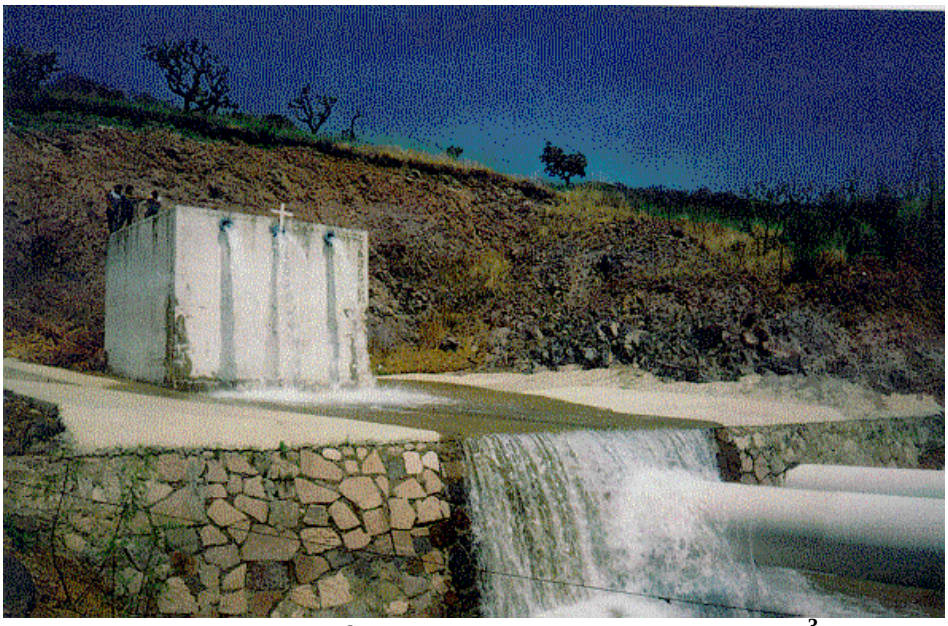

Figure 2.11: overflow over the (Tank 2), Q_w = 1.9 m^3/s

Pipe slope S	Q_w^2/gD^5 = 0.136
0.00	Air moves downstream
0.51	Air moves upstream
0.58	Air moves upstream

Table 2.3: Air behavior in the pipes downstream of the (Tank 2)

From the results presented in the table 2.3 it can be concluded that the air bubbles and pockets returned through the jump in the pipe sections with steep slope.

Hydraulic Model Investigation

In order to analyze the overflows over the (Tank 2) a model was designed and constructed in the laboratory. Due to the presence of free surface flow the Froude number was used as criterion of similarity. The used scale was 1:24. The tank was made of acrylic and the dimensions are 25 x 25 cm at the base and 18.7 cm in height. A pipe of 5 cm length is connected vertically to the tank and is followed by an elbow of 90°. Two more pipes complete the model, the first one is horizontal and 163 cm long and the last pipe has a slope, S = 0.51 and is 157 cm in length. The experimental work was performed by the use of acrylic pipes with an inner diameter of 50.8 mm. The water flow was provided by a pump of 746 W and controlled by a valve located at the discharge of a pump. A diagram of the model is shown in Figure 2.12.

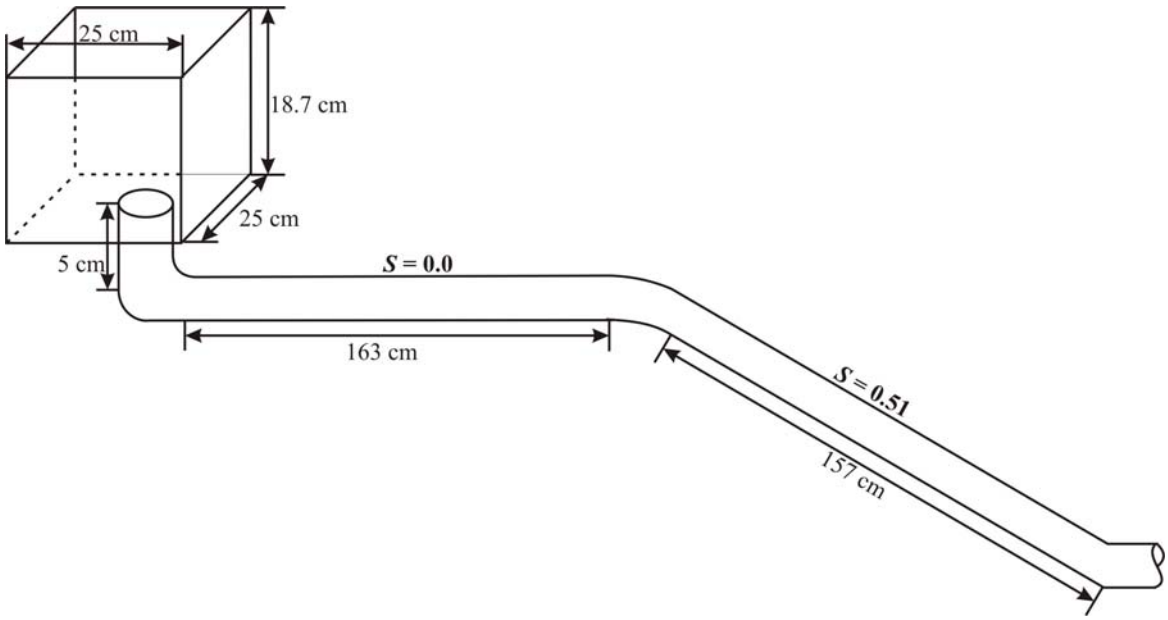

Figure 2.12: Physical model of the (Tank 2)

The water flow rate in the real pipe was Q_w = 1.9 m^3/s that corresponds in the model to Q_w = 0.67 l/s. When the model was fed with a water flow rate of Q_w = 0.67 l/s, the unstable behaviour observed was very similar as in the real pipe. The water oscillations in the model were not regular and occurred more frequently than in field. Probably the difference on time is due to the scale effects (time scale 1:4.9). On the other hand, the model does not represent a complete reproduction of the prototype. Nevertheless, the reproduction of the instability could be satisfactorily represented. The photographic sequence shown in Figure 2.13 allows observing the complete cycle of the instability in the tank.

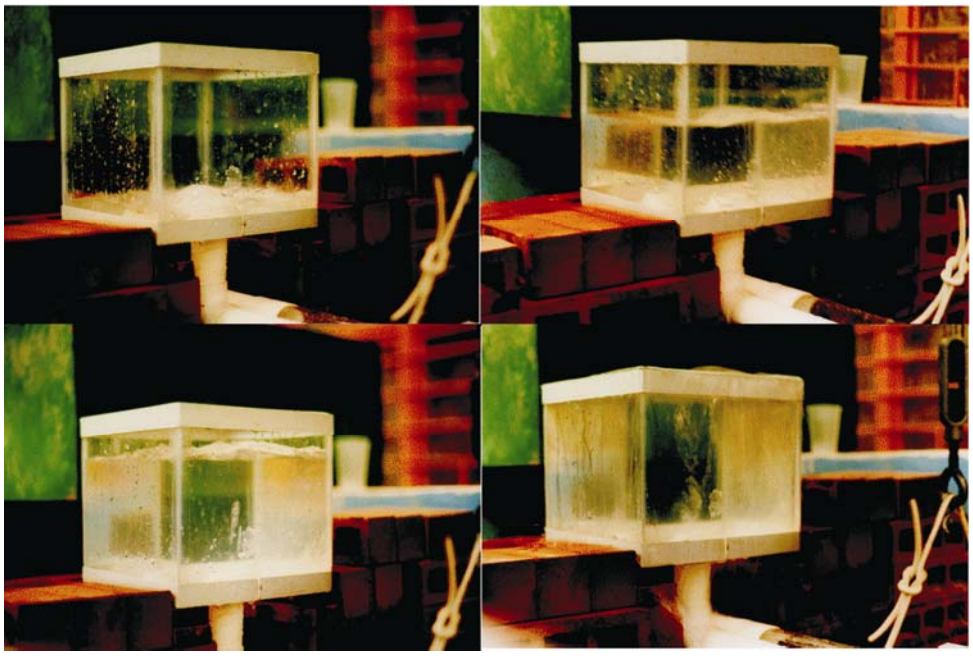

Figure 2.13: Complete cycle of the instability in the (Tank 2)

Solution to the Problem in the (Tank 2)

The Institute of Engineering proposed to place an air release valve and a vent immediately upstream and downstream of the transition from the horizontal pipe to the steep slope pipe, respectively, identified in model as the control section of the air pocket. The unstable behaviour disappeared when the vent was located in the model, see Figure 2.14. The vent allowed extracting the air that entered the pipeline and fixed the hydraulic jump at the downward sloping pipe. The open channel flow will remain at the control section, if the water discharge is lower than the nominal design flow rate.

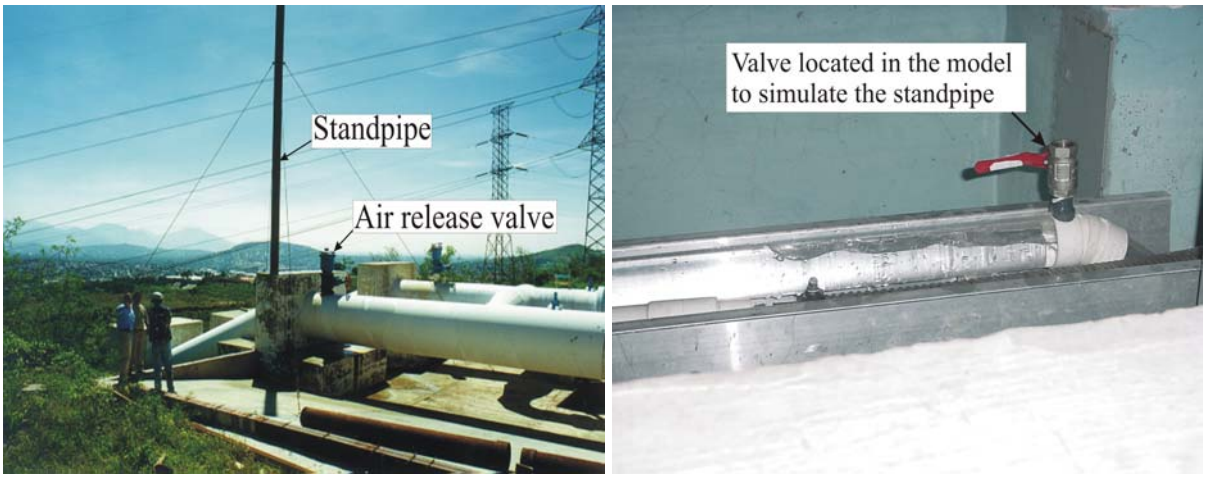

a) **b)**

Figures 2.14: Standpipe and air valve release located at the intermediate high point: a) prototype, b) model

Further blowbacks were not heard and observed, because the air pocket was not able to grow due to the air entering through the tank intake being exhausted by the standpipe and the air release valve. During the pipeline design, the air release valve and the standpipe were not placed at this intermediate high point, because it was not considered likely to accumulate air.

Analysis of the (Tank 2) by using the Program AIRE

The program AIRE is used to illustrate the problem that occurred in the (Tank 2). Figure 2.15 shows the pipeline profile from (Tank 1) to (Tank 3), the hydraulic grade line for Q_w = 1.9 m^3/s. Downstream of the (Tank 2), the hydraulic grade line intersects the pipeline profile, therefore the pipe flowing partly full will change to pipe flowing full through a hydraulic jump.

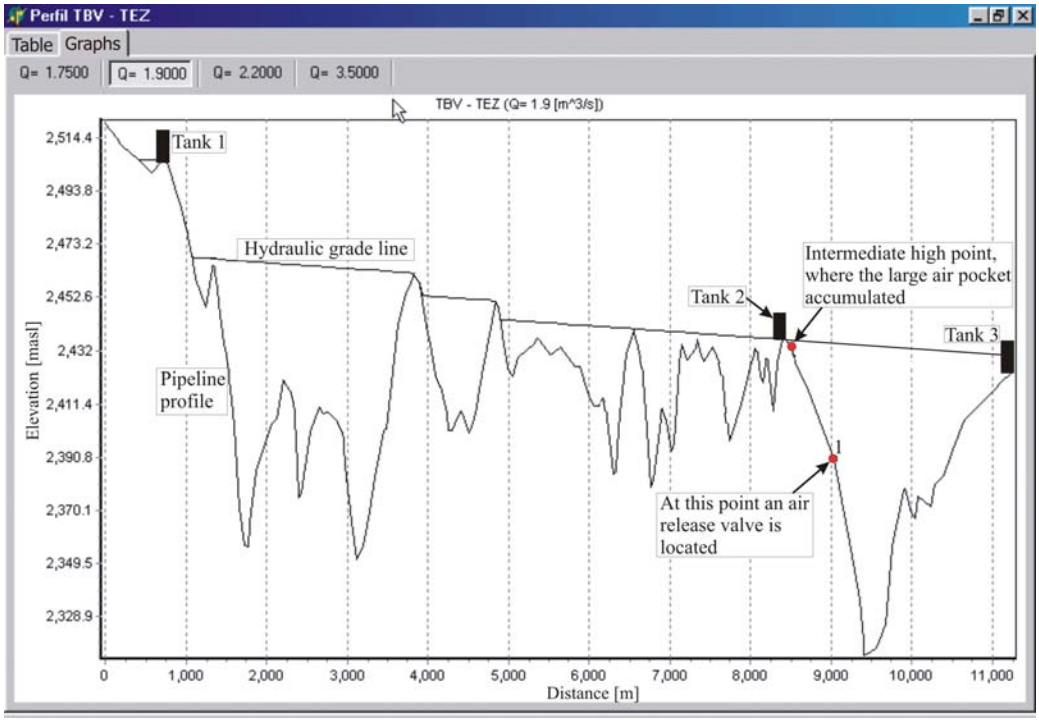

Figure 2.15: Analysis of the (Tank 2), Q_w = 1.9 m^3/s

In Figure 2.16 the analysis for a water flow rate, Q_w = 3 m^3/s is presented. The point likely to accumulate air downstream of the (Tank 2) disappeared, due to the pipe flows full and no air is carried. The point at the station 9+406.5 is not a potential location of air accumulation, because the line handles the nominal design flow rate. In addition, there is an air release valve located upstream that can exhaust the free air before it gets this station.

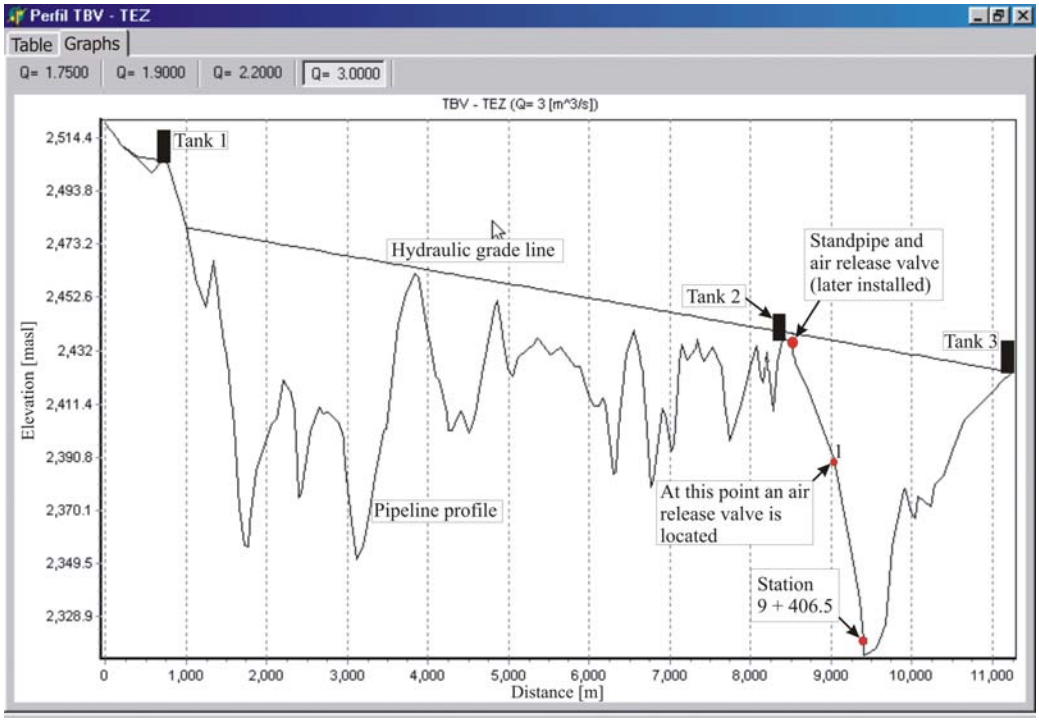

Figure 2.16: Analysis of the (Tank 2), Q_w = 3.0 m^3/s

2.6.2 Alternative Line, Cutzamala System

The second prototype to review is the Alternative Line which is part of the Cutzamala System. Due to problems of stability at the Donato Guerra Channel, the Alternative Line was designed and constructed to convey a nominal design water flow rate, Q_w = 12 m^3/s. The line is formed mainly by reinforced concrete pipes with a diameter of 2.74 m and is 10.900 km in length, approximately. A sketch of the Cutzamala System is shown in Figure 2.17. The Alternative Line is in the dotted grey.

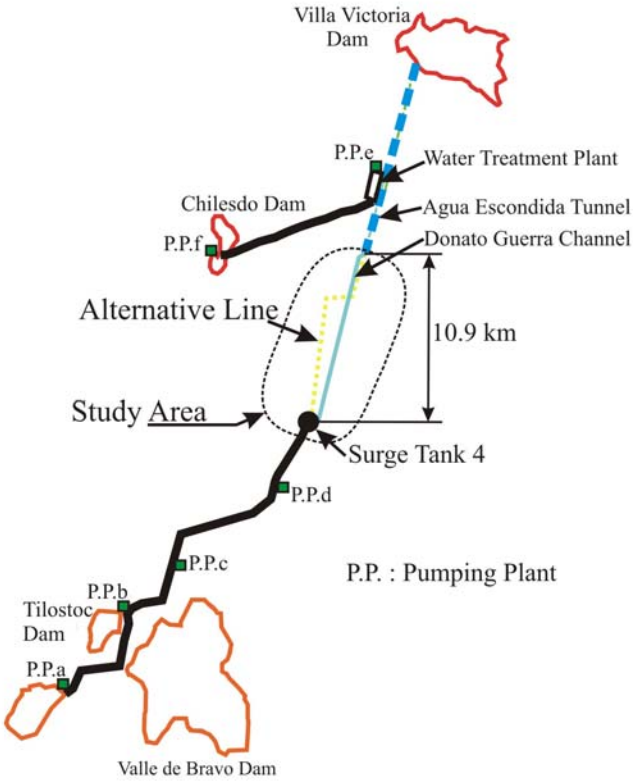

Figure 2.17: Plan of the Alternative Line, Cutzamala Pipeline System

The Alternative Line began to perform with two pumps per plant (Q_w = 8 m^3/s). The freeboard in the Surge Tank 4 was 9.90 m, when a third pump equipment was placed into operation Q_w = 12 m^3/s, the freeboard was reduced to 4.90 m. After one month of operation, the operating personnel reported a water overflow over the crown of the Surge Tank 4, see Figure 2.18.

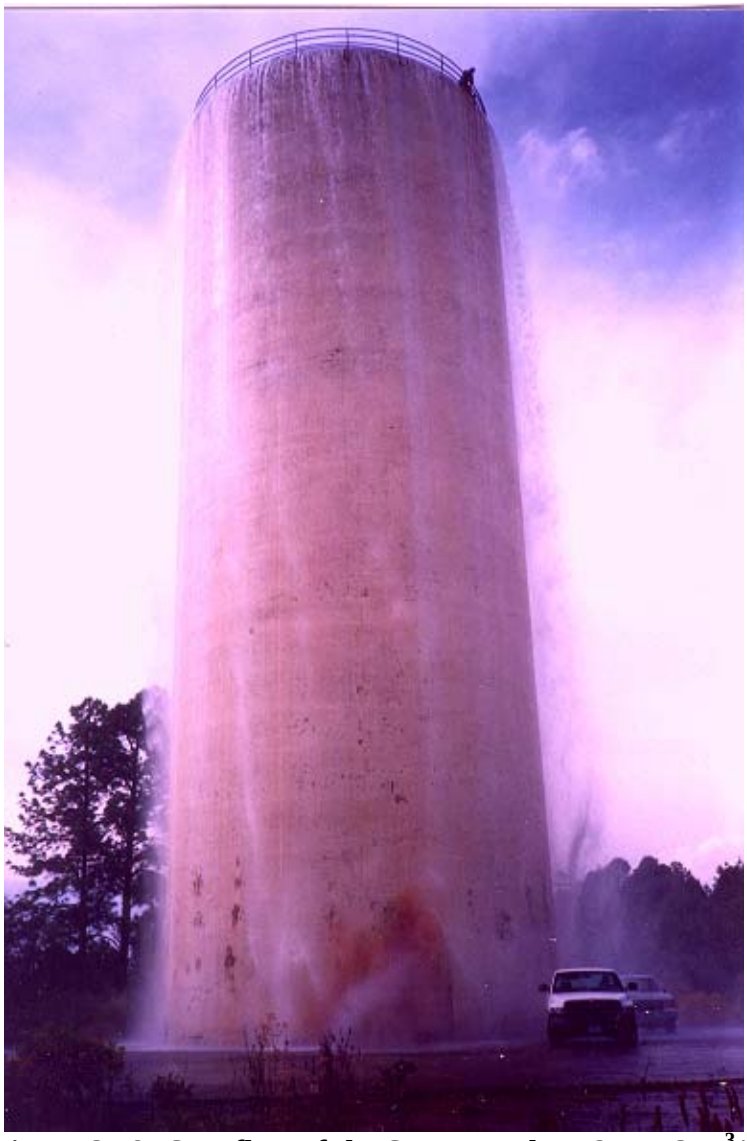

Figure 2.18: Overflow of the Surge Tank 4, Q_w = 12 m^3/s

The first hypothesis formulated was that the Surge Tank 4 spilled, due to the presence of air accumulated at the points 6 and 7, where two vents were located, see Figure 2.19. Therefore, the Institute of Engineering recommended stopping the system to purge all the air entrained and refilling the pipeline to return to the initial condition, as when the system was put in operation the first day. The personal carried out the suggested tasks but the result was not satisfactory and the overflow took place again, when the three pumps were placed into operation in the pumping plants.

Supported on the program AIRE, a second hypothesis was formulated. When the pumping plants performed with two equipments the hydraulic grade line grazed the pipe section between the highest points 6 and 7. Therefore, the vents located at these high points allowed an excessive amount of air entered the line. In addition, the air was slowly moved downstream and collected at the intermediate high point 8 that was not equipped with an air release valve

during the design, as indicated in Figure 2.19. *Colgate* (1966) [13] investigated the sizing criteria for air vent, and found that if the diameter of the vent is small, portions of large air pockets would pass by the vent. To trap all the air it was necessary for the diameter of the vent to be equal to the pipe diameter. Additional studies were done to investigate the size of the vent structure. It was observed that if the air vent diameter was less than the pipe diameter an unsteady flow was established in it, when large quantities of air exited from the vent. This unsteady flow pumped air back into the pipeline. He concluded that the diameter should be at least of one meter.

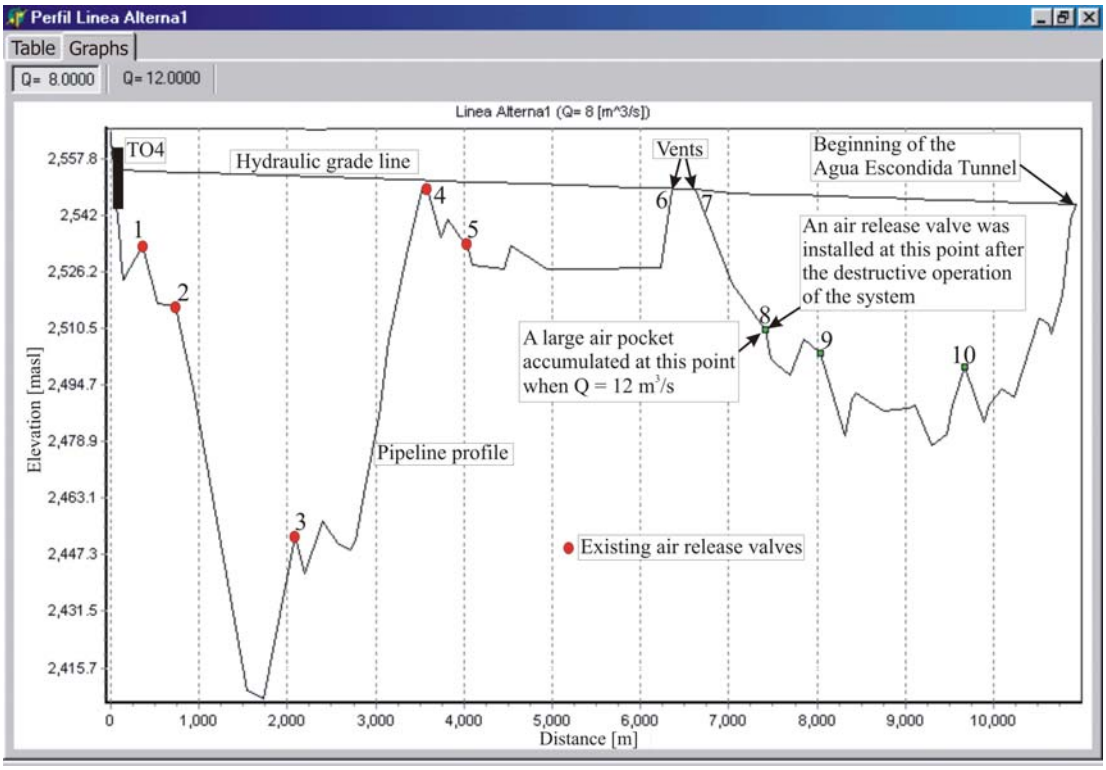

Figure 2.19: Alternative Line, Q_w = 8 m^3/s

When the pumping plants worked with three equipments, the accumulated air at points 6 and 7 was swept downstream, joining to the already existing air at point 8 forming a large air pocket that obstructed the flow and led to the overflow over the ST4. The Institute of Engineering recommended the location of an air release valve at the point 8, which is considered as an intermediate high point for air accumulation. In addition, it can be stated that air is not collected at points 9 and 10, since the air will be built up at point 8 as predicted by equation (2.6). Likewise, it is important to highlight that air did not accumulate in the form of pockets at the points 1 to 5, because air release valves are placed at these locations.

The analysis of the two gravity main pipelines revealed that problems related with entrained air may be gone unnoticed, if the hydraulic structures had not spilled. Likewise, in the case of the Surge Tank 4, if the analysis for partial flow rates had not been made the causes of the overflow might not been known.

In chapters 4 and 5, the linear equation herein presented will be used to analyze the behaviour of air bubbles/pockets, as well as the possibility of accumulation of large air pockets at high and intermediate high points in pumping pipeline systems. Furthermore, the effect of large air pockets located at the summits of pumping pipelines on hydraulic transients will be simulated with a computational program during pump shutdown. In addition, within the next chapter, the investigation developed in an experimental apparatus is presented, where large air pockets at high points of pipelines were studied, with the main aim of measuring the air volume of the pockets.

3 Experimental and theoretical investigation of air pockets located at high points of pipelines

3.1 Introduction

As described by various investigators, air pockets can accumulate at summits of water lines by air entrainment. For the purpose of studying and observing the large air pockets located at high points in pipelines, experimental investigations had been developed in a physical model with the main aim of computing the volumes of air that form the pockets. The hydraulic model investigation was focused on large air pockets located at high points of pressurized conduits for water conveyance also named pumping pipeline systems.

In the first part of the research the water depths underneath the large air pocket at a pressure greater than the atmospheric pressure, as well as for free surface flow were recorded. The experimental results have been compared with the analytical results obtained with the direct step method used in the analysis of gradually varied flow. A method of computation is presented to assess the volume of air of the pockets using some variables that result from the application of the direct step method.

The hydraulic grade line above the conduit at pressurized flow conditions was measured with and without air pocket in the test section to verify the effect of large air pockets and the hydraulic jump on the head losses. The hydraulic model investigation described in this chapter was executed in the laboratory of the Institute of Engineering at the University of Mexico (UNAM).

3.2 Preliminary observations at the test section

Preparatory runs were developed with a water flow rate range from 1.0 to 2.5 l/s to observe the behaviour of the large air pocket located at the transition of slope in the test section. When the model was filled without releasing the air through the valves, it accumulated at the transition of slope. The large air pocket extended in both legs of the test section. At the downward section the pocket ended with a hydraulic jump that sealed the duct. In addition, it was observed that part of the air pocket located at the upstream leg exceeded the length of the test section when the flow rate was lower than 1.3 l/s. In the same way, for flow rates greater than 2.3 l/s the upstream end of the pocket started within the flexible pipe. This made it impossible to measure the beginning of the pocket. Therefore, the flow rate range from 1.3 to

2.3 l/s was selected for the experiments. The photographs in Figures 3.1 and 3.2 show the large air pocket at the upstream and downstream legs, respectively.

The observations confirmed that the large air pocket remains at the transition of slope for the water flow rate range. Hence, the hypothesis formulated was that the water flow underneath the pocket behaved as open channel flow. The test section is equivalent to a pair of connected prismatic channels with the same cross section but with different slopes. At the upstream leg of the experimental apparatus the flow profiles were very similar as the profiles at open channels with adverse, horizontal and mild slope. The control section occurred at the upstream end of the supercritical slope, since the flow in a steep channel has to pass through the critical control section at the upstream end and then follows the S2 profile, see Figure 3.18. The critical depth is, therefore, the control depth.

It has been observed that during the air injection the large air pocket began to grow in the upstream direction of test section, when it reached its total length the pocket continued expanding only in the downstream direction and always ended with a hydraulic jump.

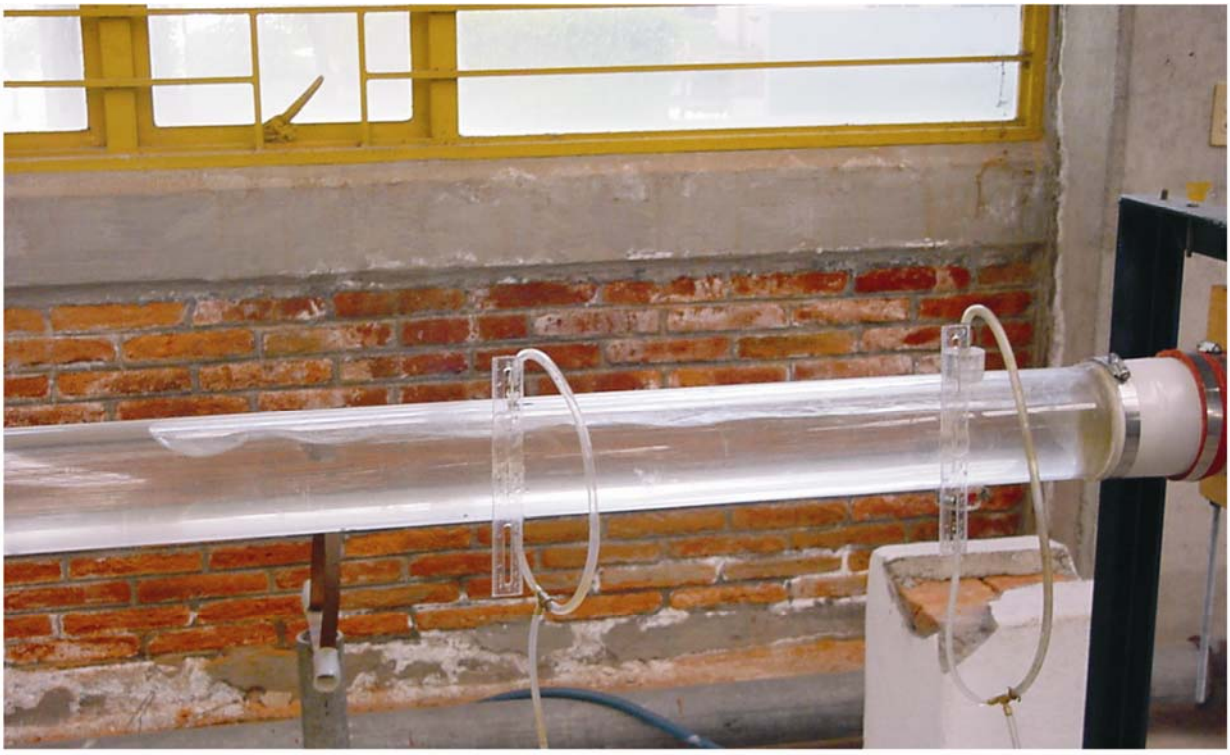

Figure 3.1: Beginning of the large air pocket in the upstream leg

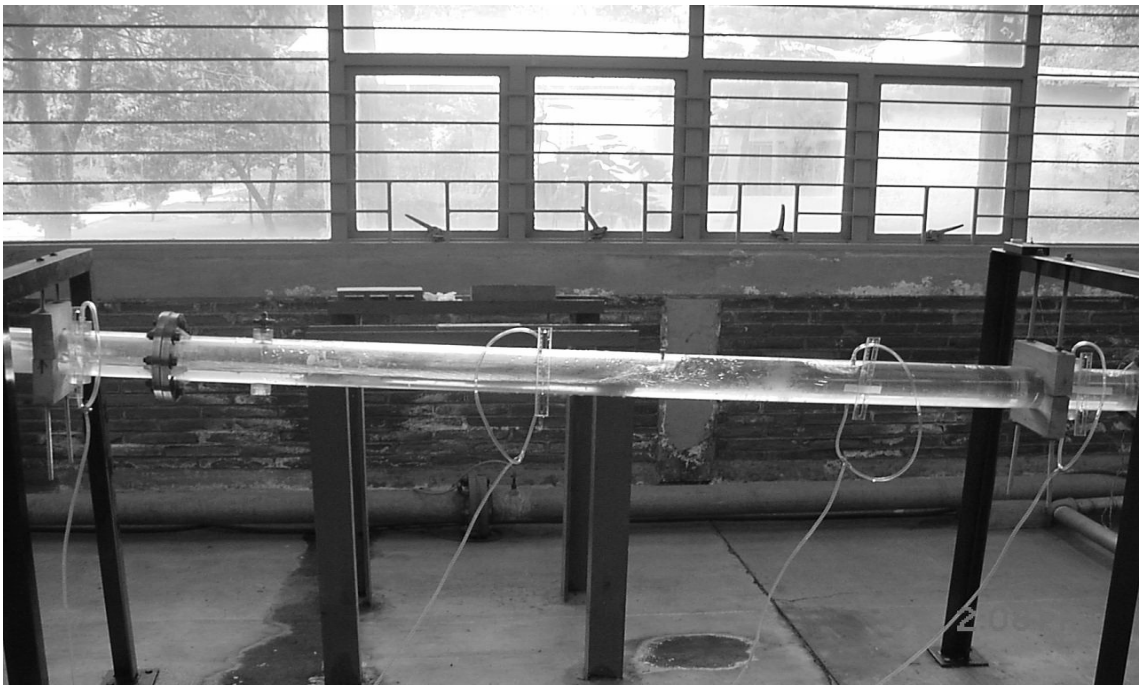

Figure 3.2: Hydraulic jump at the end of the pocket located in the downstream leg

By increasing the water flow rate without varying the volume of entrapped air, the large air pocket moved forward. It was appreciated that the air pocket did not alter its form. When the flow rate was constant and part of the air exhausted, the size of the pocket was reduced only in the downward sloping pipe of the test section and moving the hydraulic jump upstream. Likewise, when more air was injected the pocket only grew at the steep slope. Therefore, it could be concluded that the profile of the large air pocket upstream of the control section does not change its form when the flow rate remained constant and the volume of air was varied. In addition, the length of the large air pockets at the upstream leg of the test section only depends on the water flow rate and the particular critical or control depth. Therefore, the increment of head losses due to the large air pocket accumulated at the transition of slope can be associated to the part of the air pocket distributed at the downward sloping pipe of the test section, as well as the energy dissipated by the hydraulic jump.

3.3 Experimental Apparatus

3.3.1 Description of the Experimental Apparatus

The experimental apparatus was constructed as a re-circulating circuit and designed by using the Froude number, due to the presence of free surface flow. A sketch of the physical model is shown in Figure 3.3.

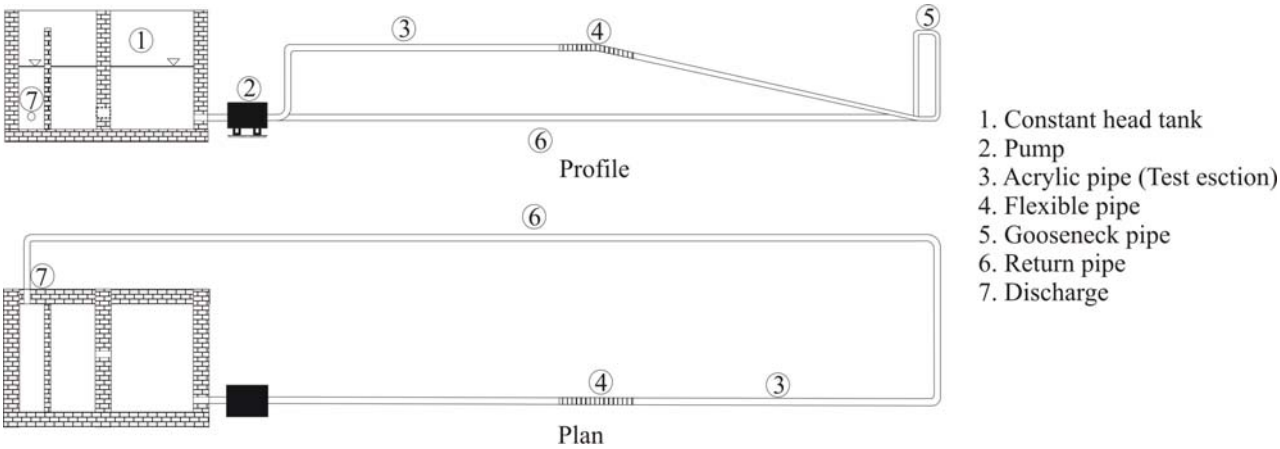

Figure 3.3: Profile and plan of the experimental apparatus

The experimental apparatus is composed of:

1) Constant Head Tank
2) Pump (1 hp)
3) Acrylic Pipe Line (Test section)

1) The dimensions of the constant head tank are 5.0 x 1.1 m at the base and 1.0 m height. The tank is divided in two deposits and interconnected by a pipe of 10 cm to avoid turbulence at the suction of the pump. The temperature of water is neglected.

2) The pump is used to feed the experimental apparatus. The maximum water flow rate that this equipment can pump is 2.5 l/s. The flow is controlled by a ball valve placed downstream of the pump discharge.

3) The test section consisted of a 76.2 mm internal diameter acrylic pipe mounted on metallic frames. It was formed by an upstream pipe of 6.8 m long followed by a flexible pipe with a length of 50 cm and by another pipe section of 6.4 m in length. Both pipe sections could be varied in slope. At the end of the test section, a gooseneck pipe was implemented and connected by a flexible pipe to a galvanized iron pipe of 101.6 mm, by which the water returned to the constant head tank. Photographs of a general view of the test section and the gooseneck pipe are shown in Figures 3.4 and 3.5, respectively.

a)

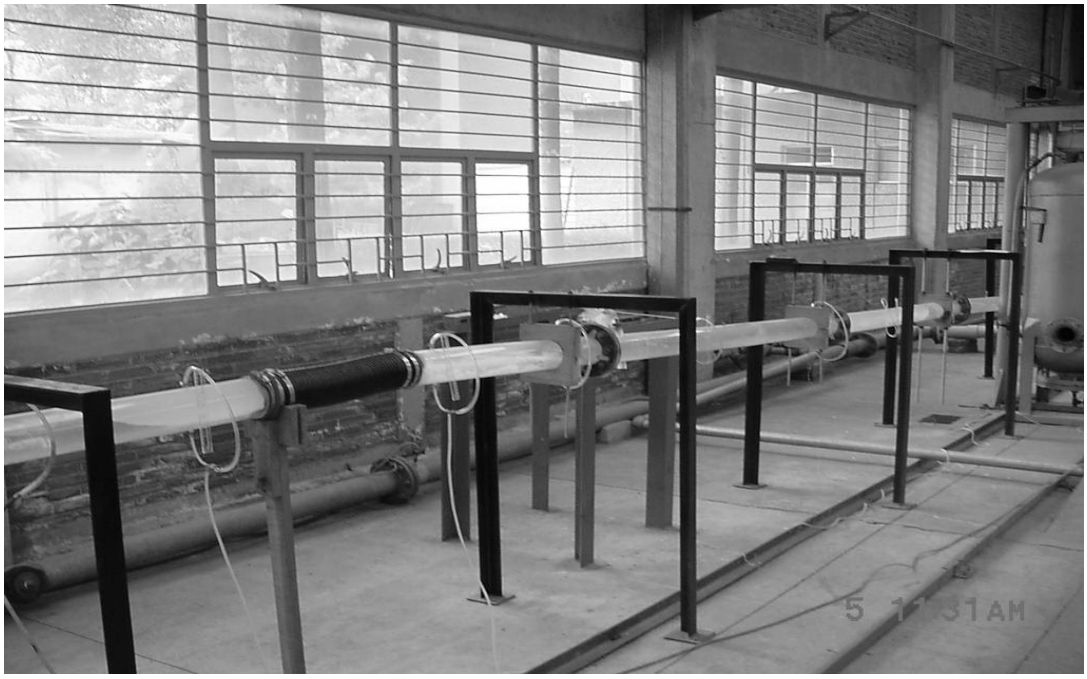

b)

Figure 3.4: Test section of the experimental apparatus: a) upstream leg, b) downstream leg

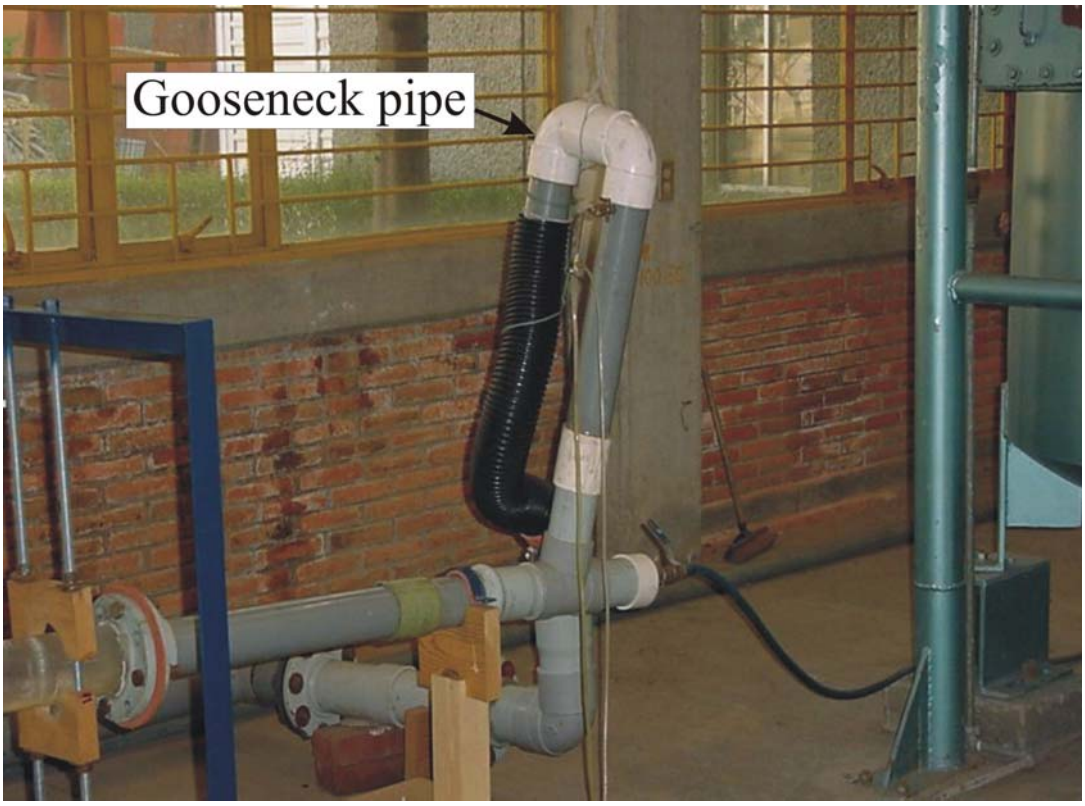

Figure 3.5: Gooseneck pipe made up of grey PVC

3.3.2 Instrumentation of the Experimental Apparatus

An orifice plate was designed according to the Norm ISO/DIS 5167-1 to measure the flow rate ranges between 0 to 2.5 l/s. The plate has a thickness of 2 mm and a concentric orifice with diameter of 19 mm.

Valves were placed throughout the test section allowing air to enter and to exhaust during filling and dewatering operations, as well as to permit the test section to flow as open channel at atmospheric pressure.

A bank of differential manometers connected by plastic tubings to the pressure tapping points placed along the test section was used to measure the variation of the hydraulic grade line above the acrylic line, when a large air pocket is located at the transition of slope in the test section. The pressure tapping points were named measuring stations (E_i). A photograph of the bank of manometers is shown in Figures 3.6, and a sketch of the test section with the measuring stations is presented in Figures 3.7.

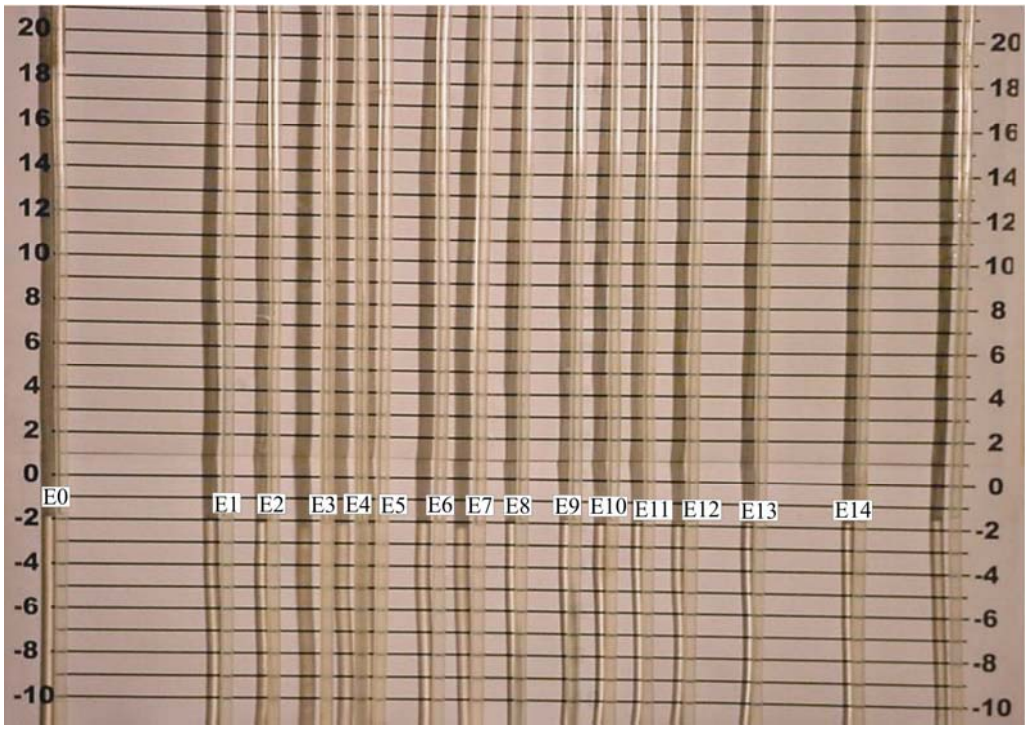

Figure 3.6: Measuring instrument, bank of manometers

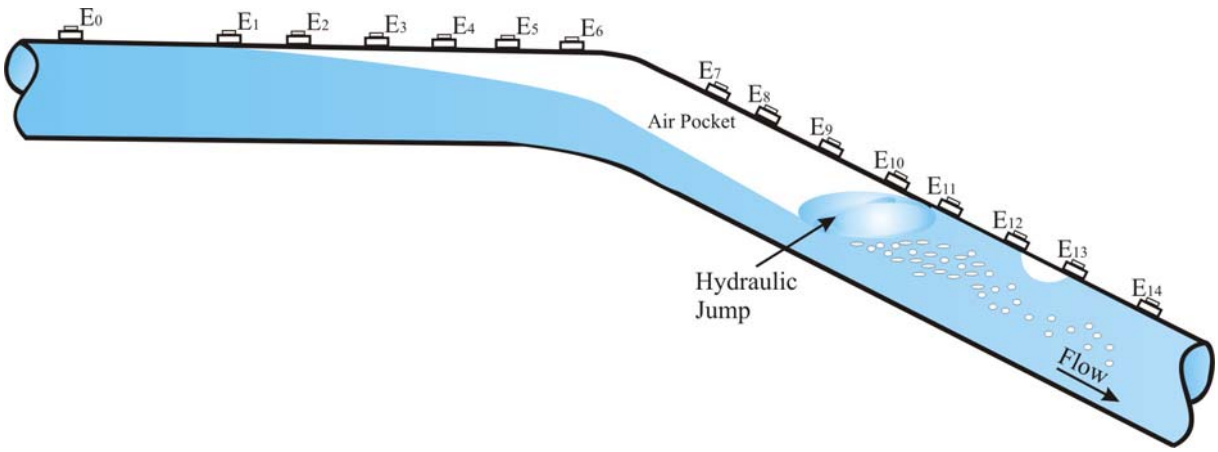

Figure 3.7: Test section with the measuring stations

An open end water manometer was used to measure the total head losses along the test section with and without air pocket, see Figure 3.8. The difference in elevation Δh read directly from the manometer was utilized to compute the friction factor λ of Darcy-Weisbach for each run.

A measuring instrument composed of an acoustic metallic sensor and an electronic sound system connected by a flexible cable was used to measure the depths of water underneath the air pockets through the measuring stations E_i. When the point of the sensor was in contact with the water surface the electronic sound system emitted a whistle, then the measurement was taken. The measuring instrument is shown by a photograph in Figures 3.9 and by a sketch in Figure 3.10.

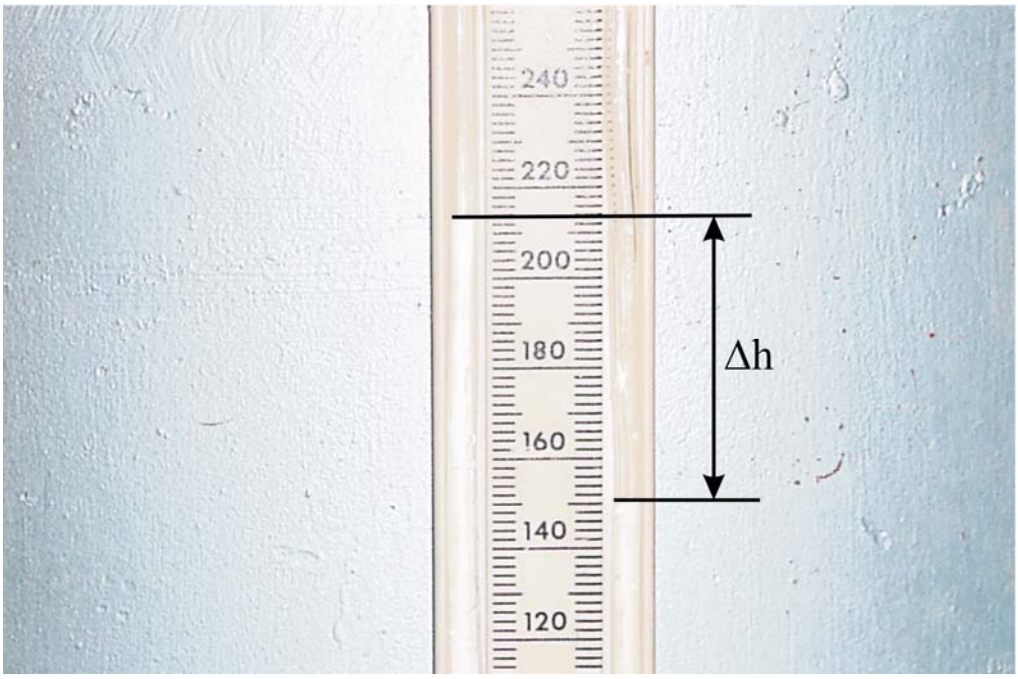

Figure 3.8: Open manometer to measure the difference in elevation Δh

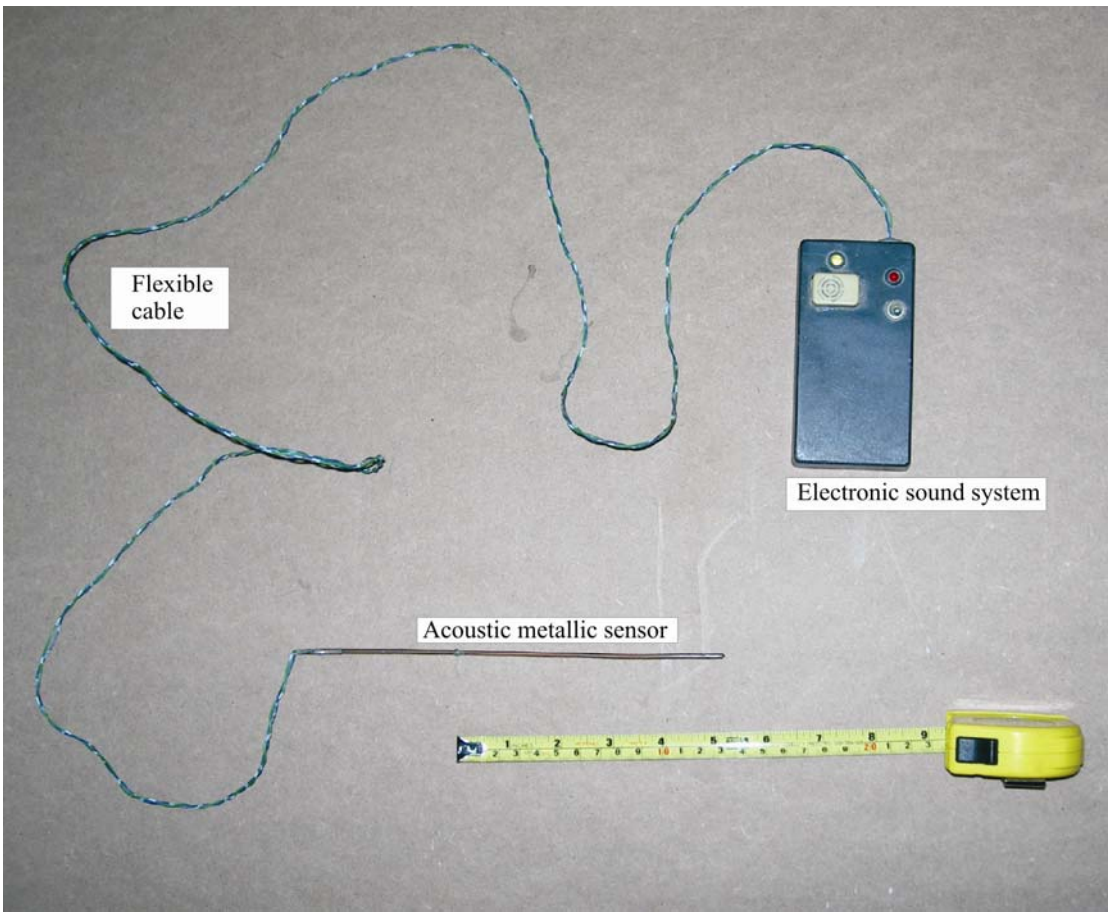

Figure 3.9: Measuring instrument to gage the depths of water

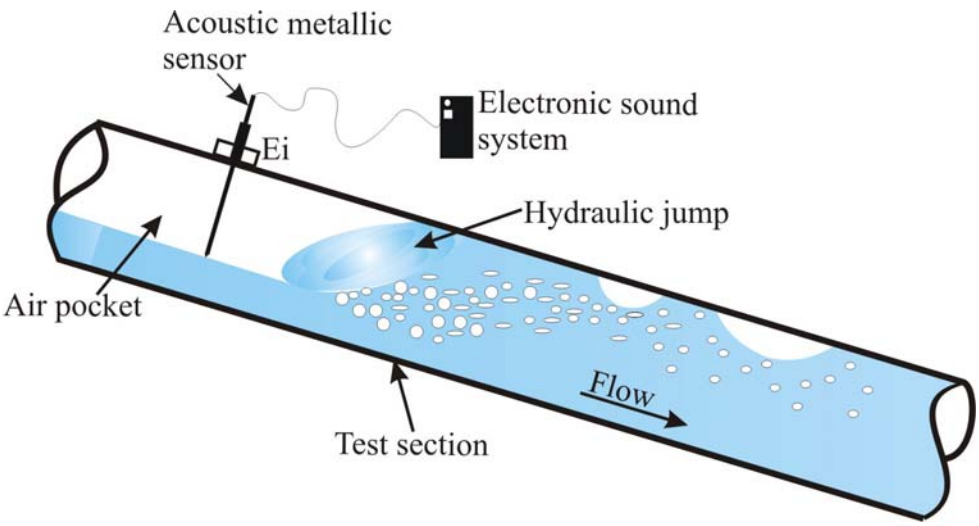

Figure 3.10: Diagrammatic sketch of the measuring instrument

The system to inject air into the test section consisted of a piston made up acrylic with an air capacity of 1 liter, two small valves and plastic tubing allowing to connect the piston to the line. In Figure 3.11 a photograph of the piston is presented.

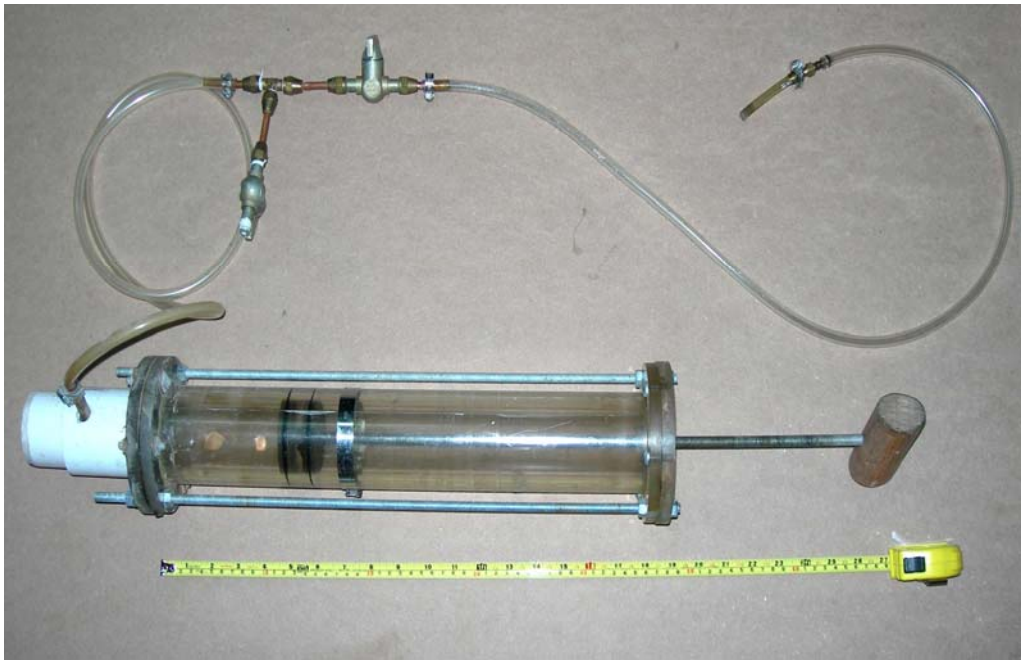

Figure 3.11: Air injection system to introduce air into the test section

3.3.3 Experimental Procedure

In order to simulate different flow profiles underneath large air pockets under pressurized flow conditions, as well as the free surface flow profiles at atmospheric pressure in a circular conduit. Three different experiments have been developed in the physical model. Subsequently, experimental data obtained during the measurements were utilized to compute the shape of the flow profiles in the test section by using the theory of the gradual varied flow to be correlated with the flow profiles obtained experimentally.

The upstream pipe leg of the experimental apparatus was set at three different slopes to reproduce the profiles A2, H2 and M2, S_{01} = - 0.0063, S_{01} = 0.0 and S_{01} = 0.0060, respectively. During the experiments the downward sloping pipe of the test section was kept constant, S_{02} = 0.060.

In each experiment three different tests were developed for a particular water flow rate and two different volumes of air.

Test 1. Pressurized flow conditions at the test section, there was **not accumulated air** at the change of slope. In each run there were four independent variables.

1) D pipe diameter [m]
2) Q_w water flow rate [m^3/s]
3) S_{01} slope of the upstream pipe leg [-]
4) S_{02} slope of the downstream pipe leg [-]

For pressurized flow conditions the hydraulic grade line was measured and observed in the bank of manometers, see Figure 3.12, as well as the difference in elevation Δh in the open end water manometer to compute experimentally the friction factor λ_{exp} by the formula of Darcy-Weisbach, written as

$$\lambda_{exp} = 12.103 \frac{\Delta h}{L_{ts}} \frac{D^5}{Q_w^2} \quad [s^2/m] \qquad (3.1)$$

λ_{exp} experimental friction factor [-]
Δh difference in elevation in the manometer [m]
L_{ts} length of the test section [m]
Q_w water flow rate [m^3/s]
D pipe diameter [m]

The coefficient of Manning n for each run is calculated in terms of the friction factor λ_{exp} by equating (3.1) with the Manning's formula (3.2).

$$Q_w = \frac{AR^{2/3}}{n} \left(\frac{\Delta h}{L_{ts}} \right)^{1/2} \quad [m^3/s] \qquad (3.2)$$

n coefficient of Manning [s/$m^{1/3}$]
A total cross section area of the pipe [m^2]
R hydraulic radius [m]

Solving equations (3.1) and (3.2) for $\Delta h/L_{ts}$ results in a relationship between the friction factors n and λ_{exp}, written as:

$$n = 0.09\lambda_{\exp}^{1/2} D^{1/6} \quad [\mathrm{s/m^{1/3}}] \qquad (3.3)$$

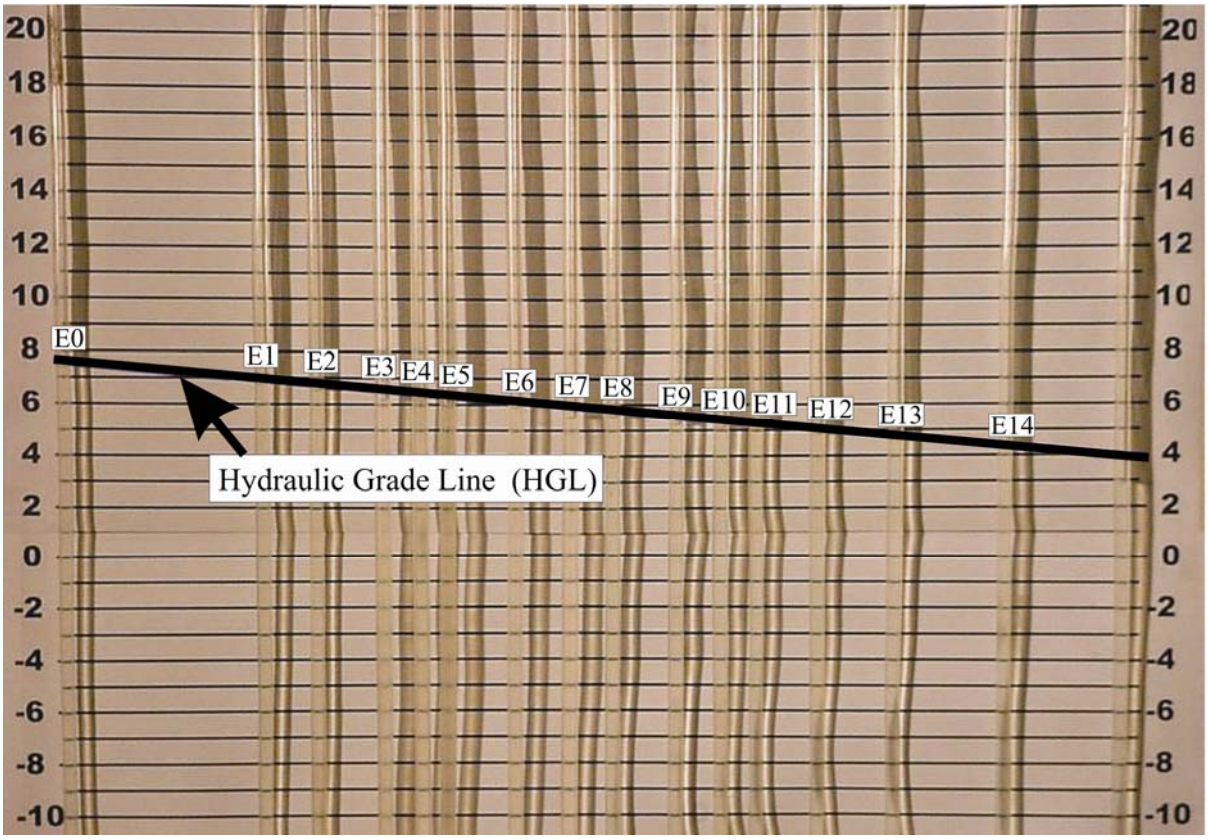

Figure 3.12: Hydraulic grade line for pressurized flow conditions

Test 2. To simulate **the flow profile under pressurized flow conditions, known volumes of air** were injected into the line by a piston at the upstream leg of the test section, while the pipe was flowing full. The air moved to the change of slope forming a large air pocket that remained at the control section. The manometric pressure of the air pocket is equal to the difference between the piezometric head and the elevation of the water surface above the horizontal datum. Likewise, the air entrained by the hydraulic jump coalesced into air bubbles that returned continuously, therefore the volume of air was considered constant during the test. Figures 3.13 and 3.14 show the hydraulic grade line, when a large air pocket is located at the transition of slope in the test section.

For each run there were six independent variables.

1) D pipe diameter [m]
2) Q_w water flow rate [m^3/s]
3) V volume of air [m^3]
4) S_{01} slope of the upstream pipe leg [-]
5) S_{02} slope of the downstream pipe leg [-]
6) L_{pocket} length of the air pocket [m]

The following variables were measured:

a) The hydraulic grade line in the bank of differential manometers

b) The difference in elevation Δh in open end water manometer that represents the head loss along the test section, due to the presence of the large air pocket

c) The air pocket and hydraulic jump length was taken by using a tape measure

d) The water depths under the air pocket were recorded by introducing the acoustic metallic sensor in the line through the orifices at the measuring stations E_i.

For this test two runs were carried out with the same water flow rate and two different volumes of air. The values are tabulated in Table 3.1.

		run 1			**run 2**		
Pipe slope	Type of flow	Q_w [m^3/s]	V_1 [m^3]	V_2 [m^3]	Q_w [m^3/s]	V_1 [m^3]	V_2 [m^3]
Adverse	Subcritical	0.0013	0.010	0.015	0.0017	0.005	0.010
Horizontal	Subcritical	0.0017	0.010	0.015	0.002	0.010	0.015
Mild	Subcritical	0.002	0.010	0.015	0.0023	0.010	0.015

Table 3.1: Water flow rates and volumes of air used in Test 2

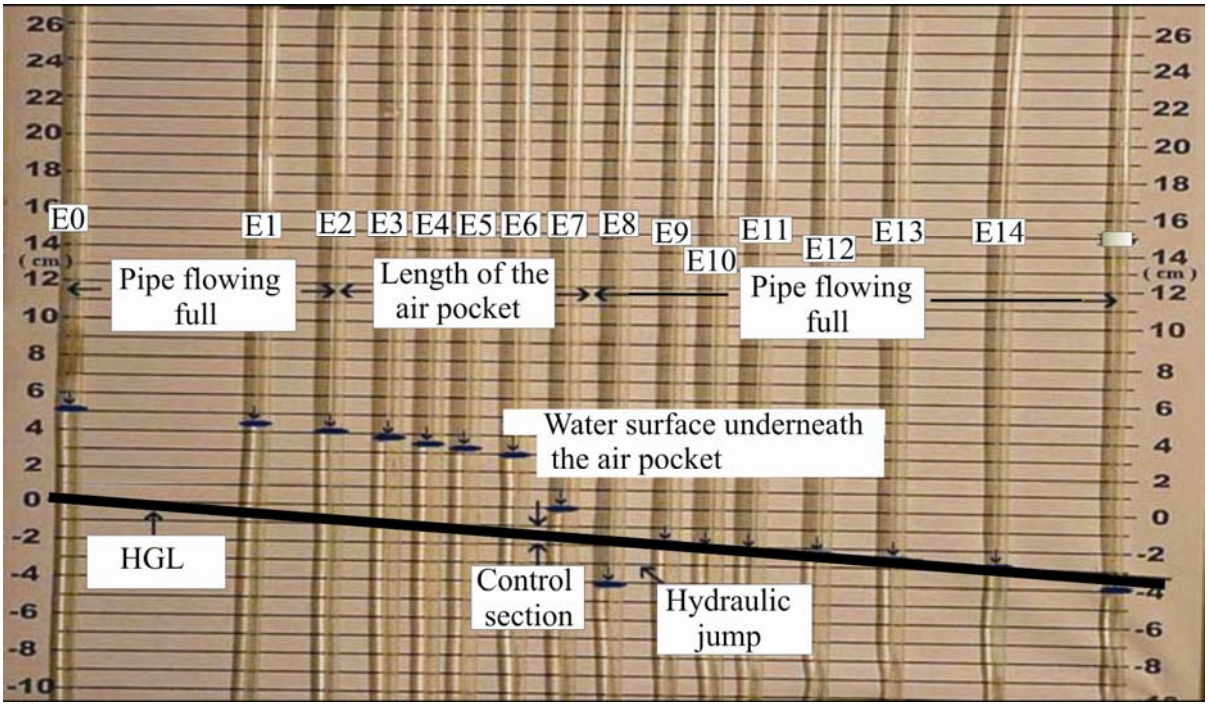

Figure 3.13: Comparison of the HGL with and without air at the transition of slope in the test section

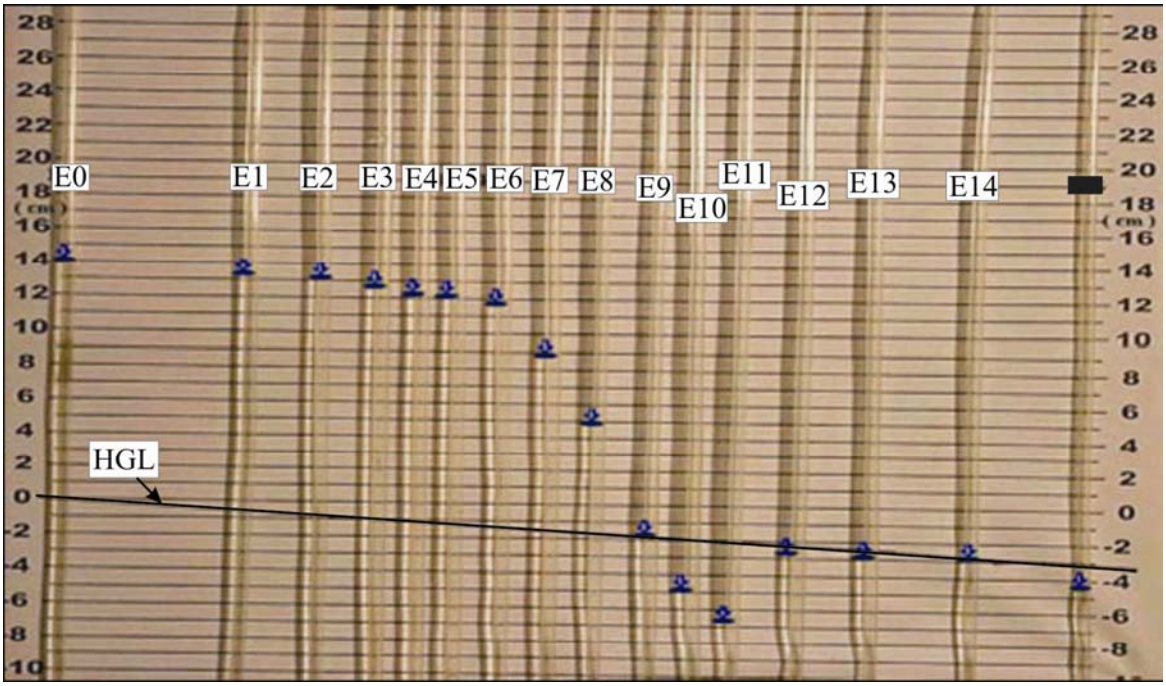

Figure 3.14: Hydraulic grade line with a large air pocket located at the transition of slope in the test section

Test 3. Free surface flow at atmospheric pressure was simulated. The runs were developed in the following manner. The valves located at the test section were opened to permit air entering the line. Likewise, the gooseneck pipe was inclined, and then the hydraulic grade line cut through the test section. The water flow rates and the length of the flow profiles were the same as in the runs of test 2. A sketch of the test section with free surface flow is presented in Figure 3.15.

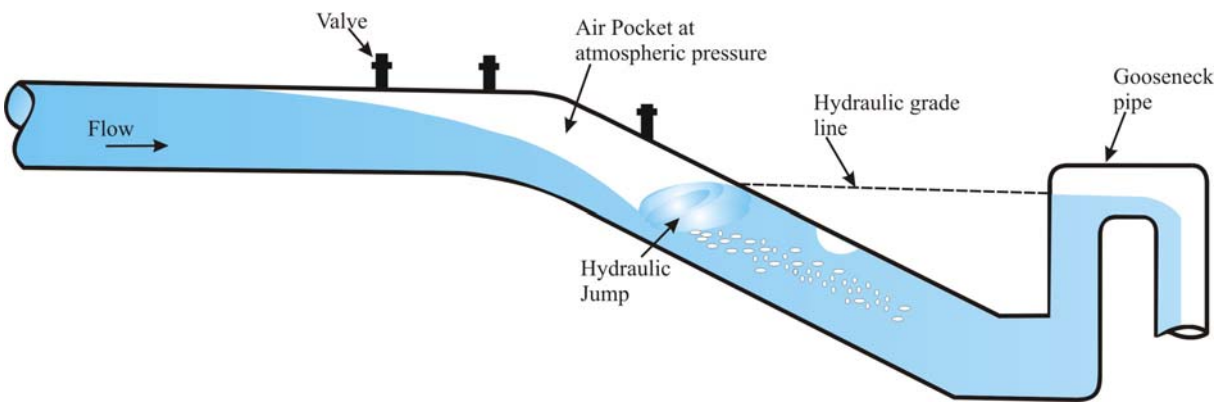

Figure 3.15: Test section with free surface flow at atmospheric pressure

In each run there were six independent variables, namely,

1) D pipe diameter [m]
2) Q_w water flow rate [m^3/s]
3) S_{01} slope of the upstream pipe leg [-]
4) S_{02} slope of the downstream pipe leg [-]
5) $L_{profile\ at\ S01}$ length of the flow profile at the upgrade pipe [m]
6) $L_{profile\ at\ S02}$ length of the flow profile at the downgrade pipe [m]

The following data were recorded:

a) The water depths of the flow profile

b) The length of the two flow profiles upstream and downstream of the control section

The results obtained during the experiments are presented at the end of the chapter.

3.4 Gradually Varied Flow

Gradually varied flow is steady nonuniform flow of a special class. The depth, roughness, channel slope, area, hydraulic radius change very slowly along the channel. The basic assumption required is that the head loss rate at a given section is given by the Manning formula, equation (3.5), *Streeter and Wylie* (1985) [74].

For a given water flow rate and channel conditions the normal depth Y_n and the critical depth Y_c lines divide the space in a channel into three zones, *Chow* (1981) [11]:

Zone 1: The space above the upper line
Zone 2: The space between the two lines
Zone 3: The space below the lower line

The flow profiles are classified according to the nature of the channel slope and the zone in which the flow surface lies. These types are designated as **A2**, **A3**; **H2**, **H3**; **M1**, **M2**, **M3**; **C1**, **C2**, **C3**; **S1**, **S2**, **S3**; where the letters describe the slope: **A** for adverse slope, **H** for horizontal, **M** for mild (subcritical), **C** for critical, **S** for steep (supercritical); and where the numeral represents the zone number. The flow profiles are shown in Figure 3.16.

3.4.1 Computation of the flow profiles

The dynamic equation of gradually varied flow was used to obtain the various flow profiles observed during the experimental work, *Chow* (1981) [11].

$$\Delta x = \frac{E_2 - E_1}{S - S_f} \quad \text{[m]} \qquad (3.4)$$

Δx length of the reach [m]
E_1 specific energy at the upstream end of the pipe reach [m]
E_2 specific energy at the downstream end of the pipe reach [m]
S pipe slope [-]
S_f friction slope [-]

$$S_f = \left(\frac{n\ v}{R^{2/3}} \right)^2 \quad [-] \qquad (3.5)$$

n coefficient of Manning [s/m$^{1/3}$]
v water velocity in the pipe [m/s]
R hydraulic radius [m]

The sketch in Figure 3.17 shows the details of the terminology used.

The main purpose of this computation is to verify that the flow profiles under the large air pockets accumulated at the break of slope in the circular conduit can be reproduced by the dynamic equation of gradually varied flow. The direct step method was applied to compute the flow profile, due to its easy applicability to prismatic channels. The step methods are characterized by dividing the channel into short reaches and carrying the computation step by step from one end of the reach to the other.

At the end of the chapter, the flow profiles computed in this section are compared with the shape of the water surfaces obtained in test 2 and test 3.

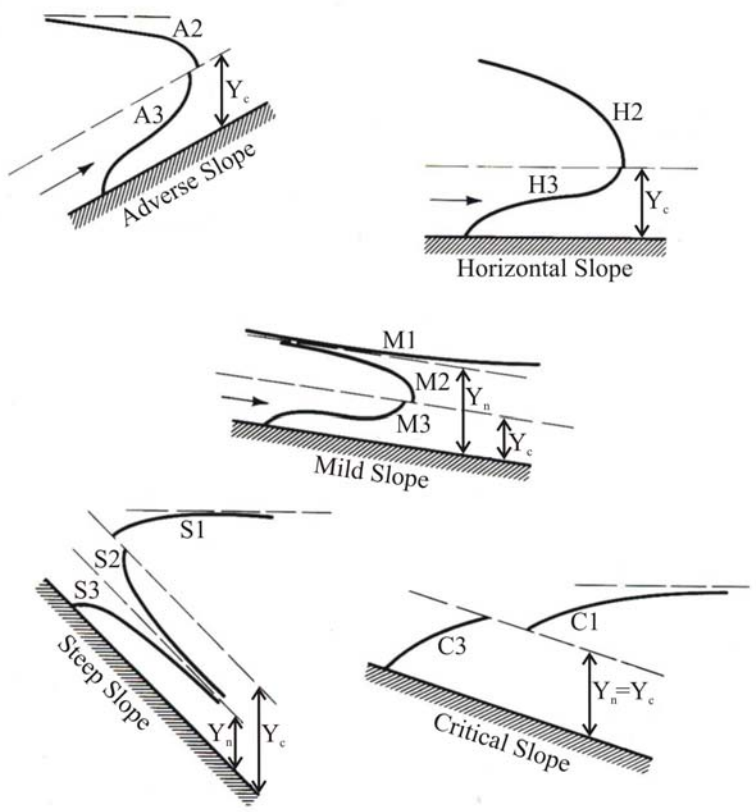

Y_c critical depth [m]
Y_n normal depth [m]

Figure 3.16 Classification of flow profiles of gradually varied flow (after Streeter and Wylie, 1985)

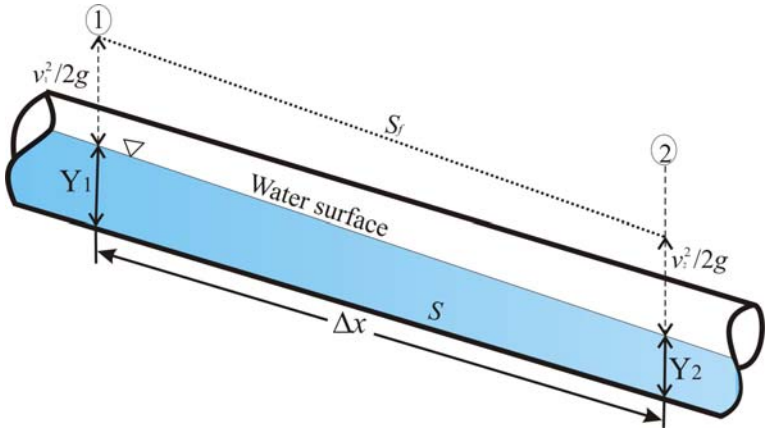

$v_1^2/2g$ velocity head at the upstream end of the pipe reach [m]

$v_2^2/2g$ velocity head at the upstream end of the pipe reach [m]

Y_1 water depth at the upstream end of the pipe reach [m]

Y_2 water depth at the downstream end of the pipe reach [m]

Figure 3.17: Pipe reach for the derivation of the direct step method

3.4.2 Computational algorithm

With the data obtained during the experimental work the flow profiles were computed. For simplicity, the water depth at the transition of the slope is the critical depth. For each run in test 2 the critical depths resulted lower than the water depths measured at the upstream leg of the test section, therefore the type of flow is subcritical. In addition, the normal depths were lower at the downgrade pipe, hence a supercritical profile S2 present.

The flow profiles at the upstream pipe of the test section were computed in the upward direction until the estimated level agreed with the inner diameter of the pipe. Likewise, the profile S2 was assessed in downstream direction until when the depth approaches the normal depth. The computation of the flow profile by the direct step method is shown in table 3.2.

1	*2*	*3*	*4*	*5*	*6*	*7*	*8*	*9*	*10*	*11*	*12*	*13*
Yi [m]	***A* [m^2]**	***R* [m]**	***R*$^{2/3}$ [m]**	***v* [m/s]**	***v*^{2}/2g [m]**	***E* [m]**	**Δ*E* [m]**	***S*$_f$**	***S*$_{fi}$**	***S* - *S*$_{fi}$**	**Δ*x* [m]**	**ΣΔ*x* [m]**
0,0366	0,0022	0,0186	0,0700	0,6002	0,0184	0,0550	----	0,0060	----	----	0,0000	0,0000
0,0406	0,0025	0,0198	0,0731	0,5268	0,0141	0,0547	0,0003	0,0042	0,0051	0,0114	0,0223	0,0223
0,0445	0,0028	0,0209	0,0757	0,4698	0,0112	0,0558	0,0011	0,0031	0,0037	0,0100	0,1067	0,0843
0,0485	0,0031	0,0218	0,0778	0,4247	0,0092	0,0577	0,0019	0,0024	0,0028	0,0091	0,2098	0,2941
0,0524	0,0033	0,0224	0,0795	0,3885	0,0077	0,0601	0,0025	0,0019	0,0022	0,0085	0,2903	0,5844

Table 3.2: Flow profile A2 estimated by the direct step method

The steps to calculate the shape of the water surface in the test section are explained as follows, *Chow* (1981) [11]:

Column 1. Depth of flow [m]
Column 2. Water area corresponding to the depth Y in column 1 [m^2]
Column 3. Hydraulic radius corresponding to Y in column 1 [m]
Column 4. Two thirds power of the hydraulic radius [$m^{2/3}$]
Column 5. Mean flow velocity [m]
Column 6. Velocity head [m]
Column 7. Specific energy obtained by adding the depth of flow in column 1 to the velocity head in column 6 [m]
Column 8. Change of specific energy, equal to the difference between the *E* value in column 7 and that of the previous step [m]
Column 9. Friction slope computed by equation (3.5)
Column 10. Average friction slope between the steps, equal to the arithmetic mean of the friction slope just computed in column 9 and that of the previous step
Column 11. Difference between the pipe slope and the average friction slope
Column 12. Length of the reach between the consecutive steps, computed by dividing the value of ΔE in column 8 by the value in column 11 [m]
Column 13. Distance of the flow profile, it is equal to the cumulative sum of the values in column 12 computed for previous steps [m]

The flow profiles evaluated by the direct step method are illustrated in Fig 3.18 through 3.20

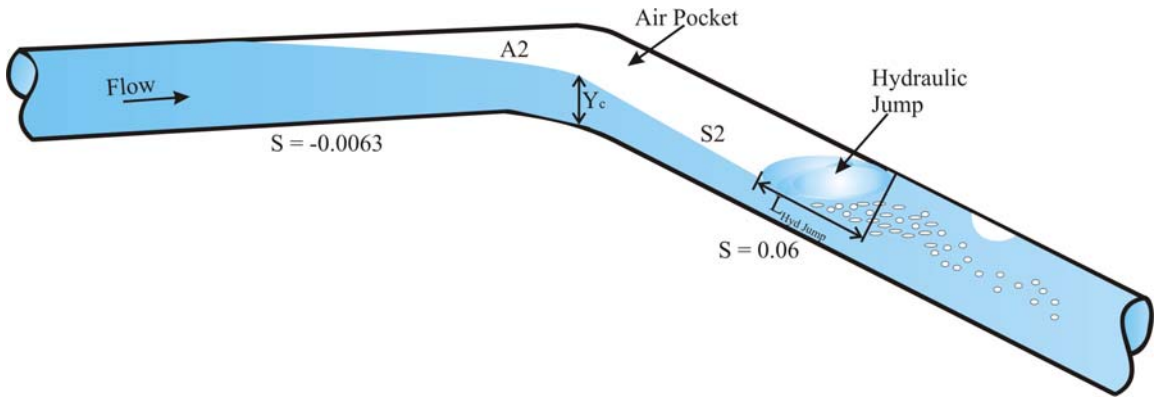

$L_{Hyd\ Jump}$ length of the hydraulic jump [m]

Figure 3.18: Flow profiles A2 and S2

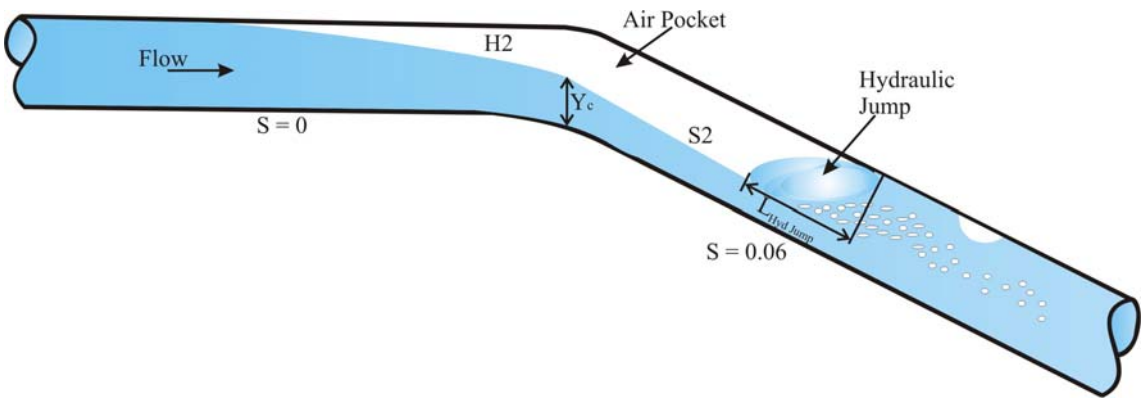

Figure 3.19: Flow profiles H2 and S2

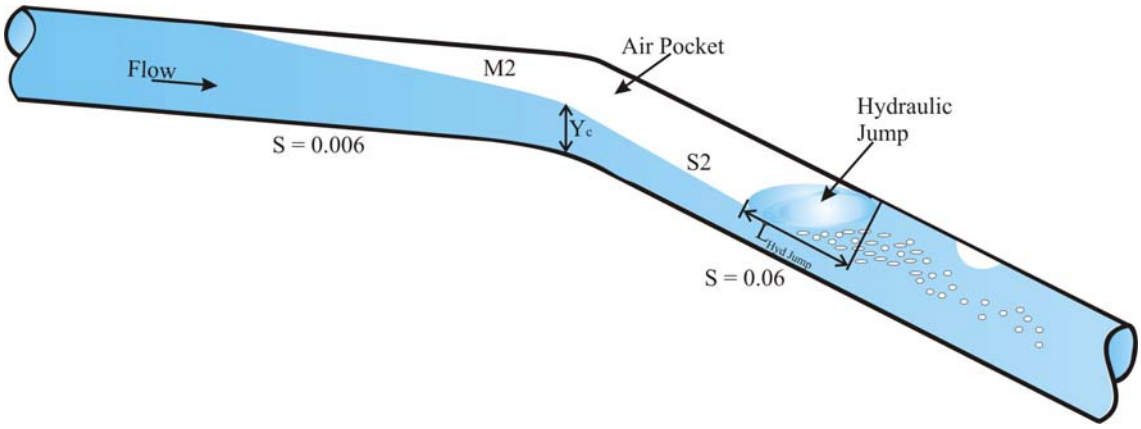

Figure 3.20: Flow profiles M2 and S2

3.5 Computation of the volume of air

As described before, air bubbles entrapped in water lines tend to join together to form large air pockets at the intermediate and high points. During the experimental work the volumes of air injected were known. In addition, Boyle´s law was used to assess the volume of air accumulated in the pockets during test 2. Boyle´s law states that the volume of a definite quantity of gas is inversely proportional to its pressure provided the temperature remains constant. The working form of the equation used to predict the changes in the volume of air due to pressure variation in the test section of the experimental apparatus can be written as

$$V_1P_1 = V_2P_2 \quad [m^4] \qquad (3.6)$$

V_1 volume of air injected in the line at atmospheric pressure [m^3]
V_2 volume of air in the test section during test 2 [m^3]
P_1 atmospheric pressure in Mexico City, equal to 8.03 [mH_2O]
P_2 absolute pressure of the air pocket during test 2 [mH_2O]

This relationship indicates that any pressure-volume product equals any other so long as temperature is constant. Three of the four variables must be known.

The volumes of air in the pockets were also estimated by applying the water areas and the lengths of the pipe reaches obtained with the direct step method, the equation utilized is

$$V_{1,2} = \left[A - \frac{A_1 + A_2}{2} \right] \Delta x_{1,2} \quad [m^3] \qquad (3.7)$$

$V_{1,2}$ volume of air at the pipe reach [m^3]
A total cross section area of the pipe [m^2]
A_1 water area at the upstream end of the pipe reach [m^2]
A_2 water area at the downstream end of the pipe reach [m^2]
$\Delta x_{1,2}$ length of the pipe reach [m]

The sketch in Figure 3.21 shows the details of the terminology used in equation (3.7).

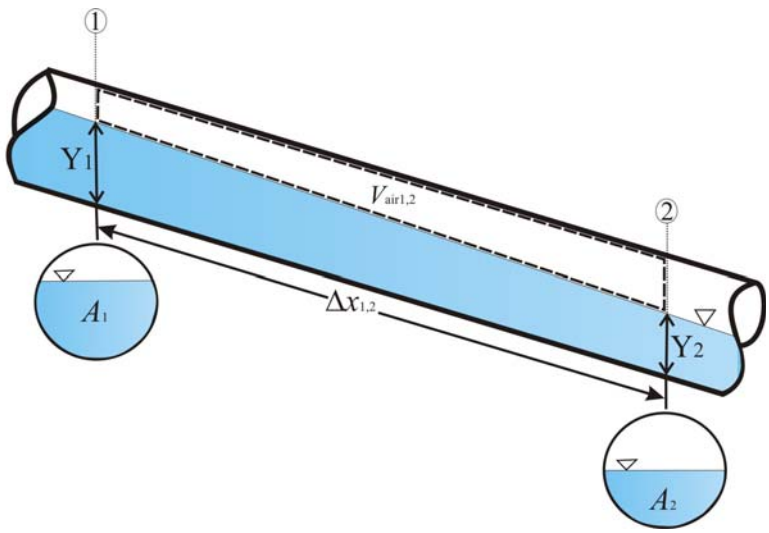

Figure 3.21: Volume of air in a pipe reach

It can be observed that the values obtained by using equation (3.6) are greater than the volumes of air computed with equation (3.7). It is because the volume of air above the surface roller of the hydraulic jump, having a length of $L_{Hyd\ Jump}$, is not taken into account in equation (3.7), see Figure 3.18 to 3.20. In addition, the pipe reaches used for the calculations are not small enough to obtain a better approximation of the volume of air. The values obtained by utilizing both equations are summarized in Tables 3.3 a), b) through 3.8 a), b).

For practical application, it is recommended to start computing the volume of the air pocket upstream of the control section, V_{Up}. This volume of air will remain constant, because as it has been observed in laboratory the air pocket grew in the upstream direction of the test section, when it reached its total length, the pocket continues growing only in the downstream direction. Downstream of the critical depth, different values of air pocket volumes V_{Down} can be computed if the cumulative sum of the length of each reach between the consecutive steps is considered as the distance of the flow profile, and also assuming that at the end of the air pocket a hydraulic jump occurs. The last value of air volume will be obtained when the water depth approaches the normal depth. The total air volume contained in the pocket will be the sum of V_{Up} and V_{Down}.

Figure 3.22 shows the details of the terminology described previously.

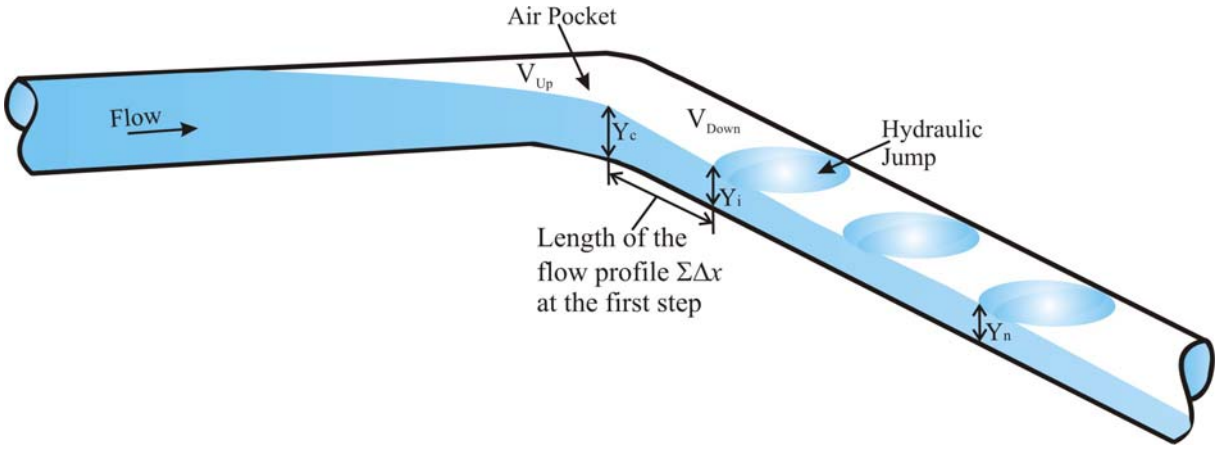

V_{Up} volume of the air pocket upstream of the control section [m^3]
V_{Down} volume of the air pocket downstream of the control section [m^3]

Figure 3.22: Volumes of the stationary air pockets

As it has been mentioned, the experimental work was focused on large air pockets located at high points of pipeline systems. Therefore, it can be stated that the volumes of air estimated with the variables obtained by using the direct step method increase the factor of safety in designing pipelines, because it has been found that small air pockets located at intermediate and high points can enhance the magnitude of surge pressures experienced by a sudden or routine pump shutdown. It could have serious implications, if entrained air is not accounted for during the design of pumping pipeline systems. Borrows and Qiu (1995) [9]; Qiu and Borrows (1996) [60]; Borrows (2003) [8].

In the next chapter, the effect of air pockets on surge pressure experienced by pumping pipeline systems is studied by using the method of the characteristics, as well as the equation (2.6) presented in chapter 2 and the direct step method to compute the volumes of air in the pockets.

3.6 Analysis of results

The comparison between experimental and analytical air pockets profiles yields interesting results. The flow profile underneath the air pocket, as computed by the dynamic equation of the gradually varied flow, shows excellent correlation with the flow profiles determined experimentally as presented in the computed curves in Figure 3.23 to Figure 3.34. In addition, tables 3.3 a), b) to 3.8 a), b) present the measurements made during the hydraulic model investigation, as well as Tables 3.3 c) to 3.8 c) tabulate the results obtained by applying the dynamic equation of the gradually varied flow.

For the same water flow rate, the hydraulic grade line measured and observed immediately downstream of the hydraulic jump in test 2 is very similar to the hydraulic grade line in test 1. The transformation of the kinetic energy of water upstream of the hydraulic jump to pressure immediately downstream of the jump, returned the hydraulic grade line to its original value as in test 1.

In the length occupied by the large air pockets the hydraulic grade lines are parallel to the water surface. The data recorded permitted to verify that the pressure throughout the air pocket was uniform, because the pressure variations are negligible in a gas.

With the measurements taken during test 2, it was possible to verify that the elevation of the hydraulic grade line with respect to the grade line of test 1 corresponded to the additional head losses, due to the reduction of the effective pipe cross section, as well as the energy dissipated by the hydraulic jump.

run 1	Q, [m³/s]	V [m³]	S_{01}	S_{02}	
	0,0013	0,01	-0,0063	0,06	
			Water Depths		Air pocket
Measuring Stations	HGL [m] Test 1	HGL [m] Test 2	Yi [m] Test 2	Yi [m] Test 3	pressure [mH2O]
E_0	0,705	0,767	0,0762	0,0762	
E_1	0,703	0,764	0,0762	0,0762	
E_2	0,701	0,763	0,0762	0,0762	
E_3	0,699	0,759	**0,0644**	**0,0640**	**0,313**
E_4	0,699	0,757	**0,0569**	**0,0570**	**0,317**
E_5	0,699	0,754	**0,0504**	**0,0500**	**0,320**
E_6	0,699	0,750	**0,0409**	**0,0400**	**0,324**
E_7	0,694	0,713	**0,0309**	**0,0320**	**0,326**
E_8	0,693	0,679	**0,0179**	**0,0190**	**0,342**
E_9	0,693	0,693	0,0762	0,0762	
E_{10}	0,694	0,694	0,0762	0,0762	
E_{11}	0,694	0,694	0,0762	0,0762	
E_{12}	0,694	0,693	0,0762	0,0762	
E_{13}	0,688	0,689	0,0762	0,0762	
E_{14}	0,691	0,692	0,0762	0,0762	
Δh [cm]	2,10	8,20			
				Volume of air [m³]	
				Test 2	
Length of the flow profiles		$L_{Hyd\ Jump}$		0.010	
Test 2 and Test 3 [m]		**[cm]**		**Boyle´s Law**	
Profile A2	**Profile S2**	24		0,0096	
2,875	1,385			**Gradually Varied Flow**	
				0,0076	
				% Error Boyle´s law vs GVF	
				20,92	

a)

run 2	Q, [m³/s]	V [m³]	S_{01}	S_{02}	
	0,0013	0,015	-0,0063	0,06	
			Water Depths		Air pocket
Measuring Stations	HGL [m] Test 1	HGL [m] Test 2	Yi [m] Test 2	Yi [m] Test 3	pressure [mH2O]
E_0	0,705	0,830	0,0762	0,0762	
E_1	0,703	0,826	0,0762	0,0762	
E_2	0,701	0,825	0,0762	0,0762	
E_3	0,699	0,821	**0,0639**	**0,0640**	**0,376**
E_4	0,699	0,819	**0,0579**	**0,0580**	**0,378**
E_5	0,699	0,817	**0,0509**	**0,0500**	**0,382**
E_6	0,699	0,811	**0,0409**	**0,0400**	**0,385**
E_7	0,694	0,774	**0,0309**	**0,0310**	**0,387**
E_8	0,693	0,737	**0,0224**	**0,0230**	**0,396**
E_9	0,693	0,678	**0,0179**	**0,0190**	**0,390**
E_{10}	0,694	0,668	0,0762	0,0762	
E_{11}	0,694	0,694	0,0762	0,0762	
E_{12}	0,694	0,693	0,0762	0,0762	
E_{13}	0,688	0,694	0,0762	0,0762	
E_{14}	0,691	0,692	0,0762	0,0762	
Δh [cm]	2,10	14,60			
				Volume of air [m³]	
				Test 2	
Length of the flow profiles		$L_{Hyd\ Jump}$		0.015	
Test 2 and Test 3 [m]		**[cm]**		**Boyle´s Law**	
Profile A2	**Profile S2**	22		0,0143	
2,875	2,515			**Gradually Varied Flow**	
				0,012	
				% Error Boyle´s law vs GVF	
				18,80	

b)

Table 3.3: Experimental results for a 76.2 mm diameter acrylic pipe, profiles A2 and S2

S_{01} =	-0,0063	n =	0,0091									
Q, [m³/s] =	0,0013	$\lambda_{m\Sigma}$ =	0,0240									
Profile A2												
Yi [m]	***A* [m²]**	***R* [m]**	**$R^{2/3}$ [m]**	***v* [m/s]**	**$v^2/2g$ [m]**	***E* [m]**	**Δ*E* [m]**	S_f	S_{fs}	$S - S_{fs}$	**Δ*x* [m]**	**ΣΔ*x* [m]**
0,0366	0,002	0,019	0,070	0,600	0,0184	0,0550	----	0,0061	----	----	0	0
0,0406	0,002	0,020	0,073	0,527	0,0141	0,0547	-0,0003	0,0043	0,0052	-0,0115	0,0221	0,0221
0,0445	0,003	0,021	0,076	0,470	0,0112	0,0558	0,0011	0,0032	0,0037	-0,0100	-0,1058	-0,0837
0,0485	0,003	0,022	0,078	0,425	0,0092	0,0577	0,0019	0,0025	0,0028	-0,0091	-0,2083	-0,2920
0,0524	0,003	0,022	0,079	0,388	0,0077	0,0601	0,0025	0,0020	0,0022	-0,0085	-0,2886	-0,5806
0,0564	0,004	0,023	0,081	0,359	0,0066	0,0630	0,0028	0,0016	0,0018	-0,0081	-0,3508	-0,9314
0,0604	0,004	0,023	0,081	0,336	0,0057	0,0661	0,0031	0,0014	0,0015	-0,0078	-0,3987	-1,3301
0,0643	0,004	0,023	0,081	0,317	0,0051	0,0694	0,0033	0,0013	0,0013	-0,0076	-0,4357	-1,7659
0,0683	0,004	0,023	0,080	0,302	0,0046	0,0729	0,0035	0,0012	0,0012	-0,0075	-0,4645	-2,2303
0,0722	0,004	0,022	0,078	0,291	0,0043	0,0766	0,0036	0,0011	0,0012	-0,0075	-0,4869	-2,7172
0,0762	0,005	0,019	0,071	0,285	0,0041	0,0803	0,0038	0,0013	0,0012	-0,0075	-0,5030	-3,2202

S_{02} =	0,06	n =	0,0091									
Q, [m³/s] =	0,0013	$\lambda_{m\Sigma}$ =	0,0240									
Profile S2												
Yi [m]	***A* [m²]**	***R* [m]**	**$R^{2/3}$ [m]**	***v* [m/s]**	**$v^2/2g$ [m]**	***E* [m]**	**Δ*E* [m]**	S_f	S_{fs}	$S - S_{fs}$	**Δ*x* [m]**	**ΣΔ*x* [m]**
0,0366	0,0022	0,0186	0,0700	0,6002	0,0184	0,0550	----	0,0061	----	----	0	0
0,0349	0,0020	0,0180	0,0686	0,6376	0,0207	0,0557	0,0007	0,0072	0,0066	0,0534	0,0129	0,0129
0,0333	0,0019	0,0174	0,0670	0,6798	0,0236	0,0568	0,0012	0,0085	0,0078	0,0522	0,0223	0,0352
0,0316	0,0018	0,0168	0,0654	0,7277	0,0270	0,0586	0,0018	0,0103	0,0094	0,0506	0,0349	0,0701
0,0299	0,0017	0,0161	0,0637	0,7823	0,0312	0,0611	0,0025	0,0125	0,0114	0,0486	0,0522	0,1223
0,0283	0,0015	0,0154	0,0619	0,8452	0,0364	0,0647	0,0035	0,0155	0,0140	0,0460	0,0771	0,1993
0,0266	0,0014	0,0147	0,0599	0,9181	0,0430	0,0695	0,0049	0,0194	0,0174	0,0426	0,1147	0,3141
0,0249	0,0013	0,0140	0,0579	1,0034	0,0513	0,0762	0,0067	0,0249	0,0221	0,0379	0,1766	0,4906
0,0232	0,0012	0,0132	0,0558	1,1043	0,0622	0,0854	0,0092	0,0325	0,0287	0,0313	0,2923	0,7829
0,0216	0,0011	0,0124	0,0535	1,2249	0,0765	0,0980	0,0127	0,0434	0,0379	0,0221	0,5725	1,3555
0,0199	0,0009	0,0116	0,0512	1,3712	0,0958	0,1157	0,0177	0,0595	0,0514	0,0086	2,0623	3,4178

Table 3.3 c): Computation of the flow profiles A2 and S2 by the direct step method

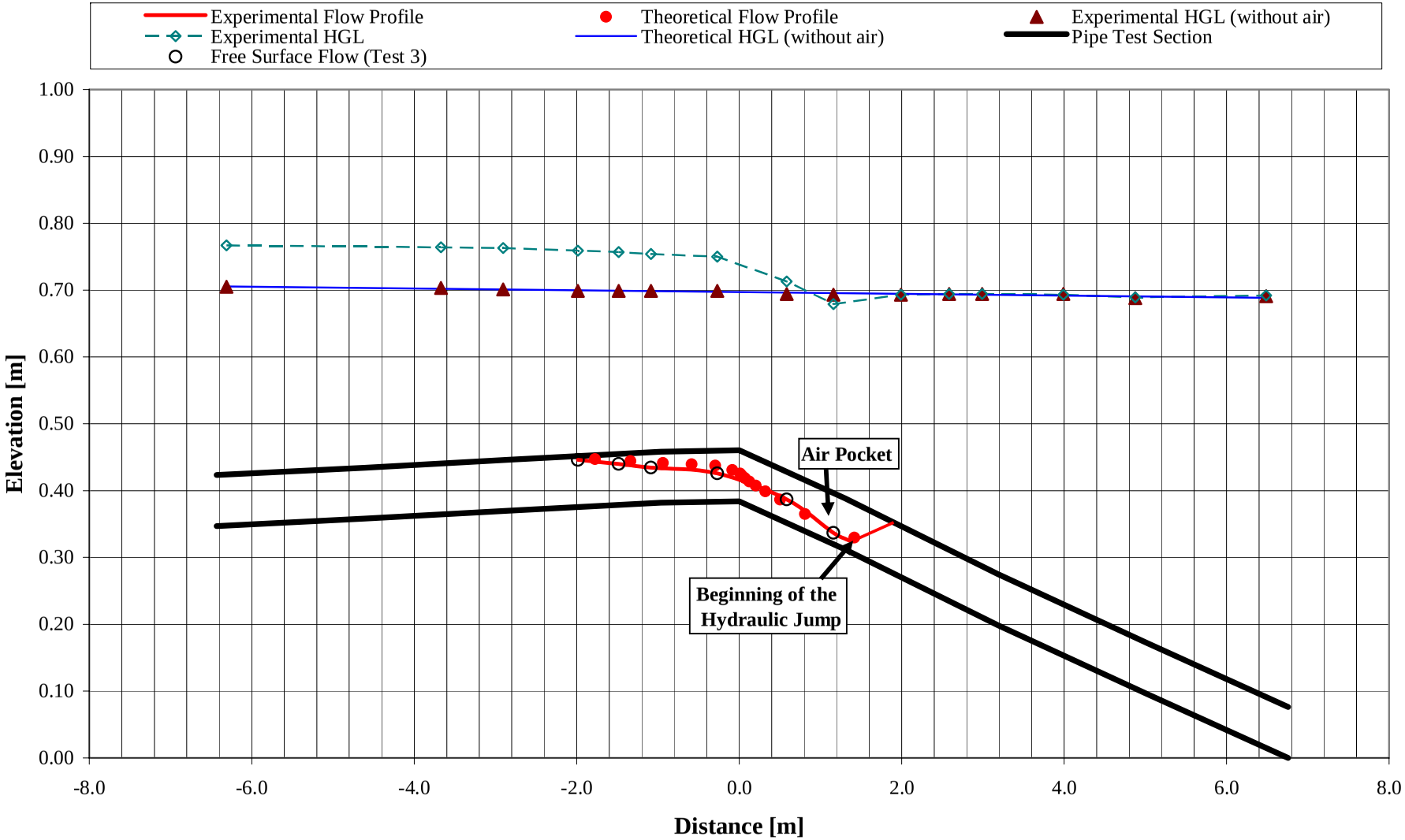

Figure 3.23: Flow profiles A2 and S2, Q_w = 0.013 m^3/s, V = 0.010 m^3

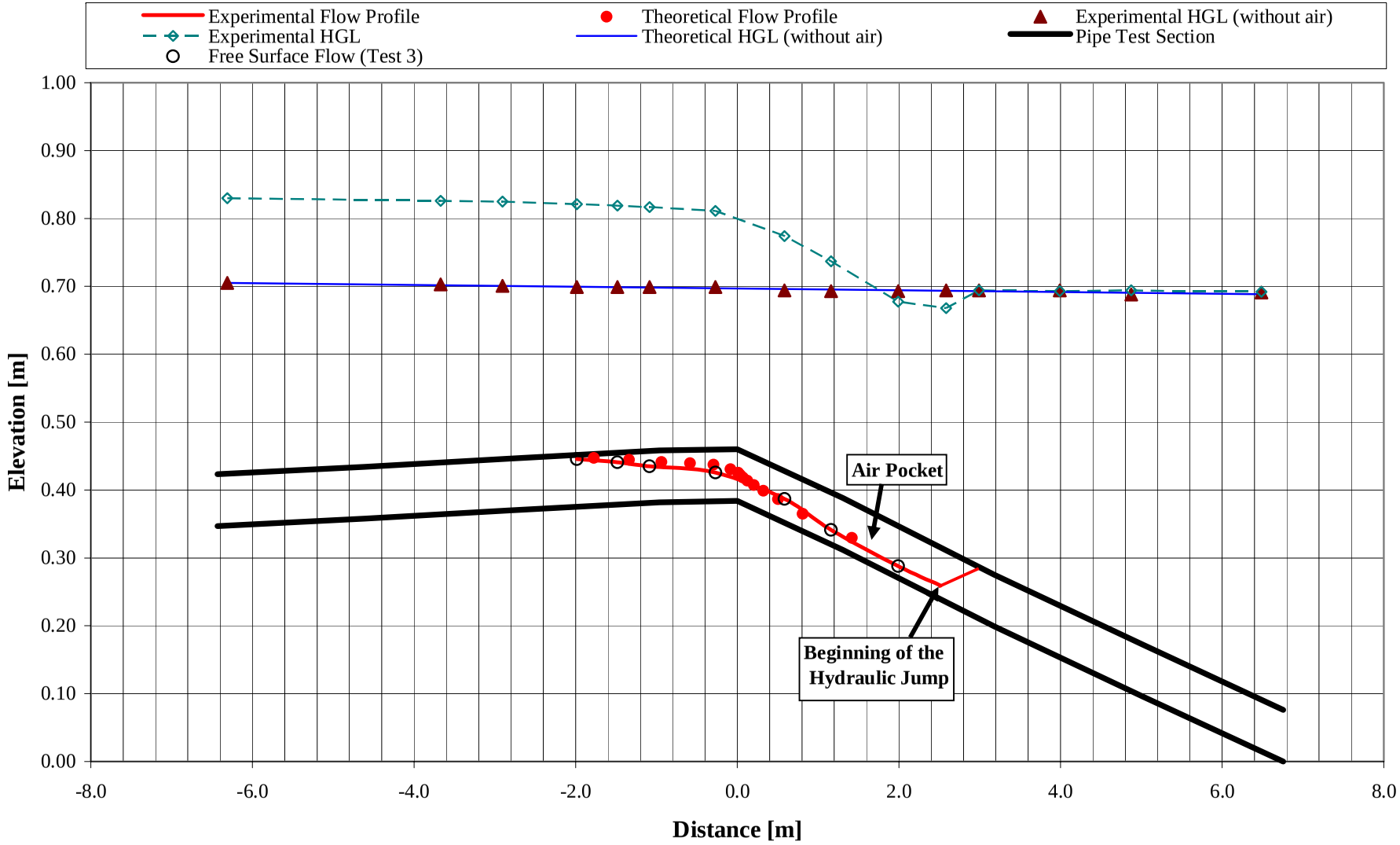

Figure 3.24: Flow profiles A2 and S2, Q_w = 0.013 m^3/s, V = 0.015 m^3

run 1	Q_w [m³/s]	V [m³]	S_{01}	S_{02}	
	0,0017	0,005	-0,0063	0,06	
			Water Depths		Air pocket
Measuring	HGL [m]	HGL [m]	Yi [m]	Yi [m]	pressure
Stations	Test 1	Test 2	Test 2	Test 3	[mH2O]
E_0	0,728	0,752	0,0762	0,0762	
E_1	0,723	0,746	0,0762	0,0762	
E_2	0,722	0,744	0,0762	0,0762	
E_3	0,718	0,740	**0,0729**	**0,073**	**0,2856**
E_4	0,718	0,738	**0,0669**	**0,068**	**0,2881**
E_5	0,718	0,736	**0,0599**	**0,06**	**0,2921**
E_6	0,717	0,730	**0,0479**	**0,049**	**0,2971**
E_7	0,713	0,692	**0,0359**	**0,037**	**0,3001**
E_8	0,712	0,712	0,0762	0,0762	
E_9	0,708	0,707	0,0762	0,0762	
E_{10}	0,708	0,709	0,0762	0,0762	
E_{11}	0,707	0,708	0,0762	0,0762	
E_{12}	0,706	0,706	0,0762	0,0762	
E_{13}	0,700	0,701	0,0762	0,0762	
E_{14}	0,703	0,704	0,0762	0,0762	
Δh [cm]	3,90	6,20			
				Volume of air [m³]	
				Test 2	
Length of the flow profiles		$L_{Hyd\ Jump}$		0.005	
Test 2 and Test 3 [m]		[cm]		Boyle´s Law	
Profile A2	Profile S2	26		0,0048	
-2,3	0,65			Gradually Varied Flow	
				0,0047	
				% Error Boyle´s law vs GVF	
				2,97	

a)

run 2	Q_w [m³/s]	V [m³]	S_{01}	S_{02}	
	0,0017	0,01	-0,0063	0,06	
			Water Depths		Air pocket
Measuring	HGL [m]	HGL [m]	Yi [m]	Yi [m]	pressure
Stations	Test 1	Test 2	Test 2	Test 3	[mH2O]
E_0	0,728	0,821	0,0762	0,0762	
E_1	0,723	0,815	0,0762	0,0762	
E_2	0,722	0,814	**0,0729**	**0,0730**	**0,3560**
E_3	0,718	0,811	**0,0669**	**0,0670**	**0,3566**
E_4	0,718	0,808	**0,0599**	**0,0600**	**0,3581**
E_5	0,718	0,806	**0,0479**	**0,0500**	**0,3621**
E_6	0,717	0,801	**0,0369**	**0,0370**	**0,3681**
E_7	0,713	0,762	**0,0299**	**0,0300**	**0,3691**
E_8	0,712	0,722	**0,0184**	**0,0190**	**0,3731**
E_9	0,708	0,666	**0,0762**	**0,0762**	**0,3776**
E_{10}	0,708	0,711	0,0762	0,0762	
E_{11}	0,707	0,710	0,0762	0,0762	
E_{12}	0,706	0,708	0,0762	0,0762	
E_{13}	0,700	0,706	0,0762	0,0762	
E_{14}	0,703	0,706	0,0762	0,0762	
Δh [cm]	3,90	13,80			
				Volume of air [m³]	
				Test 2	
Length of the flow profiles		$L_{Hyd\ Jump}$		0,01	
Test 2 and Test 3 [m]		[cm]		Boyle´s Law	
Profile A2	Profile S2	21		0,0096	
-2,3	1,985			Gradually Varied Flow	
				0,0091	
				% Error Boyle´s law vs GVF	
				5,10	

b)

Table 3.4: Experimental results for a 76.2 mm diameter acrylic pipe, profiles A2 and S2

S_{01} =	-0,0063	n =	0,0095									
Q_v [m³/s] =	0,0017	λ_{exp} =	0,0262									
Profile A2												
Yi [m]	**A [m²]**	**R [m]**	**$R^{1/3}$ [m]**	**v [m/s]**	**$v^2/2g$ [m]**	**E [m]**	**ΔE [m]**	**S_f**	**S_{fi}**	**$S - S_{fi}$**	**Δx [m]**	**$\Sigma\Delta x$ [m]**
0,0427	0,0026	0,0204	0,0746	0,6464	0,0213	0,0640	----	0,0068	----	----	0	0
0,0461	0,0029	0,0212	0,0766	0,5900	0,0177	0,0638	-0,0002	0,0054	0,0061	-0,0124	0,0168	0,0168
0,0494	0,0031	0,0219	0,0783	0,5434	0,0151	0,0645	0,0007	0,0044	0,0049	-0,0112	-0,0592	-0,0424
0,0528	0,0034	0,0225	0,0796	0,5047	0,0130	0,0657	0,0013	0,0036	0,0040	-0,0103	-0,1246	-0,1670
0,0561	0,0036	0,0229	0,0805	0,4724	0,0114	0,0675	0,0017	0,0031	0,0034	-0,0097	-0,1800	-0,3470
0,0595	0,0038	0,0231	0,0811	0,4453	0,0101	0,0696	0,0021	0,0027	0,0029	-0,0092	-0,2263	-0,5733
0,0628	0,0040	0,0232	0,0812	0,4228	0,0091	0,0719	0,0024	0,0024	0,0026	-0,0089	-0,2649	-0,8383
0,0662	0,0042	0,0230	0,0808	0,4043	0,0083	0,0745	0,0026	0,0023	0,0024	-0,0087	-0,2970	-1,1352
0,0695	0,0044	0,0226	0,0797	0,3896	0,0077	0,0772	0,0028	0,0022	0,0022	-0,0085	-0,3235	-1,4588
0,0729	0,0045	0,0217	0,0776	0,3786	0,0073	0,0802	0,0029	0,0021	0,0022	-0,0085	-0,3457	-1,8045
0,0762	0,0046	0,0190	0,0712	0,3728	0,0071	0,0833	0,0031	0,0025	0,0023	-0,0086	-0,3631	-2,1676

S_{02} =	0,06	n =	0,0095									
Q_v [m³/s] =	0,0017	λ_{exp} =	0,0262									
Profile S2												
Yi [m]	**A [m²]**	**R [m]**	**$R^{1/3}$ [m]**	**v [m/s]**	**$v^2/2g$ [m]**	**E [m]**	**ΔE [m]**	**S_f**	**S_{fi}**	**$S - S_{fi}$**	**Δx [m]**	**$\Sigma\Delta x$ [m]**
0,0427	0,0026	0,0204	0,0746	0,6464	0,0213	0,0640	----	0,0068	----	----	0	0
0,0408	0,0025	0,0199	0,0732	0,6847	0,0239	0,0647	0,0007	0,0079	0,0073	0,0527	0,0125	0,0125
0,0388	0,0023	0,0193	0,0718	0,7280	0,0270	0,0658	0,0012	0,0093	0,0086	0,0514	0,0229	0,0354
0,0369	0,0022	0,0187	0,0702	0,7772	0,0308	0,0677	0,0018	0,0110	0,0102	0,0498	0,0368	0,0722
0,0349	0,0020	0,0180	0,0686	0,8335	0,0354	0,0703	0,0027	0,0133	0,0122	0,0478	0,0560	0,1282
0,0330	0,0019	0,0173	0,0668	0,8982	0,0411	0,0741	0,0038	0,0163	0,0148	0,0452	0,0835	0,2117
0,0311	0,0017	0,0166	0,0649	0,9732	0,0483	0,0793	0,0052	0,0203	0,0183	0,0417	0,1252	0,3369
0,0291	0,0016	0,0158	0,0628	1,0610	0,0574	0,0865	0,0072	0,0257	0,0230	0,0370	0,1937	0,5306
0,0272	0,0015	0,0150	0,0606	1,1647	0,0691	0,0963	0,0098	0,0333	0,0295	0,0305	0,3223	0,8529
0,0252	0,0013	0,0141	0,0583	1,2887	0,0846	0,1099	0,0136	0,0441	0,0387	0,0213	0,6361	1,4890
0,0233	0,0012	0,0132	0,0559	1,4389	0,1055	0,1288	0,0189	0,0599	0,0520	0,0080	2,3595	3,8485

Table 3.4 c): Computation of the flow profiles A2 and S2 by the direct step method

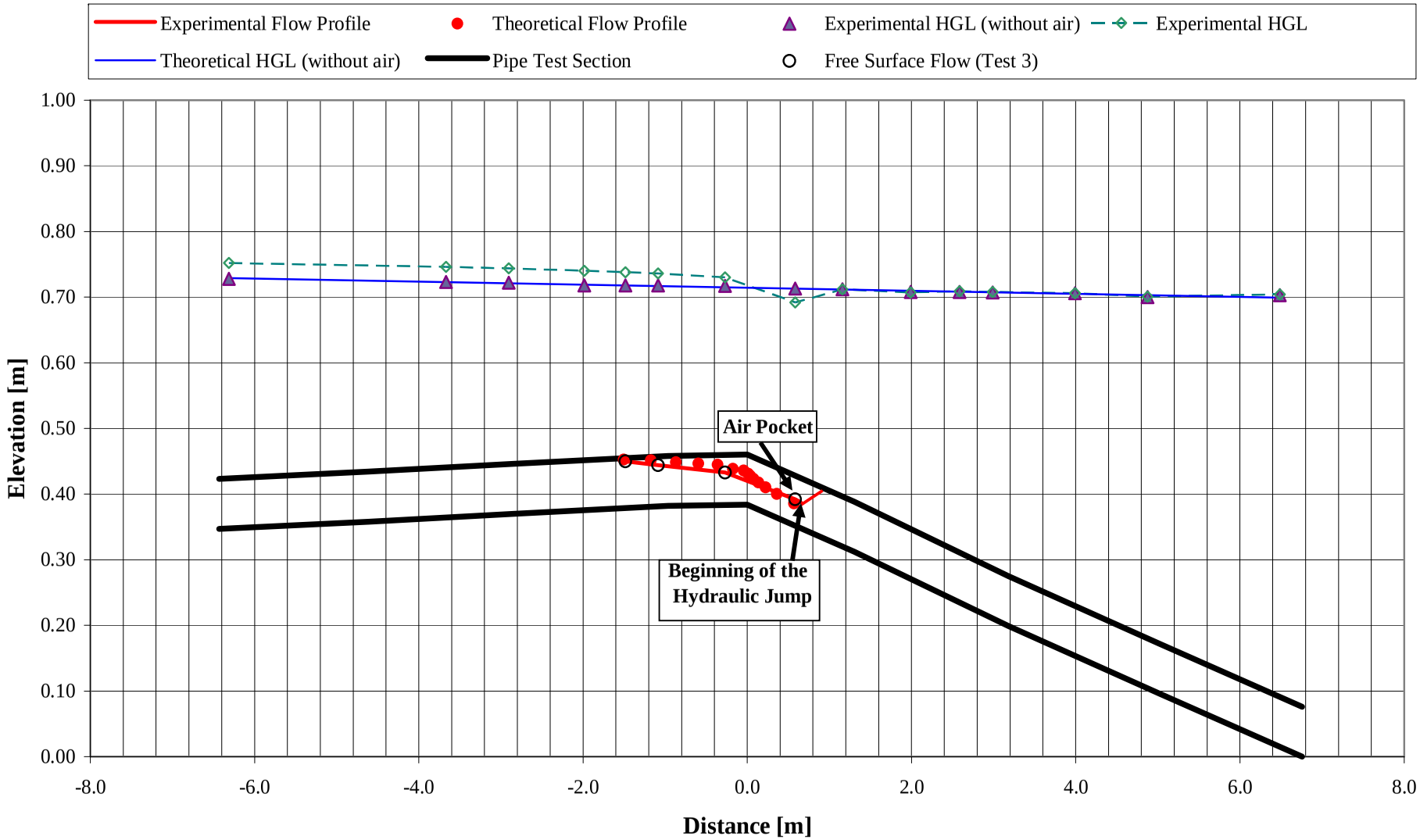

Figure 3.25: Flow profiles A2 and S2, Q_w = 0.017 m^3/s, V = 0.005 m^3

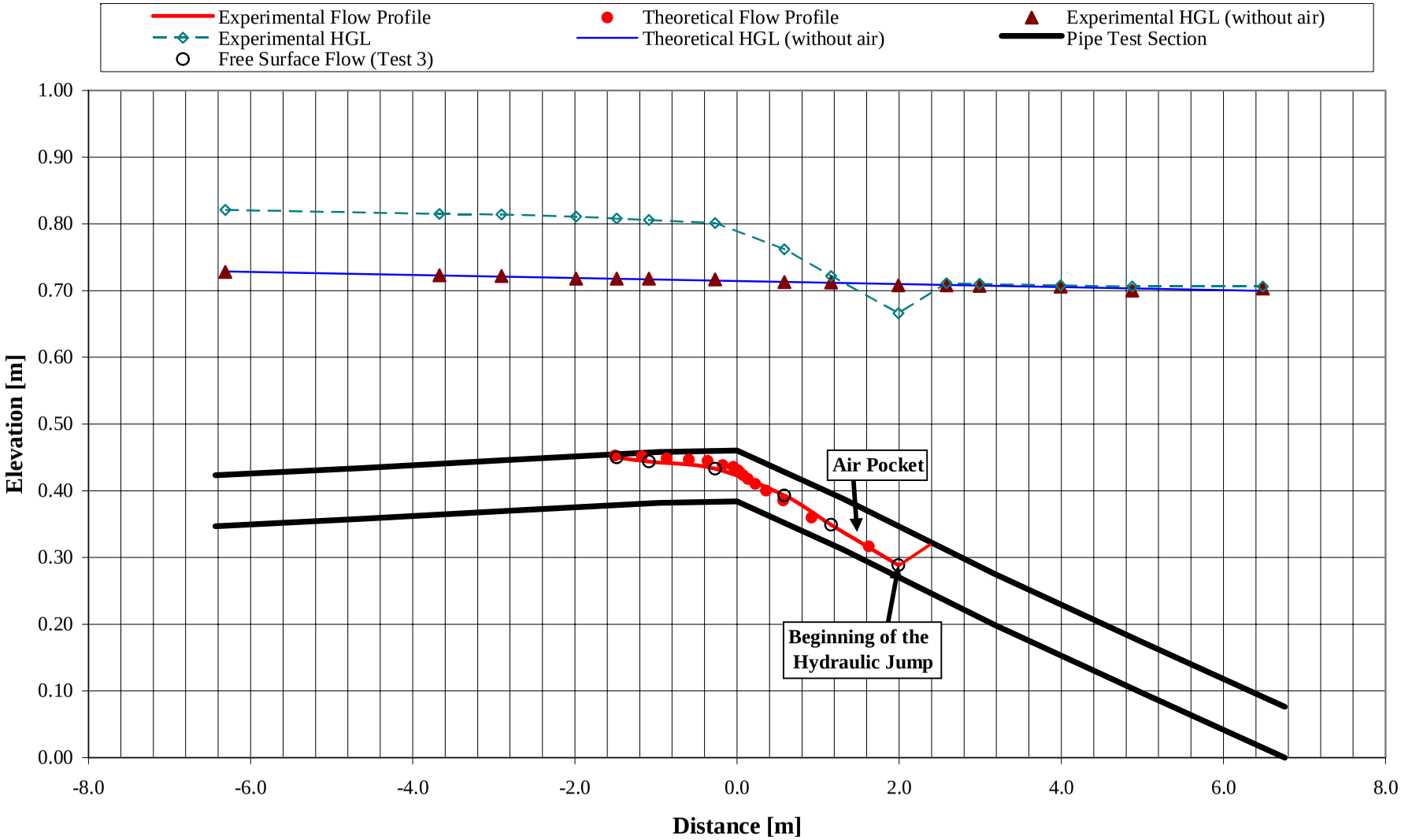

Figure 3.26: Flow profiles A2 and S2, Q_w = 0.017 m^3/s, V = 0.010 m^3

run 1	Q_w [m³/s]	V [m³]	S_{01}	S_{02}	
	0,0017	0,01	0,0	0,06	
			Water Depths		Air pocket
Measuring Stations	HGL [m] Test 1	HGL [m] Test 2	Yi [m] Test 2	Yi [m] Test 3	pressure [mH2O]
E_0	0,71200	0,77300	0,0762	0,0762	
E_1	0,70700	0,77100	0,0762	0,0762	
E_2	0,70600	0,76800	**0,0709**	**0,072**	**0,3091**
E_3	0,70300	0,76200	**0,0569**	**0,057**	**0,3171**
E_4	0,70200	0,75800	**0,0549**	**0,055**	**0,3151**
E_5	0,70200	0,75600	**0,0509**	**0,049**	**0,3171**
E_6	0,70200	0,74300	**0,0379**	**0,039**	**0,3171**
E_7	0,69700	0,71200	**0,0349**	**0,035**	**0,3211**
E_8	0,69200	0,68000	**0,0294**	**0,03**	**0,3316**
E_9	0,69500	0,69300	0,0762	0,0762	
E_{10}	0,69400	0,69300	0,0762	0,0762	
E_{11}	0,69300	0,69200	0,0762	0,0762	
E_{12}	0,69100	0,69000	0,0762	0,0762	
E_{13}	0,69000	0,68900	0,0762	0,0762	
E_{14}	0,68700	0,68800	0,0762	0,0762	
Δh [cm]	3,45	10,00			
				Volume of air [m³]	
				Test 2	
Length of the flow profiles		$L_{Hyd\ Jump}$		0.010	
Test 2 and Test 3 [m]		[cm]		Boyle´s Law	
Profile A2	Profile S2	18		0,0096	
-3,12	1,425			Gradually Varied Flow	
				0,00713	
				% Error Boyle´s law vs GVF	
				25,87	

a)

run 2	Q_w [m³/s]	V [m³]	S_{01}	S_{02}	
	0,0017	0,015	0,0	0,06	
			Water Depths		Air pocket
Measuring Stations	HGL [m] Test 1	HGL [m] Test 2	Yi [m] Test 2	Yi [m] Test 3	pressure [mH2O]
E_0	0,71200	0,83900	0,0762	0,0762	
E_1	0,70700	0,83200	0,0762	0,0762	
E_2	0,70600	0,82900	**0,0719**	**0,071**	**0,3691**
E_3	0,70300	0,82100	**0,0584**	**0,055**	**0,3746**
E_4	0,70200	0,81700	**0,0539**	**0,056**	**0,3751**
E_5	0,70200	0,81400	**0,0504**	**0,05**	**0,3756**
E_6	0,70200	0,80300	**0,0399**	**0,04**	**0,3751**
E_7	0,69700	0,77100	**0,0379**	**0,035**	**0,3771**
E_8	0,69200	0,73000	**0,0304**	**0,03**	**0,3806**
E_9	0,69500	0,67700	**0,0239**	**0,024**	**0,3831**
E_{10}	0,69400	0,68600	**0,0239**	**0,024**	**0,4271**
E_{11}	0,69300	0,65500	0,0762	0,0762	
E_{12}	0,69100	0,69300	0,0762	0,0762	
E_{13}	0,69000	0,69200	0,0762	0,0762	
E_{14}	0,68700	0,69000	0,0762	0,0762	
Δh [cm]	3,45	16,70			
				Volume of air [m³]	
				Test 2	
Length of the flow profiles		$L_{Hyd\ Jump}$		0.015	
Test 2 and Test 3 [m]		[cm]		Boyle´s Law	
Profile A2	Profile S2	18		0,0143	
-3,12	2,73			Gradually Varied Flow	
				0,0114	
				% Error Boyle´s law vs GVF	
				20,13	

b)

Table 3.5: Experimental results for a 76.2 mm diameter acrylic pipe, profiles H2 and S2

S_{01} =	0,0	n =	0,0089									
Q_w [m³/s] =	0,0017	λ_{exp} =	0,0232									
Profile H2												
Yi [m]	**A [m²]**	**R [m]**	**$R^{2/3}$ [m]**	**v [m/s]**	**$v^2/2g$ [m]**	**E [m]**	**ΔE [m]**	**S_f**	**S_{fi}**	**$S - S_{fi}$**	**Δx [m]**	**$\Sigma\Delta x$ [m]**
0,0427	0,0026	0,0204	0,0746	0,6464	0,0213	0,0640	----	0,0060	----	----	0	0
0,0461	0,0029	0,0212	0,0766	0,5900	0,0177	0,0638	-0,0002	0,0047	0,0053	-0,0053	0,0391	0,0391
0,0494	0,0031	0,0219	0,0783	0,5434	0,0151	0,0645	0,0007	0,0038	0,0043	-0,0043	-0,1550	-0,1159
0,0528	0,0034	0,0225	0,0796	0,5047	0,0130	0,0657	0,0013	0,0032	0,0035	-0,0035	-0,3661	-0,4821
0,0561	0,0036	0,0229	0,0805	0,4724	0,0114	0,0675	0,0017	0,0027	0,0030	-0,0030	-0,5887	-1,0707
0,0595	0,0038	0,0231	0,0811	0,4453	0,0101	0,0696	0,0021	0,0024	0,0026	-0,0026	-0,8155	-1,8862
0,0628	0,0040	0,0232	0,0812	0,4228	0,0091	0,0719	0,0024	0,0021	0,0023	-0,0023	-1,0376	-2,9239
0,0662	0,0042	0,0230	0,0808	0,4043	0,0083	0,0745	0,0026	0,0020	0,0021	-0,0021	-1,2440	-4,1679
0,0695	0,0044	0,0226	0,0797	0,3896	0,0077	0,0772	0,0028	0,0019	0,0019	-0,0019	-1,4206	-5,5885
0,0729	0,0045	0,0217	0,0776	0,3786	0,0073	0,0802	0,0029	0,0019	0,0019	-0,0019	-1,5477	-7,1362
0,0762	0,0046	0,0190	0,0712	0,3728	0,0071	0,0833	0,0031	0,0022	0,0020	-0,0020	-1,5424	-8,6787
S_{02} =	0,06	n =	0,0089									
Q_w [m³/s] =	0,0017	λ_{exp} =	0,0232									
Profile S2												
Yi [m]	**A [m²]**	**R [m]**	**$R^{2/3}$ [m]**	**v [m/s]**	**$v^2/2g$ [m]**	**E [m]**	**ΔE [m]**	**S_f**	**S_{fi}**	**$S - S_{fi}$**	**Δx [m]**	**$\Sigma\Delta x$ [m]**
0,0427	0,0026	0,0204	0,0746	0,6464	0,0213	0,0640	----	0,0060	----	----	0	0
0,0407	0,0025	0,0198	0,0732	0,6864	0,0240	0,0647	0,0007	0,0070	0,0065	0,0535	0,0130	0,0130
0,0387	0,0023	0,0192	0,0717	0,7319	0,0273	0,0660	0,0013	0,0083	0,0076	0,0524	0,0241	0,0372
0,0366	0,0022	0,0186	0,0700	0,7838	0,0313	0,0680	0,0020	0,0099	0,0091	0,0509	0,0391	0,0763
0,0346	0,0020	0,0179	0,0683	0,8435	0,0363	0,0709	0,0029	0,0121	0,0110	0,0490	0,0599	0,1362
0,0326	0,0019	0,0171	0,0664	0,9127	0,0425	0,0751	0,0042	0,0150	0,0135	0,0465	0,0899	0,2260
0,0306	0,0017	0,0164	0,0644	0,9936	0,0503	0,0809	0,0058	0,0189	0,0169	0,0431	0,1356	0,3616
0,0286	0,0016	0,0155	0,0622	1,0891	0,0605	0,0890	0,0081	0,0243	0,0216	0,0384	0,2112	0,5728
0,0265	0,0014	0,0147	0,0599	1,2031	0,0738	0,1003	0,0113	0,0320	0,0281	0,0319	0,3544	0,9272
0,0245	0,0013	0,0138	0,0574	1,3410	0,0917	0,1162	0,0159	0,0432	0,0376	0,0224	0,7072	1,6345
0,0225	0,0011	0,0129	0,0548	1,5103	0,1163	0,1388	0,0226	0,0602	0,0517	0,0083	2,7157	4,3502

Table 3.5 c): Computation of the flow profiles H2 and S2 by the direct step method

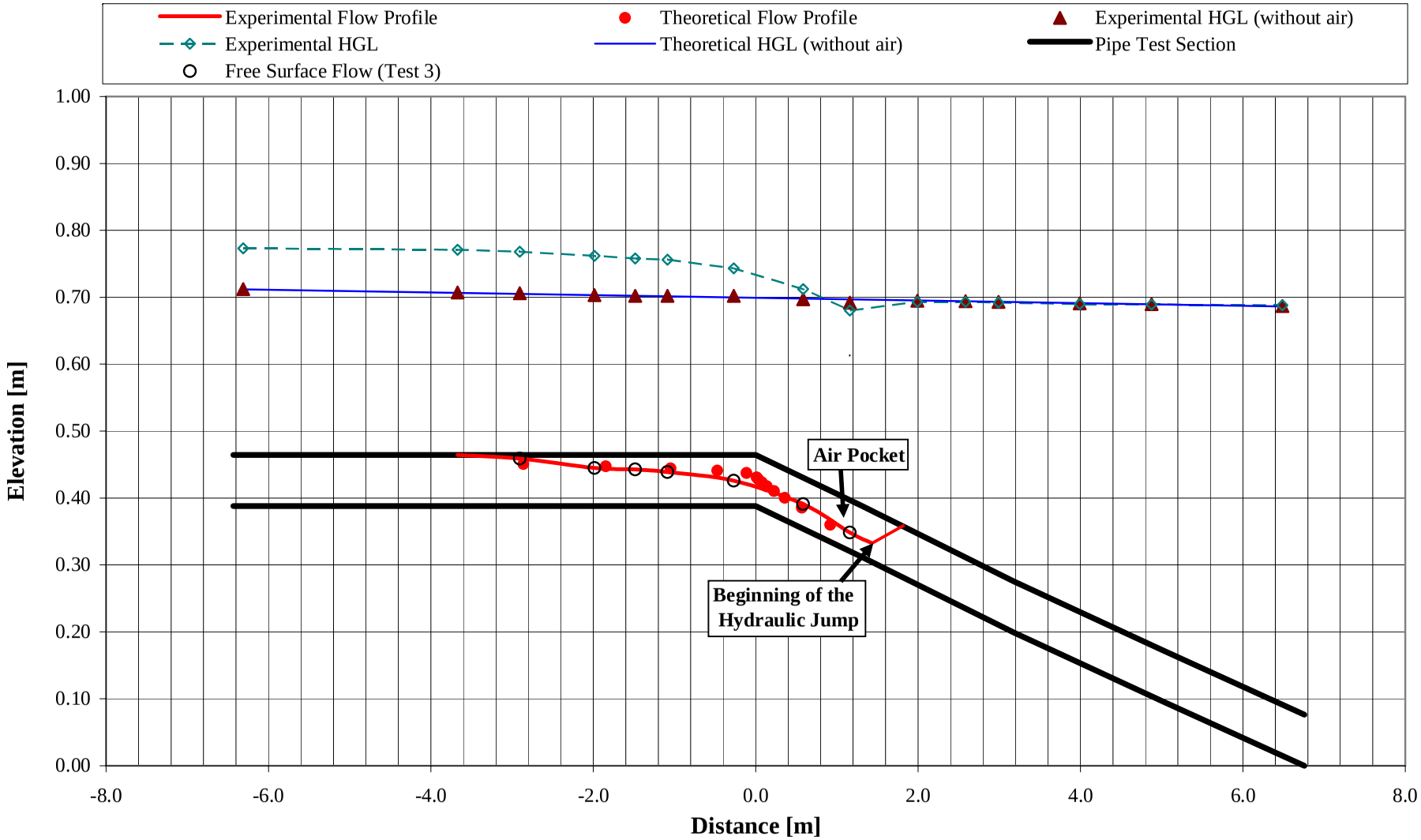

Figure 3.27: Flow profiles H2 and S2, Q_w = 0.017 m^3/s, V = 0.010 m^3

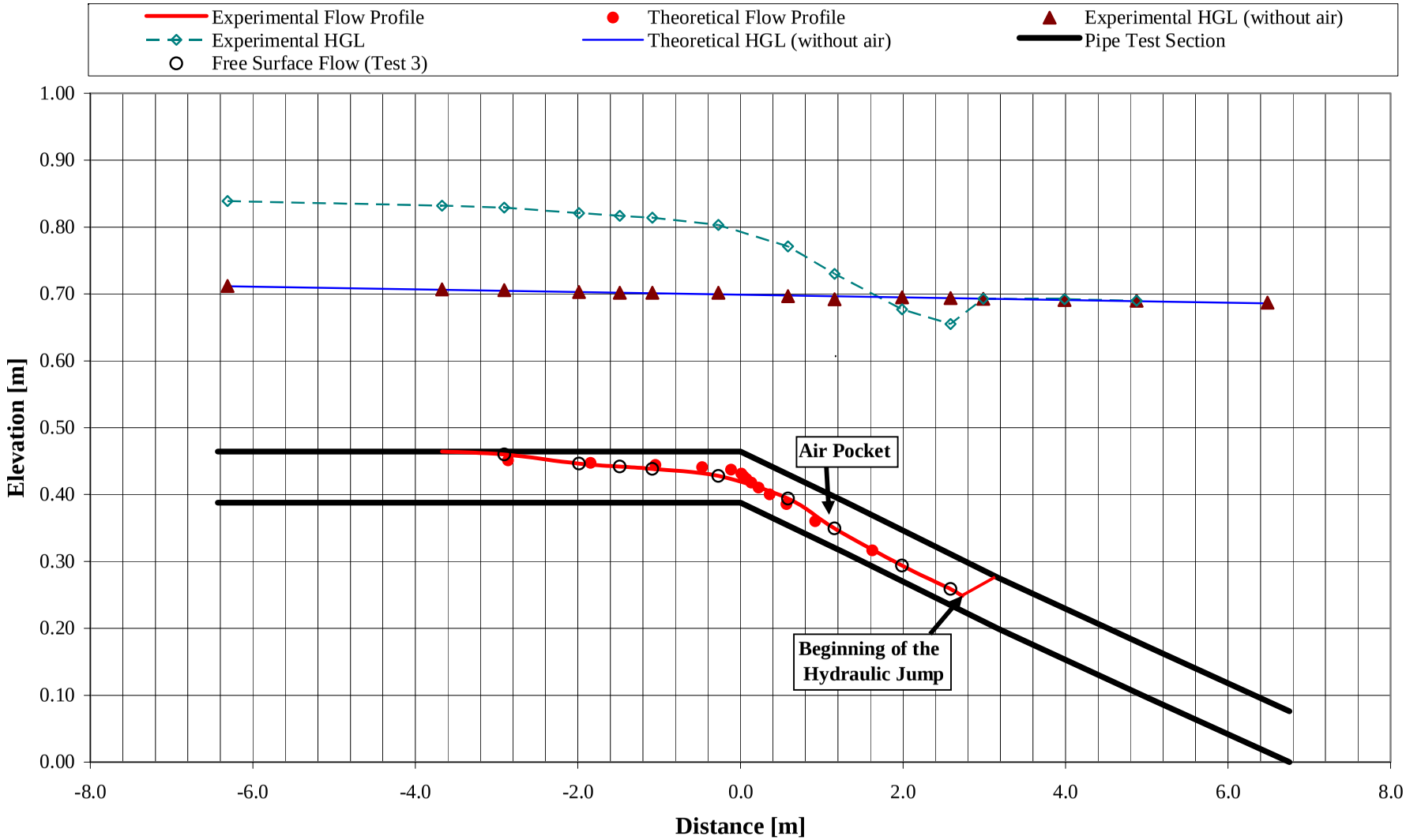

Figure 3.28: Flow profiles H2 and S2, Q_w = 0.017 m^3/s, V = 0.015 m^3

run 1	Q_w [m³/s]	V [m³]	S_{01}	S_{02}	
	0,002	0,01	0,0	0,06	
			Water Depths		Air pocket
Measuring Stations	HGL [m] Test 1	HGL [m] Test 2	Yi [m] Test 2	Yi [m] Test 3	pressure [mH2O]
E_0	0,732	0,812	0,0762	0,0762	
E_1	0,725	0,806	0,0762	0,0762	
E_2	0,723	0,805	0,0762	0,0762	
E_3	0,719	0,797	**0,0634**	**0,064**	**0,3456**
E_4	0,718	0,793	**0,0619**	**0,06**	**0,3431**
E_5	0,718	0,790	**0,0569**	**0,057**	**0,3451**
E_6	0,717	0,777	**0,0439**	**0,044**	**0,3451**
E_7	0,711	0,745	**0,0404**	**0,04**	**0,3486**
E_8	0,707	0,701	**0,0339**	**0,031**	**0,3481**
E_9	0,703	0,680	0,0762	0,0762	
E_{10}	0,705	0,705	0,0762	0,0762	
E_{11}	0,705	0,704	0,0762	0,0762	
E_{12}	0,703	0,703	0,0762	0,0762	
E_{13}	0,701	0,701	0,0762	0,0762	
E_{14}	0,698	0,699	0,0762	0,0762	
Δh [cm]	5,10	13,50			
				Volume of air [m³]	
				Test 2	
Length of the flow profiles		$L_{Hyd\ Jump}$		0.010	
Test 2 and Test 3 [m]		[cm]		Boyle´s Law	
Profile A2	Profile S2	17		0,0096	
-2,75	1,855			Gradually Varied Flow	
				0,00685	
				% Error Boyle´s law vs GVF	
				28,59	

a)

run 2	Q_w [m³/s]	V [m³]	S_{01}	S_{02}	
	0,002	0,015	0,0	0,06	
			Water Depths		Air pocket
Measuring Stations	HGL [m] Test 1	HGL [m] Test 2	Yi [m] Test 2	Yi [m] Test 3	pressure [mH2O]
E_0	0,732	0,880	0,0762	0,0762	
E_1	0,725	0,873	0,0762	0,0762	
E_2	0,723	0,861	0,0762	0,0762	
E_3	0,719	0,858	**0,0649**	**0,065**	**0,4051**
E_4	0,718	0,857	**0,0599**	**0,061**	**0,4091**
E_5	0,718	0,854	**0,0589**	**0,058**	**0,4071**
E_6	0,717	0,839	**0,0459**	**0,044**	**0,4051**
E_7	0,711	0,809	**0,0399**	**0,039**	**0,4131**
E_8	0,707	0,752	**0,0309**	**0,032**	**0,4021**
E_9	0,703	0,708	**0,0259**	**0,026**	**0,4121**
E_{10}	0,705	0,675	**0,0234**	**0,023**	**0,4166**
E_{11}	0,705	0,651	**0,0159**	**0,016**	**0,4291**
E_{12}	0,703	0,701	0,0762	0,0762	
E_{13}	0,701	0,701	0,0762	0,0762	
E_{14}	0,698	0,694	0,0762	0,0762	
Δh [cm]	5,10	19,70			
				Volume of air [m³]	
				Test 2	
Length of the flow profiles		$L_{Hyd\ Jump}$		0.015	
Test 2 and Test 3 [m]		[cm]		Boyle´s Law	
Profile A2	Profile S2	17		0,0143	
-2,75	3,235			Gradually Varied Flow	
				0,0113	
				% Error Boyle´s law vs GVF	
				20,87	

b)

Table 3.6: Experimental results for a 76.2 mm diameter acrylic pipe, profiles H2 and S2

S_{01} =	0,0	n =	0,0092									
Q_w [m³/s] =	0,002	λ_{exp} =	0,0248									
Profile H2												
Yi [m]	**A [m²]**	**R [m]**	**$R^{2/3}$ [m]**	**v [m/s]**	**$v^2/2g$ [m]**	**E [m]**	**ΔE [m]**	**S_f**	**S_{fi}**	**$S - S_{fi}$**	**Δx [m]**	**$\Sigma\Delta x$ [m]**
0,0469	0,0029	0,0214	0,0770	0,6792	0,0235	0,0704	----	0,0066	----	----	0	0
0,0498	0,0032	0,0220	0,0784	0,6330	0,0204	0,0703	-0,0002	0,0055	0,0060	-0,0060	0,0265	0,0265
0,0528	0,0034	0,0225	0,0796	0,5936	0,0180	0,0707	0,0005	0,0047	0,0051	-0,0051	-0,0921	-0,0656
0,0557	0,0036	0,0229	0,0804	0,5600	0,0160	0,0717	0,0010	0,0041	0,0044	-0,0044	-0,2164	-0,2820
0,0586	0,0038	0,0231	0,0810	0,5313	0,0144	0,0730	0,0013	0,0036	0,0039	-0,0039	-0,3437	-0,6257
0,0616	0,0039	0,0232	0,0812	0,5067	0,0131	0,0746	0,0016	0,0033	0,0035	-0,0035	-0,4705	-1,0962
0,0645	0,0041	0,0231	0,0811	0,4860	0,0120	0,0765	0,0019	0,0030	0,0032	-0,0032	-0,5929	-1,6890
0,0674	0,0043	0,0229	0,0805	0,4686	0,0112	0,0786	0,0021	0,0029	0,0030	-0,0030	-0,7060	-2,3950
0,0703	0,0044	0,0224	0,0793	0,4546	0,0105	0,0809	0,0023	0,0028	0,0028	-0,0028	-0,8040	-3,1990
0,0733	0,0045	0,0215	0,0772	0,4442	0,0101	0,0833	0,0025	0,0028	0,0028	-0,0028	-0,8786	-4,0776
0,0762	0,0046	0,0190	0,0712	0,4386	0,0098	0,0860	0,0027	0,0032	0,0030	-0,0030	-0,8914	-4,9690

S_{02} =	0,06	n =	0,0092									
Q_w [m³/s] =	0,002	λ_{exp} =	0,0248									
Profile S2												
Yi [m]	**A [m²]**	**R [m]**	**$R^{2/3}$ [m]**	**v [m/s]**	**$v^2/2g$ [m]**	**E [m]**	**ΔE [m]**	**S_f**	**S_{fi}**	**$S - S_{fi}$**	**Δx [m]**	**$\Sigma\Delta x$ [m]**
0,0469	0,0029	0,0214	0,0770	0,6792	0,0235	0,0704	----	0,0066	----	----	0	0
0,0447	0,0028	0,0209	0,0758	0,7193	0,0264	0,0711	0,0007	0,0076	0,0071	0,0529	0,0124	0,0124
0,0425	0,0026	0,0203	0,0744	0,7649	0,0298	0,0723	0,0013	0,0089	0,0083	0,0517	0,0242	0,0366
0,0403	0,0024	0,0197	0,0729	0,8171	0,0340	0,0743	0,0020	0,0106	0,0098	0,0502	0,0400	0,0766
0,0381	0,0023	0,0191	0,0712	0,8771	0,0392	0,0773	0,0030	0,0128	0,0117	0,0483	0,0618	0,1384
0,0359	0,0021	0,0183	0,0694	0,9467	0,0457	0,0816	0,0043	0,0157	0,0143	0,0457	0,0933	0,2318
0,0337	0,0019	0,0175	0,0674	1,0279	0,0539	0,0876	0,0060	0,0197	0,0177	0,0423	0,1413	0,3731
0,0315	0,0018	0,0167	0,0653	1,1237	0,0644	0,0959	0,0083	0,0251	0,0224	0,0376	0,2207	0,5938
0,0293	0,0016	0,0158	0,0630	1,2379	0,0781	0,1074	0,0115	0,0327	0,0289	0,0311	0,3707	0,9645
0,0271	0,0015	0,0149	0,0605	1,3757	0,0965	0,1236	0,0162	0,0437	0,0382	0,0218	0,7407	1,7052
0,0249	0,0013	0,0140	0,0579	1,5446	0,1216	0,1465	0,0229	0,0602	0,0520	0,0080	2,8539	4,5591

Table 3.6 c): Computation of the flow profiles H2 and S2 by the direct step method

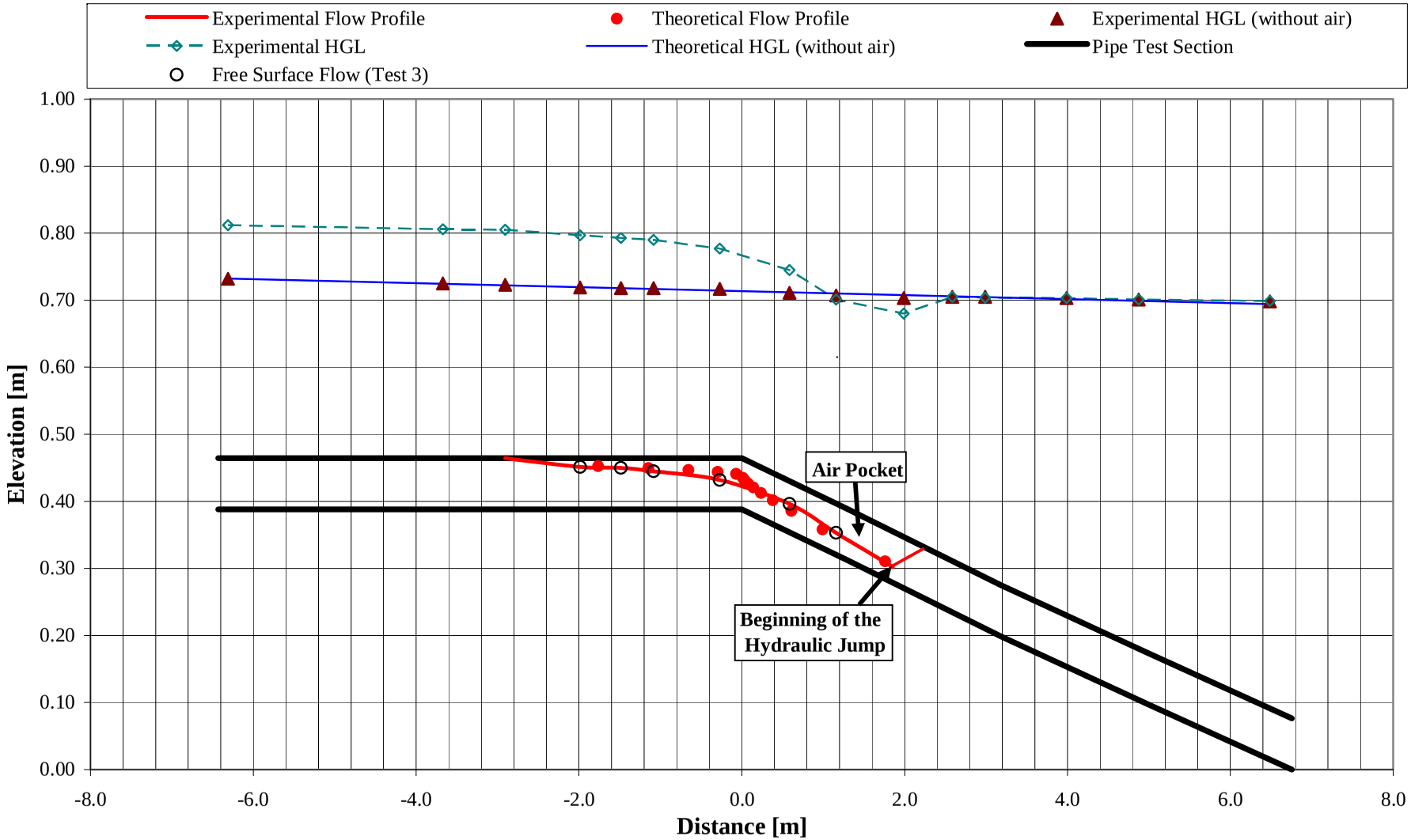

Figure 3.29: Flow profiles H2 and S2, Q_w = 0.020 m^3/s, V = 0.010 m^3

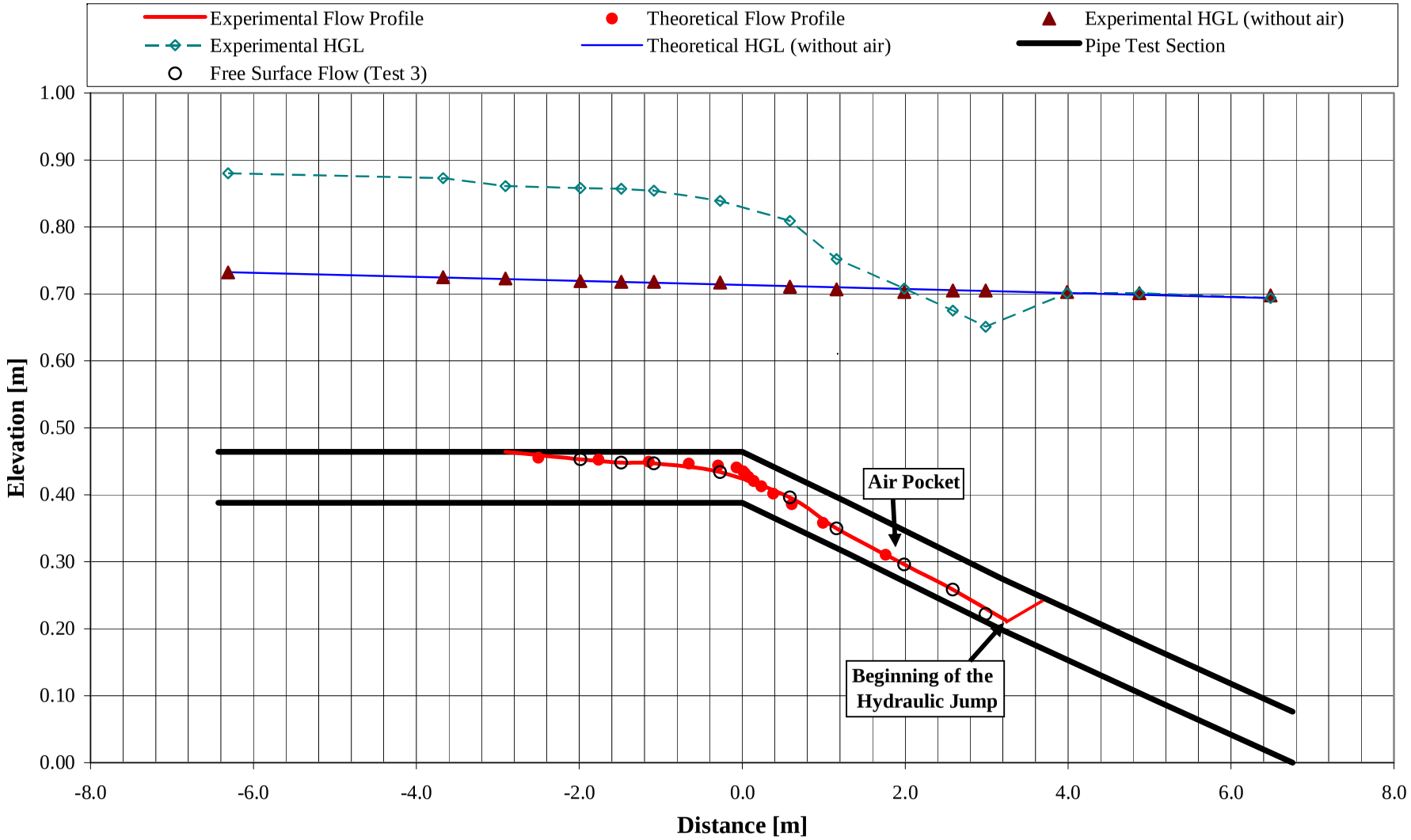

Figure 3.30: Flow profiles H2 and S2, Q_w = 0.020 m^3/s, V = 0.015 m^3

run 1	Q_w [m³/s]	V [m³]	S_{01}	S_{02}
	0,002	0,01	0,006	0,06

			Water Depths		Air pocket
Measuring Stations	HGL [m] Test 1	HGL [m] Test 2	Yi [m] Test 2	Yi [m] Test 3	pressure [mH2O]
E_0	0,732	0,812	0,0762	0,0762	
E_1	0,725	0,806	0,0762	0,0762	
E_2	0,723	0,805	0,0762	0,0762	
E_3	0,719	0,797	**0,0634**	**0,064**	**0,3456**
E_4	0,718	0,793	**0,0619**	**0,06**	**0,3431**
E_5	0,718	0,790	**0,0569**	**0,057**	**0,3451**
E_6	0,717	0,777	**0,0439**	**0,044**	**0,3451**
E_7	0,711	0,745	**0,0404**	**0,04**	**0,3486**
E_8	0,707	0,701	**0,0339**	**0,031**	**0,3481**
E_9	0,703	0,680	0,0762	0,0762	
E_{10}	0,705	0,705	0,0762	0,0762	
E_{11}	0,705	0,704	0,0762	0,0762	
E_{12}	0,703	0,703	0,0762	0,0762	
E_{13}	0,701	0,701	0,0762	0,0762	
E_{14}	0,698	0,699	0,0762	0,0762	
Δh [cm]	5,10	13,50			

Length of the flow profiles		$L_{Hyd\ Jump}$
Test 2 and Test 3 [m]		[cm]
Profile A2	Profile S2	17
-2,75	1,855	

Volume of air [m³]
Test 2
0.010
Boyle´s Law
0,0096
Gradually Varied Flow
0,00936
% Error Boyle´s law vs GVF
2,69

a)

run 2	Q_w [m³/s]	V [m³]	S_{01}	S_{02}
	0,002	0,015	0,006	0,06

			Water Depths		Air pocket
Measuring Stations	HGL [m] Test 1	HGL [m] Test 2	Yi [m] Test 2	Yi [m] Test 3	pressure [mH2O]
E_0	0,732	0,880	0,0762	0,0762	
E_1	0,725	0,873	0,0762	0,0762	
E_2	0,723	0,861	0,0762	0,0762	
E_3	0,719	0,858	**0,0649**	**0,065**	**0,4051**
E_4	0,718	0,857	**0,0599**	**0,061**	**0,4091**
E_5	0,718	0,854	**0,0589**	**0,058**	**0,4071**
E_6	0,717	0,839	**0,0459**	**0,044**	**0,4051**
E_7	0,711	0,809	**0,0399**	**0,039**	**0,4131**
E_8	0,707	0,752	**0,0309**	**0,032**	**0,4021**
E_9	0,703	0,708	**0,0259**	**0,026**	**0,4121**
E_{10}	0,705	0,675	**0,0234**	**0,023**	**0,4166**
E_{11}	0,705	0,651	**0,0159**	**0,016**	**0,4291**
E_{12}	0,703	0,701	0,0762	0,0762	
E_{13}	0,701	0,701	0,0762	0,0762	
E_{14}	0,698	0,694	0,0762	0,0762	
Δh [cm]	5,10	19,70			

Length of the flow profiles		$L_{Hyd\ Jump}$
Test 2 and Test 3 [m]		[cm]
Profile A2	Profile S2	17
-2,75	3,235	

Volume of air [m³]
Test 2
0.015
Boyle´s Law
0,0143
Gradually Varied Flow
0,0137
% Error Boyle´s law vs GVF
4,43

b)

Table 3.7: Experimental results for a 76.2 mm diameter acrylic pipe, profiles M2 and S2

S_{01} =	0,006	n =	0,0092									
Q_w (m³/s) =	0,002	λ_{exp} =	0,0248									
Profile M2												
Yi [m]	**A [m²]**	**R [m]**	**$R^{2/3}$ [m]**	**v [m/s]**	**$v^2/2g$ [m]**	**E [m]**	**ΔE [m]**	**S_f**	**S_{fi}**	**$S - S_{fi}$**	**Δx [m]**	**$\Sigma\Delta x$ [m]**
0,0469	0,0029	0,0214	0,0770	0,6792	0,0235	0,0704	----	0,0064	----	----	0	0
0,0498	0,0032	0,0220	0,0784	0,6330	0,0204	0,0703	-0,0002	0,0054	0,0059	0,0001	1,8651	1,8651
0,0528	0,0034	0,0225	0,0796	0,5936	0,0180	0,0707	0,0005	0,0046	0,0050	0,0010	-0,4706	1,3945
0,0557	0,0036	0,0229	0,0804	0,5600	0,0160	0,0717	0,0010	0,0040	0,0043	0,0017	-0,5647	0,8298
0,0586	0,0038	0,0231	0,0810	0,5313	0,0144	0,0730	0,0013	0,0036	0,0038	0,0022	-0,6020	0,2278
0,0616	0,0039	0,0232	0,0812	0,5067	0,0131	0,0746	0,0016	0,0032	0,0034	0,0026	-0,6263	-0,3985
0,0645	0,0041	0,0231	0,0811	0,4860	0,0120	0,0765	0,0019	0,0030	0,0031	0,0029	-0,6478	-1,0462
0,0674	0,0043	0,0229	0,0805	0,4686	0,0112	0,0786	0,0021	0,0028	0,0029	0,0031	-0,6714	-1,7176
0,0703	0,0044	0,0224	0,0793	0,4546	0,0105	0,0809	0,0023	0,0027	0,0028	0,0032	-0,7020	-2,4196
0,0733	0,0045	0,0215	0,0772	0,4442	0,0101	0,0833	0,0025	0,0027	0,0027	0,0033	-0,7494	-3,1690
0,0762	0,0046	0,0190	0,0712	0,4386	0,0098	0,0860	0,0027	0,0031	0,0029	0,0031	-0,8744	-4,0434

S_{02} =	0,06	n =	0,0092									
Q_w (m³/s) =	0,002	λ_{exp} =	0,0248									
Profile S2												
Yi [m]	**A [m²]**	**R [m]**	**$R^{2/3}$ [m]**	**v [m/s]**	**$v^2/2g$ [m]**	**E [m]**	**ΔE [m]**	**S_f**	**S_{fi}**	**$S - S_{fi}$**	**Δx [m]**	**$\Sigma\Delta x$ [m]**
0,0469	0,0029	0,0214	0,0770	0,6792	0,0235	0,0704	----	0,0066	----	----	0	0
0,0447	0,0028	0,0209	0,0758	0,7193	0,0264	0,0711	0,0007	0,0076	0,0071	0,0529	0,0124	0,0124
0,0425	0,0026	0,0203	0,0744	0,7649	0,0298	0,0723	0,0013	0,0089	0,0083	0,0517	0,0242	0,0366
0,0403	0,0024	0,0197	0,0729	0,8171	0,0340	0,0743	0,0020	0,0106	0,0098	0,0502	0,0400	0,0766
0,0381	0,0023	0,0191	0,0712	0,8771	0,0392	0,0773	0,0030	0,0128	0,0117	0,0483	0,0618	0,1384
0,0359	0,0021	0,0183	0,0694	0,9467	0,0457	0,0816	0,0043	0,0157	0,0143	0,0457	0,0933	0,2318
0,0337	0,0019	0,0175	0,0674	1,0279	0,0539	0,0876	0,0060	0,0197	0,0177	0,0423	0,1413	0,3731
0,0315	0,0018	0,0167	0,0653	1,1237	0,0644	0,0959	0,0083	0,0251	0,0224	0,0376	0,2207	0,5938
0,0293	0,0016	0,0158	0,0630	1,2379	0,0781	0,1074	0,0115	0,0327	0,0289	0,0311	0,3707	0,9645
0,0271	0,0015	0,0149	0,0605	1,3757	0,0965	0,1236	0,0162	0,0437	0,0382	0,0218	0,7407	1,7052
0,0249	0,0013	0,0140	0,0579	1,5446	0,1216	0,1465	0,0229	0,0602	0,0520	0,0080	2,8539	4,5591

Table 3.7 c): Computation of the flow profiles M2 and S2 by the direct step method

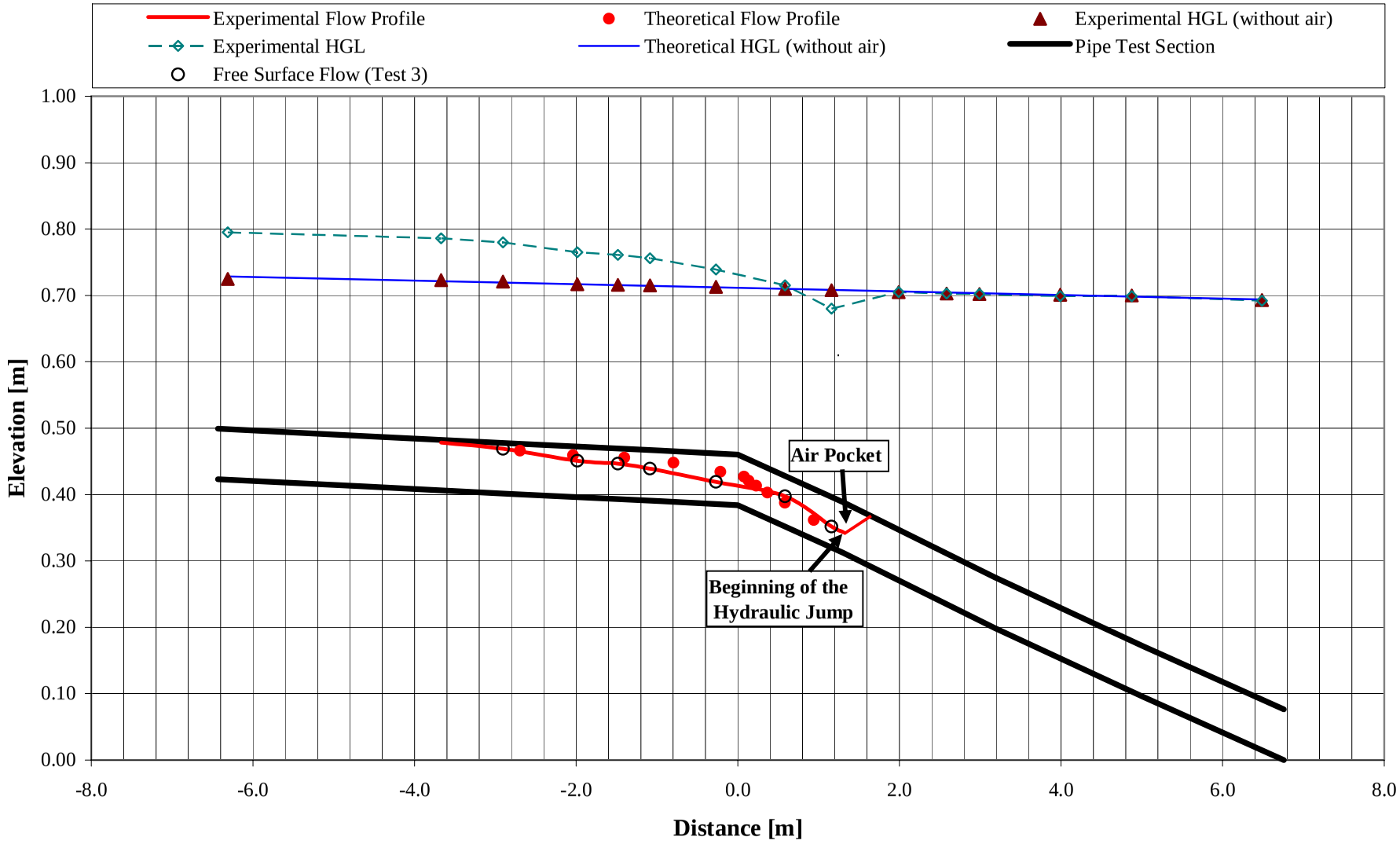

Figure 3.31: Flow profiles M2 and S2, Q_w = 0.020 m^3/s, V = 0.010 m^3

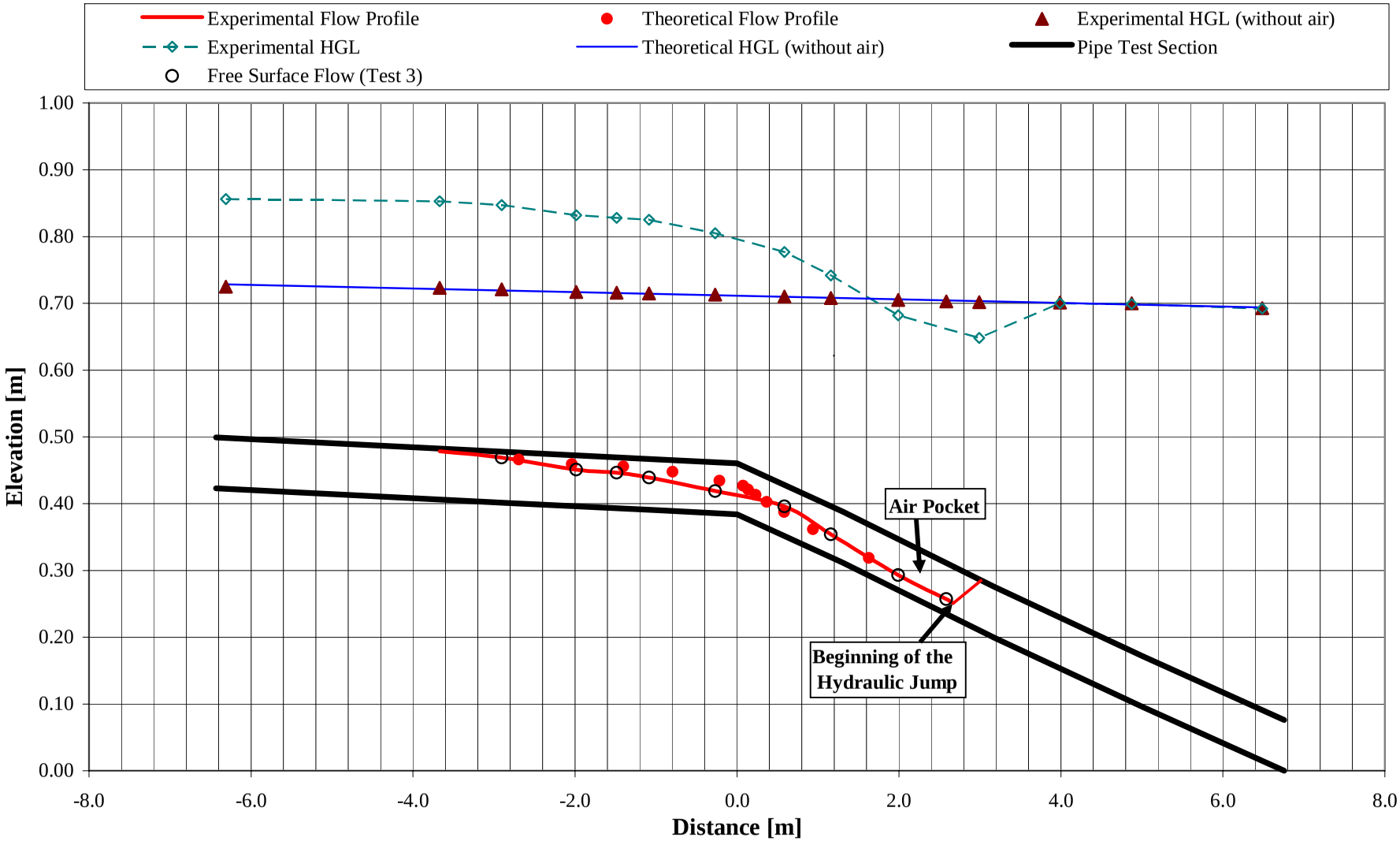

Figure 3.32: Flow profiles M2 and S2, Q_w = 0.020 m^3/s, V = 0.015 m^3

run 1	Q_w [m³/s]	V [m³]	S_{01}	S_{02}
	0,0023	0,01	0,006	0,06

Measuring Stations	HGL [m] Test 1	HGL [m] Test 2	Water Depths Yi [m] Test 2	Water Depths Yi [m] Test 3	Air pocket pressure [mH2O]
E_0	0,732	0,812	0,0762	0,0762	
E_1	0,725	0,806	0,0762	0,0762	
E_2	0,723	0,805	0,0762	0,0762	
E_3	0,719	0,797	**0,0634**	**0,064**	**0,3456**
E_4	0,718	0,793	**0,0619**	**0,06**	**0,3431**
E_5	0,718	0,790	**0,0569**	**0,057**	**0,3451**
E_6	0,717	0,777	**0,0439**	**0,044**	**0,3451**
E_7	0,711	0,745	**0,0404**	**0,04**	**0,3486**
E_8	0,707	0,701	**0,0339**	**0,031**	**0,3481**
E_9	0,703	0,680	0,0762	0,0762	
E_{10}	0,705	0,705	0,0762	0,0762	
E_{11}	0,705	0,704	0,0762	0,0762	
E_{12}	0,703	0,703	0,0762	0,0762	
E_{13}	0,701	0,701	0,0762	0,0762	
E_{14}	0,698	0,699	0,0762	0,0762	
Δh [cm]	5,10	13,50			

Length of the flow profiles Test 2 and Test 3 [m]		$L_{Hyd\ Jump}$ [cm]
Profile A2	Profile S2	17
-2,75	1,855	

Volume of air [m³] Test 2
0.010
Boyle´s Law
0,0096
Gradually Varied Flow
0,00700
% Error Boyle´s law vs GVF
27,02

a)

run 2	Q_w [m³/s]	V [m³]	S_{01}	S_{02}
	0,0023	0,015	0,006	0,06

Measuring Stations	HGL [m] Test 1	HGL [m] Test 2	Water Depths Yi [m] Test 2	Water Depths Yi [m] Test 3	Air pocket pressure [mH2O]
E_0	0,732	0,880	0,0762	0,0762	
E_1	0,725	0,873	0,0762	0,0762	
E_2	0,723	0,861	0,0762	0,0762	
E_3	0,719	0,858	**0,0649**	**0,065**	**0,4051**
E_4	0,718	0,857	**0,0599**	**0,061**	**0,4091**
E_5	0,718	0,854	**0,0589**	**0,058**	**0,4071**
E_6	0,717	0,839	**0,0459**	**0,044**	**0,4051**
E_7	0,711	0,809	**0,0399**	**0,039**	**0,4131**
E_8	0,707	0,752	**0,0309**	**0,032**	**0,4021**
E_9	0,703	0,708	**0,0259**	**0,026**	**0,4121**
E_{10}	0,705	0,675	**0,0234**	**0,023**	**0,4166**
E_{11}	0,705	0,651	**0,0159**	**0,016**	**0,4291**
E_{12}	0,703	0,701	0,0762	0,0762	
E_{13}	0,701	0,701	0,0762	0,0762	
E_{14}	0,698	0,694	0,0762	0,0762	
Δh [cm]	5,10	19,70			

Length of the flow profiles Test 2 and Test 3 [m]		$L_{Hyd\ Jump}$ [cm]
Profile A2	Profile S2	17
-2,75	3,235	

Volume of air [m³] Test 2
0.015
Boyle´s Law
0,0143
Gradually Varied Flow
0,0115
% Error Boyle´s law vs GVF
19,25

b)

Table 3.8: Experimental results for a 76.2 mm diameter acrylic pipe, profiles M2 and S2

S_{01} =	0,006	n =	0,0092									
Q_w (m³/s) =	0,0023	λ_{exp} =	0,0250									
Profile M2												
Yi [m]	**A [m²]**	**R [m]**	**$R^{2/3}$ [m]**	**v [m/s]**	**$v^2/2g$ [m]**	**E [m]**	**ΔE [m]**	**S_f**	**S_{fi}**	**$S - S_{fi}$**	**Δx [m]**	**$\Sigma\Delta x$ [m]**
0,0510	0,0032	0,0222	0,0789	0,7090	0,0256	0,0766	----	0,0068	----	----	0	0
0,0535	0,0034	0,0226	0,0798	0,6721	0,0230	0,0765	-0,0001	0,0060	0,0064	-0,0004	-0,1908	-0,1908
0,0560	0,0036	0,0229	0,0805	0,6398	0,0209	0,0769	0,0004	0,0053	0,0057	0,0003	-1,1047	-1,2954
0,0586	0,0038	0,0231	0,0810	0,6116	0,0191	0,0776	0,0007	0,0048	0,0051	0,0009	-0,7889	-2,0844
0,0611	0,0039	0,0232	0,0812	0,5870	0,0176	0,0786	0,0010	0,0044	0,0046	0,0014	-0,7394	-2,8238
0,0636	0,0041	0,0232	0,0812	0,5656	0,0163	0,0799	0,0013	0,0041	0,0043	0,0017	-0,7297	-3,5535
0,0661	0,0042	0,0230	0,0808	0,5472	0,0153	0,0814	0,0015	0,0039	0,0040	0,0020	-0,7376	-4,2911
0,0686	0,0043	0,0227	0,0801	0,5317	0,0144	0,0830	0,0017	0,0037	0,0038	0,0022	-0,7599	-5,0510
0,0712	0,0044	0,0222	0,0789	0,5190	0,0137	0,0849	0,0018	0,0037	0,0037	0,0023	-0,8006	-5,8516
0,0737	0,0045	0,0213	0,0768	0,5095	0,0132	0,0869	0,0020	0,0037	0,0037	0,0023	-0,8760	-6,7276
0,0762	0,0046	0,0190	0,0712	0,5043	0,0130	0,0892	0,0023	0,0042	0,0040	0,0020	-1,1168	-7,8444

S_{02} =	0,06	n =	0,0092									
Q_w (m³/s) =	0,002	λ_{exp} =	0,0250									
Profile S2												
Yi [m]	**A [m²]**	**R [m]**	**$R^{2/3}$ [m]**	**v [m/s]**	**$v^2/2g$ [m]**	**E [m]**	**ΔE [m]**	**S_f**	**S_{fi}**	**$S - S_{fi}$**	**Δx [m]**	**$\Sigma\Delta x$ [m]**
0,0510	0,0032	0,0222	0,0789	0,7090	0,0256	0,0766	----	0,0068	----	----	0	0
0,0486	0,0031	0,0218	0,0779	0,7495	0,0286	0,0772	0,0006	0,0078	0,0073	0,0527	0,0113	0,0113
0,0462	0,0029	0,0213	0,0766	0,7959	0,0323	0,0784	0,0012	0,0091	0,0085	0,0515	0,0239	0,0352
0,0437	0,0027	0,0207	0,0752	0,8492	0,0368	0,0805	0,0020	0,0108	0,0100	0,0500	0,0409	0,0762
0,0413	0,0025	0,0200	0,0736	0,9108	0,0423	0,0836	0,0031	0,0130	0,0119	0,0481	0,0645	0,1407
0,0389	0,0023	0,0193	0,0719	0,9824	0,0492	0,0881	0,0045	0,0158	0,0144	0,0456	0,0985	0,2391
0,0365	0,0022	0,0185	0,0699	1,0664	0,0580	0,0944	0,0063	0,0197	0,0178	0,0422	0,1503	0,3895
0,0341	0,0020	0,0177	0,0678	1,1658	0,0693	0,1033	0,0089	0,0250	0,0224	0,0376	0,2362	0,6256
0,0316	0,0018	0,0168	0,0654	1,2847	0,0841	0,1158	0,0124	0,0326	0,0288	0,0312	0,3988	1,0245
0,0292	0,0016	0,0158	0,0629	1,4288	0,1041	0,1333	0,0175	0,0436	0,0381	0,0219	0,8008	1,8252
0,0268	0,0014	0,0148	0,0602	1,6062	0,1315	0,1583	0,0250	0,0603	0,0520	0,0080	3,1095	4,9347

Table 3.8 c): Computation of the flow profiles M2 and S2 by the direct step method

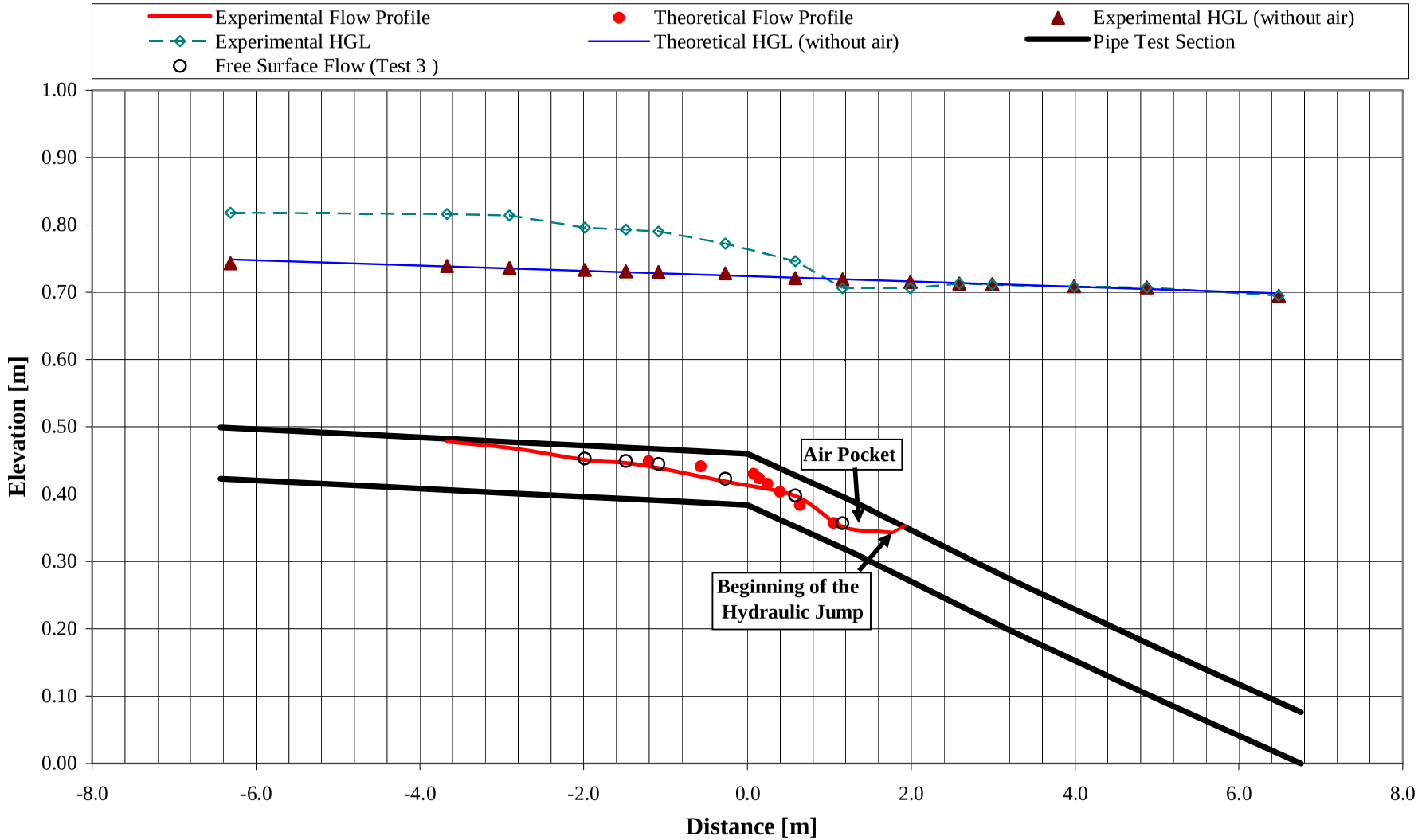

Figure 3.33: Flow profiles M2 and S2, Q_w = 0.023 m^3/s, V = 0.010 m^3

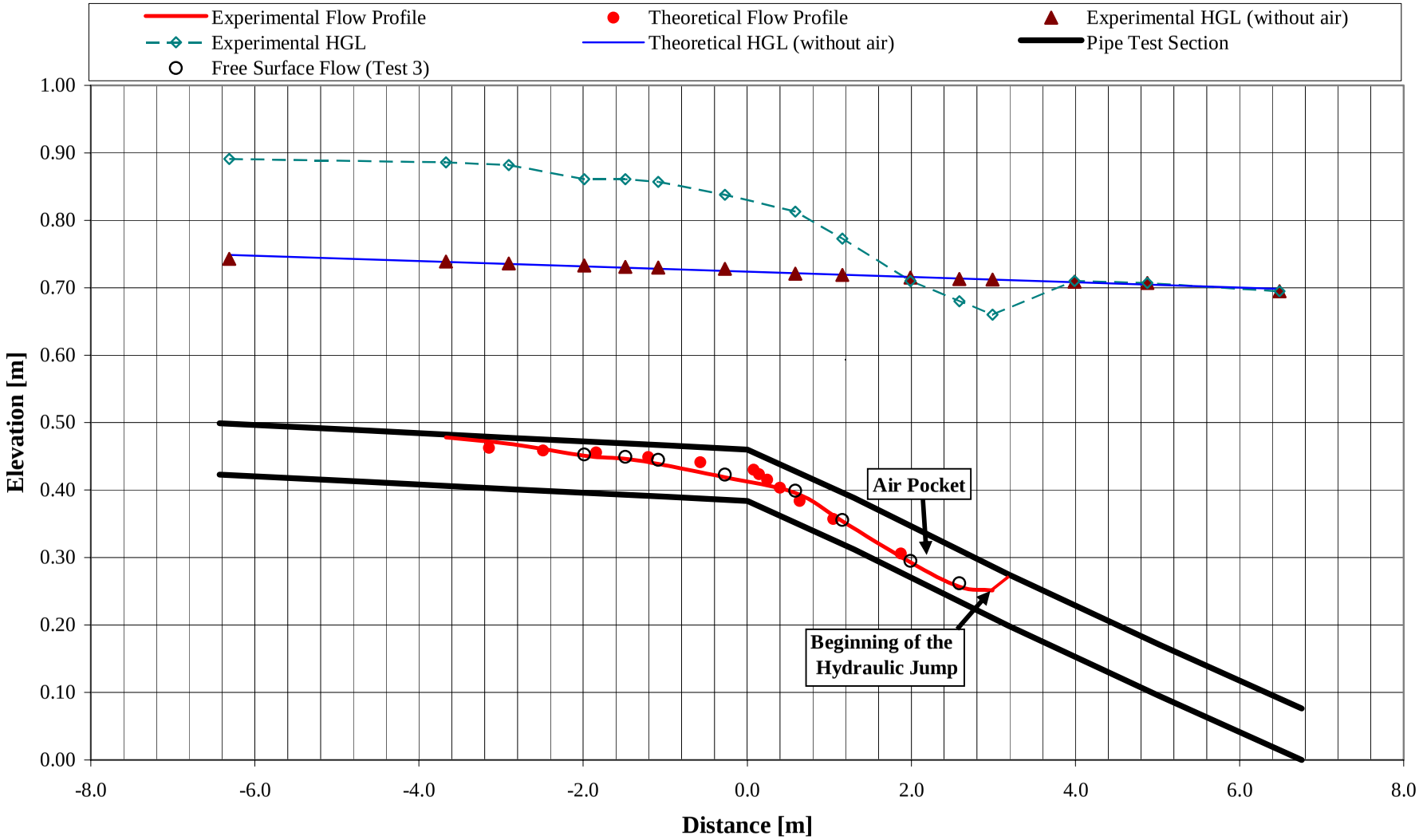

Figure 3.34: Flow profiles M2 and S2, Q_w = 0.023 m^3/s, V = 0.015 m^3

4. Effect of air pockets on hydraulic transients in pumping pipeline systems

4.1 Introduction

Hydraulic transient analysis is usually based on the assumption of no air in the water. However, in some pumping systems air entrainment can occur because pumps introduce air by the vortex action of the suction in quantities of 5% to 10% of the flow. When vacuum pressure occurs in the pipeline, air can leak in through seals at joints and valves. Likewise, water contains approximately 2% air by volume and air solubility in water is proportional to the pressure. Dissolved air may form a free gas phase at points in the pipeline where pressure drops or the temperature rises. In the same way, air pockets at intermediate or high points along the pipeline can also be presented due to the incomplete removal of air during filling and dewatering operations or progressive upward migration of air pockets. In addition, if air pockets located at high points of the pipeline cannot be carried downstream, it may occur that flow entirely stops because the cumulative head losses produced by the air pockets can be higher than the pump head capacity. The resulting pressure transients with entrained air are considerably different from that computed according to the ones without air in the line.

4.2 Effect of air pockets on hydraulic transients

The effect of entrained air in water pumping pipeline systems may be either harmful or beneficial, depending on the portion and location of the air as well as the system configuration and the causes of the transient, *Martin* (1976) [50]; *Martin* (1996) [51]. *Stephenson* (1997) [73] stated that the formation of large air pockets in pipelines can lead to further problems. However, if accepted, it may be beneficially used to reduce waterhammer.

The manner pipelines respond to the presence of this free air depends on how it is distributed. In a stationary or slowly moving flow it will tend to accumulate in pockets. If these are large, they can behave as air cushions and absorb or reflect the energy of transient pressure waves, *Horlacher and Lüdecke* (1992) [34], *Kottmann* (1992) [42], *Thorley* (2004) [78]. Likewise, the startup of pumps, or rapid opening of valves in piping systems during startup has caused many accidents during the past decades, because there is no practical form to remove all the entrained air from water lines. During startup, the air valve on the pump should be opened slowly to eliminate the air gradually from the pump discharge line to allow compression of this air without developing very high pressures. Besides, other cases of entrained air in pumping systems have caused the pipes to be pulled from their anchors, *Wylie et. al.* (1993) [89].

Qiu (1995) [59] stated that when air pockets are located at high points along the pipeline, the accumulated air is both unintended and unquantifiable. As a consequence, its potential influence on pressure transients is not often given consideration, either at design stage or in post failure inquiry. Situations where severe hydraulic transients may arise include system malfunction, temporary operation during maintenance and repair, or even during normal pump shutdown. Therefore, the effect of air pockets on hydraulic transients in pumping pipeline systems is studied in this chapter supported by the linear relationship proposed by *Gonzalez and Pozos* (2000) [29], equation (2.6), which can predict if large air pockets are likely to remain at intermediate or high points in pipelines. In the same way, the direct step method is used to obtain the flow profiles and the variables to estimate the volumes of air in the pockets by applying equation (3.7). By knowing the location of the air pockets and their volume, an analytical model based on the method of characteristics is utilized for predicting hydraulic transients caused by the shutdown in a pumping station.

4.3 Review of the effect of entrained air in pipeline systems

The effect of entrained air on hydraulic transients has been intensively investigated by many researchers and several mathematical models have been proposed. The studies of previous investigators are reviewed subsequently:

Brown (1968) [7] reported field test results and analytical investigations in two pump discharge lines, where the pressures were greater than predicted during design. The theoretical analysis was based on the method of characteristics by modifying the water column separation solution and considering the effects of entrained air in the pipeline. The total volume of entrained air is assumed to be lumped at the computing points equidistantly along the discharge line. Brown concluded that:

1) The inherent difficulty of the prediction of water column separation effects is further being complicated by the uncertainty about complete pump operating characteristics and actual momentum of inertia of pumps and motors.

2) The effects of air and gas entrained in solution in the water must be considered in the analytical solution.

3) Entrained air can have a detrimental effect on the hydraulic transients, i.e., large pressure surges in the discharge line and higher reverse speeds of the pumps can be caused by its presence.

Holley (1969) [33] developed hydraulic model investigations to study air entrainment problems when upstream control is used in water pipeline systems. Pressure oscillations in a pipeline with check structures space along the pipe were investigated. The pipe check structures serve three purposes:

1) Provide an overflow point high enough in elevation to keep the pipe from emptying when no water is flowing through the line.

2) The hydraulic gradient always passes below the top of the structure, therefore it does not overflow for the design water flow rate.

3) Provide an air source to keep negative pressure from developing when the flow rate is lower than the design value. The author found that important pressure peaks occurred when large amounts of air along the top of the pipe were exhausted from either the upstream pipe check structures or the downstream air release vent pipe.

Martin (1976) [50] investigated analytically the effect of entrapped air in pipelines for multiple configurations. The numerical solutions showed that entrapped air may be either beneficial or detrimental, depending on the amount and location of the air as well as the system configuration and the causes of the transient. Martin stated that the most severe causes of entrapped air occur during the rapid acceleration of a water column toward a volume of air that is completely confined. The resulting pressure peak can be many times the initial imposed pressure if the transient is applied rapidly. Results are also included to illustrate the effect of the initial location of an unconfined air pocket on the magnitude of the mixture pressure. The presence of the air is shown to cause peak pressures that are either greater or less than those that would occur without air.

Jönsson (1985) [35] developed analytical and experimental investigation to explain the impact of air pockets on hydraulic transients in a sewage pumping station with check valve and low water level in the pump sump. He attributed the large peak pressure predicted by the analytical study to the compression of an isolated air cushion next to the check valve. The author applied a standard model with constant wave speed to show that the pressure peaks

will arise stronger than the pressure peaks obtained when no air is let in the line and concluded that smaller volumes of air lead to larger pressure peaks. On the other hand, there is a lower limit to the volume of air that could be described as behaving as a cushion. Jönsson suggested that the strong pressure peaks must be considered at the design stage of the pipeline. Later *Jönsson* (1992) [36] presented and discussed the hydraulic transients computed and measured in three different sewage pumping pipelines. A computational model based on the air pocket concept and one dimensional compressible flow theory for the water column was developed to simulate the effect of the entrained air. The author corroborated his prior conclusions.

Hashimoto et al. (1988) [31] studied transients following the rapid opening of a valve on the upstream side of a fluid pipeline containing an air pocket, or the gas pipeline containing a liquid column. Basic equations of the lumped-element representation for the pipeline system and an equation to calculate the surge pressure were used for the theoretical computations and solved by applying the fourth-order Runge-Kutta-Gill method. The maximum pressure attained is about 2.4 times that of the supply pressure, and it is larger than the results of the system without air pocket. The theoretical results were compared with the experimental results and agreed well.

Larsen and Borrows (1992) [46] computed pressure transients and compared them with field measurements in three different pumping plastic sewer mains. The comparison highlighted the effect of cavitation (water column separation) and air pockets at the high points of the pipelines followed by pump run-down. The numerical model used in the investigation was based on the standard method of the characteristics. The authors found that only by including air pockets at the high points of the pumping systems within the numerical model could be observed that the measured and computed transient pressures adjusted reasonably well. They pointed out that air pockets can either damp or amplify the pressure transients depending on their size and causes of the transients. Accordingly one can expect that air pockets in some situations can lead to excessive load and even rupture of the line.

Förster (1997) [23] investigated the pressure absorbed by large air pockets located at aerated high points of a pipeline model during the occurrence of hydraulic transients experimentally and analytically. Likewise, several measurements were carried out in order to identify the influence of the geometry and volume of the air pocket on the absorption of the pressure. From the results obtained, it can be stated that the dampening effect on the water hammer

produced by the air pockets is affected considerably by their free surface. In the same way, the author developed a dimensionless representation of the equations utilized in the analytical model to study the effect of large air pockets on pressure transients in pipelines with larger diameters than that used during the research.

Fuertes (2000) [24] developed a mathematical model to analyze the hydraulic transients due to the compression of air pockets located at high points of pipelines. The main assumptions made in the model are the use of a lump parameter model (rigid model) and that the water-air interface coincides with the pipe cross section. Experimental investigations were carried out to validate the theoretical model. The agreement between experimental and analytical results was good during the first phase of the transient, which is when peak pressures and velocities develop. In a second stage of the investigation, the presence of air valves is included in the mathematical model to simulate air pockets and air valves within irregular profile systems. In laboratory a great number of experiments were conducted with these devices and theoretical and experimental predictions were compared.

Zhou (2000) [92] presented the results of analytical and experimental investigations on the effect of trapped air on hydraulic transients in pipelines, especially for sewer trunks during the rapid filling stage. The experimental investigation consisted of the rapid filling of different pipeline configurations containing trapped air. The computational model used during the investigation was based on the rigid column theory. The model was calibrated using the experimental data and was found to be able to predict the magnitude of maximum waterhammer peak pressure.

Burrows and Qiu (1995) [9] presented case studies to illustrate the influence of air pockets on hydraulic transients. In some cases the high peak pressures can severely arise and a catastrophic effect might be expected to occur, such as the rupture of the line. Either a single small pocket or multiple small air pockets are shown to be especially problematic. Peak pressures enhancements as high as 1.6 or even 2 times the normal steady flow duty pressures have been predicted. In addition, *Qiu and Burrows* (1996) [60] concluded that the presence of small air pockets in pumping pipeline systems may have a potential effect on hydraulic transients, due to an abrupt interruption of flow arising from routine pump shutdown. It is suggested that this could trigger serious implications for pipeline systems, where entrained air has not been taken into account.

Burrows (2003) [8] reported a real case study in which a pumping pipeline suffered from cracks and spillage. He determined that the transient pressures induced by the pump shutdown would not have been the unique cause for the failures of the line. It was found that a small air pocket located at an intermediate high point of the system was identified as likely to generate the enhancement of the pressure transients, experienced by a normal pump shutdown.

4.4 Numerical model to investigate the effects of air pockets on hydraulic transients

The numerical model was developed with the main goal to demonstrate the effect of entrained air in form of pockets on hydraulic transients caused by pump power failure. It can be considered the most severe circumstance within a pumping pipeline.

Computations corresponding to this study were evaluated by using a hydraulic transient analysis program based on the method of characteristics and the theory and procedures presented by *Wylie and Streeter* (1978) [88], *Chaudhry* (1987) [10] and *Wylie et al.* (1993) [89]. The upstream boundary is a pumping station and the downstream boundary a constant head tank. The effect of the air pockets is taken into account as outlined below. Some of the assumptions made by *Borrows and Qiu* (1995) [9] during their investigation were taken into account for the development of the numerical model:

a) The standard method of the characteristics is applied to obtain the ordinary differential equations. These are then solved along the characteristic lines with first order approximation and without interpolation to eliminate numerical damping.

b) Air pockets of pre-selected size can be located at chosen nodal points; it is assumed that the pocket included will not result in water column separation during the transients, see Figure 4.1. Also the air in the pocket does not occupy the entire cross section of the pipe and remain in its original position during the time-scale of the hydraulic transient.

c) The transient wave celerity remains invariant during the analysis.

d) The air in the pocket is supposed to follow the polytropic equation of state.

e) Friction and local losses, as well as pumping station losses are considered in the analytical model.

f) For computational convenience, the pre-selected air pocket coincides with a junction between adjacent pipe reaches.

The air pocket is located at the *i*th junction, see Figure 4.1.

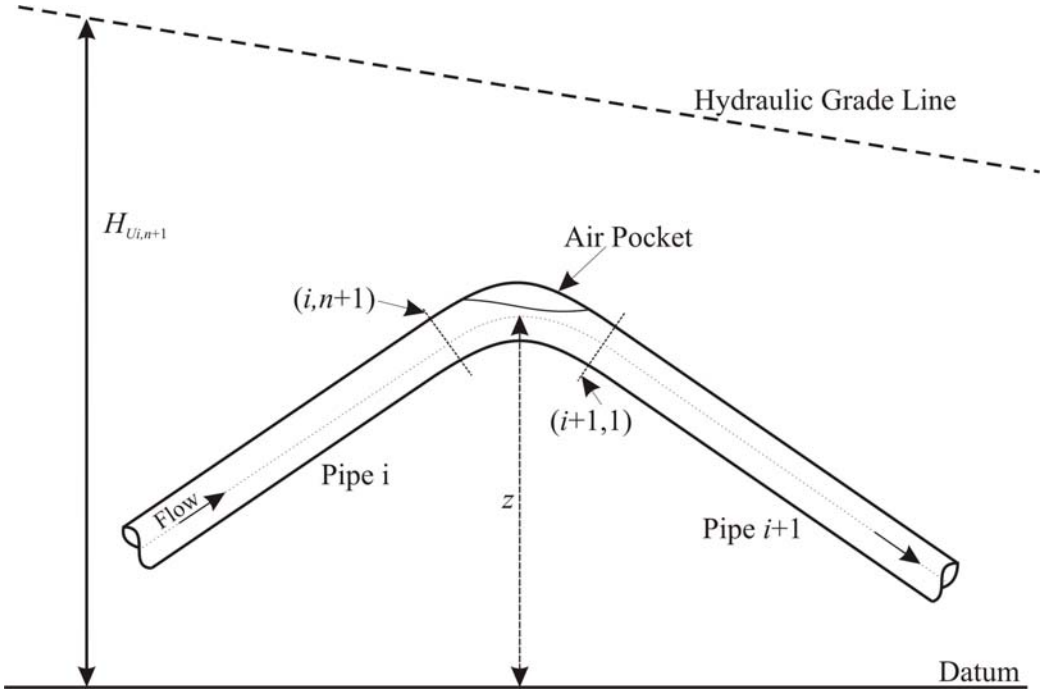

Figure 4.1: Notation for the air pocket

The following computational procedure is based on the above references.

The air pocket polytropic change given by equation (4.1) is used as boundary condition:

$$H_A V^{\psi} = c \quad [\mathrm{m}^4] \qquad (4.1)$$

in which

H_A absolute head [m]
V volume of air [m^3]
ψ polytropic index [-]
c constant determined from the initial steady state condition for the air pocket

That can be also presented as

$$(H_{U_{i,n+1}} - z + H_b)V_{Ui}^{\psi} = c_1 \quad [\mathrm{m}^4] \qquad (4.2)$$

$H_{U_{i,n+1}}$ piezometric head above the datum at the section (i,n+1) at the end of the time step [m]
z height of the pipe axis above the datum [m]
H_b barometric pressure head [m]
V_{U_i} volume of air at the end of the time step [m^3]

The value of the index ψ is equal to 1.0 for a slow isothermal process, and it is equal to 1.4 for a fast adiabatic process. An average value of $\psi = 1.2$ is here used.
Borrows and Qiu (1995) [9] found that the effect of the polytropic index ψ on the behavior of the air pockets during the hydraulic transients is of secondary importance.

The continuity equation at the air pocket can be written as

$$V_{U_i} = V_i + \frac{1}{2}\Delta t\left[(Q_{U_{i+1,1}} + Q_{i+1,1}) - (Q_{U_{i,n+1}} + Q_{i,n+1})\right] \quad [\mathrm{m}^3] \qquad (4.3)$$

V_i volume of the air at the beginning of the time step [m^3]
Δt size of the time step [s]
$Q_{i,n+1}$ water flow rate at the upstream end of the air pocket at the beginning of the time step [m^3/s]
$Q_{U_{i,n+1}}$ water flow rate at the upstream end of the air pocket at the end of the time step [m^3/s]
$Q_{i+1,1}$ water flow rate at the downstream end of the air pocket at the beginning of the time step [m^3/s]
$Q_{U_{i+1,1}}$ water flow rate at the downstream end of the air pocket at the end of the time step [m^3/s]

Note that the variables with subscript *U* indicate that these are unknown at the end of the time step $t + \Delta t$, while the variables without the subscript *U* refer to their known value at the beginning of the time step *t*.

If the method of characteristics is utilized for the analysis of the hydraulic transients, then the positive and negative characteristic equations at the end of each computational time step are defined as

$$Q_{U_{i,n+1}} = C_{(+)} - C_{a_i} H_{U_{i,n+1}} \quad [\mathrm{m}^3/\mathrm{s}] \qquad (4.4)$$

$$Q_{U_{i+1,1}} = C_{(-)} + C_{a_{i+1}} H_{U_{i+1,1}} \quad [\mathrm{m}^3/\mathrm{s}] \qquad (4.5)$$

where

$$C_{(+)} = Q_{i,n+1} + C_{a_i} H_{i,n+1} - R_i Q_{i,n+1}\left|Q_{i,n+1}\right| \quad [\mathrm{m}^3/\mathrm{s}] \qquad (4.6)$$

$$C_{(-)} = Q_{i+1,1} - C_{a_{i+1}} H_{i+1,1} - R_{i+1} Q_{i+1,1}\left|Q_{i+1,1}\right| \quad [\mathrm{m}^3/\mathrm{s}] \qquad (4.7)$$

$$R_i = \frac{\lambda_i \Delta t_i}{2 D_i A_i} \quad [\mathrm{s}/\mathrm{m}^3] \qquad (4.8)$$

$$R_{i+1} = \frac{\lambda_{i+1} \Delta t_{i+1}}{2 D_{i+1} A_{i+1}} \quad [\mathrm{s}/\mathrm{m}^3] \qquad (4.9)$$

$$C_{a_i} = \frac{gA_i}{a_i} \quad [\mathrm{m^2/s}] \tag{4.10}$$

$$C_{a_{i+1}} = \frac{gA_{i+1}}{a_{i+1}} \quad [\mathrm{m^2/s}] \tag{4.11}$$

λ Darcy – Weisbach friction factor [-]
Δt time step [s]
D pipe diameter [m]
A total cross section area of the pipe [m^2]
g gravitational acceleration [m/s^2]
a transient wave speed [m/s]

In addition, if the head losses in the pipeline at the junction are neglected, then

$$H_{U_{i,n+1}} = H_{U_{i+1,1}} \quad [\mathrm{m}] \tag{4.12}$$

Now there are five unknown variables in five equations, namely, $H_{U_{i,n+1}}$, V_{U_i}, $Q_{U_{i+1,1}}$, $Q_{U_{i,n+1}}$, $H_{U_{i+1,1}}$. The elimination of the last four unknowns, yields

$$\left(H_{U_{i,n+1}} + H_b - z\right)\left[C_{air} + \frac{1}{2}\Delta t\left(C_{a_i} + C_{a_{i+1}}\right)H_{U_{i,n+1}}\right]^{\psi} = c_1 \quad [\mathrm{m^4}] \tag{4.13}$$

$$C_{air} = V_i + \frac{1}{2}\Delta t\left(Q_{i+1,1} - Q_{i,n+1} + C_{(-)} - C_{(+)}\right) \quad [\mathrm{m^3}] \tag{4.14}$$

Equation (4.13) can be solved for $H_{U_{i,n+1}}$ by an iterative method, for example, the bisection method. No doubt other methods could also be used. The values of the other unknown variables may be evaluated from equations (4.2) through (4.12).

During the computations the finite difference scheme is stable, because the Courant-Friedrich-Lewy condition is always satisfied if Δt is appropriately selected.

$$\Delta x \geq a\Delta t \quad [\mathrm{m}] \tag{4.15}$$

The numerical model has been written by the author in COMPAQ VISUAL FORTRAN® [94]. It is called HT-PAM and is implemented on WINDOWS XP. It is supported somewhat on the program PTPS developed by *Qiu* (1995) [59], which is also based on the method of characteristics of finite differences suggested previously by *Wylie and Streeter* (1978) [88]. The new program was expanded to allow a maximum of 400 pipe sections, 30 air pockets that can be located at any junction throughout the line, as well as a set of 6 homogeneous pumps connecting in parallel per pumping plant. The program generates an output file with the

maximum and minimum heads obtained at each nodal point along the pipeline profile during the simulation time specified. These data can be transferred to graphics to plot the maximum and minimum head envelopes to compare the hydraulic transients computed with and without air pockets located at the intermediate and high points of the pipeline.

4.5 Summary of the computation steps and procedure of calculation

The flowchart of Figure 4.2 shows the computational steps for determining the transient condition in a pumping pipeline system with air pocket located at their high points. The associated equations are presented in Table 4.1.

4.6 Case Study

A study of a pumping pipeline system without surge suppression devices is presented to demonstrate the potential effect of air pockets on hydraulic transients. The boundary condition at the upstream end is a pumping station and at the downstream end a constant head tank. Only hydraulic transients generated by power failure at the pumping station are taken into account in this analysis.

The pumping station operates with four centrifugal pumps connected in parallel and each unit is able to deliver a maximum water flow rate, Q_w = 0.625 m^3/s to the constant head tank 396.92 m above the pump sump level. The conduction is 2289 m in length and made up of steel pipes with an inner diameter of 1.22 m. The sketch in Figure 4.3 illustrates schematically the investigated pumping pipeline profile.

Before applying the numerical model to investigate the effect of air pockets on hydraulic transients, an analysis was developed to identify the location of the air pockets in the pumping pipeline system and to quantify their volume. By using the linear equation proposed by *Gonzalez and Pozos* (2000) [29], equation (2.6), it was found that 4 high points are likely to accumulate air when the pumping station operates with 3 units (Q_w = 1.875 m^3/s), see Figure 4.4. During the performance of the 4 units in the pumping station (Q_w = 2.5 m^3/s) only an intermediate high point is a possible candidate for air buildup, as shown in Figure 4.5.

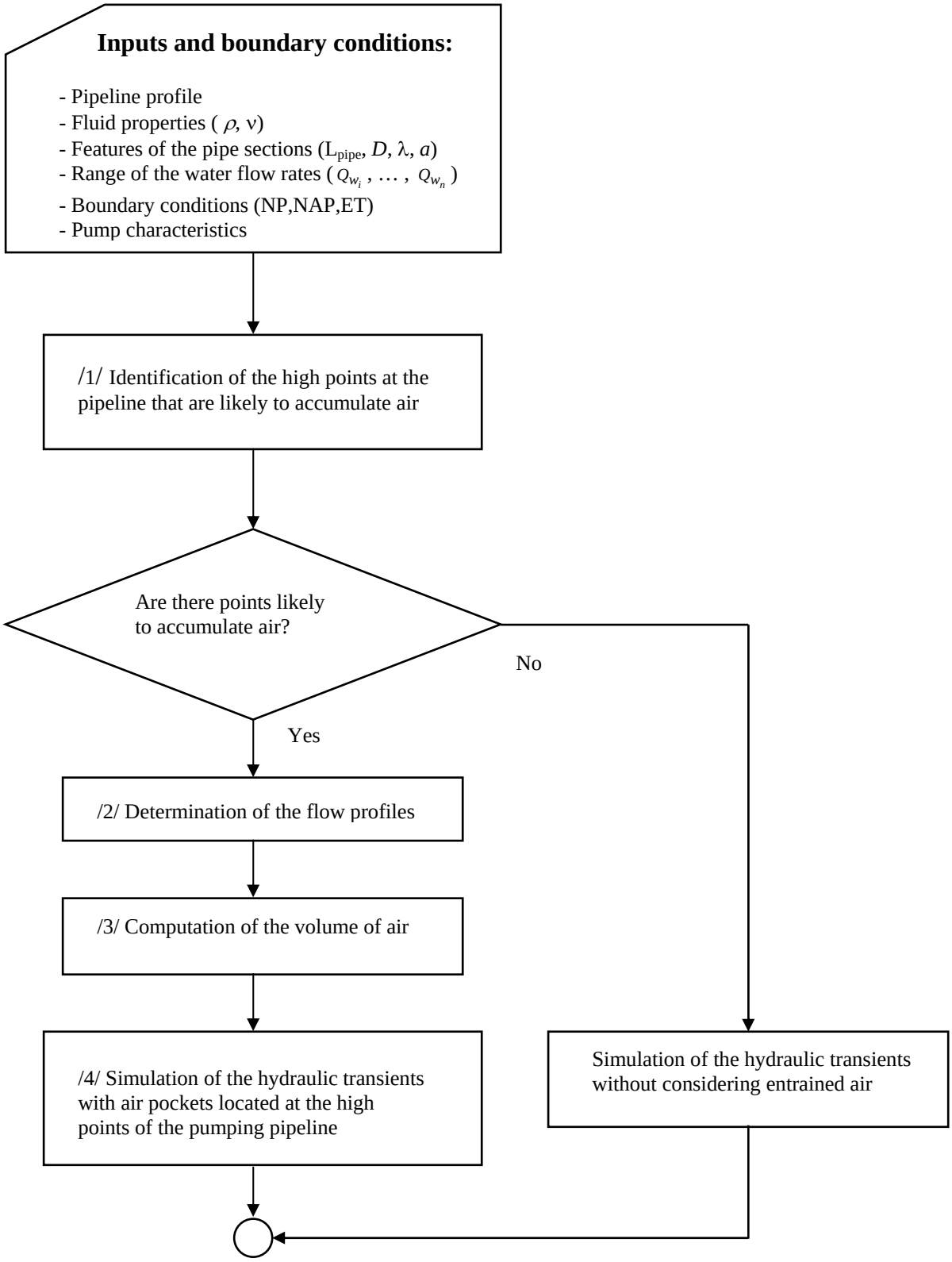

Figure 4.2 Overview of the procedure of computation of hydraulic transients with air pockets located at the high points of pumping pipeline systems

Current No. according to Figure 4.2	Associated equations
/1/	$Q_w^2 / gD^5 = S$ /Air behavior (2.6)
/2/	$\Delta x = \frac{E_2 - E_1}{S_0 - S_f}$ / Dynamic equation of the gradually varied flow (3.4)
/3/	V / Volume of air (3.7)
/4/	V_{U_i} / Volume of air at the beginning of the time step (4.3) $Q_{U_{i,n+1}}$ / Water flow rate at the upstream end of the air pocket at the end of the time step (4.4) $Q_{U_{i+1,1}}$ / Water flow rate at the downstream end of the air pocket at the end of the time step (4.5) $H_{U_{i,n+1}}$ / Piezometric head at the upstream end of the air pocket at the end of the time step (4.12)

Table 4.1: Assignment of the equations to the computation steps represented in Figure 4.2

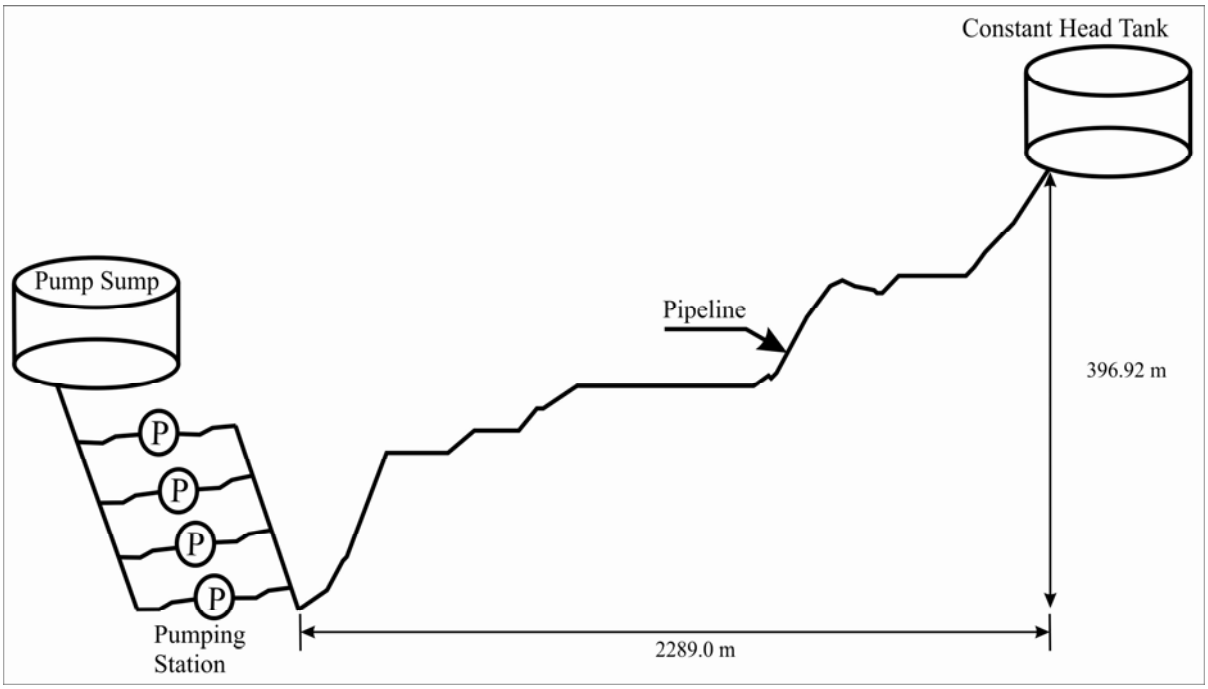

Figure 4.3: Profile of the pumping pipeline system

The results obtained with equation (2.6) are compared with the relationship presented by *Walski et al.* (1994) [83] to describe the behavior of air pockets in pumping pipeline systems. The equation can be written as

$$\frac{\xi v_{nom}^2}{gDS} = \mathrm{T}' = 1 \quad [-] \qquad (4.14)$$

T´ is the dimensionless gas pocket number and is equal to the unity when the forces acting on the air pocket are balanced.

ξ empirical dimensionless coefficient [-]
v_{nom} nominal velocity (velocity when no air pocket exist) [m/s]
S pipe slope [-]
D pipe diameter [m]
g gravitational acceleration [m/s^2]

ξ can be approximated by equation (4.15)

$$\xi = 0.88S^{0.68} \quad [-] \qquad (4.15)$$

Substituting equation (4.14) into equation (4.15) gives an equation for determining if gas pockets are likely to occur in a pipe section.

$$\frac{0.88 v_{nom}^2}{gDS^{0.32}} = \mathrm{T}' \quad [-] \qquad (4.16)$$

When T´ is greater than one for a downward sloping pipe, then the air pockets will move downstream. When it is less than one, the pocket will move upstream.

The results obtained with the equations (2.6) and (4.16) are summed up in Table 4.2. The values of the pipe slopes S correspond to the downward sloping pipes, where the air bubbles/pockets will move backward relative to the current, then air will accumulate at the high points located at the upstream end of the downgrade pipe.

Q_w [m^3/s] 1.875	**v_{nom} [m/s] 1.604**		
Pipe Slope S	**Q_w^2/gD^5 = 0.1326**	**0.88 $v_{nom}^2/gDS^{0.32}$**	**Behavior**
0.1995	Air moves upstream	0.3168	Air moves upstream
0.1354	Air moves upstream	0.3587	Air moves upstream
0.1600	Air moves upstream	0.3400	Air moves upstream
0.3226	Air moves upstream	0.2717	Air moves upstream
Q_w [m^3/s] 2.5	**v_{nom} [m/s] 2.139**		
Pipe Slope S	**Q_w^2/gD^5 = 0.1326**	**0.88 $v_{nom}^2/gDS^{0.32}$**	**Behavior**
0.3225	Air moves upstream	0.4830	Air moves upstream

Table 4.2: Movement of air bubbles/pockets in the downward sloping pipes of the pipeline

From the results presented in the Table 4.2, it can be concluded that for this pipeline configuration the equations proposed by *Walski et al.* (1994) [83] and *Gonzalez and Pozos* (2000) [29] predicted the same behavior of the air bubbles and pockets in the downward sloping pipes.

In addition, equation (3.7) was utilized to compute the volumes of air in the pockets, as described in section 3.5. The results are summarized in Tables 4.3 and 4.4.

Q_w = 1.875 [m^3/s]			
Volume of air in the pocket 1 [m^3]	**Volume of air in the pocket 2 [m^3]**	**Volume of air in the pocket 3 [m^3]**	**Volume of air in the pocket 4 [m^3]**
0.145	0.448	1.038	0.412
0.242	0.576	1.152	0.480
0.429	0.816	1.368	0.614
0.761	1.235	1.747	0.856
1.334	1.944	2.395	1.286
2.326	3.147	3.503	2.048
4.099	5.244	5.456	3.449

Table 4.3: Air pocket volumes when 3 pumps operate at the pumping station

Q_w = 2.5 [m^3/s]
Volume of air in the pocket 1 [m^3]
0.164
0.214
0.325
0.542
0.948
1.702
3.143

Table 4.4: Air pocket volumes when 4 pumps operate at the pumping station

4.7 Analysis of results

The effect of different air pocket volumes on hydraulic transients generated by simultaneous pump shutdowns at a pumping station without considering protection devices along the pipeline is theoretically analyzed within this section. The air pocket volumes summarized in tables 4.3 and 4.4 were located at intermediate and high points identified in the analysis. Subsequently, a series of numerical simulations by using the numerical model presented in the subsection 4.4 were developed to find the worst case scenarios and the critical air pocket volumes that may be present in the pumping pipeline. The most critical scenario is that when the pumping station operates with three units and the four smallest air pocket volumes computed with the equation (3.7) are placed at the points 1 to 4 of the line. In addition, to compare the hydraulic transients with and without air pockets located at the intermediate and high points of the pumping pipeline, the sudden shutdown of the pumps due to power failure

was simulated without considering air accumulated. The analysis was developed based on the method of characteristics. This numerical method is used to find the instantaneous head H and instantaneous water flow discharge Q for each nodal point throughout the pipeline until the desired time duration has been covered. From the head envelopes obtained, only the maximum and minimum head envelopes in the system are of particular interest within this investigation. The most useful manner to represent these is to plot the maximum and minimum values of the head, independently at which time step they were obtained, versus the longitudinal section of the pipeline. This provides a quick and easy way to identify critical design points in the system and it is useful when reviewing potential surge control strategies. The maximum and minimum total head envelopes achieved without regarding air are plotted in Figures 4.4 and 4.5. It can be seen from the minimum total head envelopes that part of the system will experience subatmospheric pressure that can lead to water column separation. This will take place from station 0 + 716.5 to station 0 + 996.9 and 1 + 565.6 to 1 + 719.5 when four pumps are performing at the pumping station. Subatmospheric pressure will occur between the stations 1 + 586.6 and 1 + 699.7 when three units are performing at the station. Therefore, surge protection will be required to uplift the minimum total head envelopes in the system to within acceptable limits.

When the predictions of hydraulic transients show that water column separation will occur in the pipeline, then it has to be studied if the pressures generated when the separated columns rejoin are acceptable. Hence, the provision of various control surge devices should be investigated. The following are some of the common devices usually employed to prevent water column separation or to reduce the pressure rise when the separated columns rejoin:

- Air chamber
- One way surge tank
- Flywheels
- Air-inlet valves
- Pressure relief or pressure regulating valves

Another relevant aspect that has to be taken into account during the design stage of the pipeline is that the wall thickness of the pipe has to withstand the full range of transient pressures heads that will occur in the system. For the dimensioning of the wall thickness the envelope of the upper pressures is decisive.

It is important to state that the purpose of this work is not to show a rigorous treatment of the method of characteristics nor either to simulate the hydraulic transient including surge suppression devices. Those interested in the mathematical treatment of the method of characteristics and the surge devices to reduce the effect of hydraulic transients in pipeline systems should refer to *Chaudhry* (1987) [10], *Horlacher* (1992) [34] and *Wylie et al.* (1993) [89].

4.7.1 Pumping station performing with 3 units (Q_w = 1.875 m^3/s) and 4 air pockets located at the high point 2 and intermediate points 1, 3 and 4.

Three different sets of air pocket volumes were taken into account to demonstrate the effect of multiple air pockets located at intermediate and high points of the pumping pipeline, when three pumps are performing in the station. The smallest air pocket volumes (V_1 = 0.145 m^3, V_2 = 0.448 m^3, V_3 = 1.038 m^3, V_4 = 0.412 m^3) were found to be the critical air pockets. The subscripts indicate the point where the corresponding air pocket volume is located. Two more sets of air pockets were used to compare the maximum and minimum head envelopes obtained with the smallest air volumes. The air pocket volumes (V_1 = 0.761 m^3, V_2 = 1.235 m^3, V_3 = 1.747 m^3, V_4 =0.856 m^3) are named intermediate in this specific case and the largest air pocket volumes are (V_1 = 4.099 m^3, V_2 = 5.244 m^3, V_3 = 5.456 m^3, V_4 = 3.449 m^3).

The presence of the 4 smallest volumes of air lead to the worst scenario, they caused a considerable enhancement of the maximum and minimum pressure transients throughout the system, see Figure 4.4. The predictions achieved by utilizing the numerical model indicate that these pockets absorbed only a part of the transient pressure wave and the rest is reflected towards the boundaries at upstream and downstream ends of the pipeline. The amplification of the maximum and minimum head envelopes are caused due to the reflection of the transient pressure waves at check valves of the pumps, air pockets and the constant head tank.

The maximum and minimum heads decreased with increasing the volumes of air. For example, the intermediate volumes of air considered in this analysis reduced significantly the reflection of the transient pressure waves towards to the pumping station. The minimum head is uplifted to values that are lower than those computed without air. Likewise, the pockets located at points 3 and 4 have a similar reflecting effect as the smallest air pockets placed at the same points.

It can be observed in Figure 4.4 that after the shutdown of three pumps the maximum and minimum heads along the pumping pipeline were considerably reduced by the largest air pocket volumes located at the points 1 to 4. In this case the cushioning effect produced by the air pockets absorbed considerably the transient pressures waves, and only a minor reflection is produced by the pocket located at point 3. Hence, it can be stated that these volumes of air are optimal for the configuration of the pumping pipeline system.

4.7.2 Pumping station performing with 4 units (Q_w = 2.5 m^3/s) and an air pocket located at the intermediate high point 1

To demonstrate the effect of an air pocket located at the intermediate high point 1 when four pumps are operating in the pumping station, three different volumes of air were considered. The smallest air pocket (V = 0.164 m^3), the critical air pocket (V = 0.948 m^3) and the largest air pocket (V = 3.143 m^3). The predictions are shown in Figure 4.5.

In the case of the smallest volume of air computed (V = 0.164 m^3), the minimum and maximum pressure transients along the pipeline are slightly lower than those obtained without entrained air, except for the upstream section at the pump discharge. The small pocket produced a cushioning effect, absorbing part of the transient pressure wave uplifting the minimum head and reducing the maximum head, except for the minimum and maximum head values obtained immediately downstream of the discharges of the pumps.

The critical air pocket volume (V = 0.948 m^3) caused a considerable enhancement of maximum head along the pipeline, when it was placed at point 1. The effect on minimum head was also considerable. In addition, the pocket generated an important reflection of the maximum pressure transients towards the pumping plant and the constant head tank.

Investigators have shown that peak pressure transients can be enhanced by small air pockets, *Borrows and Qiu* (1995) [9], *Qiu and Borrows* (1996) [60], *Borrows* (2003) [8]. *Gahan* (2004) [25] highlighted that the small and large air pocket volumes can be defined in terms of their effect on hydraulic transients, but there are limits to the volumes of air, outside of which, these effects do not occur.

On the contrast, the largest volume of air (V = 3.143 m^3) predicted and located at point 1 generated a positive transient that travelled upstream towards the pumping plant as downstream to the constant head tank. The pocket behaved as an air cushion and reflected the transient pressure waves in both directions with respect to the position of the pocket.

Likewise, the air pocket behaved as an air chamber uplifting the minimum head only downstream of the pocket, but produced an important minimum head immediately downstream of the pumps discharge. Therefore, it can be stated that for the largest volume of air achieved and located in this point, it does not have any beneficial effect on the hydraulic transients.

The maximum and minimum heads generated by the shutdown of four pumps were exacerbated by the range of volumes of air considered, therefore it can be stated that there was not an optimal volume of air for this pipeline, when the pocket is located at the intermediate high point 1. In the same way, it could be observed that the minimum head along the pipeline showed an enhancement at the upstream section, as the volume of air was enlarged.

For all the volumes of air, the maximum head immediately downstream of the pumping station are above that predicted under the assumption that no air is accumulated at the high or intermediate points. Only for the largest volume of air the minimum head computed is lower than that achieved without air.

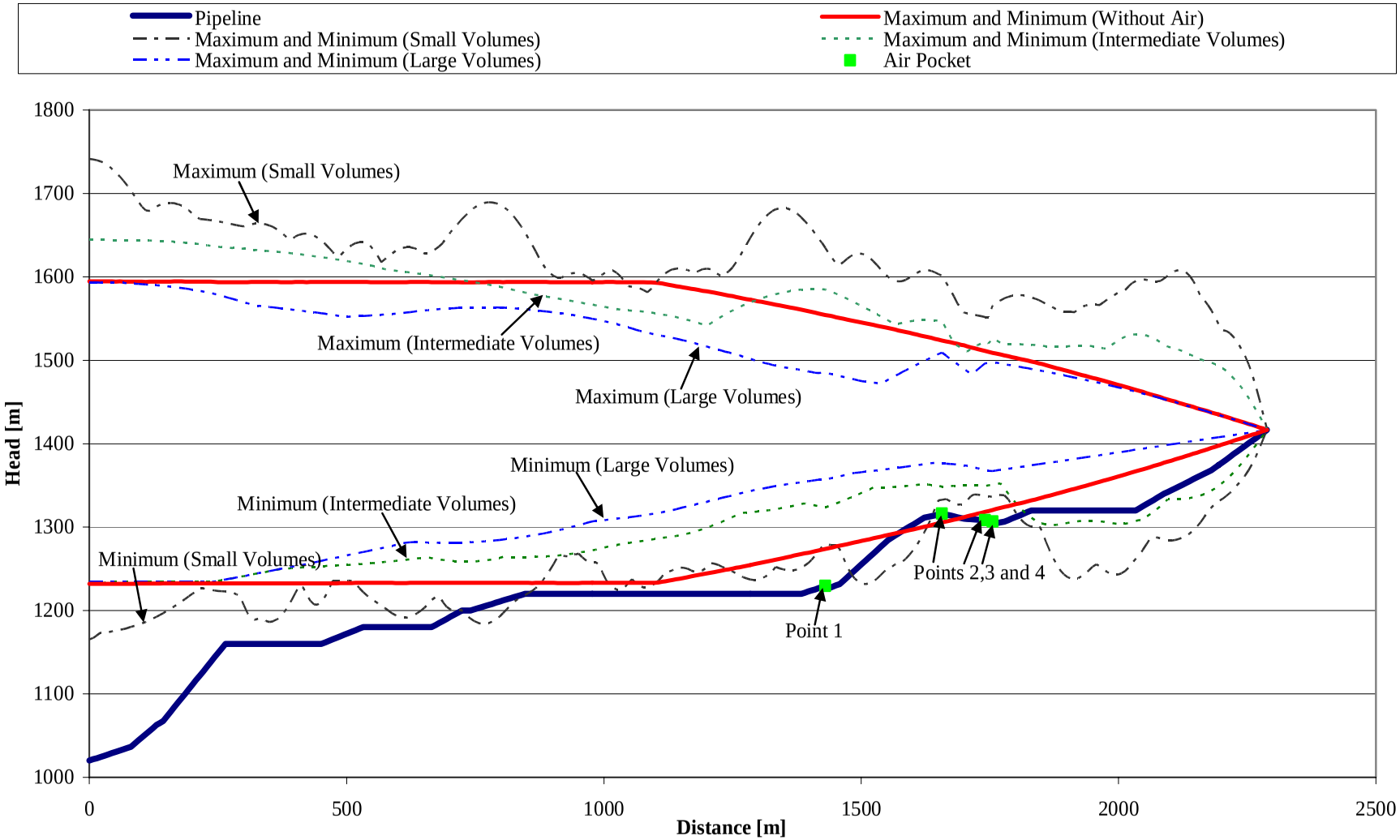

Figure 4.4: Maximum and minimum head envelopes with different air pocket volumes located at points 1, 2, 3 and 4, and flow water rate Q_w = 1.875 m^3/s

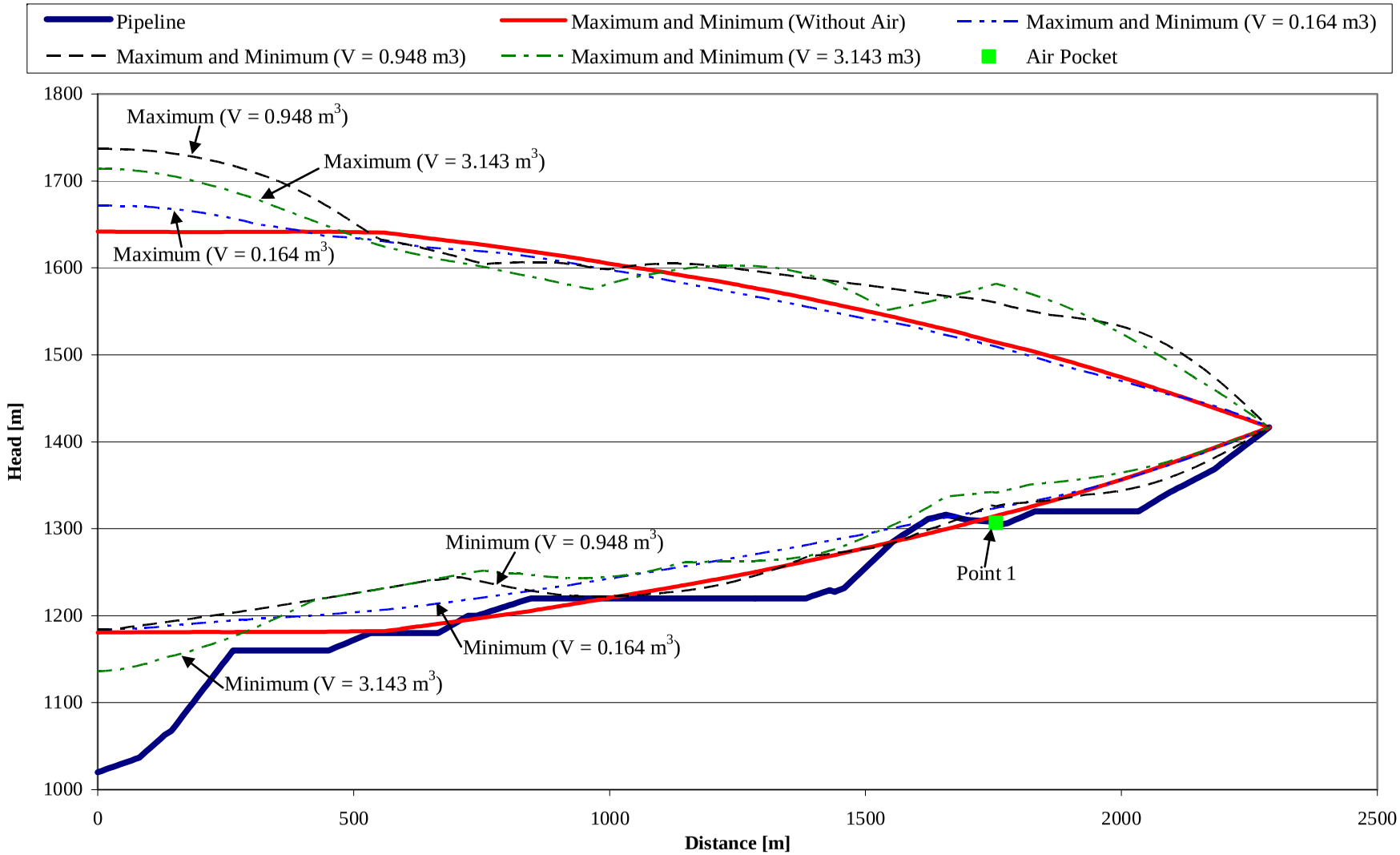

Figure 4.5: Maximum and minimum head envelopes with different air pocket volumes located at point 1, and a water flow rate Q_w = 2.5 m^3/s

5. Effects of water-air mixtures on hydraulic transients

5.1 Introduction

The numerical simulation of fluid transients caused by the shutdown of pumps, considering air pockets located at the high points of the pipeline system and a water-air bubble mixture immediately downstream of the pockets is herein presented. The air bubbles are entrained by a hydraulic jump that occurs at the end of the pocket. The computations were developed by using a numerical model based on the homogeneous model equations, which are solved with the method of characteristics, as well as the numerical model described in chapter 4. In addition, the transient pressures were simulated without surge suppression devices. Likewise, the predictions achieved are compared with the results obtained in the previous chapter, with the main goal to demonstrate the effect of the water-air mixture on fluid transients.

5.2 Two-phase flow and two-component flow in fluid transients

There are several circumstances for which a liquid flowing in a pipe contains either gas or vapour, or both as a mixture. A gas-liquid mixture of different chemical substances, such as a flow of water and air should be called two-component flow, whereas a vapour-liquid combination of the same matter would be termed two-phase flow. For convenience the term for concurrent flow of water-air is two-phase flow, but strictly speaking it has to be named two-component flow.

As described in the previous sections, free gas in pipelines may be either beneficial or detrimental during fluid transients, depending on the location and its quantity, whereas the effect of the presence of vapor is harmful with respect to waterhammer, for example water column separation. Transients associated with two-phase and two-component flow have been widely studied by several investigators. *Martin* (1996) [51] presents an excellent review on these themes.

5.2.1 Two-phase flow

The common fluid transient problems related with two-phase vapor-liquid flows are:

1) The well known problem of water column separation.
2) Rapid depressurization of liquids at high pressure and temperature linked with flashing and potential void collapse.
3) Sudden impact of steam onto water or vice versa.

The formation of a vapour pocket and its subsequent collapse (water column separation) and the direct contact of a subcooled liquid and warm vapor can give rise to important transient pressures.

5.2.2 Two-component flow

In steady and transient flow, two-component water-air mixtures may occur due to free or entrained air or because of the evolution of dissolved air from solution when the pressure drops or temperature increases above its saturation level. Examples of gas release can be found in hydraulic control systems, aviation fuel lines, and cooling water units. The effect of air compressibility on the wave celerity should be taken into account in any fluid transient analysis. Small quantities of air in form of bubbles will be favorable due to the significant reduction of the wave celerity, resulting in the diminution of potential transients. Larger amounts of air in the form of pockets in pipelines followed by a sudden pump shutdown can lead to a significant enhancement of transient pressures due to reflection or spring effect of the air pockets.

5.3 Flow Patterns

Liquid-gas two-phase flow can occur in numerous patterns depending on the velocities and flow rates of the phases, their physical properties and other variables. The determination of flow patterns has been done for various pairs of fluids and duct geometries. In transparent pipes at moderate velocities, it is possible to classify the flow pattern by direct visual observation. At higher velocities, the patterns have a chaotic behavior, therefore other techniques should be used to analyze the fluids within the pipe. Investigators have utilized flash and cine photography to slow the flow down and extend the range.

It is important to note that there is a considerable disparity in the name given to the flow patterns by different authors. Some descriptions of the various patterns in two-phase concurrent flow are (*Hewitt and Hall-Taylor*,1970 [32]) :

Bubble, gas dispersed, gas piston, liquid slug, annular, liquid dispersed, froth, mixed frothy, wall film, mist, aerated, piston, churn, wave entrainment, drop entrainment, turbulent, semi-annular, ripple, plug, wispy annular, stratify, wavy and many more.

For the purpose of this work, the most commonly accepted and recognized flow patterns classifications are used.

5.3.1 Flow patterns in horizontal concurrent flow

The flow patterns observed in concurrent two-phase flow in horizontal and inclined pipes depend on the gas velocity relative to the flow velocity and slope of the conduit. Likewise, the acceleration of gravity causes an asymmetric distribution of the phases. The sketches and photographs in Figure 5.1 show the flow patterns as described by *Alves* (1954) [2].

Bubbly Flow. The gas phase is distributed as small spherical bubbles in a continuous liquid phase, which tends to travel in the upper half of the conduit. At moderate flow rates of both gas and liquid phases the entire pipe cross section contains bubbles. This pattern is sometimes called froth flow.

Plug Flow. As the gas flow rate increases, plug flow occurs because the gas bubbles coalesce with plugs and liquid alternately flowing along the upper half of the pipe. The nose of the plug of gas is asymmetric. This pattern is also named elongated bubble flow, *Shoham* (1982) [68].

Stratified Flow. In this case the separation of the two fluids is complete, the liquid flowing at the lower half of the pipe and the gas at the top. The stratified flow develops at very low gas and liquid velocities. Some authors describe this flow pattern as stratified smooth flow due to the smoothness of its surface.

Wavy Flow. As the gas velocity is increased in stratified flow or stratified smooth flow, instability of the liquid surface gives rise to the waves that travel in the direction of the current. This pattern is also called stratified wavy flow.

Slug Flow. A further increase in the gas velocity in the wavy or stratified wavy flow causes wave amplitudes that become large enough to reach the roof of the pipe. The slugs travel with a higher velocity than the liquid velocity. The upper surface of the conduit behind the wave is wetted by a residual film that drains into the bulk of the liquid.

Annular Flow. As the gas velocity increases still further, it will result in the formation of a gas core with a thicker liquid film at the bottom of the pipe than at the top. The film may be continuous around the periphery of the duct. Alves also observed a spray or droplet flow

pattern where the majority of the flow was entrained in the gas core and is carried as dispersed droplets.

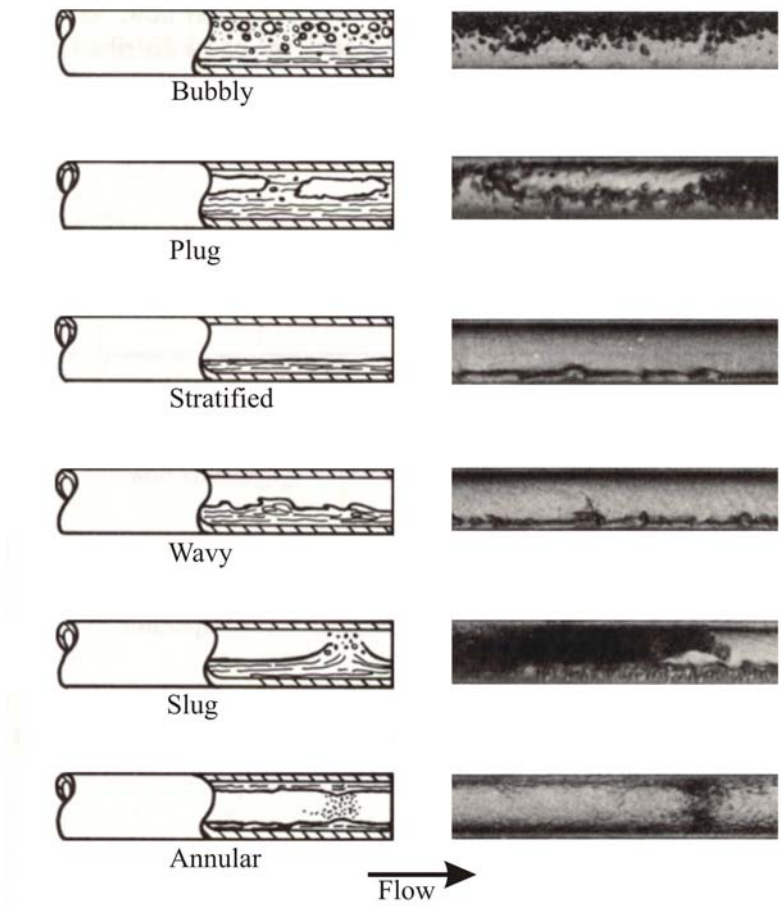

Figure 5.1: Flow patterns in horizontal concurrent flow (after Collier, 1981)

5.3.2 Flow patterns in vertical concurrent flow

The sketches and photographs of the flow patterns encountered in vertical upwards concurrent flow are presented in Figure 5.2 and are described in the following paragraphs. Note that the flow patterns in vertical pipes are more axisymmetric than flow patterns in horizontal pipes.

Bubbly Flow. At small liquid velocities, the gas phase is distributed as small spherical bubbles within the continuous liquid phase. As the liquid rate flow increases the bubbles may grow forming large bubbles with spherical cap, which are normally small with respect to the pipe diameter.

Slug Flow. From bubbly flow, with a further increase in gas flow rate some of the small bubbles join to form larger gas bubbles with a characteristic bullet-shape. The bubbles have approximately the same diameter of the pipe except for a thin liquid film on the wall of the

conduit. The slugs of gas are separated by liquid that may contain a dispersion of small bubbles. The length of the slugs of gas can vary considerably, until several times the pipe diameter. These large gas bubbles or slugs are also called Taylor bubbles.

Churn Flow. As the velocity of the two-phase mixture flowing in slug flow in a pipe is increased, the pattern will become instable due to the breakdown of the slugs of gas. The instability leads to a churning or oscillatory action, therefore the descriptive name churn flow. This pattern is also referred to as froth flow, semi-annular or slug-annular flow. However, some investigators use the more general term churn to cover the whole region.

Wispy-annular Flow. Wispy annular flow has been identified as a distinct pattern by *Hewitt et al.* (1970) [32]. The flow in this region has a form of a relatively thin liquid layer on the wall of the pipe, while a considerable quantity of liquid is entrained in a central gas core. The liquid in the layer is aerated by small gas bubbles and the entrained liquid phase appears as large droplets that have agglomerated into long irregular filaments or wisps.

Annular Flow. In annular flow a liquid layer flows on the wall of the pipe, surrounding a high velocity gas core. Large amplitude waves are usually presented on the surface of the liquid layer, the breakdown of the waves forms a source for droplet entrainment that occurs in varying amounts in the central gas core. In this pattern, the droplets are separated rather than agglomerated as in the wispy-annular flow.

5.4 Air Entrainment in Hydraulic Structures

Air entrainment is present in hydraulic structures such as siphons, pipelines, vertical dropshafts, weirs, etc. The process takes place when a supercritical water jet impacts on a body of water with a lower velocity. When the conduit is steeply inclined the process is described as impinging jet entrainment and in a slightly sloping conduit may be termed hydraulic jump entrainment, *Ahmed A. A. et al.* (1984) [1].

The process of air entrainment in closed conduits by a hydraulic jump is herein considered to compute the air void fraction α and the ratio air flow to water flow β, required to simulate the hydraulic transients with air pockets located at high points of the line and a mixture water-air flow generated by the entrained air by the jump at the end of the pocket. It is considered that the air downstream of the jump returns as predicted by equation (2.6).

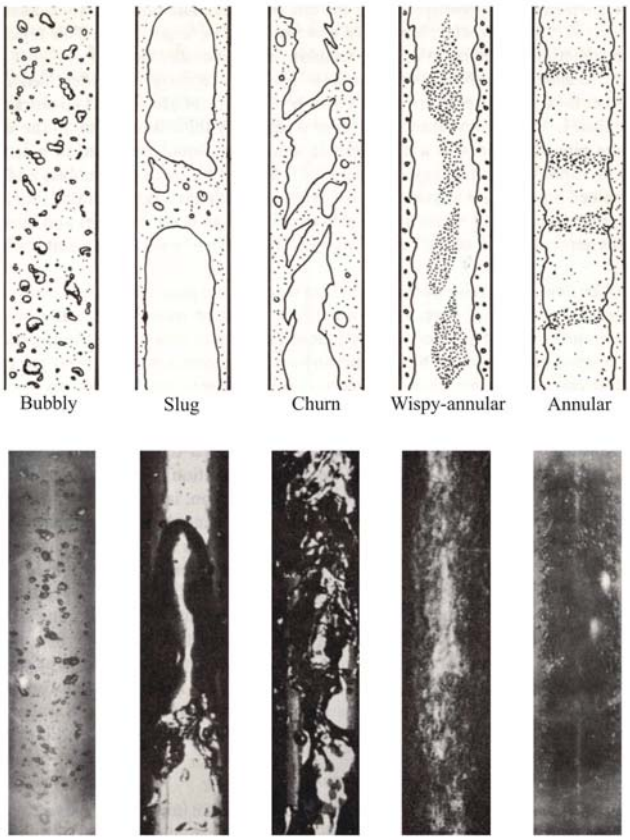

Figure 5.2: Flow patterns in vertical concurrent flow (after Collier, 1981)

5.4.1 Hydraulic jumps in water pipelines systems

From pipeline designers' point of view, water-air flows in closed conduits can be divided in four general categories. Each category may present only one or a combination of the flow patterns described previously. These categories are (*Falvey* 1980 [20]):

- Flow in partially filled conduits
- Flow having a hydraulic jump that fills the conduit
- Flow from control devices
- Falling water surfaces

For the purpose of this work only the flow having a hydraulic jump that fills the conduit is considered. Two-phase water-air flow in which the transition from supercritical flow to pressurized conduit flow occurs by a hydraulic jump has been investigated by *Lane and Kindsvater* (1938) [45], *Kalinske and Robertson* (1943) [38], *Fasso* (1955) [21], *Cohen de Lara* (1955) [12], *Haindl* (1957) [30], *Rajaratnam* (1965) [61], *Ahmed et al.* (1984) [1], *Matsushita* (1989) [54], and *Smith and Chen* (1989) [71] and many others.

One of the most recent investigations related with hydraulic jumps in circular pipes was carried out by *Stahl and Hager* (1999) [72]. They studied the main characteristics of these jumps in Plexiglas pipes of internal diameter of 240 mm and 6 m in length. The free surface flow and the hydraulic jumps were simulated at atmospheric pressure at the test section of the physical model.

During the investigation developed in the laboratory of the Institute of Engineering at the University of Mexico (UNAM), and described in Chapter 3, it was stated that the large air pockets subjected to pressurized flow conditions ended with a hydraulic jump that sealed the pipe. The main flow features of these jumps were measured and are compared with those jumps studied by *Stahl and Hager* (1999) [72]. They classified the types and appearances of hydraulic jumps in function of the filling ratio y_1/D and the Froude number F_1 upstream of the jump, where y_1 is the upstream depth and D is the pipe diameter.

For $F_1 > 2$, two types of hydraulic jumps were observed in circular pipes:

- For a filling ratio $y_1/D > 1/3$ and $F_1 = 2.3$, a direct hydraulic jump took place, its appearance is similar to the classical jump with a surface roller, straight front, bottom forward flow zone and width almost constant along the jump, see Figures 5.3 and 5.4.

- For a filling ratio $y_1/D < 1/3$ and $F_1 = 4.1$, a hydraulic jump with a flow recirculation occurred. The width along the jump increased and lateral wings formed at the beginning of the jump, as is shown in Figure 5.6 a) and b). It is noticed in Figure 5.6 a) that the forward flow concentrates axially as a superficial jet, but it is not apparent in Figure 5.6 b) and also the lateral recirculation with the characteristic wedge-shape is weak. Probably the differences are due to the scales used for both experimental investigations and other factors.

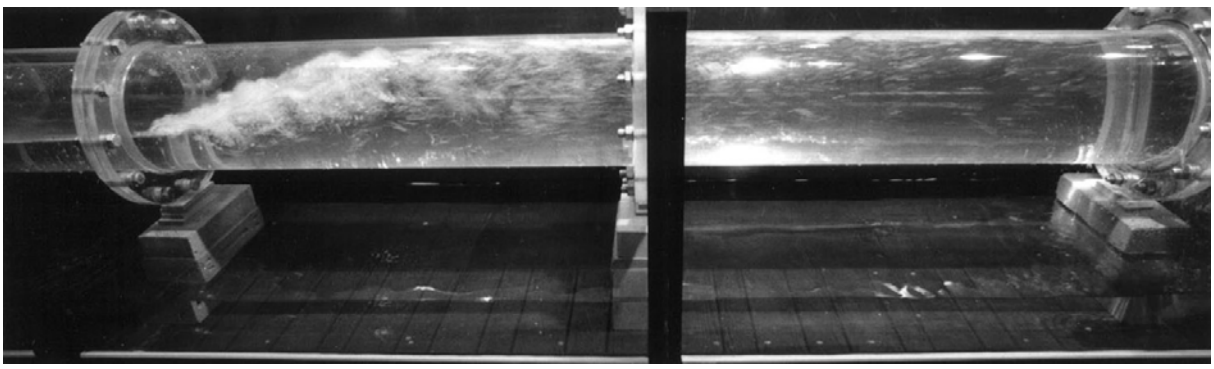

a)

b)

Figure 5.3: Profile of a direct hydraulic jump: a) (after Stahl and Hager, 1999), b) picture of the author.

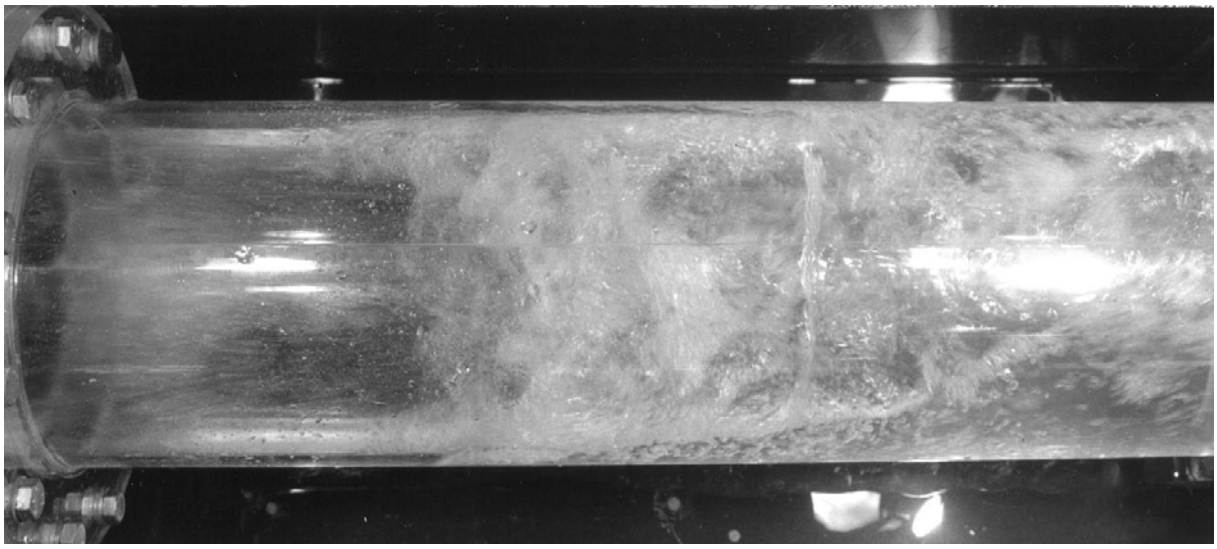

a)

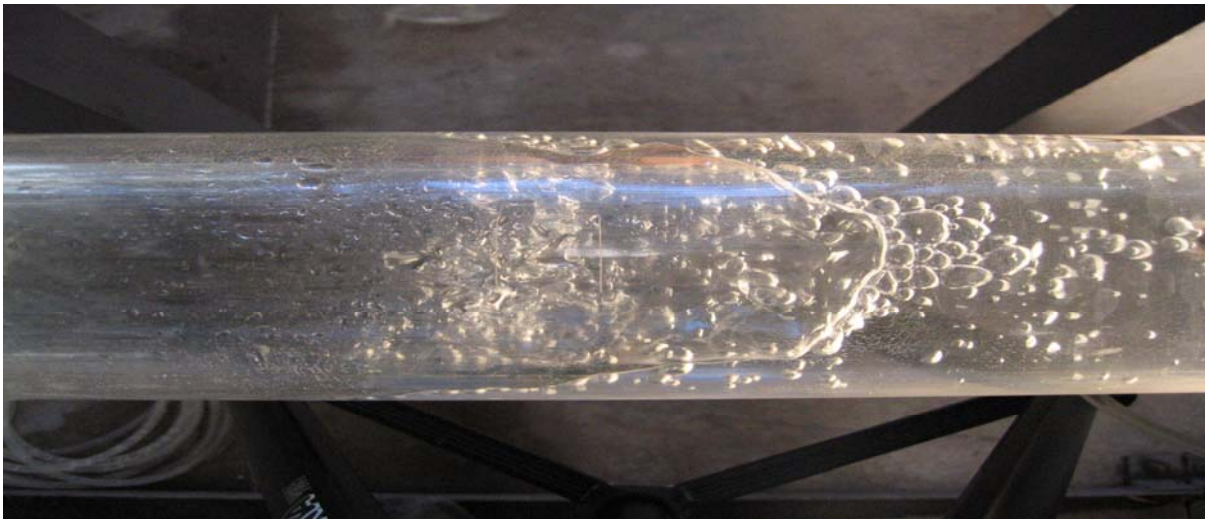

b)

Figure 5.4: Plan of a direct hydraulic jump: a) (after Stahl and Hager, 1999), b) picture of the author

- For a filling ratio $y_1/D < 1/3$ and $F_1 = 4.1$, a hydraulic jump with a flow recirculation occurred. The width along the jump increased and lateral wings formed at the beginning of the jump, as is shown in Figure 5.6 a) and b). It is noticed in Figure 5.6 a) that the forward flow concentrates axially as a superficial jet, but it is not apparent in Figure 5.6 b) and also the lateral recirculation with the characteristic wedge-shape is weak. Probably the differences are due to the scales used for both experimental investigations and other factors.

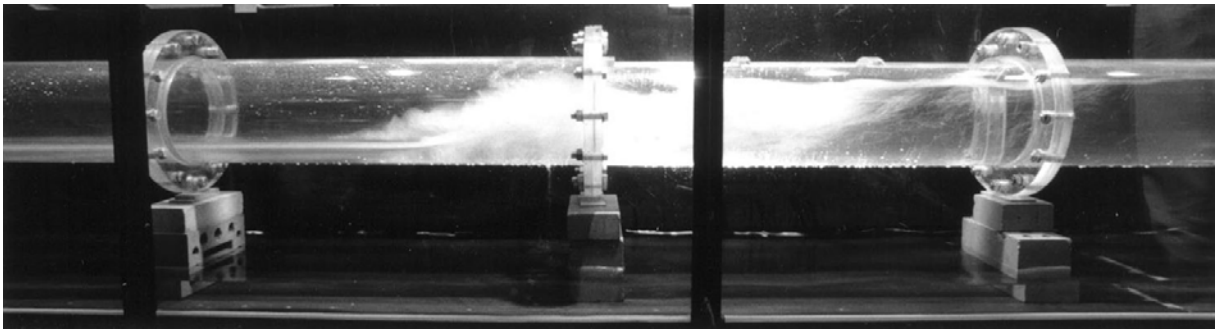

a)

b)

Figure 5.5: Profile of a hydraulic jump with flow recirculation: a) (after Stahl and Hager, 1999), b) picture of the author

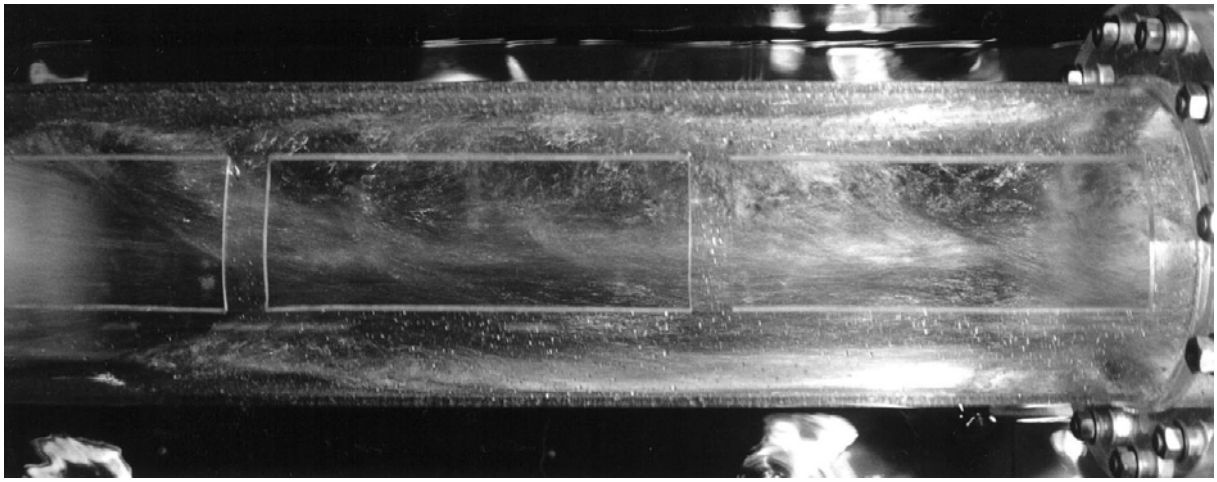

a)

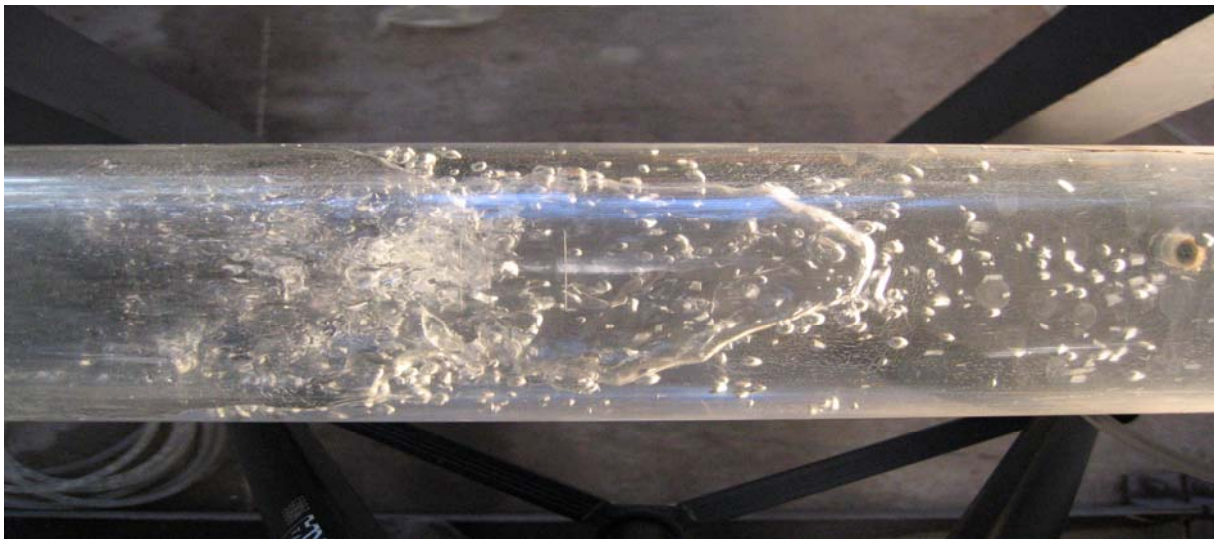

b)

Figure 5.6: Plan of a hydraulic jump with flow recirculation: a) (after Stahl and Hager, 1999), b) picture of the author

Figure 5.7 presents a set of pictures that highlight the large quantity of air that a hydraulic jump may entrain.

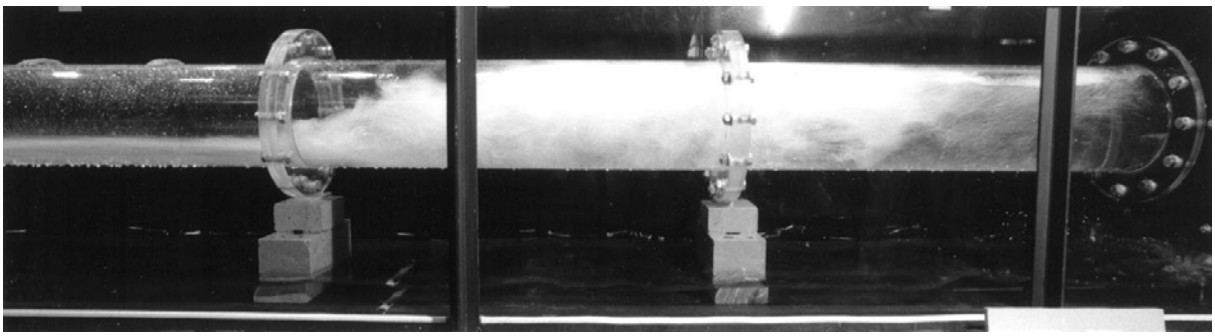

a)

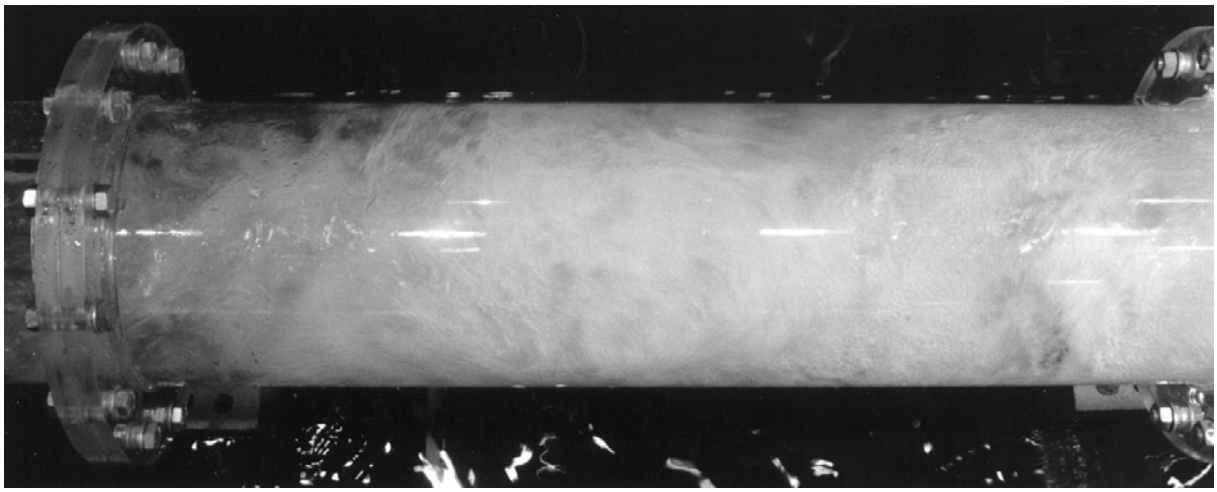

b)

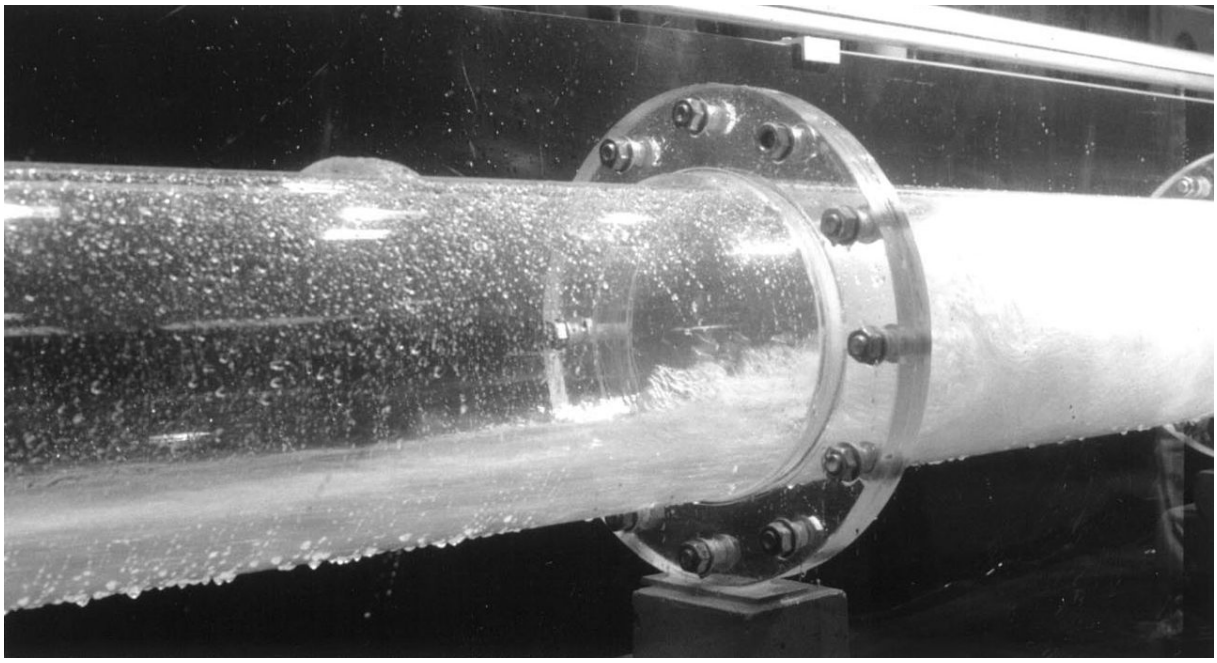

c)

Figure 5.7: Hydraulic jump with a transition to pressurized conduit flow (after Stahl and Hager, 1999): a) profile view, b) plan view, c) side view

The Froude numbers obtained during the experiments described in chapter 3 ($1.7 < F_1 < 4.7$, $F_1 = 1.35$ and $F_1 = 7.34$) are in the range of the Froude numbers achieved by Stahl and Hager.

5.5 Air entrainment mechanisms

Ervin (1998) [16] investigated the air entrainment in closed conduits and stated that there are at least three mechanisms of air entrainment at the plunge or entrainment point, which can be listed as follows:

First mechanism. The first mechanism regarding air entrainment in the absence of surface disturbances is presented in Figure 5.8. A smooth jet may drag a thin air boundary layer. Likewise, the air may be able to enter the slower moving body of water when a gap is formed between the recirculating flow and the jet.

Second mechanism. It is related with the role of surface disturbances of the upstream jet on the aeration process. Surface disturbances can take place due to different phenomena, such as turbulent eddies reaching the free surface, longitudinal vorticity, instabilities, as well as shock waves. It has been proposed that the amount of entrained air can be represented by a shaded area as shown in Figure 5.9. The size of the surface disturbances can be related to the velocity head. The simplicity of this argument was confirmed by dimensional analysis, but it is required to be validated with experimental investigation.

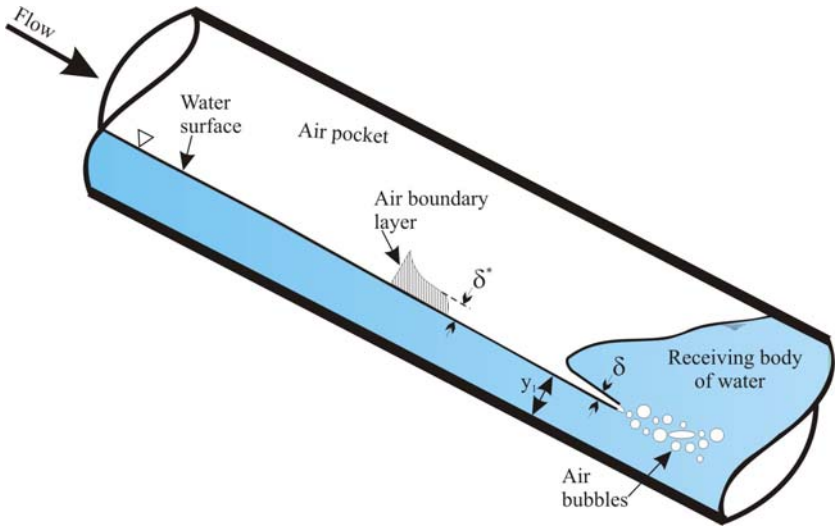

Figure 5.8: Aeration due to air boundary layer

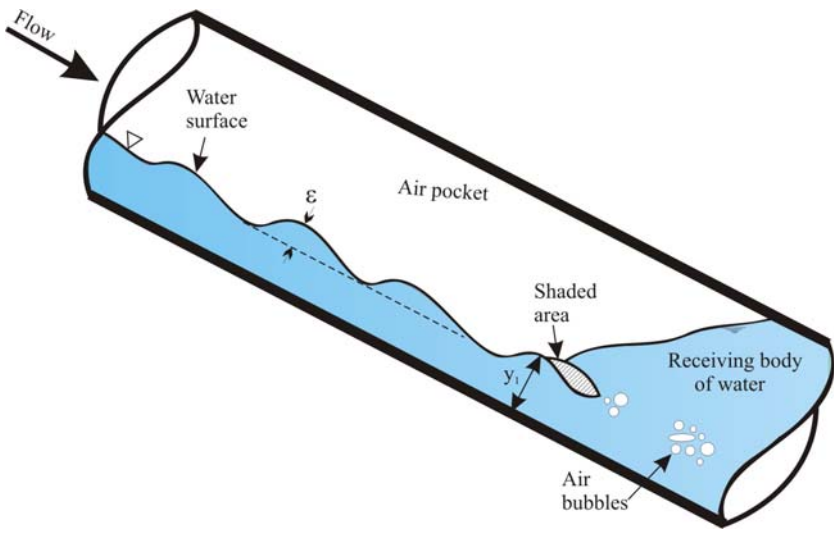

Figure 5.9: Aeration due to surface disturbances in an upstream jet

Third mechanism. This is a free surface aeration mechanism that contributes to the overall aeration rate. At high velocities, free surface aeration can be present in the upstream jet. It can also arise due to the turbulence on the surface of the receiving body of water as is commonly observed in hydraulic jumps, which gives rise to air entrainment through the free surface over the part of the length d. The sketch in Figure 5.10 shows the details of the mechanism of air entrainment.

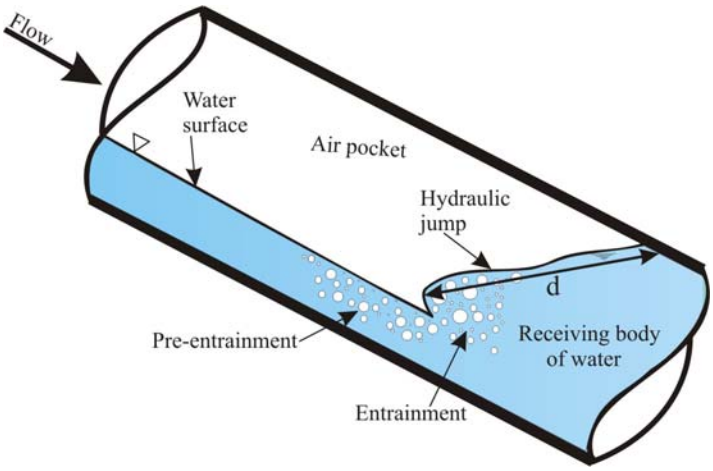

d length of the free surface of the receiving body of water [m]

Figure 5.10: Free surface aeration in a shear layer

It can be seen that the development of a relationship for the entrainment or plunge point aeration is not possible, because at least three different mechanisms of air entrainment exist.

5.6 Transport of air bubbles in downward sloping pipes

The discussion so far has focused on the air entrainment process at the plunge point in hydraulic structures. Just as significant is the air bubble transport process downstream of the plunge point. When air is entrained at the plunge point it is then either detrained or transported downstream, as sketched in Figure 5.11.

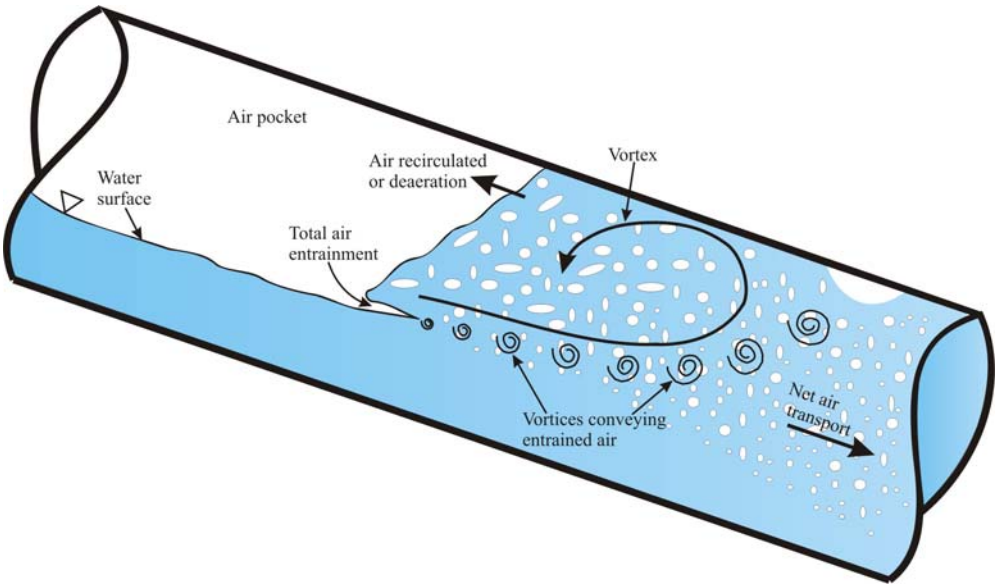

Figure 5.11: Air entrained by a supercritical jet in a closed conduit

Experimental and theoretical investigations have been conducted to study the ability of the vortices in the shear layer to trap air bubbles in their vortex cores and convey them long distances along the conduit beyond that expected from the average velocity field. During

these investigations also the main forces acting on air bubbles downstream of the entrainment point have been identified. These are drag, buoyant, inertia and the lift force due to the shear layer velocity. In addition, dimensional numbers have been developed to characterize the air bubbles behavior in the shear layer, *Thomas et al.* (1983) [76] and *Sene at al.* (1994) [67].

5.7 Quantity of air transported in downward sloping pipes

Ervin (1998) [16] stated that the quantity of air transported along a closed conduit depends not only on the rate of air entrainment at the plunge point, but also on the flow conditions downstream of the shear layer, as well as on the pipe slope. If flow conditions have exceeded the threshold of air bubbles transport, then the single most important parameter affecting transport is the length of the pipe downstream of the entrainment point, as demonstrated in Figure 5.12. Experimental investigations have shown that there exist broadly three different conduit lengths that affect the net rate of air transport.

Short conduits. Short conduits have a length to the conduit diameter ratio (L/D) less than 5. In these conduits all the air entrained at the plunge point is transported downstream and removed from the pipe. Figure 5.12 a) shows the phenomenon. Once air is entrained at the plunge point and trapped in the shear layer vortices, air bubbles reaching the reattachment point $L/D > 4$, can then be transported out of the line. In this case the net air transport rate is equal to the entrainment rate.

Intermediate conduits. Intermediate closed conduits have a ratio $5 < L/D < 20$. This length is sufficient to transport air bubbles that rise to the conduit roof due to their buoyancy force. Some of the bubbles coalesce, forming small air pockets at the conduit roof. In this case the flow regime presented is a mixture of air bubbles and small air pockets that may reach the exit of the conduit, as shown in Figure 5.12 b).

Long conduits. Long conduits have ratio L/D greater than 20. In this third category, the coalescence of air bubbles produces the formation of distinct air pockets at the conduit roof, and will only be removed along the downward sloping pipe when the flow has the capacity to transport or exhaust large air pockets downstream of the conduit. If the flow does not have this capacity then air pockets grow in size and eventually blowback upstream through the jump towards the large air, see Figure 5.12 c).

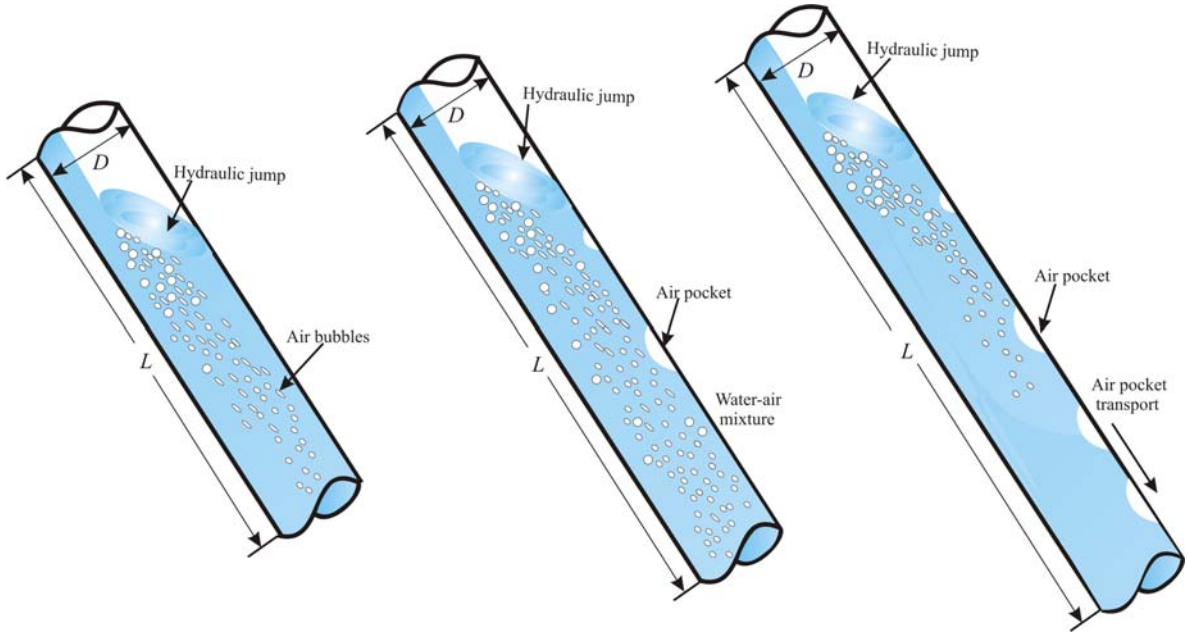

a) **b)** **c)**

Figure 5.12: Air transported in downward sloping pipes in function of the length and conduit diameter (*L*/*D*)

5.8 Relationships to compute air entrainment in hydraulic structures

Consider an air pocket that ends in a hydraulic jump at the downward sloping pipe. The turbulence action at the jump generates small air bubbles. The air entry will depend on different variables, as the upstream Froude number of the jet *Kalinske and Robertson* (1943) [38], jet velocity *Kenn and Zanker* (1967) [39], the recirculating vortex *Goldring et. al.* (1980) [28], the surface roughness of the jet *Ervin and Mckeogh* (1980) [17], and other factors. The air entrainment will be transported along the pipe in form of small bubbles, part of the bubbles join and form larger bubbles that travel on the upper half of the pipe. A portion of the air bubbles will return upstream. This phenomenon is named detrainment or recirculation.

Some factors that influence the detrainment may be summarized as follows (*Ahmed et al.* 1984 [1]):

- The slope of the pipe that influences the balance between the buoyant and drag forces on an air bubble.
- The effective air bubble rise velocity in a turbulent shear field.
- The velocity of the jet when impacting on a slower moving body of water, the angle of spread of shear layer, and the velocities or turbulence intensity generated in the vortex cores.

- The value of the water outlet velocity in the pipe downstream of the hydraulic jump.

Ahmed et al. (1984) [1], supported on hydraulic model research, stated that air transport as a water-air mixture will have a maximum air void fraction α of 42%. The void fraction is given by:

$$\alpha = \frac{\beta}{1+\beta} \quad [-] \qquad (5.1)$$

α air void fraction [-]
β ratio of air flow to water flow [-]

$$\beta = \frac{Q_a}{Q_w} \quad [-] \qquad (5.2)$$

where

Q_a air flow rate [m^3/s]
Q_w water flow rate [m^3/s]

The two variables presented in equations 5.1 and 5.2 are later used to compute the two-component fluid transients in a pumping pipeline system, produced by the shutdown of the units in a pumping station.

The values of air entrainment by the hydraulic jump can be estimated from the empirical relationship proposed by *Kalinske and Robertson* (1943) [38].

$$\beta = 0.0066(F_1 - 1)^{1.4} \quad [-] \qquad (5.3)$$

F_1 Froude number upstream of the jump [-]

The previous relationship is only valid if all the air entrained by the jump is carried out of the water line.

Wisner (1965) [86] conducted experiments for higher velocity flows for hydraulic jumps in a rectangular conduit and obtained the following equation

$$\beta = 0.014(F_1 - 1)^{1.4} \quad [-] \qquad (5.4)$$

After their experiments the U.S. Corps of Engineers [79] found an upper envelop for air entrainment in hydraulic jumps in closed conduits, which can be written in the form

$$\beta = 0.03(F_1 - 1)^{1.06} \quad [-] \qquad (5.5)$$

The disadvantage of the relationships above presented is that these do not consider the scale effects.

A relationship regarding air entrainment in model siphons was produced by *Thomas* (1982) [75], the parenthesis to the power of three is a factor that allows scale effects.

$$\beta = 0.01F_1^2\left(1-\frac{0.8}{v_1}\right)^3 \quad [-] \qquad (5.6)$$

v_1 water velocity upstream of the jump [m/s]

Recently, *Escarameia et al.* (2005) [18] investigated the rate of expulsion of air through a hydraulic jump in circular pipes and provided a relationship to estimate the rate of air entrained by the jump with the following equation.

$$\beta = 0.0025(F_1-1)^{1.8} \quad [-] \qquad (5.7)$$

Supported on several tests, *Ahmed et al.* (1984) [1] proposed a relationship for air bubbles transport that includes a term dependent of the scale, useful for the comparison between model and prototype air-water ratios.

$$\beta = 0.04(F_1-1)^{0.85}\left[\left(1-\frac{0.8}{v_{jet}}\right)^3\left(1-\exp^{-2(v_0-v_0^*)/v_{br}}\right)\right] \quad [-] \qquad (5.8)$$

v_{jet} supercritical jet velocity [m/s]
v_0 outlet water velocity [m/s]
v_0^* critical outlet velocity to transport air [m/s]
v_{br} bubble rise velocity [m/s]

The influence of the scale factor is only significant for values of $v_0 - v_0^*$ lower than 0.25 m/s, corresponding to values of $(v_0 - v_0^*)/v_{br} < 1$. Therefore the terms within the square brackets can be considered as unity. Therefore, equation (5.8) can be written as

$$\beta = 0.04(F_1-1)^{0.85} \quad [-] \qquad (5.9)$$

This relationship is used to calculate the air void fraction α in the numerical model implemented to simulate the two-component fluid transients, because it is supported on a three-year testing programme. A total of 2250 test runs had been made in closed conduits

sloping from horizontal to vertical. Likewise, the relationship includes the scale effects arising during the air entrainment process.

5.9 Variation of wave speed in water-air mixtures

It is well known that small quantities of free air in the form of bubbles in liquids cause the wave propagation speed to be decreased substantially from that in the pure liquid itself, *Giesecke and Mosonyi* (2005) [27]. The effect of gas concentration in a bubbly mixture has been investigated in laboratory, *Silberman* (1957) [70]. Numerous researchers have measured the wave celerity in two-phase and two-component flow. Many of the tests were conducted in the bubbly-flow regime. The values obtained by *Kobori et al.* (1955) [41] are representative for homogeneous flow wave propagation speeds. *Pearsall* (1965) [57] found by measurements in two sewage pumping pipelines that the wave celerity can be reduced by as much as 86 percent as a result of gas content.

Knowledge of the wave propagation speed for other flow patterns such as plug, annular, or slug is not as complete. Except for the formation and propagation of shock waves in a bubbly mixture in short vertical columns there have been relatively few studies performed on the effect of the presence of gas bubbles on pressure surge. For longer conduits in which the pressure and void fraction varies along the pipe as a result of boundary friction and elevation change, a simple knowledge of acoustic wave speed is inadequate for the prediction of the peak pressure caused by a transient.

The theoretical wave propagation speed or acoustic velocity of a pressure wave in a two-phase mixture under the associated assumptions of homogeneous flow and no relative motion or slip between the phases can be written as, *Martin et al.* (1976) [53]:

$$a_{mix} = \left[\frac{1}{(1-\alpha)\rho \left[(D \cdot \mu / E \cdot e) + (\alpha / E_a) + ((1-\alpha)/E_w) \right]} \right]^{1/2} \quad \text{[m/s]} \qquad (5.10)$$

a_{mix} velocity of the pressure wave in a water-air mixture [m/s]
α void fraction [-]
ρ water density [kgs^2/m^4]
E Young's modulus of elasticity of the pipe material [kg/m^2]
E_w modulus of elasticity of water [kg/m^2]
E_a modulus of elasticity of air [kg/m^2]
μ pipe constraint factor [-]
e pipe wall thickness [m]

The term *D/Ee* can be important in single-phase liquid flow or in two-component flow. For moderate to low values of α the pipe wall elasticity effect is minimal. The effect of the gaseous component is represented by two quantities, the air void fraction α and the pressure, as represented by the bulk modulus of elasticity of the gas E_a . It has been found by *Martin* (1976) [50], and by *Martin and Padmanabhan* (1979) [52] that the no-slip homogeneous model is quite effective even in the slug-flow regime.

Equation (5.10) will be utilized to evaluate the wave propagation speed in the water-air mixture during the fluid transients.

5.10 Models for analyzing hydraulic transients with water–air mixture

A great effort has been done in performing computational programs to simulate transient two-phase flow in pipelines. The nuclear industry is the pioneer in the development of these computer codes to analyze the possible occurrence of accidents in nuclear reactors. Some of the codes have been modified by the oil and gas industry to study the transients in oil pipelines. Programming the equations of continuity, momentum and energy for the two fluids lead to codes of thousands of lines that require a lot of time to be developed and are very complex to use, because the equations are merely more numerous and complicated than those for single-phase flow.

The differences among the flow patterns presented above suggest that the development of a universal two-phase analytical model is rather remote. As a matter of fact, phase interaction, the relative velocity between the fluids and momentum, mass and heat transfer can have an important effect on one regime than another. Even though the most adequate model may vary depending on the flow pattern investigated, for flow in long pipelines the assumption of one-dimensionality is usually quite successful. Likewise, the most extensively utilized methods of analysis are the homogeneous model, the separated-flow model, and the drift-flux model.

These analytical models are defined by *Wallis* (1969) [82] as follows:

5.10.1 Homogeneous flow model

The homogeneous model is the simplest method of analysis for studying two-phase or two-component flow. Convenient average properties have to be determined and the mixture

is treated as a pseudofluid that follows the common equations of single-component flow. Therefore, all the standard methods of fluid mechanics can then be applied. The average properties required are the velocity, transport properties (e.g., viscosity) and thermodynamic properties (e.g., temperature and density). These pseudo properties are weighted averages and are not necessarily the same as the properties of either fluid. The method to determine suitable properties often begins with the more complex relationships and rearranges them until they resemble equivalent equations of single-phase flow.

5.10.2 Separated-flow model

The separated-flow model considers that the two phases can have varying properties and different velocities. It may be developed with various degrees of complexity. In the most sophisticated formulation, the model will necessitate six equations to represent the conservation of mass, momentum, and energy of each of the phases. These equations are solved simultaneously, together with rate equations that describe the interaction between the phases and with the walls of the pipe. In the simplest version of the model only the velocity is allowed to differ from the two phases as the equations of conservation are only written for the combined flow. When the number of equations is exceeded in number by the variables to be determined, correlations or simplifying assumptions are introduced.

5.10.3 Drift-flux model

The drift-flux model is basically a separated-flow model in which the attention is concentrated on the relative motion rather than the motion of the two phases individually. This model is particularly remarkable, as the effects of velocity and concentration profiles can be included. However, since several empirical relationships are an essential part of the drift-flux model, it may not have a general applicability for an ample range of problems.

The advantages and disadvantages of the above models depend on the causes of the transient two-phase flow. In some transient and steady flows, the gravitational and inertial effects can have an important influence, therefore the relative velocity between the two-phases should be taken into account.

5.11 <u>Homogeneous flow model equations</u>

A one dimensional homogeneous model is used to study the fluid transients considering a water-air-mixture. The constitutive equations – conservation of the gas mass, of the liquid

mass, and the mixture momentum – yield a set of differential equations that will be solved by the method of characteristics.

For the homogeneous model presented herein the two phases or components (water-air bubbly mixture) are treated as a single pseudofluid with average properties. As explained by *Martin et al.* (1976) [53] and later in *Wiggert and Sundquist* (1979) [85], it is assumed that there is no relative motion or slip between the components in the development of the mass conservation equation for each phase, as well as for the momentum equation for the mixture. In the same way to the compressibility of the gas, the liquid compressibility and the pipe wall elasticity are included in the system of equations. The equation of energy is not used due to the moderate change in temperature of the mixture during the transient.

The following assumptions are used with regard to the homogenous model:

a) The water-air mixture is a homogenous two-component bubbly flow. Although the growing bubbles may join, for the most part they remain uniformly distributed in a continuous liquid phase along the pipe.
b) The difference in pressure across the air bubble surface is neglected.
c) The momentum interchange between the air and water components is ignored; then for momentum considerations, the air bubbles and water possess the same velocity.
d) The momentum of the air component relative to the liquid is small and hence can be neglected.
e) The average cross-sectional representation of air void fraction, water-air mixture velocity, and component densities can be employed.
f) No gas release and absorption takes place during the transients.
g) The circulation region also called net air transport does not extend beyond the end of downward sloping pipe section, as equation 2.6 predicted, see Figure 5.11 and Table 4.2, respectively.

The following mathematical development is mainly based on the two above references. By using a control-volume approach, *Yadigaroglu and Leahy* (1976) [90], the conservation of mass can be developed for each phase. This formulation is not strictly speaking a separated flow model because it is assumed that there is not relative motion between the fluids. Therefore, the continuity equation for the gas phase is written as:

$$\frac{\partial}{\partial t}(\rho_a \alpha A) + \frac{\partial}{\partial x}(\rho_a \alpha A v_a) = \Gamma A \qquad (5.11)$$

α void fraction [-]
ρ_a air density [kgs^2/m^4]
Γ gas production rate per unit volume [kg/m^3/s]
A pipe cross sectional area [m^2]
v_a average air velocity [m/s]
t time [s]
x axial distance along the pipe [m]

For the liquid phase the continuity equation is given by

$$\frac{\partial}{\partial t}\left[\rho\ (\alpha - 1)A\right] + \frac{\partial}{\partial x}\left[\rho\ (\alpha - 1)Av\ \right] = -\Gamma A \qquad (5.12)$$

ρ liquid density [kgs^2/m^4]

v water velocity in the pipe, which has been assumed equal to the gas phase velocity [m/s]

Neglecting the contribution of the gas phase, the mixture momentum balance can be formulated from a control-volume as

$$\frac{\partial}{\partial t}\left[\rho\ (1-\alpha)v_m A\right] + \frac{\partial}{\partial x}\left[\rho\ (1-\alpha)v_m{}^2 A\right] + A\frac{\partial p}{\partial x} + \pi D \tau_o - g\rho\ (1-\alpha)A\sin\theta = 0 \qquad (5.13)$$

p average pressure at the particular cross section [kg/m^2]
$v_m = v_a = v$ mixture velocity [m/s]
D pipe diameter [m]
τ_o boundary shear stress [kg/m^2]
θ angle of pipe inclination from the horizontal [°]

The boundary shear stress is based on the definition of the Darcy-Weisbach resistance coefficient λ:

$$\tau_o = \frac{\lambda}{8}(1-\alpha)\rho\ v_m|v_m| \quad [\text{kg/m}^2] \qquad (5.14)$$

λ Darcy – Weisbach friction factor [-]

The mixture density is

$$\rho_m = (1-\alpha)\rho\ + \alpha\rho_a \quad [\text{kgs}^2/\text{m}^4] \qquad (5.15)$$

ρ water density [kgs^2/m^4]

and can be approximated by $\rho_m = (1-\alpha)\rho$ for most of the gas-liquid mixtures.

The above equations can be expressed in characteristic form for application of the method of characteristics. By introducing the elastic properties of air, water and pipe material, the equations (5.11 to 5.13) can be presented in the form:

$$\frac{\partial \alpha}{\partial t} + v_m \frac{\partial \alpha}{\partial x} - \varphi_1 \frac{\partial v_m}{\partial x} = \zeta_1 \tag{5.16}$$

$$\frac{\partial p}{\partial t} + v_m \frac{\partial p}{\partial x} + \varphi_2 \left(\frac{\partial \alpha}{\partial t} + v_m \frac{\partial \alpha}{\partial x} \right) = \zeta_2 \tag{5.17}$$

$$\frac{\partial v_m}{\partial t} + v_m \frac{\partial v_m}{\partial x} + \varphi_3 \frac{\partial p}{\partial x} = \zeta_3 \tag{5.18}$$

in which

$$\varphi_1 = \alpha(1-\alpha)\left(\frac{1}{E_a} - \frac{1}{E_w} \right)\left[\frac{D \cdot \mu}{E \cdot e} + \frac{\alpha}{E_a} + \frac{(1-\alpha)}{E_w} \right]^{-1} \tag{5.19}$$

$$\varphi_2 = \left[\alpha(1-\alpha)\left(\frac{1}{E_a} - \frac{1}{E_w} \right) \right]^{-1} \tag{5.20}$$

$$\varphi_3 = \frac{1}{\rho(1-\alpha)} \tag{5.21}$$

$$\zeta_1 = \Gamma\left[\rho\ (1-\alpha)\left(\frac{D \cdot \mu}{E \cdot e} + \frac{1}{E_w} \right) + \rho_a \alpha \left(\frac{D \cdot \mu}{E \cdot e} + \frac{1}{E_a} \right) \right] * \left[\rho_a \rho_w \left(\frac{D \cdot \mu}{E \cdot e} + \frac{\alpha}{E_a} + \frac{1-\alpha}{E_w} \right) \right]^{-1} \tag{5.22}$$

$$\zeta_2 = \Gamma\left[\frac{1}{\rho(1-\alpha)} + \frac{1}{\rho_a \alpha} \right]\left[\frac{1}{E_a} - \frac{1}{E_w} \right]^{-1} \tag{5.23}$$

$$\zeta_3 = g \sin\theta - \frac{\lambda}{2D} v_m |v_m| \tag{5.24}$$

Gas release is not considered for the computations ($\Gamma = 0$), therefore $\zeta_1 = \zeta_2 = 0$.

E Young's modulus of elasticity of the pipe material [kg/m^2]
E_w modulus of elasticity of water [kg/m^2]
E_a modulus of elasticity of air [kg/m^2]
μ pipe constraint factor [-]
e pipe wall thickness [m]
$\varphi_1, \varphi_2, \varphi_3$ terms in the characteristic equations
$\zeta_1, \zeta_2, \zeta_3$ terms in the characteristic equations

In equation (5.24) a steady frictional factor of Darcy-Weisbach is assumed. *Shuy and Aplet* (1983) [69], *Fok* (1987) [22] and *Lee* (1991) [48] have shown that the utilization of a steady friction factor or an unsteady friction factor will not achieve significantly different results.

Equations (5.16) to (5.24) form a base from which a numerical solution can proceed. The dependent variables are p = pressure, v_m = mixture velocity and α = air void fraction. The terms φ and ζ account for the gas release, elastic properties of the fluids and pipe, and force terms. The compatibility and characteristic relations derived from equations (5.16) to (5.18) are

$$\frac{dp}{dt} \pm \frac{a_{mix}}{\varphi_3}\frac{dV}{dt} \mp \frac{a_{mix}\zeta_3}{\varphi_3} = 0 \qquad (5.25)$$

valid along the $C_{(+)}$ and $C_{(-)}$ characteristics lines

$$\frac{dx}{dt} = a_{mix} \pm v_m \qquad (5.26)$$

For the third characteristic

$$\frac{dp}{dt} + \varphi_2 \frac{d\alpha}{dt} = 0 \qquad (5.27)$$

the compatibility equation or pathline C is

$$\frac{dx}{dt} = v_m \qquad (5.28)$$

The relationship (5.25) relates to the propagation of pressure waves along the characteristic lines in the x-t plane defined by the relationship (5.26). On the other side, equation (5.27) establishes the variation of the air void fraction α along the pathline characteristic, represented by equation (5.28). The three compatibility equations can be integrated, each along its respective characteristic to yield a simultaneous solution for p, v_m and α. The characteristic lines are illustrated in Figure 5.13. It is also convenient to develop equation (5.25) with the water flow rate Q and the head H as dependent variables, that yields

$$\frac{dH}{dt} \pm \frac{a_{mix}}{C_{mix}A\varphi_3}\frac{dQ}{dt} \mp \frac{a_{mix}\zeta_3}{C_{mix}\varphi_3} = 0 \qquad (5.29)$$

In which $C_{mix} = \rho_m g$ and A is the total cross section area of the pipe.

For the situation in which no gas is released from the liquid, equation (5.29) can be used in conjunction with equation (5.10) to predict the fluid transients, considering air pockets located at the intermediate and high points of the pipeline and a water-air mixture immediately downstream of them. The equations (5.30) to (5.37) of the numerical process of characteristics derived from equation (5.29) are the same as equations (4.4) to (4.11) with different wave celerity.

$$Q_{U_{i,n+1}} = C_{(+)_{mix}} - C_{mix} K_{mix_i} \varphi_3 H_{U_{i,n+1}} \quad [\mathrm{m^3/s}] \tag{5.30}$$

$$Q_{U_{i+1,1}} = C_{(-)_{mix}} + C_{mix} K_{mix_{i+1}} \varphi_3 H_{U_{i+1,1}} \quad [\mathrm{m^3/s}] \tag{5.31}$$

where

$$C_{(+)_{mix}} = Q_{i,n+1} + C_{mix} K_{mix_i} \varphi_3 H_{i,n+1} + R_{mix_i} \zeta_3 \quad [\mathrm{m^3/s}] \tag{5.32}$$

$$C_{(-)_{mix}} = Q_{i+1,1} - C_{mix} K_{mix_{i+1}} \varphi_3 H_{i+1,1} + R_{mix_{i+1}} \zeta_3 \quad [\mathrm{m^3/s}] \tag{5.33}$$

$$R_{mix_i} = A_i \Delta t_i \quad [\mathrm{m^2 s}] \tag{5.34}$$

$$R_{mix_{i+1}} = A_{i+1} \Delta t_{i+1} \quad [\mathrm{m^2 s}] \tag{5.35}$$

$$K_{mix_i} = \frac{A_i}{a_{mix_i}} \quad [\mathrm{ms}] \tag{5.36}$$

$$K_{mix_{i+1}} = \frac{A_{i+1}}{a_{mix_{i+1}}} \quad [\mathrm{ms}] \tag{5.37}$$

Δt time step [s]
A total cross section area of the pipe [m^2]
a_{mix} velocity of the pressure wave in a water-air mixture [m/s]

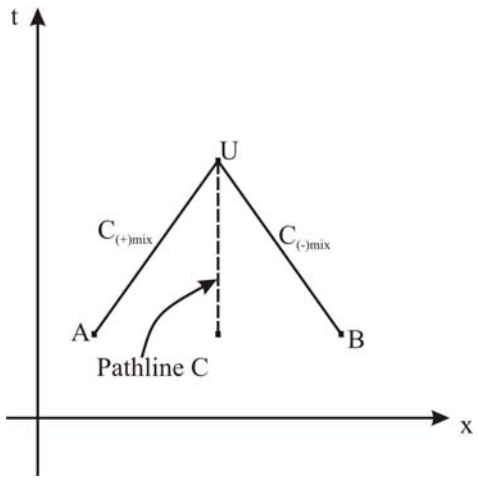

Figure 5.13: Characteristic lines in the x-t plane

5.12 Summary of the computation steps and procedure of calculation

The flowchart of Figure 5.14 shows the computational steps for determining the transient condition in a pumping pipeline system with air pockets located at their high points and a water-air bubble mixture immediately downstream of them. The associated equations are presented in Table 5.1.

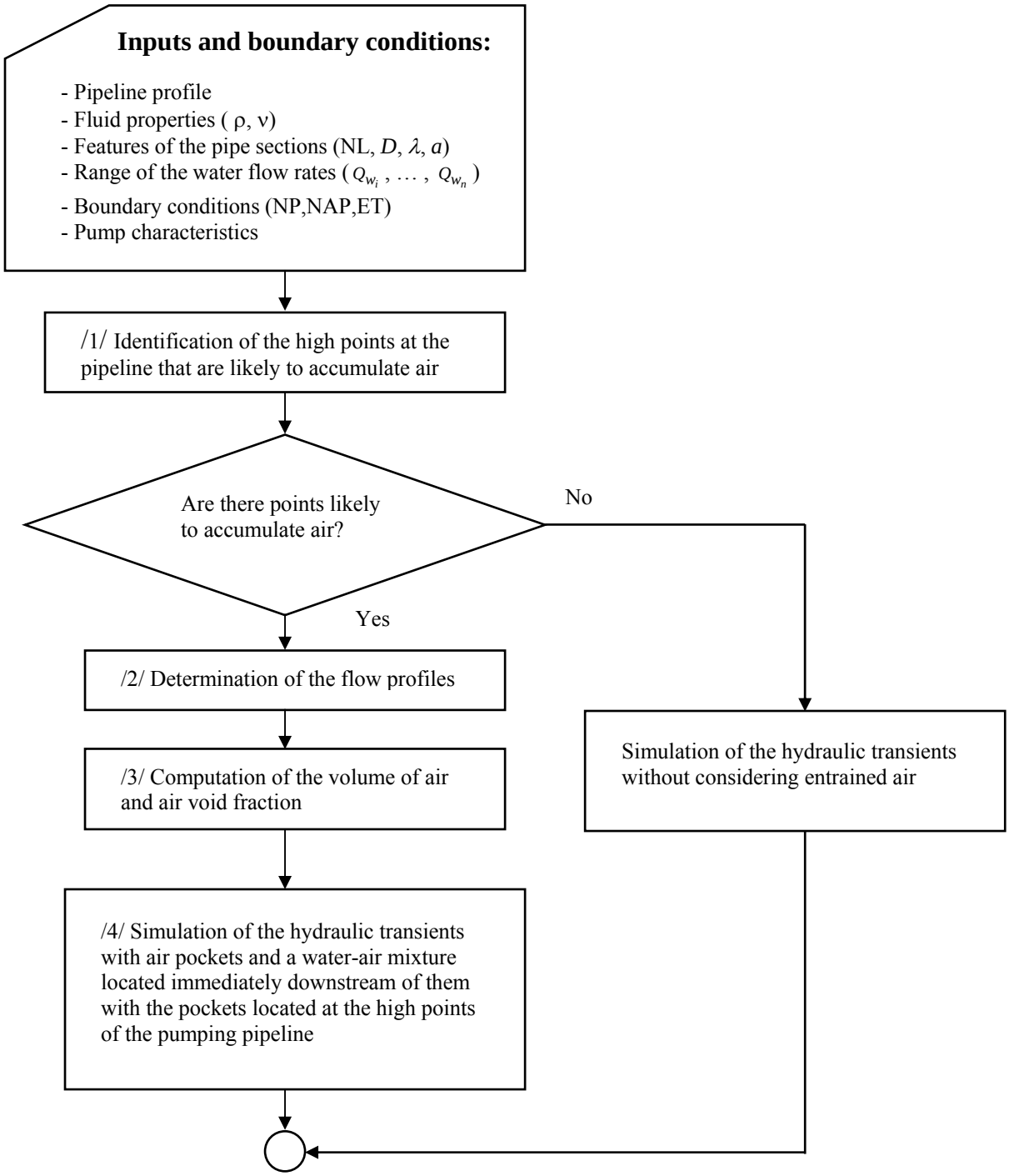

Figure 5.14: Overview of the procedure of computation of hydraulic transients with air pockets and a water-air bubble mixture immediately downstream of the pockets

Current No. according to Fig. 5.14	Associated equations
/1/	$Q_w^2 / gD^5 = S$ /Air behavior (2.6)
/2/	$\Delta x = \frac{E_2 - E_1}{S_0 - S_f}$ / Dynamic equation of the gradually varied flow (3.4)
/3/	V / Volume of air (3.7)
/4/	V_{U_i} / Volume of air at the beginning of the time step (4.3) a_{mix} / wave celerity of a pressure wave in a water-air mixture (5.10) $Q_{U_{i,n+1}}$ / Water flow rate at the end of the time step for - upstream end of the air pocket (4.4) - upstream end of the water-air mixture (5.30) $Q_{U_{i+1,1}}$ / Water flow rate at the end of the time step for - downstream end of the air pocket (4.5) - downstream end of the water-air mixture (5.31) $H_{U_{i,n+1}}$ / Piezometric head at the end of the time step for - upstream end of the air pocket (4.12) - upstream end of the water-air mixture (5.30) $H_{U_{i+1,1}}$ / Piezometric head at the upstream end of the water-air mixture at the end of the time step (5.31)

Table 5.1: Assignment of the equations to the computation steps represented in Figure 5.14

5.13 Case Study

In this section the same pumping pipeline system that has been presented in the chapter 4 is studied. The profile is sketched in Figure 4.3. The boundary condition at the upstream end is a pumping plant with four centrifugal pumps connected in parallel, Q_w = 0.625 m^3/s per unit, and at the downstream end a constant head tank.

The numerical simulation of fluid transients caused by a sudden pump shutdown in two-component flows has been developed. For this analysis the propagation of the pressure waves through a two-component water-air mixture were analytically investigated. It is assumed that

the air bubbles are entrained by the hydraulic jumps occurring at the end of the air pockets. The computations were performed with the numerical model implemented by using the homogeneous model equations. The transient pressures are simulated without surge suppression devices to demonstrate the potential effect of air pockets and the water-air mixture on hydraulic transients.

The high points that are likely to accumulate air, when the pumping station operates with 3 and 4 units identified by utilizing the equations (2.6) and (4.16) are summarized in Table 4.2. In addition, the relationships (3.7) and (5.1) were used to calculate the volumes of air in the pockets and the air void fraction downstream of them, respectively. The results are summed up in Tables 5.2 and 5.3.

Q_w = 1.875 [m^3/s]

Small volumes of air		**Intermediate volumes of air**		**Large volumes of air**	
***V* [m^3]**	α [%]	***V* [m^3]**	α [%]	***V* [m^3]**	α [%]
0.145	0.64	0.761	2.76	4.099	6.32
0.448	0.61	1.235	2.55	5.244	5.66
1.038	0.63	1.747	2.64	5.456	5.94
0.142	0.69	0.856	2.99	3.449	7.13

Table 5.2: Air pocket volumes and void fractions when 3 unit operate at the pumping station

Q_w = 2.500 [m^3/s]

Small volumes of air		**Intermediate volumes of air**		**Large volumes of air**	
***V* [m^3]**	α [%]	***V* [m^3]**	α [%]	***V* [m^3]**	α [%]
0.164	0.66	0.948	3.98	3.143	7.04

Table 5.3: Air pocket volumes and void fractions when 4 unit operate at the pumping station

The values of the variables to estimate the wave celerity a_{mix} in the water-air mixture, and the terms of the characteristic equations are listed subsequently:

E = 2.1 x 10^{10} [kg/m^2] (steel pipe)
E_w = 2.14 x 10^8 [kg/m^2]
E_a = 1.45 x 10^4 [kg/m^2]
μ = 1 [-]
e = 0.0254 [m]
ρ = 101.8 [kgs^2/m^4]
ρ_a = 0.123 [kgs^2/m^4]

5.14 Analysis of the results

This section presents the results achieved with the numerical model developed for the treatment of flow transients in a two-phase homogenous water-air mixture. The envelopes of the maximum and minimum heads with and without air pockets obtained in the previous chapter are compared with those achieved with the same air pocket volumes located at the same high points, but in this case downstream of the pockets a water-air mixture occurs. Likewise, the effect of the water-air mixture on the maximum and minimum heads envelopes will be herein analyzed. The marked differences among the groups of results show the potential attenuation during the propagation of the transient pressure wave along the pipeline profile. The transient pressure is absorbed considerably by the water-air mixture and the air pockets. As stated in chapter 4, the envelopes are plotted by using the maximum and minimum heads achieved at each nodal point along the pipeline during the simulation time, independent at which time step were recorded. For the dimensioning of the wall thickness the envelope of the upper pressures is decisive.

The essential effects of free air on fluid transients are well known. For example, if the air remains localized at a high point it usually behaves as an air cushion that absorbs the transient pressure waves, but also it can act as an unwanted nonlinear spring magnifying surge, *Ewing* (1980) [19]. If the air is uniformly distributed in form of small bubbles its effect is more difficult to predict. The most noticeable effect is a large drop in the waterhammer wave speed, even with a small mass of free air. The dampening of the pressure waves has an overall beneficial effect on the pipeline system. *Ewing* (1980) [19] stated that the damping occurs due to dispersion breaking down of the main wave surge into shorter wave length components, which are damped out more readily. *Pearsall* (1965) [57] found that in the presence of water-air mixtures, the most likely cause of the damping observed is due to the internal reflection of the wave celerity in bubbly water.

The following figures show that there is a difference between the maximum and minimum heads envelopes, when a water-air mixture presents downstream of the air pockets, as well as those with only water.

5.14.1 Pumping station performing with 4 units (Q_w = 2.5 m^3/s) with an air pocket located at the intermediate high point 1 and a water-air mixture immediately downstream of it

Figures 5.15 to 5.17 show the numerical comparisons of the calculated results from the simulations of fluid transients with an air pocket located at the intermediate high point 1 with and without a water-air mixture immediately downstream of it, as well as the envelopes of the maximum and minimum heads without air. The latter forms a good basis for comparison to assist in the judgment of degree of the dampening effect. From the graphs, it can be demonstrated that the distribution of the air void fraction greatly influence the pressure transient. Comparing Figures 5.15 to 5.17, it can be observed that the maximum and minimum heads decrease considerably throughout the pipeline profile with increasing the air void fraction α and the air pocket volume.

From the computations obtained, it can be seen in Figure 5.15 that the worst scenario takes place when a water-air mixture occurs downstream of the smallest air pocket. For this specific situation this volume of air with its corresponding air void fraction (V = 0.164 m^3, α = 0.66 %) can be called critical, see Table 5.3. It is observed that the maximum head envelope obtained with this pocket and the water-air mixture is slightly greater than that computed without water-air mixture. The enhancement is produced immediately downstream of the pumps discharge and near the downstream end boundary. *Ngoh and Lee* (1998) [56] found that the transient pressure varies with the void fraction α and is sometimes above that predicted without considering air. They suggest that this effect is produced by the expansion and contraction processes of the air bubbles. In the same way, it is observed that the minimum head achieved with a mixture immediately downstream of the pocket is lower than those obtained without mixture and no air accumulated.

The results have shown that the air pocket volume (V = 0.948 m^3, α = 3.98 %) located at the point 1, see Figure 5.16, only partially absorbed the pressure transient even with the presence of the water-air mixture. The pocket generated a reflection of the maximum pressure transients towards the downstream end boundary and an enhancement at the discharges of the pumps. However, the air pocket and water-air mixture produced an important dampening effect along the pipeline and the computed values of the maximum head are lower compared with those predicted under the assumption of no air accumulated in the line. Therefore, the volume of air (V = 0.948 m^3) cannot be named critical in this specific case. On the other side, it can be said that the pressure transients generated by this air pocket volume with a water-air

mixture downstream of it, may have a detrimental effect within the pipeline, mainly close to the pumps and from the point 1 towards the constant head tank.

It has been demonstrated that the presence of the largest air pocket with a water-air mixture immediately downstream of it (V = 3.143 m^3, α = 7.04 %) acts as an effective accumulator and suppresses the pressure transients, when four pumps are shutdown at the pumping station, as can be seen in Figure 5.17. It is important to highlight that with the occurrence of the water-air mixture the maximum head envelope has a lower value than that obtained without air; on the other side the wave reflection is marginal. Therefore, it can be stated that this large air pocket volume and the water-air mixture in this location have a beneficial effect on this pipeline configuration by lowering significantly the transient pressures.

In all the simulations performed with an air pocket located at point 1 and a water-air mixture immediately downstream of it, the minimum pressure along the pipeline profile was never less than the minimum head envelope without air. Likewise, it has been observed that the maximum and minimum head envelopes have similar shapes compared with single-phase water flow and are symmetric with respect to the static head. In the same way, the shapes of the maximum and minimum head envelopes are roughly the same, independent of the value of the air pocket volume and air void fraction, as illustrated in Figure 5.18.

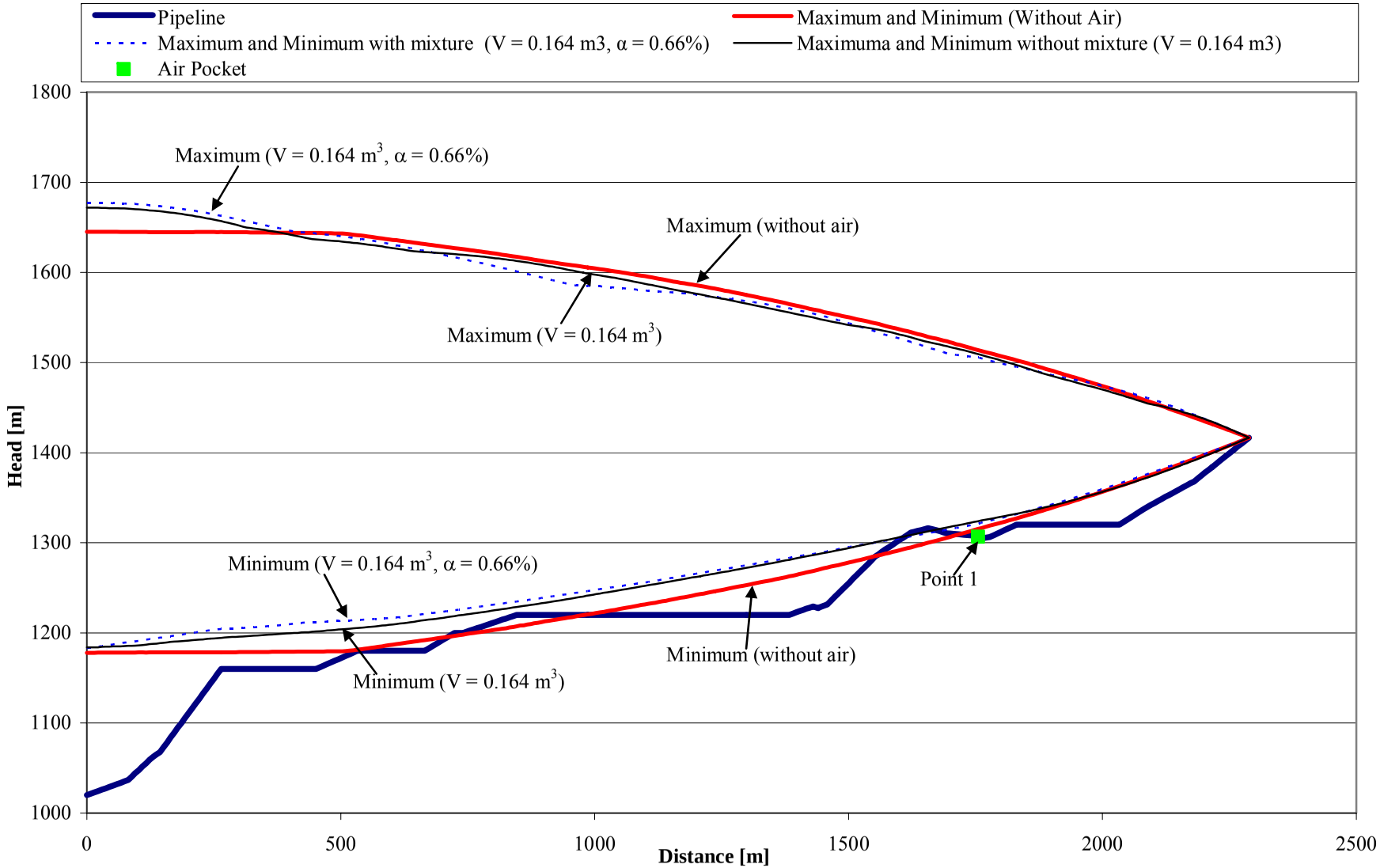

Figure 5.15: Maximum and minimum head envelopes with a small air pocket volume V = 0.164 m^3, located at point 1with and without a water-air mixture immediately downstream of the pocket, α = 0.66 %

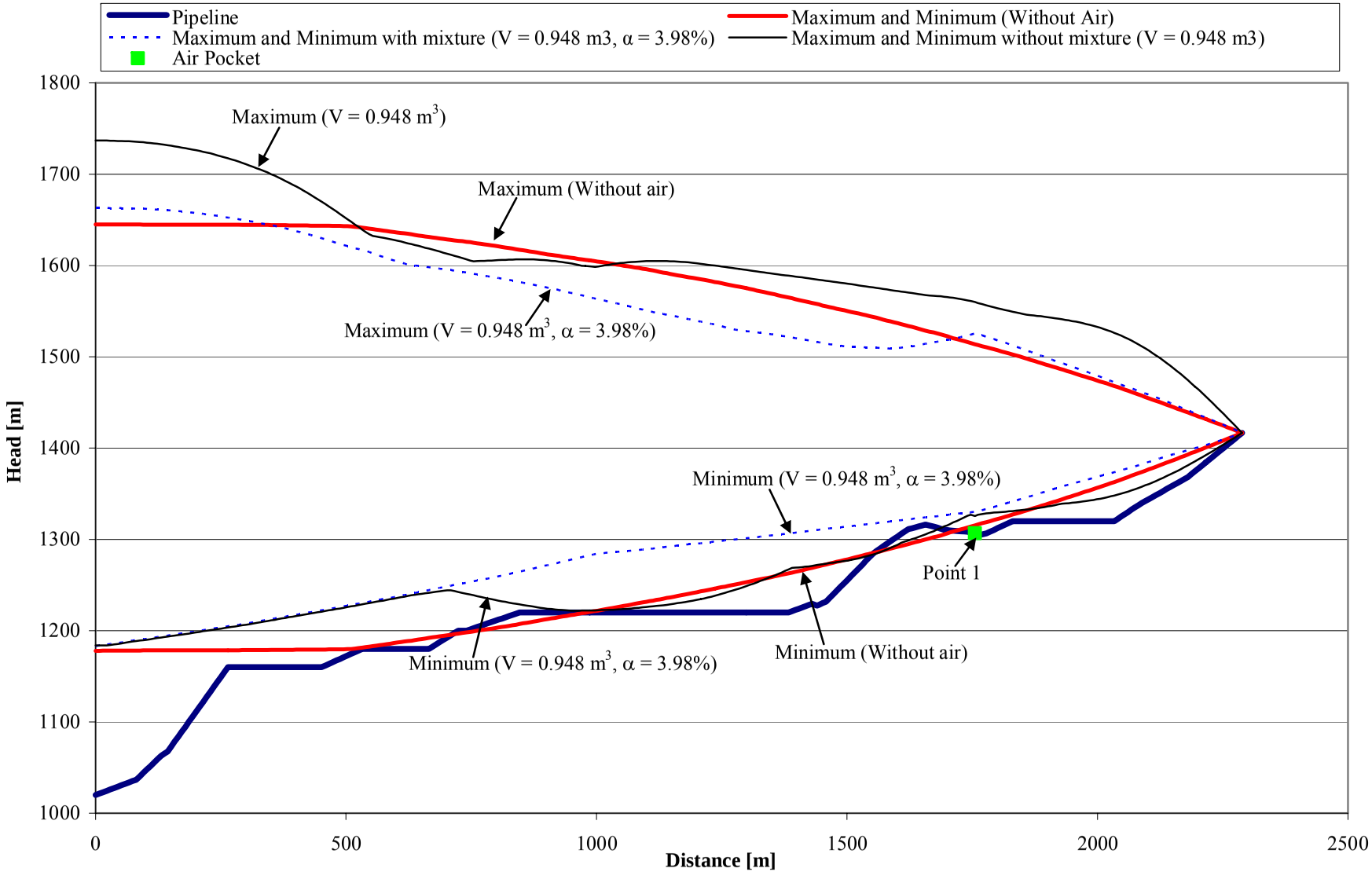

Figure 5.16: Maximum and minimum head envelopes with and intermediate air pocket volume V = 0.948 m^3, located at point 1 with and without water-air mixture immediately downstream of the pocket, α = 3.98 %

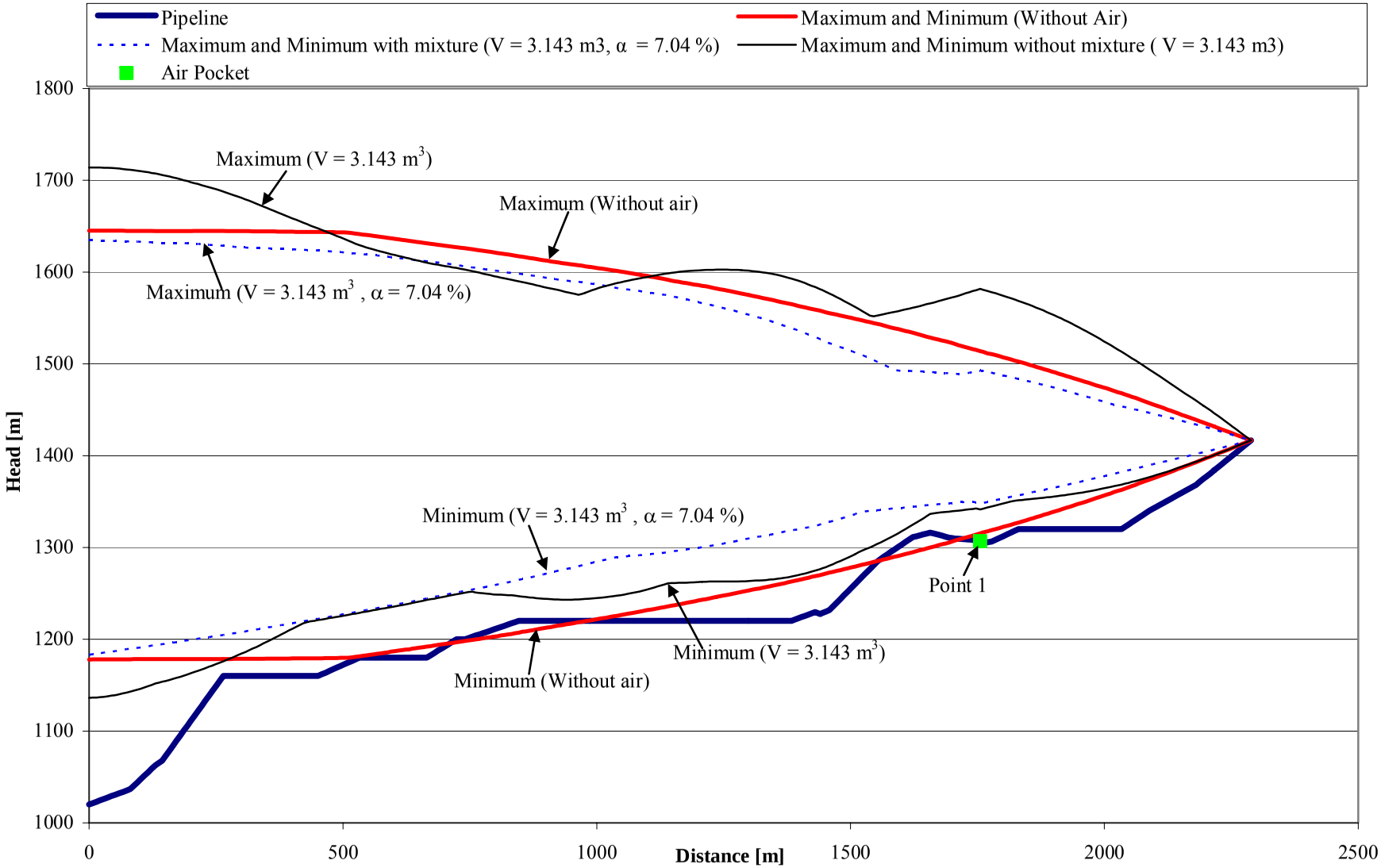

Figure 5.17: Maximum and minimum head envelopes with a large air pocket volume V = 3.143 m^3, located at point 1 with and without a water-air mixture immediately downstram of the pocket, a = 7.04 %

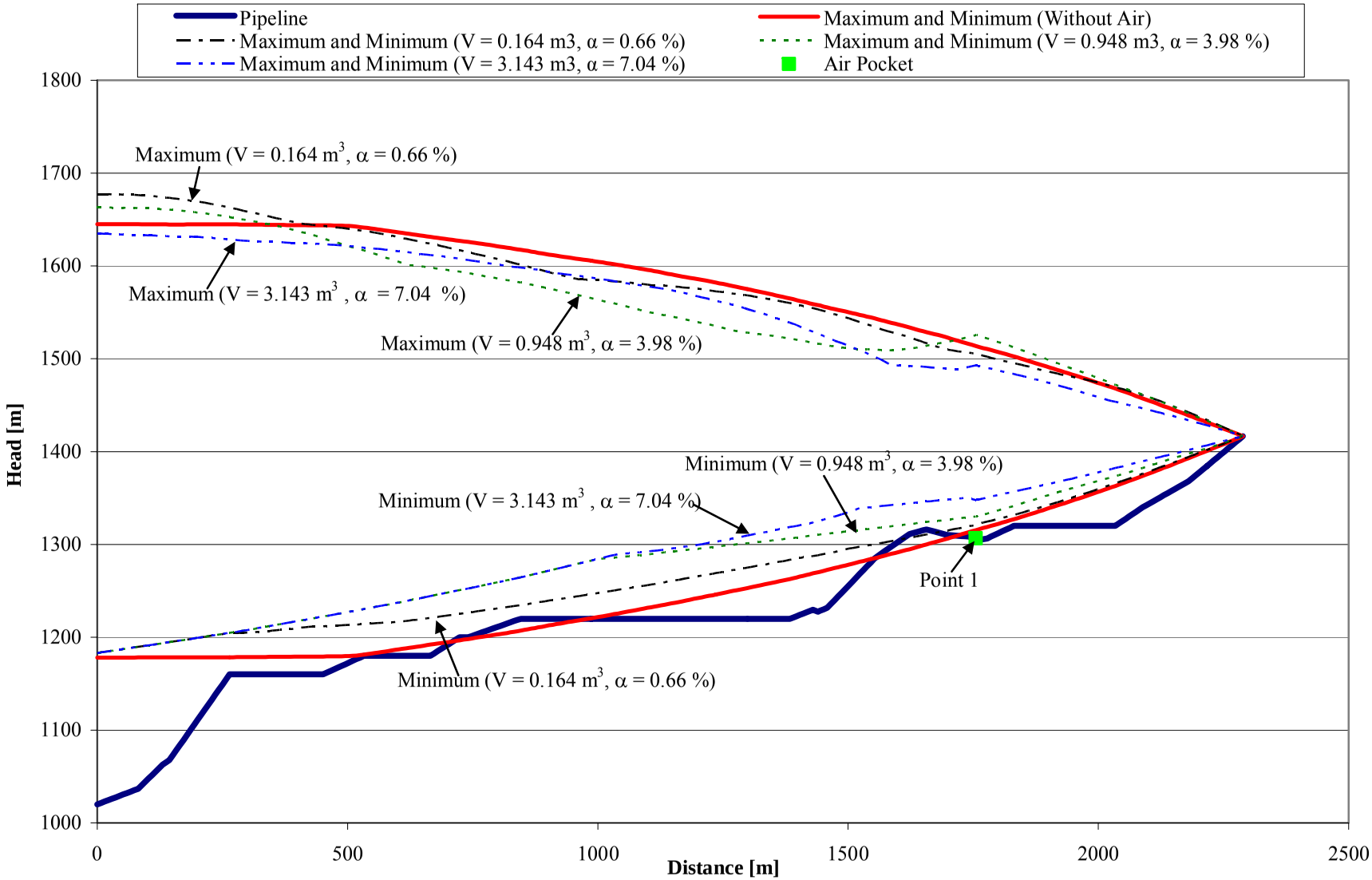

Figure 5.18: Comparison of the maximum and minimum head envelopes with different air pocket volumes located at point 1, and a water-air mixture immediately downstram of the pocket

5.14.2 Pumping station performing with 3 units (Q_w = 1.875 m^3/s) and 4 air pockets located at the high point 2 and intermediate points 1, 3 and 4 with a water-air mixture immediately downstream of the pockets

From the results obtained and depicted in Figure 5.19, it is noticeable that the worst situation remains when the four smallest air pocket volumes are placed at the points found as likely to accumulate air. Even though a water-air mixture exists immediately downstream of each pocket, these are not enough to absorb the energy transient wave considerably. Likewise, the maximum head at the pump discharge is greater than that obtained without considering air accumulation at the pipeline. In addition, a slight reflection of the maximum head is generated by the air pockets located at the points 3 and 4 towards the downstream end boundary.

It is observed in Figure 5.20 that when a water-air mixture occur downstream of the intermediate air pockets, the maximum and minimum head profiles are reduced significantly. It is important to point out that the reflection of the transient pressure waves almost disappears due to the presence of the water-air mixture, although a reflection is evident above the high points where the pockets are located and towards the downstream end boundary, but it seems not to be detrimental for the system.

It is possible to suggest from Figure 5.21 that the largest air pocket volumes with a water-air mixture downstream of them contribute to reduce considerably the maximum and minimum head envelopes in the pumping pipeline system. It is important to highlight that the greatest and lowest values of the maximum and minimum envelopes occurred at the discharge side of the pumps. They are slightly the same, as those obtained without water-air mixture downstream of the pockets and under the assumption of no air accumulated. The cushioning effect produced by the large air volumes and the corresponding air void fractions on the maximum head is even more considerable than that compared without water-air mixture. In addition, a minor reflection is observed in both envelopes compared with that obtained without considering a water-air mixture downstream of the pockets.

From the previous results, it can be said that the intermediate and large pockets with a water-air mixture downstream of them have an important effect by lowering the transient pressure. The dampening effect is more noticed on the maximum head envelopes. However, the simulation which includes small air pockets and water-air mixture presents an important exacerbation of the maximum head towards the upstream and downstream end boundaries.

As in the previous subsection, it is observed that the minimum head envelopes generated after the shutdown of 3 units at the pumping plant, when 4 air pockets are located at the high points of the line and with a water-air mixture immediately downstream of the pockets. These minima were never lower than those computed in the absence of air and with air pockets without a water-air mixture. Likewise, the results show that the shape of the maximum and minimum head envelopes obtained are slightly the same, when the air pockets with their corresponding water-air mixture are located at the high points 1 to 4. The value of the air void fraction and air pocket volumes, see Figure 5.22, are of no influence.

To highlight the effect of the water-air mixture on pressure transients, a comparison between maximum and minimum head envelopes computed with air pockets located at the high points of the pumping pipeline with and without a water-air mixture immediately downstream of them was done. It can be seen in Figures 5.23 that the results obtained for the simulations with small air pockets and a water-air mixture immediately downstream of them, and the maximum and minimum head envelopes when intermediate air pockets without water-air mixture downstream of them are located at the high points, give similar values across the majority of the pipeline profile, except at the points where the intermediate air pockets are placed. In this case a pressure wave reflection between the pockets located at points 3 and 4 and the downstream end boundary exists, due to the small air pockets and the water-air mixture were not enough to absorb the reflection. Likewise, the minimum head envelope achieved did not show a wave reflection.

In Figure 5.24 are shown the pressure transient simulations with intermediate air pocket volumes and a water-air mixture immediately downstream of them and those with large air pockets and no water-air mixture. It can again be observed that there are marginal differences between the computations. The most notable difference in the two sets of results is the shape of maximum head reflection near the locations of the air pockets. On the other side, it can be stated that the two minimum head envelopes are very similar.

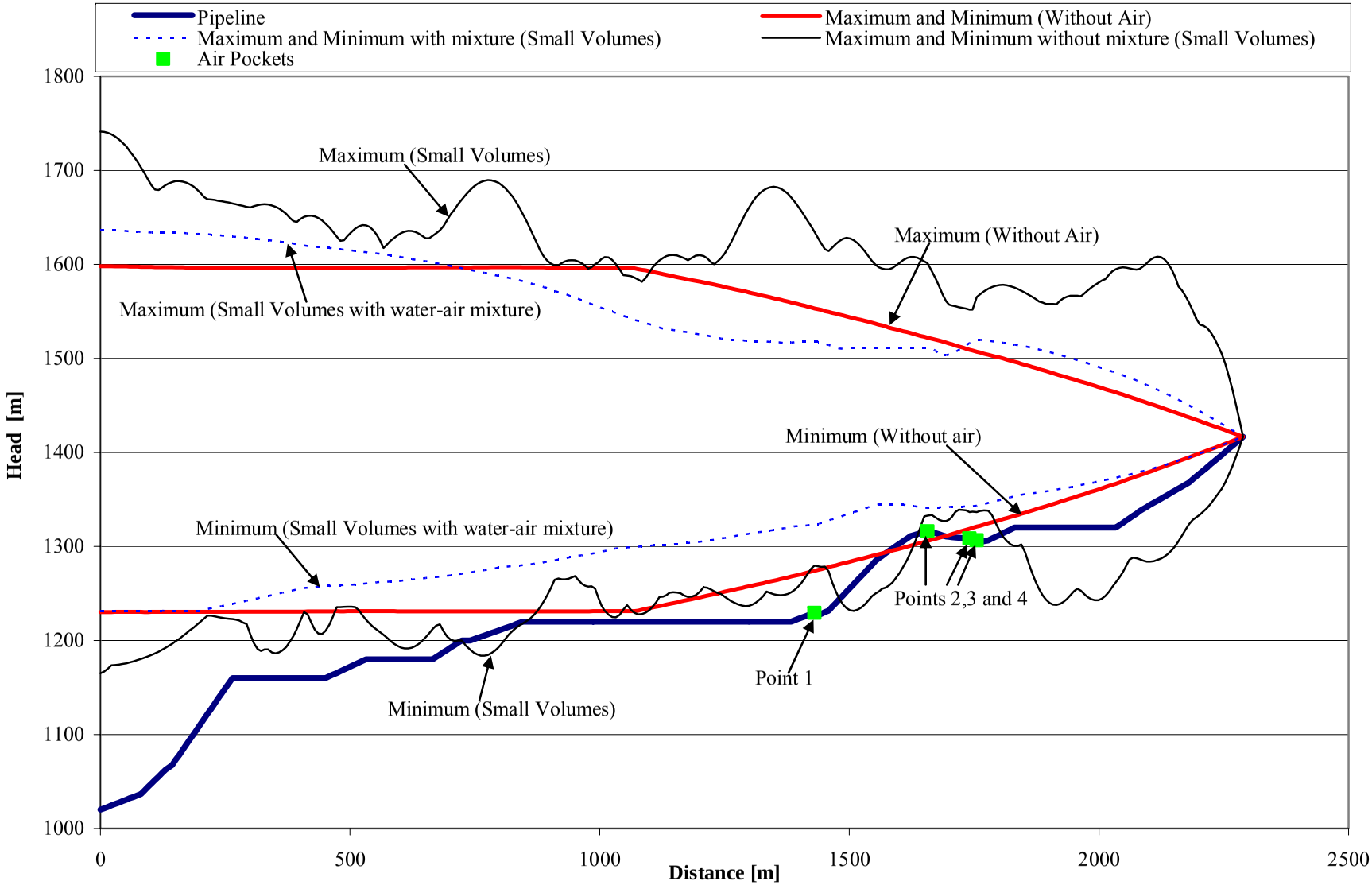

Figure 5.19: Maximum and minimum head envelopes with 4 small air pockets located at points 1, 2, 3 and 4 with and without a water-air mixture immediately downstream of the pockets

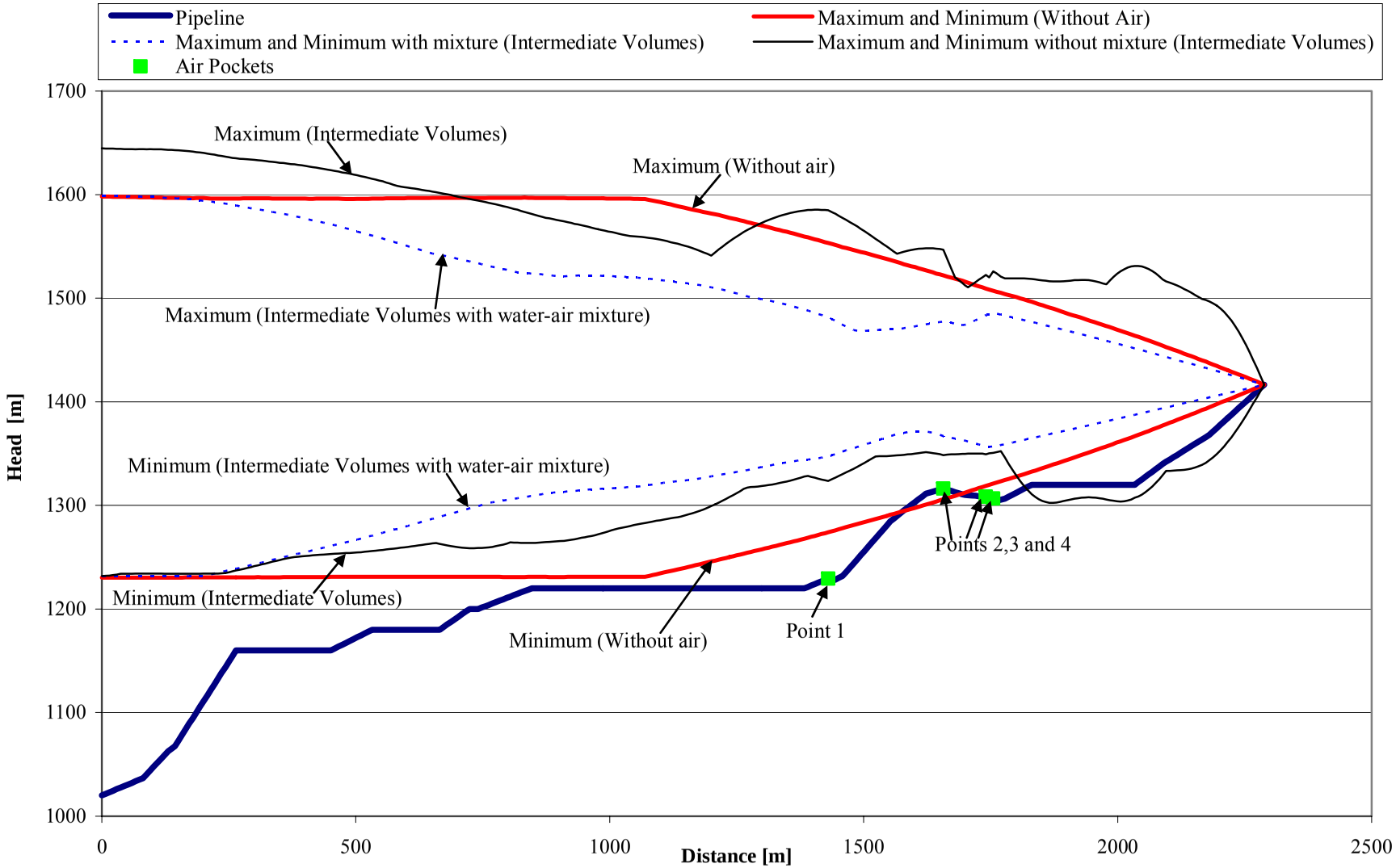

Figure 5.20: Maximum and minimum head envelopes with 4 intermediate air pockets located at points 1, 2, 3 and 4 with and without a water-air mixture immediately downstream of the pockets

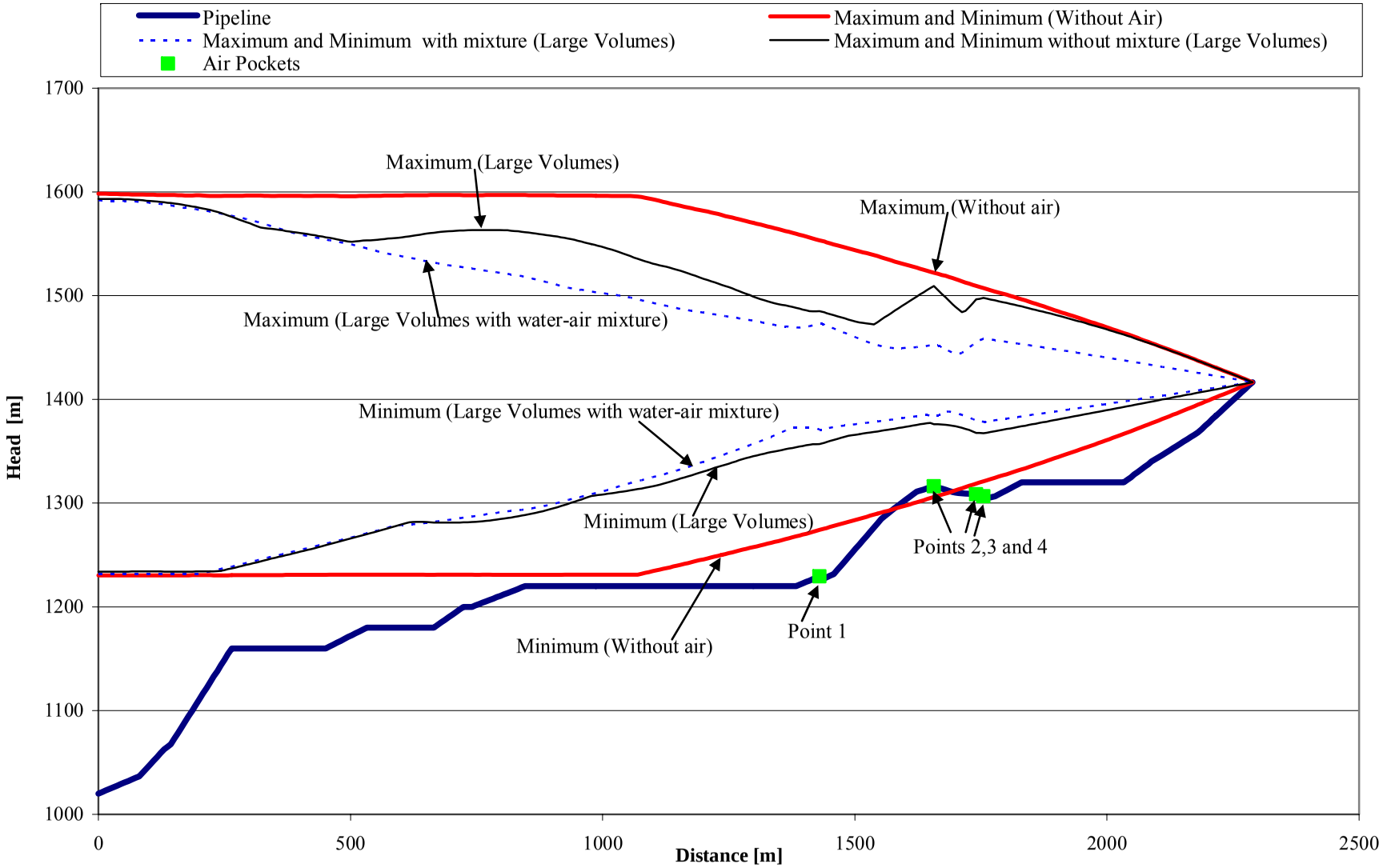

Figure 5.21: Maximum and minimum head envelopes with 4 large air pockets located at points 1, 2, 3 and 4 with and without a water-air mixture immediately downstream of the pockets

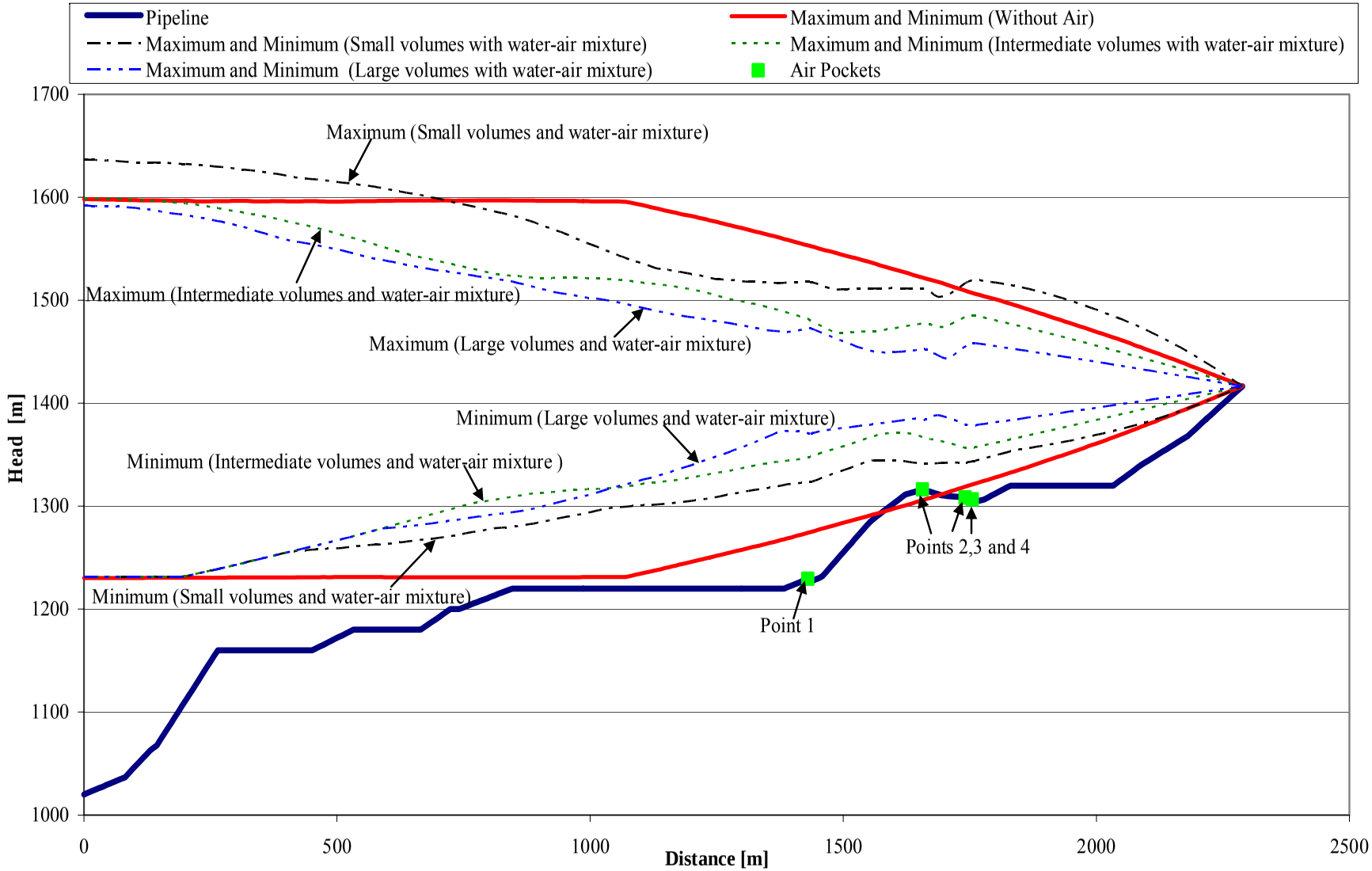

Figure 5.22: Comparison of the minimum head envelopes with different air pocket volumes located at points 1, 2, 3 and 4 with and without a water-air mixture immediately downstream of the pockets

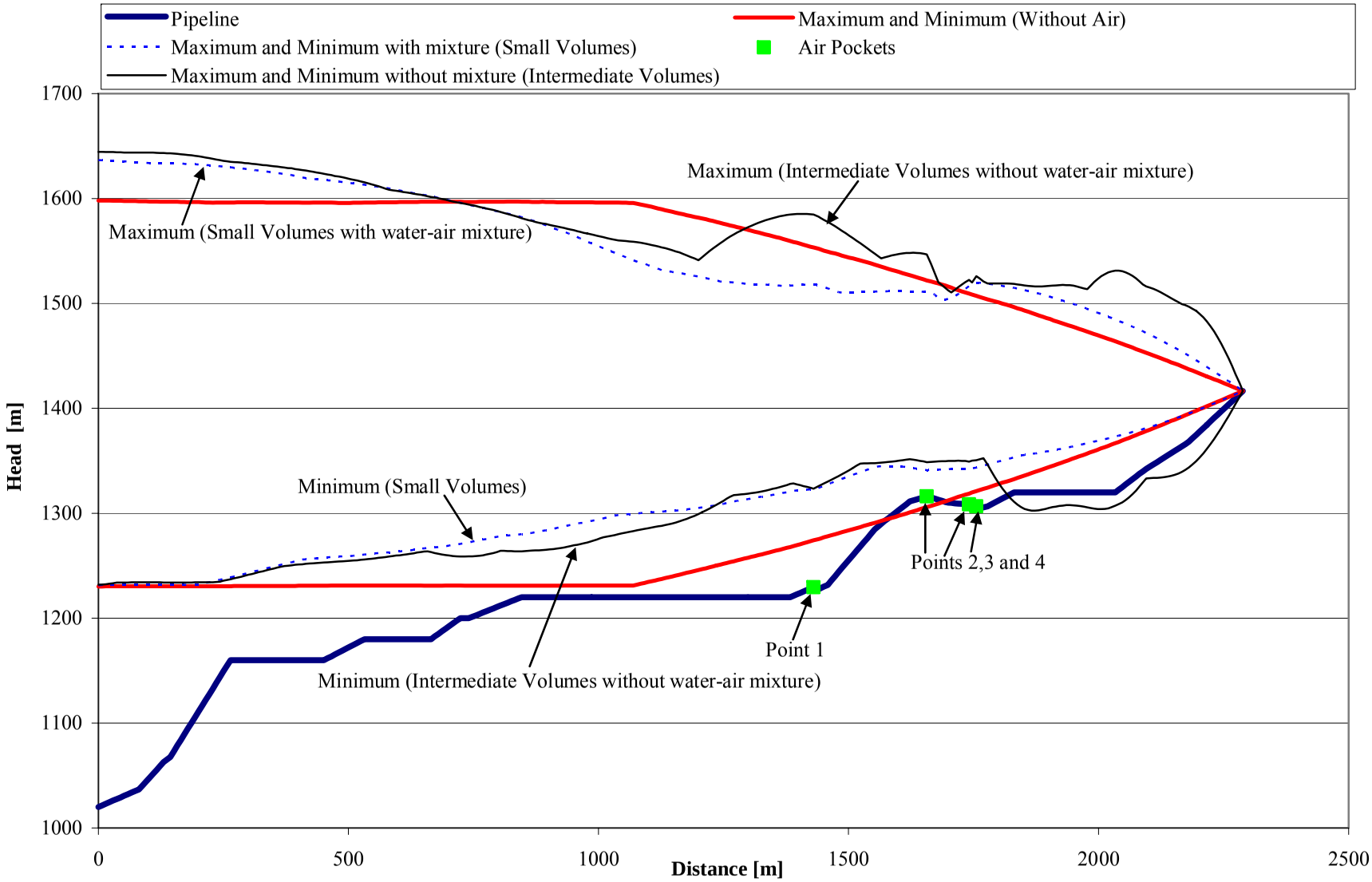

Figure 5.23: Comparison of the maximum and minimum head envelopes with small air pocket volumes located at points 1, 2, 3 and 4 with a water-air mixture immediately downstream of them, and intermediate air pockets at the same high points without water-air mixture

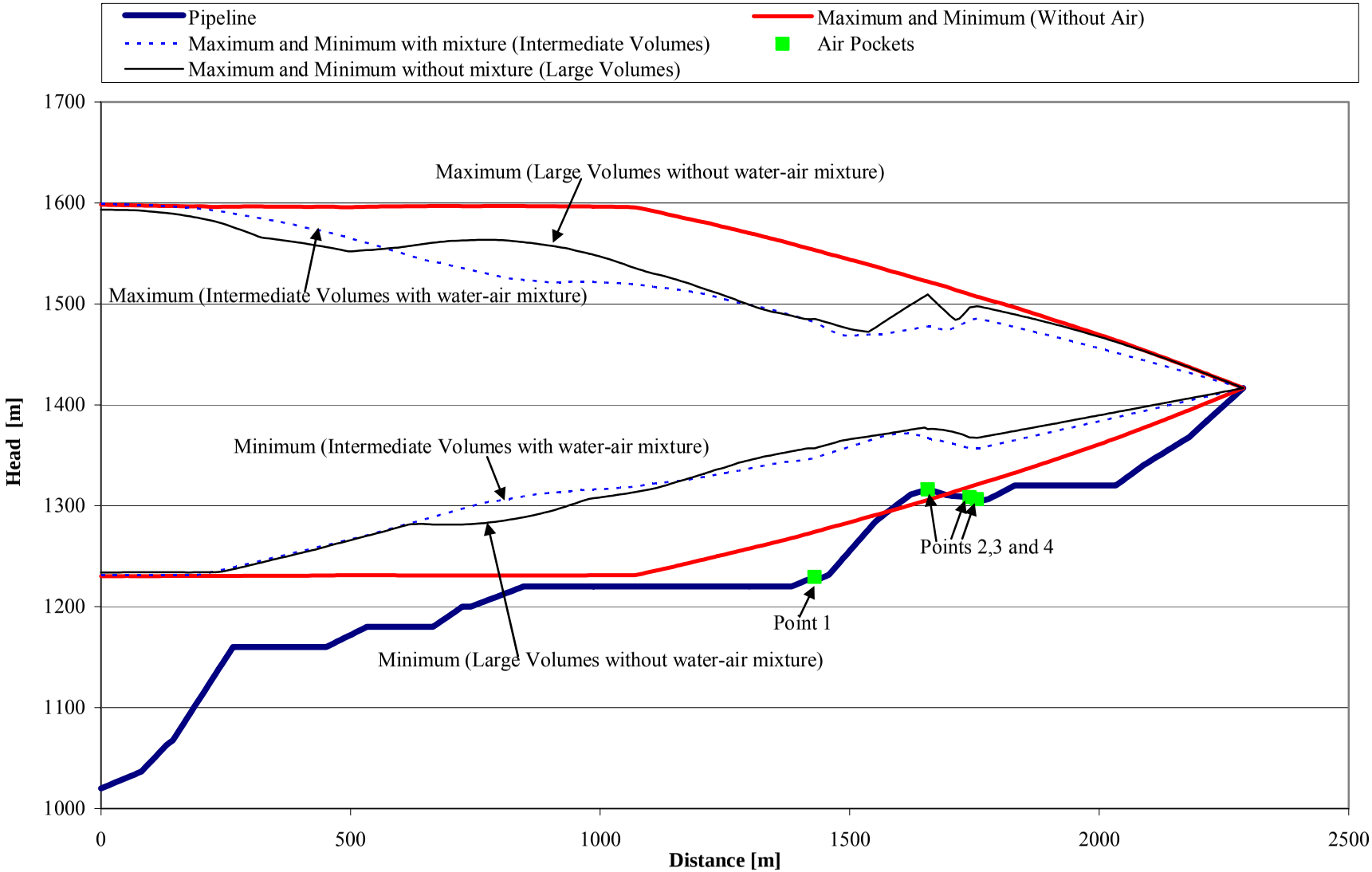

Figure 5.24: Comparison of the maximum and minimum head envelopes with intermediate air pocket volumes located at points 1, 2, 3 and 4 with a water-air mixture immediately downstream of them, and large air pockets at the same high points without water-air

6. Conclusions and Recommendations

6.1 Conclusions

A numerical model based on the homogeneous model equations has been developed to investigate the effects of air pockets with a water-air mixture downstream of them on pressure transients in pumping pipeline systems. It is assumed that the air bubbles are entrained by the hydraulic jumps occurring at the end of the air pockets. The equations of the system are solved by the method of characteristics. Likewise, pressure transients two-phase flow with air pockets located at the high points of the line with and without a water-air mixture downstream of them were simulated. The main purpose was to analyze the influence of the air void fraction, size of the air pocket volumes, their locations and pipeline system configuration.

The comparison of the maximum and minimum head envelopes with and without a water-air mixture downstream of the pockets highlighted the combined effects of both air pockets and water-air mixture on transient pressures. As it has been stated, the small and large air pockets can be defined in terms of their effects on fluid transients. For example, small air pockets can exacerbate the maximum peak pressure, even though a water-air mixture occurs immediately downstream of them. On the other side, large air pockets can behave as an energy accumulator that absorbs the transient wave in pipelines. Likewise, there are limits to the volumes of air, outside of which these effects do not occur. This implies that there is a critical air pocket volume for a particular pipeline configuration.

A case study of a pumping pipeline system without surge suppression devices was simulated to demonstrate the potential detrimental and beneficial effects of air pockets with and without a water-air mixture downstream of them on hydraulic transients. The boundary condition at the upstream end is a pumping station with four units connected in parallel and at the downstream end a constant head tank. Only hydraulic transients generated by the sudden shutdown of the pumps are taken into account in this analysis. A series of numerical simulations has been developed to give guidance for prevention of the problems or else for the reduction of the risks of pipeline damage. Likewise, hydraulic model investigations were made to understand the behaviour of air pockets at the high points of pipelines and to compute the volume of air contained within the pockets.

6.1.1 Effect of air pockets with and without a water-air mixture on hydraulic transients

From the computations obtained, it can be seen that the worst scenarios occurred either when a single small air pocket or multiple small air pocket volumes are located at the intermediate and high points of the pumping pipeline, and a water-air mixture occurs immediately downstream of the pockets, as is shown in Figures 5.15 and 5.19. It was found that although a water-air mixture occurs downstream of the small pockets, the maximum head enveloped can be slightly greater than that achieved without water-air mixture immediately downstream of the pockets. It was suggested that this effect is produced by the expansion and contraction processes of the air bubbles, see Figure 5.15.

The results have shown that an air pocket located at a high point of the pipeline can give rise to the worst situation, when a water-air mixture does not exist immediately downstream of it, i.e. the air pocket volume is the critical value for this pipeline configuration. Nevertheless, when the bubbly mixture is considered together with the pocket in the computations, it was observed that the air pocket and the water-air mixture produced an important dampening effect along the pipeline, and the achieved values of the maximum head enveloped are even lower than those predicted under the assumption of no air accumulated in the pipeline, therefore in this case this air pocket volume cannot be called critical, see Figure 5.16.

It has been demonstrated that the presence either of a single large air pocket or multiple large air pockets with a water-air mixture immediately downstream of them act as effective accumulators, suppressing the pressure transients, as can be seen in Figures 5.17 and 5.21. It is important to highlight that with the occurrence of the water-air mixture, the maximum head envelopes have lower values than those obtained without considering air; on the other side the wave reflection is marginal. Therefore, it can be stated that the large air pocket volumes with a water-air mixture have a beneficial effect for pipelines by lowering significantly the transient pressure.

The results have shown that the transient pressures, as well as the wave reflections are significantly reduced by increasing the air pocket volume and the air void fraction. It has to be pointed out that the maximum head envelopes have a more significant reduction than the minimum head envelopes, when a water-air mixture occurs immediately downstream of the air pockets.

In all the simulations performed either with an air pocket or multiple air pockets located at the intermediate or high points of the pipeline and a water-air mixture immediately downstream of the pockets, the minimum head envelopes along the pipeline profile were never less than the minimum head envelopes without air. In the same way, it has been observed that the maximum and minimum head envelopes have similar shapes compared with single-phase water flow and are symmetric with respect to the static head. Likewise, the shapes of the maximum and minimum head envelopes are roughly the same, see Figures 5.18 and 5.22. It is independent of the values of the air pocket volumes and the air void fraction.

6.1.2 Hydraulic model investigation

Previous to this work, experimental investigation in laboratory was made. Two models were designed and constructed to analyze the behavior of stationary air pockets at intermediate and high points of gravity pipelines, as well as to analyze the air entrained by the hydraulic jump at the end of the pocket located in the downward sloping pipe section of the model. The main aim of the research was to validate the use of a proposed equation, which describes the movement of air bubbles and pockets downstream of the jump. Supported on this relation a computational algorithm was developed. From a comparison of the experimental measures with the results obtained with the program, it can be concluded that these agreed well. Likewise, the proposed relationship was used in this work to determine the location of the air pockets in pumping pipeline systems. The results obtained with the equation adjusted well with the predictions obtained from other investigators for the pipeline configuration analyzed in the case study.

For the purpose of studying and observing the large air pockets located at high points in pipelines, experimental investigations were developed in laboratory. The research was carried out in a physical model with the main aim of measuring the volumes of air that form the pockets. The hydraulic model investigation was focused on large air pockets located at high points of pumping pipeline systems.

During the measurements the water depths underneath the large air pocket at atmospheric pressure, as well as for pressurized conduit flow were recorded. The experimental results were compared with the analytical results obtained with the direct step method used in the analysis of gradually varied flow. The comparison of the air pockets profiles yield interesting results. The flow profile underneath the air pocket, as computed by the dynamic equation of the

gradually varied flow, shows excellent correlation with the flow profiles determined experimentally.

The volumes of air of the pockets were calculated by using an equation based on the direct step method and were compared with the experimental results obtained in laboratory. The computed values are lower than the volumes of air measured in the experiments. Therefore, it can be stated that the volumes of air estimated with the variables obtained by using the direct step method increase the factor of safety in the pipeline design. This is because the author and other investigators have found that small air pockets located at intermediate and high points can enhance the magnitude of surge pressures experienced by a sudden or routine pump shutdown. It could have serious implications, if entrained air is not accounted for during the design of pumping pipeline systems.

A photographic study was developed to reinforce the assumptions made in the numerical model for the simulation of pressure transients with air pockets and a water-air mixture downstream of them. The supercritical flow to pressurized conduit flow was explored, as well as the characteristics of the hydraulic jumps in circular pipes at atmospheric pressure and pressurized flow conditions. The observations indicated that the hydraulic jumps may entrain a considerable quantity of air into the water-air mixture.

6.2 Recommendations

6.2.1 Design and operation of pipelines

Air accumulation in pipeline systems is both unintentional and unavoidable and cannot be always completely eliminated but understanding the ways how it enters a pipe helps the engineers to minimize its occurrence. Unfortunately, many engineers design under the assumption that pipelines flow full all the time and never part-full and this hypothesis may lead to critical problems, because the presence of entrained air was not taken into account during the design stage of pipelines. Therefore, the pipeline designer should have the knowledge to predict the worst case scenarios and in the case of a likely negative impact, modify the profile of the pipeline or suggest operational remediation measures to reduce an important detrimental effect. It is known that the simplest pipeline systems can suffer from air entrainment problems. Hence, all systems especially those with several slope changes have to be analyzed in detail for all flow conditions to locate the potential high and intermediate high points, where air may be accumulated. In addition, hydraulic transient analysis is usually

based on the assumption of no air accumulated in the pipeline system. That may explain the collapse or burst of the line that could not be predicted with a standard surge analysis. Likewise, when the profile of an existing pipeline is modified, due to the construction of an open channel, a highway or other civil structure, a new complete analysis of the water line has to be carried out. The summits in the pipeline that are susceptible to build up air have to be identified. If high points likely to accumulate air exist, a simulation of hydraulic transients has to be developed to intent to reduce the potential detrimental effect.

During the analysis of hydraulic transients, the pipeline designer should take into account that all the water systems are dynamically different in terms of operation and pipeline configuration. It is also not possible to obtain a definitive answer in terms of the critical air pocket volume and its location. However, the results obtained during the simulations could serve to assist the designer to predict more accurately the critical conditions for various pipeline configurations. As a result of the progress of numerical methods, there has been a tendency to attempt the design of pipeline systems only by numerical simulations. However, experimental investigation would be recommended additionally as the ideal in order to develop a detailed and rigorous analysis of the effect of air pockets with and without water air mixture on pressure transients.

It is recommended to the designers to incorporate the analysis of entrained air in pipelines as a matter of routine to be able to report the possible operational scenarios likely to give rise to severe pressure transients. Moreover, many pipeline designers can consider that the idea to develop numerical and experimental investigation would be extremely time consuming and costly. However, the cost of repairing the pipeline and the lawsuit against the system operator by the people and businesses affected due to a pipeline failure can rise to thousands or even millions of euros.

The comprehensive method developed by the author for the identification and quantification of the volume of air entrained into the pumping pipeline systems, can be used by the pipeline designers to allow for the effects of air pockets with and without a water-air mixture immediately downstream of them on fluid transients, and its impact on the safety of pipeline operation. The procedure of computation is summarized in the flowcharts presented in chapter 4 and chapter 5.

6.3 Suggestions for further studies

6.3.1 Numerical and experimental investigation

As it has been stated, a numerical model based on the homogeneous model equations has been developed to analyze the problem of transient two-phase flow. The method of characteristics was chosen to solve the system of equations, due to its simplicity, accuracy and numerical efficiency. However, additional work is required to implement more sophisticated methods and schemes to compare the results herein achieved and supporting the numerical model. Likewise, the numerical model proposed herein this work has not yet been verified experimentally, hence a hydraulic model research is needed to be developed to investigate the effects of air pockets with a water-air mixture downstream of them on pressure transients in pumping pipeline systems.

Normally in the literature simple reservoir/pipe/valve arrangements are presented with low air void fractions $\alpha < 1$ % and the pressure transients are induced by a quick valve closure, therefore experiments in more realistic and elaborated hydraulic models with upward and downward sloping pipe sections, should be carried out to simulate the transient response of air pockets with a flowing bubbly water-air mixture downstream of them subsequent to a shutdown of pumps.

6.3.2 Structural safety

The amplification of the maximum and minimum head, due to the reflection produced by the air pockets has to be considered during the design stage of the reservoirs or suctions tanks of the pumping plants. The pressures may give rise to cracks or to important fractures in the structure. In addition, the degree of the pressure transient waves enhancement experienced by the upstream end boundary should be taken into account for the selection and design of the check valves located at the discharges of the pumps.

As previously highlighted, the transient pressures are simulated without surge suppression devices to demonstrate the potential effect of air pockets with and without water-air mixture downstream of them on hydraulic transients. In extreme cases the large pressure transients arising may be expected to have a potentially catastrophic effect. This numerical investigation can be used as guidance for the pipeline designers to minimize the effect of entrapped air on pressure transients. However, it is envisaged that further numerical and experimental

investigation can provide more specific guidelines. Therefore, the simulation of additional case studies is needed, incorporating in the numerical model to analyze the effect of suppressor devices as air vessels, surge tanks, air release and vacuum valves on pressure transients with entrapped air pockets with and without water-air mixture downstream of them.

References

[1] Ahmed, A.A., Ervine, D.A., and McKeogh, E.J. 1984. The process of aeration in closed conduit hydraulic structures. In Proceedings of a Symposium on Scale Effects in Modelling Hydraulic Structures. *Edited by* H. Kobus. Technische Akademie Esslingen, Germany, Vol. 4(13), pp. 1-11.

[2] Alves, G.E., 1954. Chemical Engineering Progress, Vol. 50 (9), pp. 449-456.

[3] Babb, A.F., Johnson, W.K., Performance characteristics of siphons outlets, Journal of the Hydraulics Division, ASCE, November 1968, pp. 1421-1437.

[4] Balutto, A., 1996. Air valve technology reviewed, Introducing controlled air transferred technology, VENT-O-MAT, http://internationalvalve.com.

[5] Balutto, A., 1998. The application of controlled air transfer technology to new and existing pipeline systems, http://www.ventomat.com.

[6] Bendiksen, K.H., 1984. An experimental investigation of the motion of long bubbles in inclined tubes, Int. J. Multiphase Flow, Vol. 10, No. 4, pp. 467-483.

[7] Brown, R.J., 1968. Water column separation at two pumping plants, Journal of Basic Engineering, ASME, Vol. 90, N° 4, pp. 521-531.

[8] Burrows, R., 2003. A cautionary note on the operation of pumping mains without appropriate surge control and the potentially detrimental impact of small air pockets, Paper submission for IAHR / IWA International Conference - PEDS-2003 - Valencia, Spain, April 22nd-25th.

[9] Burrows, R. and Qiu, D.Q., 1995. Effect of air pockets on pipeline surge pressure, Proceedings of the Institution of Civil Engineers, Journal of Water, Maritime and Energy, Volume 112, December, Paper 10859, pp. 349-361.

[10] Chaudhry, M.H., 1987. Applied Hydraulic Transients, 2nd Edition, Van Nostrand Reinhold, New York, USA.

[11] Chow, V.T., 1981. Open channel hydraulics, 17th Edition, McGraw Hill.

[12] Cohen de Lara, G. 1955. Degazage naturel dans les puits inclines reliant les adductions secondaires aux galéries en charge. In Proceedings of the 6th International Association for Hydraulic Research Congress, La Haye, Vol. 3(C19), pp. 1–20.

[13] Colgate, D. 1966. Hydraulic model studies of the flow characteristics and air entrainment in the check towers of the main aqueduct, Canadian river project Texas. Department of the Interior Bereau of Reclamation, Report N° Hyd-555, USA.

[14] Collier, J.G., 1981. Convective boiling and condensation, 2nd Edition, McGraw Hill.

[15] Edmunds, R. C, 1979. Air binding in pipes, Journal AWWA, Water Technology/Distribution, pp. 273-277.

[16] Ervine, D.A., 1998. Air entrainment in hydraulic structures: a review. Proc. Instn Civ. Engrs Wat., Marit. and Energy, Vol. 130, Sept, pp. l42-153.

[17] Ervin, R.A., McKeogh, E., Elsawy, E.M., 1980. Effect of turbulence intensity on the rate of air entrainment by plunging water jets. Proc Instn Civ Engrs, 69, 2, pp. 425-445.

[18] Escarameia, M., Dabrowski, C., Gahan, C. and Lauchlan, C., 2005. Experimental and numerical studies on movement of air in water pipelines. HR Wallingford Report SR661.

[19] Ewing, D.J.F., 1980. Allowing for free air in waterhammer analysis, Proceedings of the 3rd International Conference on Pressure Surge, BHRA, Canterbury, England, pp. 127-146.

[20] Falvey, H.T., 1980. Air-water flow in hydraulic systems, Bureau of Reclamation, Engineering monograph No. 41.

[21] Fasso, C. 1955. Experimental research on air entrainment in gated outlet works. *In* Proceedings of the 6th International Association for Hydraulic Research Congress, La Haye, Vol. X(C26), pp. 1-18.

[22] Fok. T.K., 1987. A contribution to the analysis of energy losses in transient pipe flow, Doctor of Philosophy Thesis, University of Ottawa, Canada.

[23] Förster, G., 1997. Druckstoßdämpfung durch große Luftblasen in Hochpunkten von Rohrleitungen. In: Mitteilungen des Institutes für Wasserbau der Universität Stuttgart, Heft 1994.

[24] Fuertes, V.S., 2000. Hydraulic transients with entrapped air, PhD Thesis, Universidad Politécnica de Valencia, Departamento de Ingeniería Hidráulica y Medio Ambiente, España (in spanish)

[25] Gahan, C.M., 2004. A review of the problem of air release/collection in water pipelines with in-depth study of the effects of entrapped air on pressure transients, MRes Thesis, Department of Civil Engineering, Universty of Liverpool, UK.

[26] Gandenberger, W., 1957. Uber die wirtshaftliche und betriebssichere Gestaltung von Fernwasserleitungen, R. Oldenbourg Verlag, Munich, Germany Design of overland water supply pipelines for economy and operational reliability (rough translation by W.A. Mechler, discussion of "Factors influencing flow in large conduits.", Report of the Task Force on Flow in Large Conduits of the Committee on Hydraulic Structures, ASCE, Vol. 92, No. HY4, 1966.

[27] Giesecke, J., Mosonyi, E., 2005. Wasserkraftanlagen: Planung, Bau und Betrieb Planung - 4., aktualis. u. erw. Aufl.. - Berlin ; Heidelberg : Springer.

[28] Goldring, B.T., Mawer, W.T., Thomas, N.H., 1980. Level surges in the circulating water downshaft of large generating stations. Third International Pressure Surges Conference, BHRA, Canterbury, England.

[29] Gonzalez, C.A., Pozos, O., 2000. Análisis experimental del ingreso de aire en un acueducto, Thesis, Univesidad Nacional Autónoma de México, México. (in spanish).

[30] Haindl, K. 1957. Hydraulic jump in closed conduits. *In* Proceedings of the 7th International Association for Hydraulic Research Congress, Lisboa, Vol. 2(D32), pp. 1-12.

[31] Hashimoto, K., Imaeda, M., Osayama, A., 1988. Transients of fluid lines containing and air pocket or liquid column, Journal of Fluid Control, Vol. 18, N° 4, pp. 38-54.

[32] Hewitt, G.F. and Hall-Taylor, N.S., 1970. Annular two-phase flow, 1st Edition, Pergamon Press Ltd.

[33] Holley, E.P., 1969. Surging in laboratory pipeline with steady inflow, Journal of Hydraulic Engineering, ASCE, Vol. 95, N° 3, pp. 961-979.

[34] Horlacher, H.-B., Lüdecke, H.-J., 1992. Strömungsberechnung für Rohrsysteme. Ehningen: Expert-Verlag.

[35] Jönsson, L., 1985. Maximum transient pressures in a conduit with check valve and air entrainment, Proceeding of the International Conference on the Hydraulics of Pumping Stations, British Hydromechanics Research Association, Manchester, pp. 55-76.

[36] Jönsson, L., 1992. Anomalous pressure transients in sewage lines, Proceedings of the International Conference on Unsteady Flow and Transients, Durham, UK, pp. 251-258.

[37] Kalinske, A.A. and Bliss, P.H., 1943. Removal of air from pipelines by flowing water, ASCE Vol. 13, No. 10, pp. 480-482.

[38] Kalinske, A.A, Robertson, J.M., 1943. Closed conduit flow, ASCE Vol. 108, pp. l453-1516.

[39] Kenn, M.J., Zanker, K.J., 1967. Aspects of similarity for air-entraining water flows, Nature, 213, 5071, pp. 59-60.

[40] Kent, J.C., 1952. The entrainment of air by water flowing in circular conduits with downgrade slopes. Doctoral thesis, University of California, Berkley, California, USA.

[41] Kobori, T., Yokoyama, S., Miyashiro, H., 1955. Propagation velocity of pressure wave in pipe line, Hitachi Hyoron, Vol. 37, N° 10, pp. 1407-1411.

[42] Kottmann, A., 1992. Druckstoßermittlung in der Wasserversorgung. Essen: Vulkan-Verlag.

[43] Landon, P.O. Air in Pipe? Time to review air valve basics, Opflow AWWA, March 1994, pp. 1-5.

[44] Landon, P.O., 1997. Air in pipelines: sources, system impact, removal by air valves, Val-Matic Valve & Mfg. Corp.

[45] Lane, E.W., Kindsvater, C.E. 1938. Hydraulic jump in enclosed conduits. Engineering News Record, Dec. 29, pp. 815–817.

[46] Larsen, T., Burrows, R., 1992. Measurements and computations of transients in pumped sewer plastic mains, Proceedings of the BHR Group / IAHR International Conference on Pipeline Systems, Manchester, pp. l17-123.

[47] Lauchlan, C.S., Escarameia, M., May, R. W. P., Borrows, R. and Gahan, C., 2005. Air in pipelines – A Literatur review. HR Wallingford Report SR649.

[48] Lee, T.S., 1991. Numerical computation of fluid transients in pumping installations with air entrainment, International Journal for Numerical Methods in Fluids, Vol. 12, pp. 747-763.

[49] Little, M.J., 2002. Air Transport in Water and Effluent Pipelines, 2nd International Conference on Marine Waste Discharges, Istanbul, September 16-20.

[50] Martin, C.S., 1976. Entrapped air in pipelines, Proceedings of the Second International Conference on Pressure Surges, British Hydromechanics Research Association, The City University, London, September 22nd - 24th, Paper F2, F2-15 - F2-28.

[51] Martin, C.S., 1996. Two-phase gas-liquid experiences in fluid transients, Proceedings of the 7th International Conference on Pressure Surge and Fluid Transients in Pipelines and Open Channels, BHRA, Harrogate, UK, pp. 65-81.

[52] Martin, C.S., Padmanabhan, M., 1979. Pressure pulse propagation in two-component slug flow, Transaction of the ASME, Vol. 101, pp. 44-52.

[53] Martin, C.S., Padmanabhan, M., Wiggert, D.C., 1976. Pressure wave propagation in two-phase bubbly air-water mixtures, Proceedings of the 2nd International Conference on Pressure Surges, BHRA, Cranfield, Bedford, England.

[54] Matsushita, F. 1989. On the hydraulic jump in a downward sloping closed conduit. Transactions of the Japanese Society of Irrigation Drainage and Reclamation Engineering, 144, pp. 33-42.

[55] Mosvell, G., 1976. Luft I utslippsledninger (Air at outfalls), Prosjektkomiteen for rensing av avkrpsvann (Project committee on sewage), PRA report 8, NIVA (Norwegian Water Institute), Oslo, 1976 (in norwegian).

[56] Ngoh, K.L., Lee, T.S., 1998. Air influence on pressure transients with air vessel, Proceedings of the XIX Symposium on Hydraulic Machinery and Cavitation, IAHR, Singapur, pp. 665-672.

[57] Pearsall, I.S., 1965. The velocity of water hammer waves, Symposium on Surge in Pipelines, Institution of Mechanical Engineers, Vol. 180, Part 3E, pp. 12-20.

[58] Pozos Estrada, O., 2002. Desarrollo de un programa de cómputo para detectar las posibles zonas de acumulación de aire en acueductos, y ejemplos de su aplicación. Tesis para obtener el grado de Maestro en Ingeniería, DEPFI, Universidad Nacional Autónoma de México, México. (in spanish)

[59] Qiu, D.Q., 1995. Transient analysis and the effect of air pockets in a pipeline, Master of Philosophy Thesis, University of Liverpool, UK.

[60] Qiu, D.Q., Borrows, R., 1996. Prediction of pressure transients with entrapped air in a pipeline, Proceedings of the 7th International Conference on Pressure Surge and Fluid Transients in Pipelines and Open Channels, BHRA, Harrogate, UK, pp. 251-263.

[61] Rajaratnam, N. 1965. Hydraulic jump in horizontal conduits. Water Power and Dam Construction, **17**(2), pp. 80–83.

[62] Richards, R.T., 1957. Air binding in large pipe lines flowing under vacuum. Journal of the Hydraulics Division, ASCE, Vol. 83, No. HY6, paper 1454, pp. l-10.

[63] Richards, R.T., Air binding in water pipelines, AWWA, June 1962, pp. 719-730.

[64] Rodal E.A., Carmona, R., Gonzalez, C.A., Pozos, O., 2000. Aumento de la pérdida de carga en conduciones debido a aire atrapado, XIX Congreso Latinoamericano de Hidráulica, IAHR, Cordoba, Argentina, pp. 583-592. (in spanish)

[65] Runge, D.E. and Wallis, G.B., 1965. AEC Rept. NYO-3114-8 (EURAEC-1416).

[66] Sailer, R. E. 1955. San Diego aqueduct, Journal of civil engineering, ASCE, Vol. 25, N° 5, pp. 38-40.

[67] Sene, K.J., Hunt, J.C.R., Thomas, N.H., 1994. The role of coherent structures in bubble transport by turbulent share flows. Journal of Fluid Mechanics, 259, pp. 219-240.

[68] Shoham, O., 1982. Flow pattern transition and characterisation in gas-liquid two-phase flow, PhD Thesis, Tel-Aviv University, Ramat-Aviv, Israel.

[69] Shuy, E.B., Aplet, C.J., 1983. Friction effects in unsteady pipe flow, 4th International Conference on Pressure Surge, BHRA, pp. 147-164.

[70] Silberman, E., 1957. Sound velocity and attenuation in bubbly mixture measured in standing wave tubes, Journal of the Acoustical Society of America, Vol. 29, N° 8, pp. 925-933.

[71] Smith, C.D., and Chen, W. 1989. The hydraulic jump in a steeply sloping square conduit. Journal of Hydraulic Research, 27(3): pp. 385–399.

[72] Stahl, H., Hager, W.H., 1999. Hydraulic jump in circular pipes, Canadian Journal of Civil Engineering. 26**,** pp. 368–373.

[73] Stephenson, D., 1997. Effects of air valves and pipework on water hammer pressure, Journal of Transportation Engineering, Vol. 123, N° 2, pp. 101-106.

[74] Streeter, V.L., Wylie, E.B., 1985. Fluid mechanics, 8th Edition, McGraw-Hill International Book Company, New York, USA.

[75] Thomas, N.H., 1982. Air demand distortion in hydraulic models: experimental evidence of bi-modal structure in air entraining flows and scaling analysis of detrainment with special application to siphon priming, International Conference on the Hydraulic Modelling of Civil Engineering Structures, BHRA, Coventry, England.

[76] Thomas, N. H., et. al., 1983. Entrapment and transport of bubbles by transient large eddies in multi-phase turbulent shear flows. International conference on physical modeling of Multi-phase flow, Coventry, pp. 169-184.

[77] Thomas, S., 2003. Air management in water distribution systems, A new understanding of air transfer, Clear water legacy, Ontario, Canada.

[78] Thorley, A.R.D., 2004. Fluid transients in pipeline systems, 2nd Edition, Ed. D. & L. George Ltd., London, UK.

[79] U.S. Corps of Engineers, Air demand – Regulated outlet works, Hydraulic Design Criteria, Chart 050-1.

[80] Veronese (1937): Veronese, A., 1937. Sul motto delle bolle d'aria nelle condotte d'acqua, Estrato dal fasciacolo X, Vol. XIV, October, p.XV (in italian).

[81] Viana, F., Pardo, R, Yanez, R, Trallero, J.L., Joseph, D.D., 2003. Universal Correlation for the rise velocity of long gas bubbles in round pipes, Journal of Fluid Mechanics, vol. 494, pp. 379-398.

[82] Wallis, G.B. 1969. One dimensional two-phase flow, McGraw Hill, New York, USA.

[83] Walski, T.M., Barnhart T., Driscoll J. and Yencha R., 1994. Hydraulics of corrosive gas pockets in force mains. Water Environment Research, Vol. 66, No. 6, Sept/Oct, pp. 772-778.

[84] Wiggert, D.C., Sundquist, M.J., 1977. Fixed-grid characteristics for pipeline transients, Journal of the Hydraulics Division, Vol. 101, pp. 79-86.

[85] Wiggert, D.C., Sundquist, M.J., 1979. The effect of gaseous cavitation on fluid transients, Journal of Fluids Engineering, Vol. 101, pp. 79-86.

[86] Wisner, P.E., 1965. Role of the Froude number in the study of air entrainment, Proc. 11th Cong. IAHR, Leningrad, Paper 1.15.

[87] Wisner, P.E., Mohsen, F.N. and Kouwen, N., 1975. Removal of air from water lines by hydraulic means. ASCE, Journal of the Hydraulics Division, Vol. 101, HY2, pp. 243-25.

[88] Wylie, E.B. and Streeter, V.L. 1978. Fluid Transients, McGraw-Hill International Book Company, New York, USA.

[89] Wylie, E.B., Streeter, V.L., Suo, L., 1993. Fluid transients in systems, Ed. Prentice Hall, Englewood Cliffs, New Jersey, USA.

[90] Yadigaroglu, G., Lahey, R.T.Jr., 1976. On the various forms of the conservation equations in two-phase flow, International Journal of Multi-phase Flow, Vol. 2, pp. 477-494.

[91] Zukoski, E.E., 1966. Influence of viscosity, surface tension and inclination on motion of long bubbles in closed tubes, J. of Fluid Mechanics, 25(4), pp. 821-837.

[92] Zhou, F., 2000. Effects of trapped air on flow transients in rapidly filling sewers, Doctor of Philosophy Thesis, University of Alberta, Canada.

[93] OPTIMAS® Software for WINDOWS 95: Version 5.23, 1996, OPTIMAS Corporation.

[94] COMPAQ VISUAL FORTRAN® for WINDOWS XP: Version 6.6, 2001, Compaq Computer Corporation

Institut für Wasserbau
Universität Stuttgart

Pfaffenwaldring 61
70569 Stuttgart (Vaihingen)
Telefon (0711) 685 - 64717/64741/64752/64679
Telefax (0711) 685 - 67020 o. 64746 o. 64681
E-Mail: iws@iws.uni-stuttgart.de
http://www.iws.uni-stuttgart.de

Verzeichnis der Mitteilungshefte

1 Röhnisch, Arthur: *Die Bemühungen um eine Wasserbauliche Versuchsanstalt an der Technischen Hochschule Stuttgart*,
und
Fattah Abouleid, Abdel: *Beitrag zur Berechnung einer in lockeren Sand gerammten, zweifach verankerten Spundwand*, 1963

2 Marotz, Günter: *Beitrag zur Frage der Standfestigkeit von dichten Asphaltbelägen im Großwasserbau*, 1964

3 Gurr, Siegfried: *Beitrag zur Berechnung zusammengesetzter ebener Flächentragwerke unter besonderer Berücksichtigung ebener Stauwände, mit Hilfe von Randwert- und Lastwertmatrizen*, 1965

4 Plica, Peter: *Ein Beitrag zur Anwendung von Schalenkonstruktionen im Stahlwasserbau*, und Petrikat, Kurt: *Möglichkeiten und Grenzen des wasserbaulichen Versuchswesens*, 1966

5 Plate, Erich: *Beitrag zur Bestimmung der Windgeschwindigkeitsverteilung in der durch eine Wand gestörten bodennahen Luftschicht*,
und
Röhnisch, Arthur; Marotz, Günter: *Neue Baustoffe und Bauausführungen für den Schutz der Böschungen und der Sohle von Kanälen, Flüssen und Häfen; Gestehungskosten und jeweilige Vorteile*, sowie Unny, T.E.: *Schwingungsuntersuchungen am Kegelstrahlschieber*, 1967

6 Seiler, Erich: *Die Ermittlung des Anlagenwertes der bundeseigenen Binnenschiffahrtsstraßen und Talsperren und des Anteils der Binnenschiffahrt an diesem Wert*, 1967

7 *Sonderheft anläßlich des 65. Geburtstages von Prof. Arthur Röhnisch mit Beiträgen von* Benk, Dieter; Breitling, J.; Gurr, Siegfried; Haberhauer, Robert; Honekamp, Hermann; Kuz, Klaus Dieter; Marotz, Günter; Mayer-Vorfelder, Hans-Jörg; Miller, Rudolf; Plate, Erich J.; Radomski, Helge; Schwarz, Helmut; Vollmer, Ernst; Wildenhahn, Eberhard; 1967

8 Jumikis, Alfred: *Beitrag zur experimentellen Untersuchung des Wassernachschubs in einem gefrierenden Boden und die Beurteilung der Ergebnisse*, 1968

9 Marotz, Günter: *Technische Grundlagen einer Wasserspeicherung im natürlichen Untergrund*, 1968

10 Radomski, Helge: *Untersuchungen über den Einfluß der Querschnittsform wellenförmiger Spundwände auf die statischen und rammtechnischen Eigenschaften*, 1968

11 Schwarz, Helmut: *Die Grenztragfähigkeit des Baugrundes bei Einwirkung vertikal gezogener Ankerplatten als zweidimensionales Bruchproblem*, 1969

12 Erbel, Klaus: *Ein Beitrag zur Untersuchung der Metamorphose von Mittelgebirgsschneedecken unter besonderer Berücksichtigung eines Verfahrens zur Bestimmung der thermischen Schneequalität*, 1969

13 Westhaus, Karl-Heinz: *Der Strukturwandel in der Binnenschiffahrt und sein Einfluß auf den Ausbau der Binnenschiffskanäle*, 1969

14 Mayer-Vorfelder, Hans-Jörg: *Ein Beitrag zur Berechnung des Erdwiderstandes unter Ansatz der logarithmischen Spirale als Gleitflächenfunktion*, 1970

15 Schulz, Manfred: *Berechnung des räumlichen Erddruckes auf die Wandung kreiszylindrischer Körper*, 1970

16 Mobasseri, Manoutschehr: *Die Rippenstützmauer. Konstruktion und Grenzen ihrer Standsicherheit*, 1970

17 Benk, Dieter: *Ein Beitrag zum Betrieb und zur Bemessung von Hochwasserrückhaltebecken*, 1970

18 Gàl, Attila: *Bestimmung der mitschwingenden Wassermasse bei überströmten Fischbauchklappen mit kreiszylindrischem Staublech*, 1971, vergriffen

19 Kuz, Klaus Dieter: *Ein Beitrag zur Frage des Einsetzens von Kavitationserscheinungen in einer Düsenströmung bei Berücksichtigung der im Wasser gelösten Gase*, 1971, vergriffen

20 Schaak, Hartmut: *Verteilleitungen von Wasserkraftanlagen*, 1971

21 *Sonderheft zur Eröffnung der neuen Versuchsanstalt des Instituts für Wasserbau der Universität Stuttgart mit Beiträgen von*
Brombach, Hansjörg; Dirksen, Wolfram; Gàl, Attila; Gerlach, Reinhard; Giesecke, Jürgen; Holthoff, Franz-Josef; Kuz, Klaus Dieter; Marotz, Günter; Minor, Hans-Erwin; Petrikat, Kurt; Röhnisch, Arthur; Rueff, Helge; Schwarz, Helmut; Vollmer, Ernst; Wildenhahn, Eberhard; 1972

22 Wang, Chung-su: *Ein Beitrag zur Berechnung der Schwingungen an Kegelstrahlschiebern*, 1972

23 Mayer-Vorfelder, Hans-Jörg: *Erdwiderstandsbeiwerte nach dem Ohde-Variationsverfahren*, 1972

24 Minor, Hans-Erwin: *Beitrag zur Bestimmung der Schwingungsanfachungsfunktionen überströmter Stauklappen*, 1972, vergriffen

25 Brombach, Hansjörg: *Untersuchung strömungsmechanischer Elemente (Fluidik) und die Möglichkeit der Anwendung von Wirbelkammerelementen im Wasserbau*, 1972, vergriffen

26 Wildenhahn, Eberhard: *Beitrag zur Berechnung von Horizontalfilterbrunnen*, 1972

27 Steinlein, Helmut: *Die Eliminierung der Schwebstoffe aus Flußwasser zum Zweck der unterirdischen Wasserspeicherung, gezeigt am Beispiel der Iller*, 1972

28 Holthoff, Franz Josef: *Die Überwindung großer Hubhöhen in der Binnenschiffahrt durch Schwimmerhebewerke*, 1973

29 Röder, Karl: *Einwirkungen aus Baugrundbewegungen auf trog- und kastenförmige Konstruktionen des Wasser- und Tunnelbaues*, 1973

30 Kretschmer, Heinz: *Die Bemessung von Bogenstaumauern in Abhängigkeit von der Talform*, 1973

31 Honekamp, Hermann: *Beitrag zur Berechnung der Montage von Unterwasserpipelines*, 1973

32 Giesecke, Jürgen: *Die Wirbelkammertriode als neuartiges Steuerorgan im Wasserbau*, und Brombach, Hansjörg: *Entwicklung, Bauformen, Wirkungsweise und Steuereigenschaften von Wirbelkammerverstärkern*, 1974

33 Rueff, Helge: *Untersuchung der schwingungserregenden Kräfte an zwei hintereinander angeordneten Tiefschützen unter besonderer Berücksichtigung von Kavitation*, 1974

34 Röhnisch, Arthur: *Einpreßversuche mit Zementmörtel für Spannbeton - Vergleich der Ergebnisse von Modellversuchen mit Ausführungen in Hüllwellrohren*, 1975

35 *Sonderheft anläßlich des 65. Geburtstages von Prof. Dr.-Ing. Kurt Petrikat mit Beiträgen von*: Brombach, Hansjörg; Erbel, Klaus; Flinspach, Dieter; Fischer jr., Richard; Gàl, Attila; Gerlach, Reinhard; Giesecke, Jürgen; Haberhauer, Robert; Hafner Edzard; Hausenblas, Bernhard; Horlacher, Hans-Burkhard; Hutarew, Andreas; Knoll, Manfred; Krummet, Ralph; Marotz, Günter; Merkle, Theodor; Miller, Christoph; Minor, Hans-Erwin; Neumayer, Hans; Rao, Syamala; Rath, Paul; Rueff, Helge; Ruppert, Jürgen; Schwarz, Wolfgang; Topal-Gökceli, Mehmet; Vollmer, Ernst; Wang, Chung-su; Weber, Hans-Georg; 1975

36 Berger, Jochum: *Beitrag zur Berechnung des Spannungszustandes in rotationssymmetrisch belasteten Kugelschalen veränderlicher Wandstärke unter Gas- und Flüssigkeitsdruck durch Integration schwach singulärer Differentialgleichungen*, 1975

37 Dirksen, Wolfram: *Berechnung instationärer Abflußvorgänge in gestauten Gerinnen mittels Differenzenverfahren und die Anwendung auf Hochwasserrückhaltebecken*, 1976

38 Horlacher, Hans-Burkhard: *Berechnung instationärer Temperatur- und Wärmespannungsfelder in langen mehrschichtigen Hohlzylindern*, 1976

39 Hafner, Edzard: *Untersuchung der hydrodynamischen Kräfte auf Baukörper im Tiefwasserbereich des Meeres*, 1977, ISBN 3-921694-39-6

40 Ruppert, Jürgen: *Über den Axialwirbelkammerverstärker für den Einsatz im Wasserbau*, 1977, ISBN 3-921694-40-X

41 Hutarew, Andreas: *Beitrag zur Beeinflußbarkeit des Sauerstoffgehalts in Fließgewässern an Abstürzen und Wehren*, 1977, ISBN 3-921694-41-8, vergriffen

42 Miller, Christoph: *Ein Beitrag zur Bestimmung der schwingungserregenden Kräfte an unterströmten Wehren*, 1977, ISBN 3-921694-42-6

43 Schwarz, Wolfgang: *Druckstoßberechnung unter Berücksichtigung der Radial- und Längsverschiebungen der Rohrwandung*, 1978, ISBN 3-921694-43-4

44 Kinzelbach, Wolfgang: *Numerische Untersuchungen über den optimalen Einsatz variabler Kühlsysteme einer Kraftwerkskette am Beispiel Oberrhein*, 1978, ISBN 3-921694-44-2

45 Barczewski, Baldur: *Neue Meßmethoden für Wasser-Luftgemische und deren Anwendung auf zweiphasige Auftriebsstrahlen*, 1979, ISBN 3-921694-45-0

46 Neumayer, Hans: *Untersuchung der Strömungsvorgänge in radialen Wirbelkammerverstärkern*, 1979, ISBN 3-921694-46-9

47 Elalfy, Youssef-Elhassan: *Untersuchung der Strömungsvorgänge in Wirbelkammerdioden und -drosseln*, 1979, ISBN 3-921694-47-7

48 Brombach, Hansjörg: *Automatisierung der Bewirtschaftung von Wasserspeichern*, 1981, ISBN 3-921694-48-5

49 Geldner, Peter: *Deterministische und stochastische Methoden zur Bestimmung der Selbstdichtung von Gewässern*, 1981, ISBN 3-921694-49-3, vergriffen

50 Mehlhorn, Hans: *Temperaturveränderungen im Grundwasser durch Brauchwassereinleitungen*, 1982, ISBN 3-921694-50-7, vergriffen

51 Hafner, Edzard: *Rohrleitungen und Behälter im Meer*, 1983, ISBN 3-921694-51-5

52 Rinnert, Bernd: *Hydrodynamische Dispersion in porösen Medien: Einfluß von Dichteunterschieden auf die Vertikalvermischung in horizontaler Strömung*, 1983, ISBN 3-921694-52-3, vergriffen

53 Lindner, Wulf: *Steuerung von Grundwasserentnahmen unter Einhaltung ökologischer Kriterien*, 1983, ISBN 3-921694-53-1, vergriffen

54 Herr, Michael; Herzer, Jörg; Kinzelbach, Wolfgang; Kobus, Helmut; Rinnert, Bernd: *Methoden zur rechnerischen Erfassung und hydraulischen Sanierung von Grundwasserkontaminationen*, 1983, ISBN 3-921694-54-X

55 Schmitt, Paul: *Wege zur Automatisierung der Niederschlagsermittlung*, 1984, ISBN 3-921694-55-8, vergriffen

56 Müller, Peter: *Transport und selektive Sedimentation von Schwebstoffen bei gestau tem Abfluß*, 1985, ISBN 3-921694-56-6

57 El-Qawasmeh, Fuad: *Möglichkeiten und Grenzen der Tropfbewässerung unter besonderer Berücksichtigung der Verstopfungsanfälligkeit der Tropfelemente*, 1985, ISBN 3-921694-57-4, vergriffen

58 Kirchenbaur, Klaus: *Mikroprozessorgesteuerte Erfassung instationärer Druckfelder am Beispiel seegangsbelasteter Baukörper*, 1985, ISBN 3-921694-58-2

59 Kobus, Helmut (Hrsg.): *Modellierung des großräumigen Wärme- und Schadstofftransports im Grundwasser*, Tätigkeitsbericht 1984/85 (DFG-Forschergruppe an den Universitäten Hohenheim, Karlsruhe und Stuttgart), 1985, ISBN 3-921694-59-0, vergriffen

60 Spitz, Karlheinz: *Dispersion in porösen Medien: Einfluß von Inhomogenitäten und Dichteunterschieden*, 1985, ISBN 3-921694-60-4, vergriffen

61 Kobus, Helmut: *An Introduction to Air-Water Flows in Hydraulics*, 1985, ISBN 3-921694-61-2

62 Kaleris, Vassilios: *Erfassung des Austausches von Oberflächen- und Grundwasser in horizontalebenen Grundwassermodellen*, 1986, ISBN 3-921694-62-0

63 Herr, Michael: *Grundlagen der hydraulischen Sanierung verunreinigter Porengrundwasserleiter*, 1987, ISBN 3-921694-63-9

64 Marx, Walter: *Berechnung von Temperatur und Spannung in Massenbeton infolge Hydratation*, 1987, ISBN 3-921694-64-7

65 Koschitzky, Hans-Peter: *Dimensionierungskonzept für Sohlbelüfter in Schußrinnen zur Vermeidung von Kavitationsschäden*, 1987, ISBN 3-921694-65-5

66 Kobus, Helmut (Hrsg.): *Modellierung des großräumigen Wärme- und Schadstofftransports im Grundwasser*, Tätigkeitsbericht 1986/87 (DFG-Forschergruppe an den Universitäten Hohenheim, Karlsruhe und Stuttgart) 1987, ISBN 3-921694-66-3

67 Söll, Thomas: *Berechnungsverfahren zur Abschätzung anthropogener Temperaturanomalien im Grundwasser*, 1988, ISBN 3-921694-67-1

68 Dittrich, Andreas; Westrich, Bernd: *Bodenseeufererosion, Bestandsaufnahme und Bewertung*, 1988, ISBN 3-921694-68-X, vergriffen

69 Huwe, Bernd; van der Ploeg, Rienk R.: *Modelle zur Simulation des Stickstoffhaushaltes von Standorten mit unterschiedlicher landwirtschaftlicher Nutzung*, 1988, ISBN 3-921694-69-8, vergriffen

70 Stephan, Karl: *Integration elliptischer Funktionen*, 1988, ISBN 3-921694-70-1

71 Kobus, Helmut; Zilliox, Lothaire (Hrsg.): *Nitratbelastung des Grundwassers, Auswirkungen der Landwirtschaft auf die Grundwasser- und Rohwasserbeschaffenheit und Maßnahmen zum Schutz des Grundwassers*. Vorträge des deutsch-französischen Kolloquiums am 6. Oktober 1988, Universitäten Stuttgart und Louis Pasteur Strasbourg (Vorträge in deutsch oder französisch, Kurzfassungen zweisprachig), 1988, ISBN 3-921694-71-X

72 Soyeaux, Renald: *Unterströmung von Stauanlagen auf klüftigem Untergrund unter Berücksichtigung laminarer und turbulenter Fließzustände*,1991,ISBN 3-921694-72-8

73 Kohane, Roberto: *Berechnungsmethoden für Hochwasserabfluß in Fließgewässern mit überströmten Vorländern*, 1991, ISBN 3-921694-73-6

74 Hassinger, Reinhard: *Beitrag zur Hydraulik und Bemessung von Blocksteinrampen in flexibler Bauweise*, 1991, ISBN 3-921694-74-4, vergriffen

75 Schäfer, Gerhard: *Einfluß von Schichtenstrukturen und lokalen Einlagerungen auf die Längsdispersion in Porengrundwasserleitern*, 1991, ISBN 3-921694-75-2

76 Giesecke, Jürgen: *Vorträge, Wasserwirtschaft in stark besiedelten Regionen; Umweltforschung mit Schwerpunkt Wasserwirtschaft*, 1991, ISBN 3-921694-76-0

77 Huwe, Bernd: *Deterministische und stochastische Ansätze zur Modellierung des Stickstoffhaushalts landwirtschaftlich genutzter Flächen auf unterschiedlichem Skalenniveau*, 1992, ISBN 3-921694-77-9, vergriffen

78 Rommel, Michael: *Verwendung von Kluftdaten zur realitätsnahen Generierung von Kluftnetzen mit anschließender laminar-turbulenter Strömungsberechnung*, 1993, ISBN 3-92 1694-78-7

79 Marschall, Paul: *Die Ermittlung lokaler Stofffrachten im Grundwasser mit Hilfe von Einbohrloch-Meßverfahren*, 1993, ISBN 3-921694-79-5, vergriffen

80 Ptak, Thomas: *Stofftransport in heterogenen Porenaquiferen: Felduntersuchungen und stochastische Modellierung*, 1993, ISBN 3-921694-80-9, vergriffen

81 Haakh, Frieder: *Transientes Strömungsverhalten in Wirbelkammern*, 1993, ISBN 3-921694-81-7

82 Kobus, Helmut; Cirpka, Olaf; Barczewski, Baldur; Koschitzky, Hans-Peter: *Versuchseinrichtung zur Grundwasser und Altlastensanierung VEGAS, Konzeption und Programmrahmen*, 1993, ISBN 3-921694-82-5

83 Zang, Weidong: *Optimaler Echtzeit-Betrieb eines Speichers mit aktueller Abflußregenerierung*, 1994, ISBN 3-921694-83-3, vergriffen

84 Franke, Hans-Jörg: *Stochastische Modellierung eines flächenhaften Stoffeintrages und Transports in Grundwasser am Beispiel der Pflanzenschutzmittelproblematik*, 1995, ISBN 3-921694-84-1

85 Lang, Ulrich: *Simulation regionaler Strömungs- und Transportvorgänge in Karstaquiferen mit Hilfe des Doppelkontinuum-Ansatzes: Methodenentwicklung und Parameteridentifikation*, 1995, ISBN 3-921694-85-X, vergriffen

86 Helmig, Rainer: *Einführung in die Numerischen Methoden der Hydromechanik*, 1996, ISBN 3-921694-86-8, vergriffen

87 Cirpka, Olaf: *CONTRACT: A Numerical Tool for Contaminant Transport and Chemical Transformations - Theory and Program Documentation -*, 1996, ISBN 3-921694-87-6

88 Haberlandt, Uwe: *Stochastische Synthese und Regionalisierung des Niederschlages für Schmutzfrachtberechnungen*, 1996, ISBN 3-921694-88-4

89 Croisé, Jean: *Extraktion von flüchtigen Chemikalien aus natürlichen Lockergesteinen mittels erzwungener Luftströmung*, 1996, ISBN 3-921694-89-2, vergriffen

90 Jorde, Klaus: *Ökologisch begründete, dynamische Mindestwasserregelungen bei Ausleitungskraftwerken*, 1997, ISBN 3-921694-90-6, vergriffen

91 Helmig, Rainer: *Gekoppelte Strömungs- und Transportprozesse im Untergrund - Ein Beitrag zur Hydrosystemmodellierung-*, 1998, ISBN 3-921694-91-4

92 Emmert, Martin: *Numerische Modellierung nichtisothermer Gas-Wasser Systeme in porösen Medien*, 1997, ISBN 3-921694-92-2

93 Kern, Ulrich: *Transport von Schweb- und Schadstoffen in staugeregelten Fließgewässern am Beispiel des Neckars*, 1997, ISBN 3-921694-93-0, vergriffen

94 Förster, Georg: *Druckstoßdämpfung durch große Luftblasen in Hochpunkten von Rohrleitungen 1997*, ISBN 3-921694-94-9

95 Cirpka, Olaf: *Numerische Methoden zur Simulation des reaktiven Mehrkomponententransports im Grundwasser*, 1997, ISBN 3-921694-95-7, vergriffen

96 Färber, Arne: *Wärmetransport in der ungesättigten Bodenzone: Entwicklung einer thermischen In-situ-Sanierungstechnologie*, 1997, ISBN 3-921694-96-5

97 Betz, Christoph: *Wasserdampfdestillation von Schadstoffen im porösen Medium: Entwicklung einer thermischen In-situ-Sanierungstechnologie*, 1998, ISBN 3-921694-97-3

98 Xu, Yichun: *Numerical Modeling of Suspended Sediment Transport in Rivers*, 1998, ISBN 3-921694-98-1, vergriffen

99 Wüst, Wolfgang: *Geochemische Untersuchungen zur Sanierung CKW-kontaminierter Aquifere mit Fe(0)-Reaktionswänden*, 2000, ISBN 3-933761-02-2

100 Sheta, Hussam: *Simulation von Mehrphasenvorgängen in porösen Medien unter Einbeziehung von Hysterese-Effekten*, 2000, ISBN 3-933761-03-4

101 Ayros, Edwin: *Regionalisierung extremer Abflüsse auf der Grundlage statistischer Verfahren*, 2000, ISBN 3-933761-04-2, vergriffen

102 Huber, Ralf: *Compositional Multiphase Flow and Transport in Heterogeneous Porous Media*, 2000, ISBN 3-933761-05-0

103 Braun, Christopherus: *Ein Upscaling-Verfahren für Mehrphasenströmungen in porösen Medien*, 2000, ISBN 3-933761-06-9

104 Hofmann, Bernd: *Entwicklung eines rechnergestützten Managementsystems zur Beurteilung von Grundwasserschadensfällen*, 2000, ISBN 3-933761-07-7

105 Class, Holger: *Theorie und numerische Modellierung nichtisothermer Mehrphasenprozesse in NAPL-kontaminierten porösen Medien*, 2001, ISBN 3-933761-08-5

106 Schmidt, Reinhard: *Wasserdampf- und Heißluftinjektion zur thermischen Sanierung kontaminierter Standorte*, 2001, ISBN 3-933761-09-3

107 Reinhold Josef:, *Schadstoffextraktion mit hydraulischen Sanierungsverfahren unter Anwendung von grenzflächenaktiven Stoffen*, 2001, ISBN 3-933761-10-7

108 Schneider, Matthias: *Habitat- und Abflussmodellierung für Fließgewässer mit unscharfen Berechnungsansätzen*, 2001, ISBN 3-933761-11-5

109 Rathgeb, Andreas: *Hydrodynamische Bemessungsgrundlagen für Lockerdeckwerke an überströmbaren Erddämmen*, 2001, ISBN 3-933761-12-3

110 Lang, Stefan: *Parallele numerische Simulation instätionärer Probleme mit adaptiven Methoden auf unstrukturierten Gittern*, 2001, ISBN 3-933761-13-1

111 Appt, Jochen; Stumpp Simone: *Die Bodensee-Messkampagne 2001, IWS/CWR Lake Constance Measurement Program 2001*, 2002, ISBN 3-933761-14-X

112 Heimerl, Stephan: *Systematische Beurteilung von Wasserkraftprojekten*, 2002, ISBN 3-933761-15-8

113 Iqbal, Amin: *On the Management and Salinity Control of Drip Irrigation*, 2002, ISBN 3-933761-16-6

114 Silberhorn-Hemminger, Annette: *Modellierung von Kluftaquifersystemen: Geostatistische Analyse und deterministisch-stochastische Kluftgenerierung*, 2002, ISBN 3-933761-17-4

115 Winkler, Angela: *Prozesse des Wärme- und Stofftransports bei der In-situ-Sanierung mit festen Wärmequellen*, 2003, ISBN 3-933761-18-2

116 Marx, Walter: *Wasserkraft, Bewässerung, Umwelt - Planungs- und Bewertungsschwerpunkte der Wasserbewirtschaftung*, 2003, ISBN 3-933761-19-0

117 Hinkelmann, Reinhard: *Efficient Numerical Methods and Information-Processing Techniques in Environment Water*, 2003, ISBN 3-933761-20-4

118 Samaniego-Eguiguren, Luis Eduardo: *Hydrological Consequences of Land Use / Land Cover and Climatic Changes in Mesoscale Catchments*, 2003, ISBN 3-933761-21-2

119 Neunhäuserer, Lina: *Diskretisierungsansätze zur Modellierung von Strömungs- und Transportprozessen in geklüftet-porösen Medien*, 2003, ISBN 3-933761-22-0

120 Paul, Maren: *Simulation of Two-Phase Flow in Heterogeneous Poros Media with Adaptive Methods*, 2003, ISBN 3-933761-23-9

121 Ehret, Uwe: *Rainfall and Flood Nowcasting in Small Catchments using Weather Radar*, 2003, ISBN 3-933761-24-7

122 Haag, Ingo: *Der Sauerstoffhaushalt staugeregelter Flüsse am Beispiel des Neckars - Analysen, Experimente, Simulationen -*, 2003, ISBN 3-933761-25-5

123 Appt, Jochen: *Analysis of Basin-Scale Internal Waves in Upper Lake Constance*, 2003, ISBN 3-933761-26-3

124 Hrsg.: Schrenk, Volker; Batereau, Katrin; Barczewski, Baldur; Weber, Karolin und Koschitzky, Hans-Peter: *Symposium Ressource Fläche und VEGAS - Statuskolloquium 2003, 30. September und 1. Oktober 2003*, 2003, ISBN 3-933761-27-1

125 Omar Khalil Ouda: *Optimisation of Agricultural Water Use: A Decision Support System for the Gaza Strip*, 2003, ISBN 3-933761-28-0

126 Batereau, Katrin: *Sensorbasierte Bodenluftmessung zur Vor-Ort-Erkundung von Schadensherden im Untergrund*, 2004, ISBN 3-933761-29-8

127 Witt, Oliver: *Erosionsstabilität von Gewässersedimenten mit Auswirkung auf den Stofftransport bei Hochwasser am Beispiel ausgewählter Stauhaltungen des Oberrheins*, 2004, ISBN 3-933761-30-1

128 Jakobs, Hartmut: *Simulation nicht-isothermer Gas-Wasser-Prozesse in komplexen Kluft-Matrix-Systemen*, 2004, ISBN 3-933761-31-X

129 Li, Chen-Chien: *Deterministisch-stochastisches Berechnungskonzept zur Beurteilung der Auswirkungen erosiver Hochwasserereignisse in Flussstauhaltungen*, 2004, ISBN 3-933761-32-8

130 Reichenberger, Volker; Helmig, Rainer; Jakobs, Hartmut; Bastian, Peter; Niessner, Jennifer: *Complex Gas-Water Processes in Discrete Fracture-Matrix Systems: Upscaling, Mass-Conservative Discretization and Efficient Multilevel Solution*, 2004, ISBN 3-933761-33-6

131 Hrsg.: Barczewski, Baldur; Koschitzky, Hans-Peter; Weber, Karolin; Wege, Ralf: *VEGAS - Statuskolloquium 2004*, Tagungsband zur Veranstaltung am 05. Oktober 2004 an der Universität Stuttgart, Campus Stuttgart-Vaihingen, 2004, ISBN 3-933761-34-4

132 Asie, Kemal Jabir: *Finite Volume Models for Multiphase Multicomponent Flow through Porous Media*. 2005, ISBN 3-933761-35-2

133 Jacoub, George: *Development of a 2-D Numerical Module for Particulate Contaminant Transport in Flood Retention Reservoirs and Impounded Rivers*, 2004, ISBN 3-933761-36-0

134 Nowak, Wolfgang: *Geostatistical Methods for the Identification of Flow and Transport Parameters in the Subsurface*, 2005, ISBN 3-933761-37-9

135 Süß, Mia: *Analysis of the influence of structures and boundaries on flow and transport processes in fractured porous media*, 2005, ISBN 3-933761-38-7

136 Jose, Surabhin Chackiath: *Experimental Investigations on Longitudinal Dispersive Mixing in Heterogeneous Aquifers,* 2005, ISBN: 3-933761-39-5

137 Filiz, Fulya: *Linking Large-Scale Meteorological Conditions to Floods in Mesoscale Catchments,* 2005, ISBN 3-933761-40-9

138 Qin, Minghao: *Wirklichkeitsnahe und recheneffiziente Ermittlung von Temperatur und Spannungen bei großen RCC-Staumauern,* 2005, ISBN 3-933761-41-7

139 Kobayashi, Kenichiro: *Optimization Methods for Multiphase Systems in the Subsurface - Application to Methane Migration in Coal Mining Areas,* 2005, ISBN 3-933761-42-5

140 Rahman, Md. Arifur: *Experimental Investigations on Transverse Dispersive Mixing in Heterogeneous Porous Media,* 2005, ISBN 3-933761-43-3

141 Schrenk, Volker: *Ökobilanzen zur Bewertung von Altlastensanierungsmaßnahmen,* 2005, ISBN 3-933761-44-1

142 Hundecha, Hirpa Yeshewatesfa: *Regionalization of Parameters of a Conceptual Rainfall-Runoff Model,* 2005, ISBN: 3-933761-45-X

143 Wege, Ralf: *Untersuchungs- und Überwachungsmethoden für die Beurteilung natürlicher Selbstreinigungsprozesse im Grundwasser,* 2005, ISBN 3-933761-46-8

144 Breiting, Thomas: *Techniken und Methoden der Hydroinformatik - Modellierung von komplexen Hydrosystemen im Untergrund,* 2006, 3-933761-47-6

145 Hrsg.: Braun, Jürgen; Koschitzky, Hans-Peter; Müller, Martin: *Ressource Untergrund: 10 Jahre VEGAS: Forschung und Technologieentwicklung zum Schutz von Grundwasser und Boden,* Tagungsband zur Veranstaltung am 28. und 29. September 2005 an der Universität Stuttgart, Campus Stuttgart-Vaihingen, 2005, ISBN 3-933761-48-4

146 Rojanschi, Vlad: *Abflusskonzentration in mesoskaligen Einzugsgebieten unter Berücksichtigung des Sickerraumes,* 2006, ISBN 3-933761-49-2

147 Winkler, Nina Simone: *Optimierung der Steuerung von Hochwasserrückhaltebeckensystemen,* 2006, ISBN 3-933761-50-6

148 Wolf, Jens: *Räumlich differenzierte Modellierung der Grundwasserströmung alluvialer Aquifere für mesoskalige Einzugsgebiete,* 2006, ISBN: 3-933761-51-4

149 Kohler, Beate: *Externe Effekte der Laufwasserkraftnutzung,* 2006, ISBN: 3-933761-52-2

150 Hrsg.: Braun, Jürgen; Koschitzky, Hans-Peter; Stuhrmann, Matthias: *VEGAS-Statuskolloquium 2006,* Tagungsband zur Veranstaltung am 28. September 2006 an der Universität Stuttgart, Campus Stuttgart-Vaihingen, 2006, ISBN: 3-933761-53-0

151 Niessner, Jennifer: *Multi-Scale Modeling of Multi-Phase - Multi-Component Processes in Heterogeneous Porous Media*, 2006, ISBN: 3-933761-54-9

152 Fischer, Markus: *Beanspruchung eingeerdeter Rohrleitungen infolge Austrocknung bindiger Böden*, 2006, ISBN: 3-933761-55-7

153 Schneck, Alexander: *Optimierung der Grundwasserbewirtschaftung unter Berücksichtigung der Belange der Wasserversorgung, der Landwirtschaft und des Naturschutzes*, 2006, ISBN 3-933761-56-5

154 Das, Tapash: *The Impact of Spatial Variability of Precipitation on the Predictive Uncertainty of Hydrological Models*, 2006, ISBN: 3-933761-57-3

155 Bielinski, Andreas, *Numerical Simulation of CO_2 sequestration in geological formations*, 2007, ISBN: 3-933761-58-1

156 Mödinger, Jens: *Entwicklung eines Bewertungs- und Entscheidungsunterstützungssystems für eine nachhaltige regionale Grundwasserbewirtschaftung*, 2006, ISBN: 3-933761-60-3

157 Manthey, Sabine: *Two-phase flow processes with dynamic effects in porous media - parameter estimation and simulation*, 2007, ISBN: 3-933761-61-1

158 Pozos Estrada, Oscar: *Investigation on the Effects of Entrained Air in Pipelines*, 2007, ISBN: 3-933761-62-X

Die Mitteilungshefte ab dem Jahr 2005 stehen als pdf-Datei über die Homepage des Instituts: www.iws.uni-stuttgart.de zur Verfügung.